FATIGUE CRACK GROWTH IN ADHESIVELY BONDED STRUCTURES AND COMPOSITE REPAIRS

by

WENCHEN HU

B.Eng. (Hons.) Mechanical Engineering

A thesis submitted in fulfilment of
the requirements for the degree of
Doctor of Philosophy

Department of Mechanical and Aerospace Engineering
Monash University
2017

Copyright Notice

Declaration

I hereby declare that this thesis contains no material which has been accepted for the award of any other degree or diploma at any university or equivalent institution and that, to the best of my knowledge and belief, this thesis contains no material previously published or written by another person, except where due reference is made in the text of the thesis.

W. Hu

[redacted]

Acknowledgements

Firstly, I would like to give my deepest gratitude to my supervisors. Prof. Rhys Jones has constantly provided me support and guidance since the very start of my PhD study. His unique and humorous style of talking is always inspiring and interesting. Dr. Daren Peng is a respectable and intelligent researcher who always helped me with great patience for finite element analysis and experiment setups. Prof. Anthony Kinloch from Imperial College London also provided many valuable thoughts and suggestions during my study.

Next, I would like to acknowledge Dr John Wang from Defence Science and Technology Group whom put a great effort on preparing and arranging the fatigue experiment. Dr. Simon Barter and Mr. Richard Mazeika also from Defence Science and Technology Group taught me everything about quantitative fractography and were patient with all my questions and inquiries.

For those who supported and inspired me during conferences and communications, I would like to give them my warmest appreciation. Mr. Lorrie Molent, Prof. Andrea Brunner, Dr. John-Alan Pascoe, Prof. Wenyi Yan, Prof. Raman Singh. Then my friends and colleagues in my department Pu, Khawla, Dinaz, Michael, Wencheng and Yaohui, I would like to thank them for their support and help.

Lastly and most importantly, I would like to dedicate this thesis to my family, especially my wife, Jialin. Her constant support and encouragement are the source of strength to push me to challenge the shardships I have encountered during this journey.

Abstract

Before 2009, the US Federal Aviation Administration (FAA) required composite and adhesively bonded structures on aircraft to be designed based on no growth approach. This means that there should be no crack growing during the designed life. However, many incidents associated with disbands still occurred. Consequently, FAA changed its requirement to slow growth approach in 2009. The new requirement allows disbond to grow during the designed life if the growing is slow, stable and predictable. Thus, the development of methodology for predicting disbond growth is necessary.

The range of strain energy release rate, ΔG, is a prevalent parameter used to characterise the delamination and disbond growth for composite and adhesively bonded structures. However, ΔG is no longer a valid crack driving force (CDF) as it would cause R-ratio anomaly when it is plotted against fatigue crack growth rate, da/dN. R ratio anomaly represents the phenomenon that for the same CDF, the increase of mean stress would lead the decrease if the growth rate. Consequently, $\Delta\sqrt{G}$ (= $\sqrt{G_{max}}$ - $\sqrt{G_{min}}$) is proposed as the new CDF as its ability to plot a more physically intuitive result.

The Hartman-Schijve variant of NASGRO equation first used to predict the crack growth in metal is extended to composite and adhesively bonded structures with the new CDF, $\Delta\sqrt{G}$. By using the Hartman-Schijve representation, $(\Delta\sqrt{G}-\Delta\sqrt{G_{thr}})/(\sqrt{(1-\sqrt{G}/\sqrt{A})})$, plot against da/dN, a master curve is produced so that fatigue data with scatters, different R ratios, different temperature and different initial length can collapse onto it. In addition, the master line has lower exponential value which is beneficial for design process. The Hartman-Schijve equation is also capable of predicting disbond growing from naturally occurring material discontinuity with information from standard laboratory tests which contain long artificial disbond.

According to the report of US Air Force, the operational life of aircraft is barely equal to its designed life. As a result, the schedule of maintenance and repair is an important part of the airworthiness. Laboratory test results are often used to predict cracks which growing in operational aircraft. However, ASTM E647-13a points out that fatigue crack growth data obtained using cracks growing from long artificial notches is inappropriate for assessing aircraft sustainment as the threshold of long cracks is much higher than those of short cracks.

A program cooperated with Australia Defence Science and Technology Group (DSTG) allows fatigue cracks growing from small surface damage, i.e. laser notches and corrosion pits, which both have depth of less than 0.3 mm. Then the cracked specimens are patched with boron/epoxy prepreg. The result of this experiment shows that the cracks grow exponentially both before and after patching and are simulated with finite element model and Cubic rule. Both methods demonstrated their capability of predicting crack growth after patching with information obtained from unpatched condition. This experiment also reveals that there are marker bands on the fracture surface of adhesive film. This shows a potential to predict the time of patch failure.

Table of Contents

List of Figures

List of Tables

Abbreviations

AA	Aluminium Alloy
ASIP	Aircraft Structural Integrity Program
ASTM	American Society for the Testing and Materials
CA	Constant Amplitude
CCT	Centre Cracked Tension
COD	Crack Opening Displacement
CPCA	Compression Pre-cracking Constant Amplitude
DSTG	Defence Science and Technology Group
DSTO	Defence Science and Technology Organisation
EIFS	Equivalent Initial Flaw Size
EPFM	Elastic Plastic Fracture Mechanics
EPS	Equivalent Pre-crack Size
FAA	Federal Aviation Administration
FAST	Fatigue Analysis of Structure
FALSTAFF	Fighter Aircraft Loading STAndard For Fatigue Evaluation
FCG	Fatigue Crack Growth
FEA	Finite Element Analysis
FSFT	Full-Scale Fatigue Testing
HS	Hartman-Schijve
IFS	Initial Flaw Size
JSSG	Joint Service Specification Guide
IR	Infrared
LEFM	Linear Elastic Fracture Mechanics
LOV	Limit Of Validity
MED	Multiple Element fatigue Damage
MSD	Multiple Site fatigue Damage
NASA	National Aeronautics and Space Administration
NDI	Non-Destructive Inspection
PABST	Primary Adhesively Bonded Structure Technology
PROF	Probability of Fracture
QF	Quantitative Fractography
RAAF	Royal Australian Air Force
RAM	Repair Assessment Methodology
SAM	Structural Analysis Methodology
SEM	Scanning Electron Microscope
SERR	Strain Energy Release Rate
SENT	Single Edge Notch Tension
SIF	Stress Intensity Factor
SLAP	Service Life Assessment Program
S-N	Stress-Life curve
TR	Technical Report
USAF	United States Air Force
VA	Variable amplitude
VCCT	Virtual Crack-Closure Technique
WSD	Widespread Fatigue Damage

Nomenclature

a	Crack depth in 3D, Crack size in 2D
a_0	Initial crack length
A	Cyclic fracture toughness
c	Crack length
C	A parameter in power relation for metals
D	A parameter in power relation for composites and adhesively bonded structures
$\mathrm{d}a/\mathrm{d}N$	Crack growth rate per cycle
E	Young's modulus
G	Strain energy release rate
G_{max}	Maximum strain energy release rate during a load cycle
G_{min}	Minimum strain energy release rate during a load cycle
K	Stress intensity factor
K_c	Fracture toughness
K_{max}	Maximum stress intensity factor during a load cycle
K_{min}	Minimum stress intensity factor during a load cycle
K_{op}	Crack opening stress intensity factor
m	Exponent in power relation for composites and adhesively bonded structure
n	Exponent in power relation for metals
N	Number of load cycles
P	Remote load
R	Stress ratio
T	Thickness
U	Crack closure factor or Strain energy
W	Strain energy density
x, y, z	Coordinate system
Y	Geometry correction factor
ΔG	Strain energy release rate range
$\Delta\sqrt{G}$	Crack driving force for composites and adhesively bonded structure in HS equation
$\Delta\sqrt{G_{thr}}$	Threshold strain energy release rate range in HS equation
ΔK	Stress intensity factor range
ΔK_{op}	Crack opening stress intensity range
ΔK_{th}	Stress intensity range threshold for long cracks
ΔK_{thr}	Threshold stress intensity range in HS equation
β	Geometric factor
γ	Surface tension
ε	strain
υ	Poisson ratio
σ	Local stress
$\Delta\sigma$	Stress amplitude
σ_∞	Applied remote stress
ω	Exponential term in Cubic rule

Publications

- R. Jones, W. Hu and A. J. Kinloch, "Characterising crack growth in structural adhesives," 8th Australasian Congress on Applied Mechanics, ACAM 8, Melbourne, Australia, 23rd - 26th November 2014.
- A. J. Kinloch, R. Jones and W. Hu, "Modelling Fatigue Crack Growth in Structural Adhesive Joints", Proceedings Adhesion Society 2015 Annual Meeting, Savannah, United States, 20th –25th February 2015.
- R. Jones, W. Hu and A. J. Kinloch, "A Convenient Way to Represent Fatigue Crack Growth in Structural Adhesives," Fatigue and Fracture of Engineering Materials and Structures, vol. 38, no. 4, pp. 379-391, 2015.
- W. Hu, R. Jones and A. J. Kinloch, "Computing the growth of naturally-occurring disbonds in adhesively-bonded patches to metallic structures," Engineering Fracture Mechanics, vol. 152, pp. 162-173, 2016.
- R. Jones, A. J. Kinloch and W. Hu, "Cyclic-fatigue crack growth in composite and adhesively-bonded structures: The FAA slow crack growth approach to certification and the problem of similitude," International Journal of Fatigue, vol. 88, pp. 10-18, 2016.
- W. Hu, R. Jones and A. J. Kinloch, "Discussion of the stress ratio effect on the fatigue delamination growth characterization in composite structures," Procedia Structural Integrity, vol. 2, pp. 66-71, 2016.
- A. J. Kinloch, R. Jones and W. Hu, "Modelling and predicting fatigue crack growth in structural adhesive joints," Procedia Structural Integrity, vol. 2, pp. 221-226, 2016.
- W. Hu, S. Barter, J. Wang, R. Jones and A. J. Kinloch, "Extending the USAF risk of failure approach to composite repairs," 17th Australian International Aerospace Congress, Melbourne, Australia, 27th - 28th February 2017.
- W. Hu, S. Barter, J. Wang, R. Jones and A. J. Kinloch, "On the USAF 'risk of failure' approach and its applicability to composite repairs to metal airframes," Composite Structures, vol. 167, pp. 103-111, 2017.
- W. Hu, R. Jones and A. J. Kinloch, "Computing the Growth of Naturally-Occurring Disbonds in Adhesively-Bonded Joints," in Aircraft Sustainment and Repair by Jones et al., Elsevier. (Proceeding)

Chapter 1

Introduction

There is a crack in everything. That's how the light gets in.

Leonard Cohen

1.1 Background

As the famous Canadian singer, Leonard Cohen, wrote, "*There is a crack in everything. That's how the light gets in.*" Indeed every physical material contains small naturally occurring material discontinuities, such as voids and inclusion particles [1]. They can often be caused during manufacturing, machining, transporting and assembling. We can't discover the majority of those discontinuities either visually or by touch. It is therefore important to study and understand how cracks form, grow and finally fail. Although there are numerous mechanisms and conditions that can cause cracks to fail, this thesis will only focus on failures that are caused by fatigue.

As failure by fatigue can occur as a result of repeated loads that are lower than the design load level it is a particularly dangerous failure mechanism. Between the late 1940s and early 1950, aircraft designs were primarily focused on static strength and there was less attention paid to aircraft fatigue. During this period, there was no requirement for full-scale fatigue testing (FSFT). A catastrophic incident summarized by Charles F. Tiffany illustrates the importance of fatigue failure, which should always be considered during aircraft design [2]:

"Comet 1 (DH 106-1) registration number G-ALYP was the first jet transport to enter scheduled airline service on May 2, 1952. On January 19, 1954 after only 1286 pressurized flights this aircraft suffered an explosive decompression failure and crashed in the

Mediterranean off Elba. Investigations revealed that the failure of G-ALYP originated near the aft automatic direction finding (ADF) window."

The Comet incident highlighted the need of considering fatigue in airframe design led to the recognition that in addition to static strength, aircraft designers needed to consider fatigue performance [3]. One outcome of the Comet incident was the implementation of the fail-safe design principle to ensure the structural safety of commercial transport aircraft, i.e. '*The fail-safe design concept requires having multiple load paths with the residual strength requirement in the event of failure of one structural element or an obvious partial failure'* [3]. Fatigue resistance and residual strength tests were required to verify fail-safe design. The analysis and prediction of fatigue crack growth now form an essential part of the aircraft certification process [3].

In early 1958, US Air Force lost five B-47 bombers due to fatigue. As a consequence, in May 1958 the Aircraft Structural Integrity Program (ASIP) was established [4]. This program had three objectives [5]:

- *Control structural failure of operational aircraft*
- *Determine methods of accurately predicting aircraft service life*
- *Provide design and test approaches that would avoid structural fatigue problems in future aircraft*

The new 1958 Air Force ASIP required a safe-life fatigue design approach based on the assumption of an initial-flaw-free structure. A stress-life fatigue analysis (using Miner's rule) plus a scatter factor of **FOUR** were required to arrive at the safe-life estimates. In addition, FSFTs were required to achieve **FOUR** times of the design [2]. Even with a safety factor of four, the new safe-life design and test requirements did not prevent failures from occurring and the loss of many military aircraft in the 1960s and early 1970s was directly due to fatigue [2].

Consequently, the introduction of damage tolerance requirements in 1974, which proposed as a result the F-111 wing failure, had a positive effect on structural safety for military aircraft. Damage tolerance guidelines for ensuring the structural safety of military aircraft was incorporated in Military Specification, MIL-A-83444 [6]. In this approach, it was mandatory to assume that there were initial flaws existing in aircraft.

On April 28, 1988, Aloha Airline flight 243, a Boeing 737-200 experienced an explosive decompression of fuselage. The upper forward fuselage was torn away and this incident caused one fatality. Investigation showed that the loss of fuselage skin was caused by rapid link-up of many relatively small fatigue cracks in a single structural element. This kind of fatigue damage was subsequently called multiple site fatigue damage (MSD). It is one of the two types of widespread fatigue damage (WFD). The other type of WFD is multiple element fatigue damage (MED) used to categorize those simultaneously present fatigue damages in adjacent structural elements [3]. Either type of WFD can lead to catastrophic accidents.

WFD can rapidly reduce the residual strength to the extent that below the residual strength requirements. In 2011 the US Federal Aviation Administration (FAA) introduced the concept of Limit of Validity (LOV) to try to prevent WFD [7]. The definition of LOV given in 2011 [7] is:

"The period of time (in flight cycles, flight hours, or both), up to which it has been demonstrated by test evidence, analysis and, if available, service experience and teardown inspection results of high-time airplanes, that widespread fatigue damage will not occur in the airplane structure."

In 2008. Babish [8] summarized thirty-seven losses due to structural failures of USAF aircrafts since 1972. Babish found that 16 out of 37 or 43% of structural failures were caused by fatigue, as can be seen Figure 1.1. Despite of much effort put in over the years, fatigue damage is still a crucial factor that leads to structural failures.

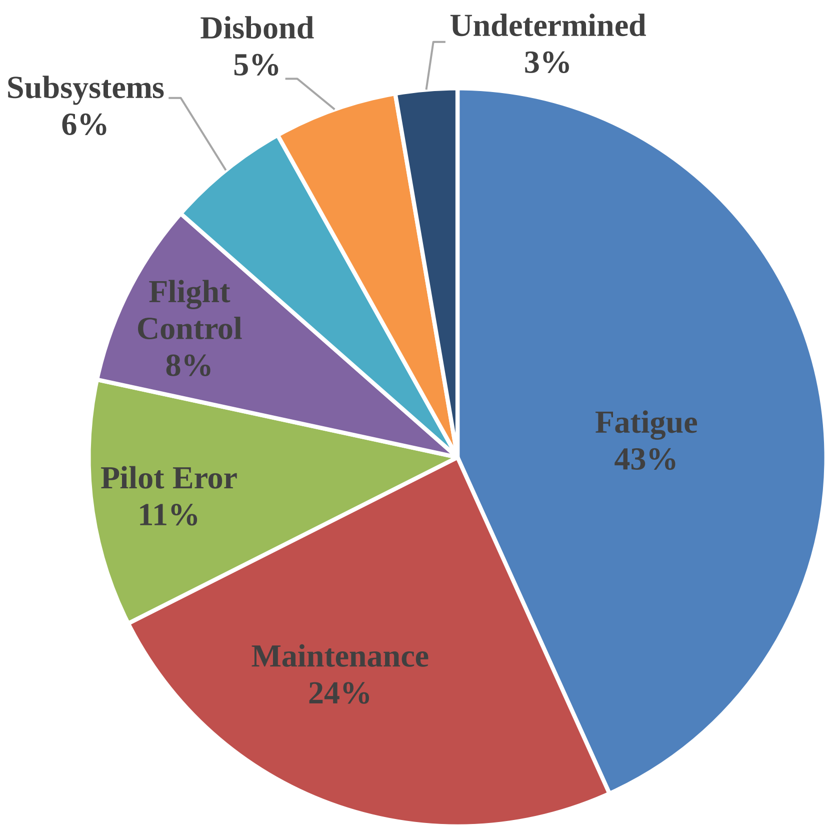

Figure 1.1 Percentages associated with types of causes of 37 USAF structureal Failures [8].

1.2 Motivation

Section 1.1 provides a briefing history on the effort of engineers to ensure the airworthiness in both military and civilian aviation industries. Since the late 1960s, fracture mechanics approaches focused on fatigue problems have been demonstrated to be an effective approach to predict:

- Critical crack sizes in aircraft structure
- Crack growth behaviour
- The effects of various structural configurations on crack behaviour

The ability of fracture mechanics approaches to predict the crack in aircraft makes it one of the most growth popular options for determining inspection requirements and operational limits. Such an approach can also provide aircraft designers with the ability to correlate fatigue test results with the expected in-service behaviour. The ultimate goal is to simulate the growth of fatigue cracks based on a well-established fracture mechanics model.

Most of those structural safe design philosophies have focused on metallic airframes (e.g. fuselage). However, adhesively bonded joints are now common in modern aircraft design. Bonded joints possess a number of potential advantages [9]:

- As they do not need to create extra holes, adhesively bonded joints generally have lower stress concentration factors than bolted joints.
- Due to the larger contact surfaces, the stress transfer through adhesively bonded joints is smoother than that is through bolted joints.
- Being lighter, adhesively bonded joints also have economic benefits. In other words, they have the potential to result in a lighter structure and therefore consume less fuel.

However, adhesively bonded joints on aircraft have demonstrated considerable variations in their reliability [10]. The lack of understanding about the fatigue of bonded joints is one major obstruction that prevents them from being applied on primary aircraft structures. Between 1984 and 2009, the US FAA approach to composite aircraft structures [11] mandated a no-growth approach for aircraft design. By this the FAA meant that *a method that requires demonstration that the structure, with defined flaws present, is able to withstand appropriate repeated loads without detrimental flaw growth for the life of the structure* [12].

Even though the phrase, “no-growth”, is mentioned **FIVE** times in FAA Advisory Circular 120-107A [11], in-service experience associated with RAAF F-111C aircraft is that extensive disbonds were found on 7 out of 40 composite doublers within 1000 flight hours of installation.

This is despite the fact that as required in MIL-STD-1530 [13] prior to installation the doublers passed the requisite building block tests, both static and fatigue, and that all of the fleet passed cold proof load tests at a temperature of -40 °C. As such the doublers met all of the certification requirements outlined in MIL-STD-1530 and in the Composite Materials Handbook CMH-17-3F [14]. Nevertheless, disbonds between the upper surface of wings and the boron/epoxy doublers still arose in service [15, 16]. Other examples of disbonds both service and full-scale fatigue tests are given in [17, 18]. As a consequence in 2009 the US FAA introduced a slow growth approach to certify composite and adhesively bonded structures as well as bonded repairs. The precise wording given in FAA Advisory Circular 120-107B [12] is:

"The traditional slow growth approach may be appropriate for certain damage types found in composites if the growth rate can be shown to be ***slow****,* ***stable*** *and* ***predictable****. Slow growth characterization should yield conservative and reliable results. As part of the slow growth approach, an inspection program should be developed consisting of the frequency, extent, and methods of inspection for inclusion in the maintenance plan."*

Consequently, a method that can be used for the damage tolerance assessment of adhesively bonded joints is urgently needed.

1.3 Research Aims

In 2009, the US FAA changed its guidance for composite and adhesively bonded aircraft structures to allow a slow growth approach which is based on the damage tolerance design philosophy [12]. Such a change opens up a new opportunity to apply adhesively bonded structures (e.g. adhesively bonded joint and adhesively bonded repairs) on primary aircraft structures. Unfortunately a lack of understanding of and an inability to predict the growth of cracks that arise from small naturally occurring material discontinuities is an obstacle that hampers the establishment of a slow growth approach to adhesively bonded structures.

Consequently, this research aims to develop a methodology for predicting the growth of large cracks as well as cracks that have grown from small natural occurring material discontinuities in adhesively bonded structures and bonded repairs. Attention will focus on developing a single formulation (i.e. a master curve approach) that holds for Mode I, Mode II and Mixed Mode I and II fatigue crack growth. A key aim of this research is to ensure that a is independent of fracture modes, and can account for the scatter that is seen in disbond growth. Specific aims in this thesis are:

- Understand the behaviour of short crack growth in adhesively bonded joints and bonded repairs;
- Use the information from long crack to predict the crack growing from small naturally occurring discontinuity;
- Be able to account for scatter seen for both long and short cracks in adhesively bonded joints and bonded repairs;
- Establish a model that can predict the behaviour of cracks, which have grown from small naturally occurring discontinuities, before and after they have been repaired using an externally bonded fibre reinforced composite patch.

1.4 Thesis Outline

This thesis consists SEVEN chapters including the Introduction Chapter. Chapter 2 presents the literature review. A detailed part of literature review focuses on fatigue problems associated with adhesively bonded structures. Chapter 3 introduces the Hartman-Schijve variant of the NASGRO crack-growth equation and its ability to account for load ratio effects, scatter, both for long disbonds and disbonds growing from small naturally occurring discontinuities and the effect of temperature on disbond growth. Chapter 4 investigates the possibility of using long crack data associated with adhesively bonded joints to predict disbonds growing from small naturally occurring discontinuities. Chapter 5 presents experimental work collaborated with the Australian Defence Science and Technology Group (DSTG), which focuses on discovering the effect of different fibre reinforced composite patch configurations on cracked metallic structures. Chapter 6 illustrates the possibility of using the Hartman-Schijve equation with Finite Element Analysis (FEA) and the Cubic Rule to predict the life of cracked metallic structures repaired using a bonded composite patch. Chapter 7 summarises the main findings and makes recommendations for the future work.

Chapter 2

Literature Review

Looking into a mirror you may trim your garments.

Looking into a soul you may find out how well you rule.

Looking into the histories you may foresee the future

Shimin Li -- The Second Emperor of Tang Dynasty

2.1 A Short History of Fatigue and Fracture Mechanics

The problem of fatigue has been an issue throughout human history. It is undeniable that the quality of physical matter will gradually decline as time goes by. Axes become blunter every time they hack trees. Wheels of carts become more fragile after a journey from Melbourne to Sydney. Human knees get damaged with age. It was not until 1837 that the first scientific fatigue test was performed by Wihelm Albert in Clausthal, Germany [19]. Albert constructed a test machine to study how conveyor chains would fail in service in the Clausthal mines. In 1853 a Frenchman, Morin, in his book "Resistance des Materiaux" discussed the reports of two engineers who were responsible for horse-drawn mail coaches. The replacement of the axles of the coaches was prescribed after 60000 km. This was an early example of the "safe life" design approach. In 1870 August Wöhler, who performed fatigue tests in order to study the of railway axles, concluded:

"Material can be induced to fail by many repetitions of stresses, all of which are lower than the static strength. The stress amplitudes are decisive for the destruction of the cohesion of the

material. The maximum stress is of influence only in so far as the higher it is, the lower are the stress amplitudes which lead to failure [19].*"*

This was the first statement to mention that the stress range was more important than the maximum stress in mechanism of fatigue failure. The Basquin in 1910 used Wöhler's tests data to present the relationship between stress and life cycles in a log – log form [20]. Such plots are now referred to as an S-N curve.

In 1920, Griffith [21] established the discipline of fracture mechanics which would subsequently become one of the most popular approaches as to address the problems of fatigue and fracture. In this work Griffith used an energy approach, instead of a stress based approach, to study crack propagation in glass. Here he used the first law of thermodynamics to characterise the energy balance under plane strain condition, the glass materials were not thin, see Equation (2.1),

$$\sigma_\infty = \sqrt{\frac{2E\gamma}{\pi a}} \tag{2.1}$$

where σ_∞ is the applied remote tensile stress at material, a is the length of half crack, E is the Young's modulus of material and γ is the "surface tension" of the material which indicates the resistance of forming new surfaces. Griffith found that the product of σ_∞ and $\sqrt{a}$ was almost a constant, even in different geometries, e.g. spherical bulbs and circular tubes [21]. Both Griffith and Irwin [21, 22] believed that the change in fracture work per unit crack extension should equal the energy required to create a unit new surface. Thus, the surface tension, γ, in Equation (2.1) and the strain energy release rate (SERR), G, which is the result of crack extension, can be considered as equivalent. Irwin noticed, from Griffith's work, that $\sqrt{EG}$ (or $\sqrt{E\gamma}$) is a constant and named this term the stress intensity factor (SIF) or K [23]. Consequently, for metals the SERR and K are related by Equation (2.2).

$$K = \sqrt{GE'} \tag{2.2}$$

where E′ equals to E for plain stress or E/(1-υ^2) for plain strain and υ is the Poisson ratio. The crack would propagate if K is beyond the SIF threshold, K_{th}, and it would propagate very quickly and unstably if K is approaching to the material's fracture toughness, K_c.

There are three different modes of fracture that a crack can experience. Thus, the SIF can have three components which are commonly denoted as K_I, K_{II} and K_{III}. K_I represents Mode I fracture on which the crack propagation caused by the stress acting perpendicular to the crack face. K_{II} represents Mode II fracture for which the crack propagation is caused by the in-plane shear parallel to the crack face. K_{III} represents Mode III fracture for which crack propagation is due to the out-plane shear stresses acting as shown in Figure 2.1.

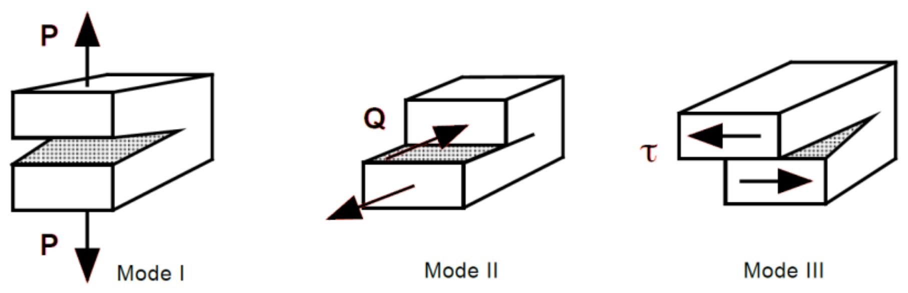

Figure 2.1 Three modes of fracture

The near tip stress field is a function of these three different modes. For Mode I fracture the stress field can be written as per Equations (2.3) – (2.5) [24].

$$\sigma_x = \frac{K_I}{\sqrt{2\pi r}} cos\frac{\theta}{2}\left(1 - sin\frac{\theta}{2} sin\frac{3\theta}{2}\right) \tag{2.3}$$

$$\sigma_y = \frac{K_I}{\sqrt{2\pi r}} cos\frac{\theta}{2}\left(1 + sin\frac{\theta}{2} sin\frac{3\theta}{2}\right) \tag{2.4}$$

$$\tau_{xy} = \frac{K_I}{\sqrt{2\pi r}} cos\frac{\theta}{2} sin\frac{\theta}{2} sin\frac{3\theta}{2} \tag{2.5}$$

where σ_x and σ_y are local stresses in x and y direction respectively, τ_{xy} is the local shear and (r, θ) is a crack tip centred local polar coordinate system such that the crack faces lie on the lines ±π. The equations also demonstrate that the near crack tip stress field has a $\frac{1}{\sqrt{r}}$ singularity. As such the SIF is believed to characterize the crack tip stress field. It is common to write K in the form:

$$K = \beta\sigma_\infty\sqrt{\pi a} \tag{2.6}$$

where β is a geometric factor, also called the beta factor, and σ_∞ is the remote applied stress. As a parameter that characterises the crack tip stress field K makes fracture mechanics based approaches ideal for studying cyclic fatigue.

2.2 Fatigue and Prediction in Metal

2.2.1 Fatigue crack growth and Paris equation

Based on the work of Griffith and Irwin [21, 22], Martin and Sinclair [25] were the first to use SERR to characterise the fatigue crack growth in 1958. In the early 1960s Paris and co-workers [26, 27] proposed a power relationship between the crack propagation rate and the range of SIF (ΔK)

$$\frac{da}{dN} = C(\Delta K)^n \tag{2.7}$$

where C and n are material constants and ΔK is the range of K caused by the cyclic fatigue loading, i.e. K_{max} - K_{min}. This equation is commonly referred to as the Paris crack growth equation. Hartman and Schijve [28] subsequently suggested that the fatigue crack growth rate may be proportional to the amount by which ΔK exceeds its threshold value ΔK_{th}., i.e. to ΔK - ΔK_{th}. Lindley et al. [29] argued that the Paris equation underestimates the crack growth rate when K_{max} approaches the value of 70% K_C, the static fracture toughness of the material. Thus, the fatigue crack growth behaviour is divided into three regions as shown in Figure 2.2. Region I is called threshold region where the crack barely has any propagation. Region II is Paris region where the crack grows in accordance with Equation (2.7). In Region III crack growth is rapid.

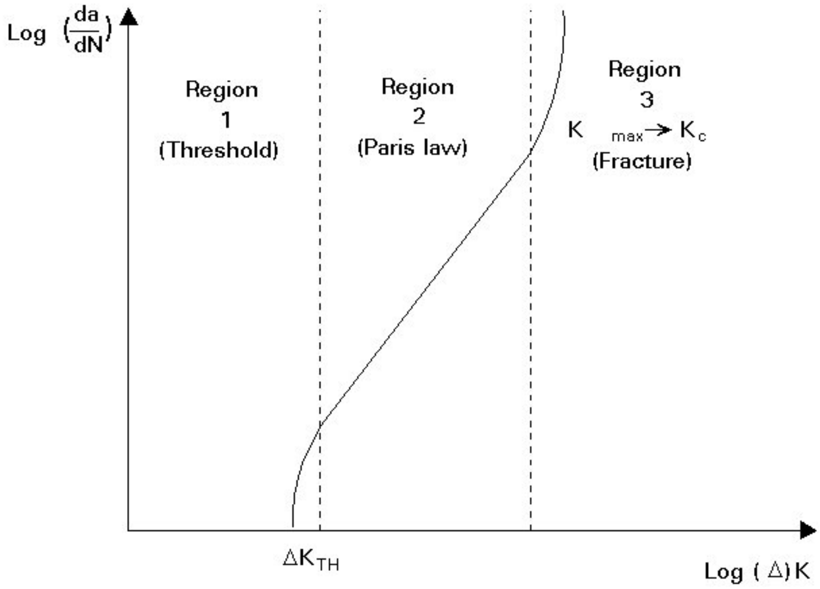

Figure 2.2 Three regions of fatigue crack growth behaviour.

2.2.2 Fatigue crack closure

In 1970 Elber [30] proposed that crack closure occurred under cyclic fatigue. Elber found that, for long cracks growing from artificially induced notches in centre cracked tension (CCT) specimens, the crack tip only opened for a part of the loading cycle test with a load of zero-to-tension. This led to the suggestion that crack closure occurs in the wake of the crack tip and that crack closure is often caused by the residual plastic deformations. In long cracks, this effect is a function of the R ratio which is defined as:

$$\mathrm{R} = \frac{\sigma_{min}}{\sigma_{max}} \tag{2.8}$$

where σ_{min} and σ_{max} are the minimum and maximum stresses in a single fatigue load cycle. Low R ratio tests are associated with low values of K_{min} which may be smaller than the opening value of K, K_{op}. Hence, the effective ΔK, ΔK_{eff}, defined as $K_{max} – K_{op}$, is can be smaller than the actual range $\Delta K = K_{max} – K_{min}$. As part of this work Elbert suggested a crack closure factor, namely U, which provided a relation for those with R ratio between -1 and 0.7. U was defined as shown in Equation (2.9) [31].

$$\mathrm{U} = \frac{\sigma_{max} - \sigma_{op}}{\sigma_{max} - \sigma_{min}} \tag{2.9}$$

where σ_{op} is the minimum stress that can just fully open the crack tip. Based on his results, Elbertdeveloped an empirical formula for U:

$$\mathrm{U} = 0.5 + 0.4R \tag{2.10}$$

whence, ΔK_{eff} was expressed as:

$$\Delta K_{eff} = (0.5 + 0.4R)\Delta K \tag{2.11}$$

This relation implied that the minimum crack opening force was 50% of the maximum tensile stress. Other researchers have suggested that that the minimum of 50% to open the crack might be too high for the aluminium alloy 2024-T3 [32]. Adams [33] suggested that for 2024-T3 a value of 40% of the maximum load was needed to open crack. Roberts and Schmidt [34] declared that only around 25% of maximum load was required.

Fatigue crack growth (FCG) data in near the threshold is particularly important, since the significant fraction of structural life is spent when crack is small or short [35]. However, the crack closure effect is thought to prevent researchers for obtaining such a true FCG rate, because part of tensile stress is used to overcome the compressive residual stress. In contrast it is thought that negative (compressive) loads can accelerate the crack growth rate by inducing a residual tensile force around the crack tip. One good example of this approach is the

Compression Pre-cracking Constant Amplitude (CPCA) test [36]. The work of Newman Jr. and Yamada has suggested that, because of the tensile residual stresses induced by the compressive yielding, a crack grown under CPCA loading spectrum will be fully open at the start of a constant amplitude tensile load. Hence, the subsequent constant tensile loads will be fully effective, i.e. there will be no crack closure effect [36]. A typical CPCA spectrum is shown in Figure 2.3.

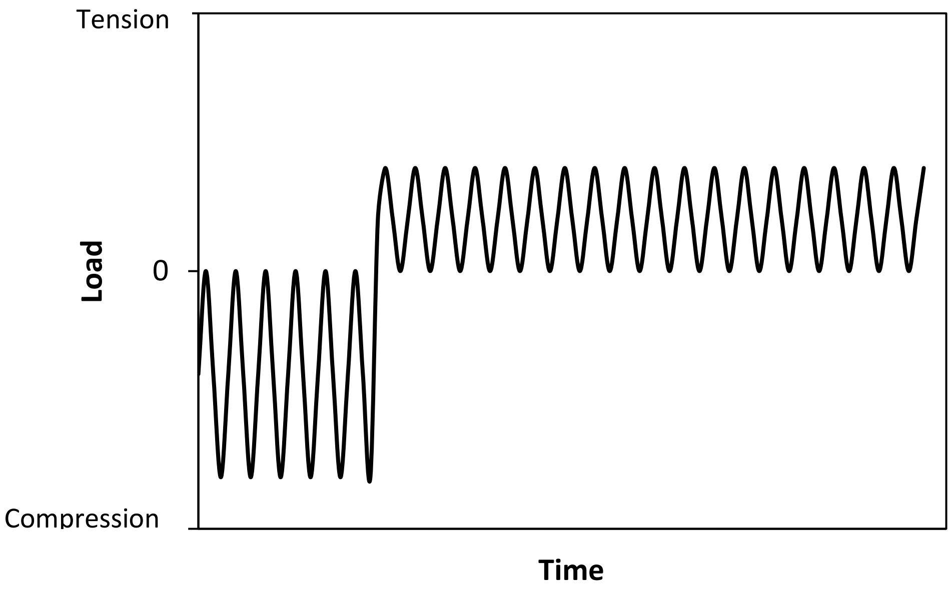

Figure 2.3 A typical schematic CPCA spectrum [36].

2.2.3 Short crack effect

It is believed that in many engineering structures and components fatigue fractures account for the majority of in-service failures [8]. It has been suggested that cracks that grow from small naturally occurring material discontinuities under cyclic fatigue load can be categorised into the following five stages [37]:

1. Initial cyclic damage in the form of cyclic hardening or softening
2. Creation of initial microscopic flaws
3. Coalescence of these micro cracks to form a short crack

4. Subsequent macroscopic propagation of this crack
5. Final catastrophic failure or instability

All materials contain naturally occurring material discontinuities. They can be voids, inclusion particles, grain boundaries and others which are normally caused during manufacturing, machining, transporting and assembling [38]. Experiment data suggests that the order of 0.01 mm would be a reasonable assumption for a typically average initial defect/flaw size and crack growth essentially starts from day one when the aircraft enters service [39, 40]. The time growing from such small material dicontinuities to a size that can be readily detected occupies a significant fraction of the structural life [35].

According to ASTM 647-13a [35] and Suresh and Ritchie [37], there are three ways to define short cracks:

1. Continuum mechanics limitation: *cracks which are of a length comparable to the scale of the microstructure, e.g. of the order of the grain size.*
2. Linear elastic fracture mechanics limitation: *cracks which are of a length comparable to the scale of local plasticity, e.g. small cracks embedded in the plastic zone of a notch or of a length comparable with their own crack tip plastic zones, typically* $\leq 10^{-2}$ *mm in ultrahigh strength materials and* $\leq 10^{-1}$ *mm in low strength materials.*
3. Physical limitation: *cracks which are simply physically small, e.g.* ≤ 1 *mm.*

This research takes the third option as the definition of short crack. Therefore, it is fairly reasonable to state that in smooth specimens, most of the lifetime is spent on the formation of a short crack that is equal or smaller than 1 mm. Hence, it is essential to calculate the FCG behaviour of short cracks as accurately as possible, because it determines the most of the structural life.

It is interesting to notice that physically short cracks, which are 'long' in terms of continuum mechanics and LEFM analyses, have also been shown to propagate more rapidly than corresponding long cracks under the same nominal driving force. The crack growth rate is faster for short cracks, as compared with its corresponding long cracks at certain values of ΔK, e.g. when ΔK approach to threshold. Lados et al. [41] stated that: "*The use of long crack data can lead to significantly non-conservative estimates of the fatigue response and serious design errors.*" Such a phenomenon has been confirmed by many other researchers [42, 43, 44, 45, 46, 47, 48, 49, 50] and quoted ASTM E647-13a [35]. An example of AA 7050-T7451 from Jones et al. [49] is shown in Figures 2.4. The result reviewed that the FCG of short cracks has a much lower threshold than long cracks. Consequently, it was explained in ASTM R647-13a [35] that the prediction of the growth of short cracks using data of long cracks can lead to a non-conservative life estimation.

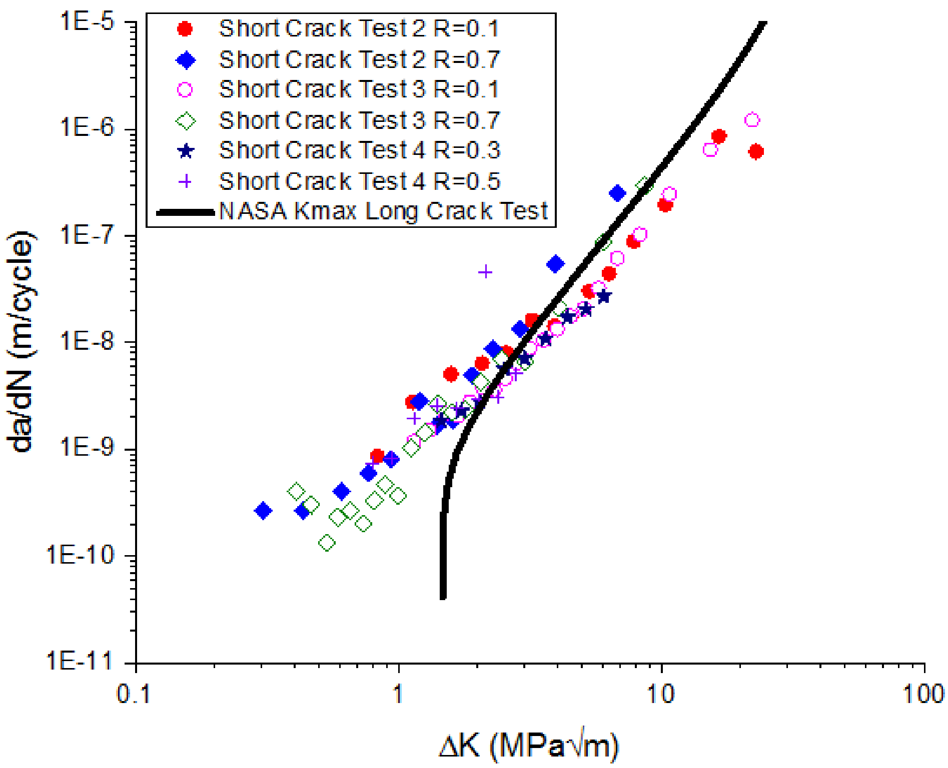

Figure 2.4 AA7050-T7451 fatigue rack growth behaviour [49].

It is worth noting that, compared to long cracks, short cracks growing from naturally occurring material discontinuities have little R ratio effect [48, 49, 50]. Consequently, short cracks have little crack closure. In this context Alaoui et al. [48] noted that "*load ratio does not have a real influence on the short fatigue crack propagation, while checking propagation rate different load ratios collapse into one single line. Such little R ratio dependency proves that short cracks have little or no crack closure effect.*" Jones et al. [46] summarised several fatigue crack growth test data of Aluminium Alloy 7050-T7451 in Figure 2.4. The data sets contain four different load ratios in short crack tests. The short crack FCG rate data points for all four different load ratios which collapse onto one single line. Such little R ratio dependency means that short cracks have little or no crack closure effect.

2.2.4 NASGRO crack growth equation

It is very clear that, for long cracks, the power relation proposed by Paris and his co-workers [26, 27] can only describe Region 2 as shown in Figure 2.2. In order to extend prediction range to Region 3 as well as to account for R ratio effect, Forman et al. [51] proposed Equation (2.12) to predict the cyclic fatigue crack propagation rate.

$$\frac{da}{dN} = \frac{C(\Delta K)^n}{(1-R)K_c - \Delta K} \tag{2.12}$$

Most commonly used commercial available crack growth codes now use the NASGRO equation [52]:

$$\frac{da}{dN} = C(\frac{1-f}{1-R}\Delta K)^n \frac{\left(1-\frac{\Delta K_{th}}{\Delta K}\right)^p}{\left(1-\frac{K_{max}}{K_c}\right)^q} \tag{2.13}$$

where C, n, p and q are empirically derived constants and f is the crack opening function for plasticity induced crack closure defined by Newman [53].

$$f = \frac{K_{op}}{K_{max}} = \begin{cases} A_0 + A_1 R + A_2 R^2 + A_3 R^3 & R \geq 0 \\ A_0 + A_1 R & -1 \leq R < 0 \end{cases} \tag{2.14}$$

Details on how to determine these various constants can be found in [52]. Jones et al. [54] simplified the crack growth equation [51, 52, 53] to establish the Hartman-Schijve variant of the NASGRO equation:

$$\frac{da}{dN} = C \left(\frac{\Delta K - \Delta K_{thr}}{\sqrt{1 - \frac{K_{max}}{A}}} \right)^n \tag{2.15}$$

where ΔK_{thr} is the apparent fatigue threshold range and A is the apparent cyclic fracture toughness. ΔK_{thr} and A are best interpreted as parameters chosen to fit the measured da/dN data [55]**.** Jones and Tamboli [50] showed that the Hartman-Schijve equation is capable of describing the growth of both short and long cracks.

It might be noticed that the Hartman-Schijve equation can be derived from the NASGRO equation by assuming n = p, q = p/2 and crack closure effect will be described within the term ΔK_{thr}, e.g. (1-f)/(1-R) = 1. Even with such simplifications, the Hartman-Schijve equation can account for:

- Both short and long cracks as shown in Figure 2.5.
- R-ratio effect as shown in Figure 2.5 and Figure 2.6.
- Different materials that within the same series, e.g. Aluminium alloys 2000 series as shown in Figure 2.6.
- Different types of loading spectrums, e.g. constant and variable amplitude load, as shown in Figure 2.7.

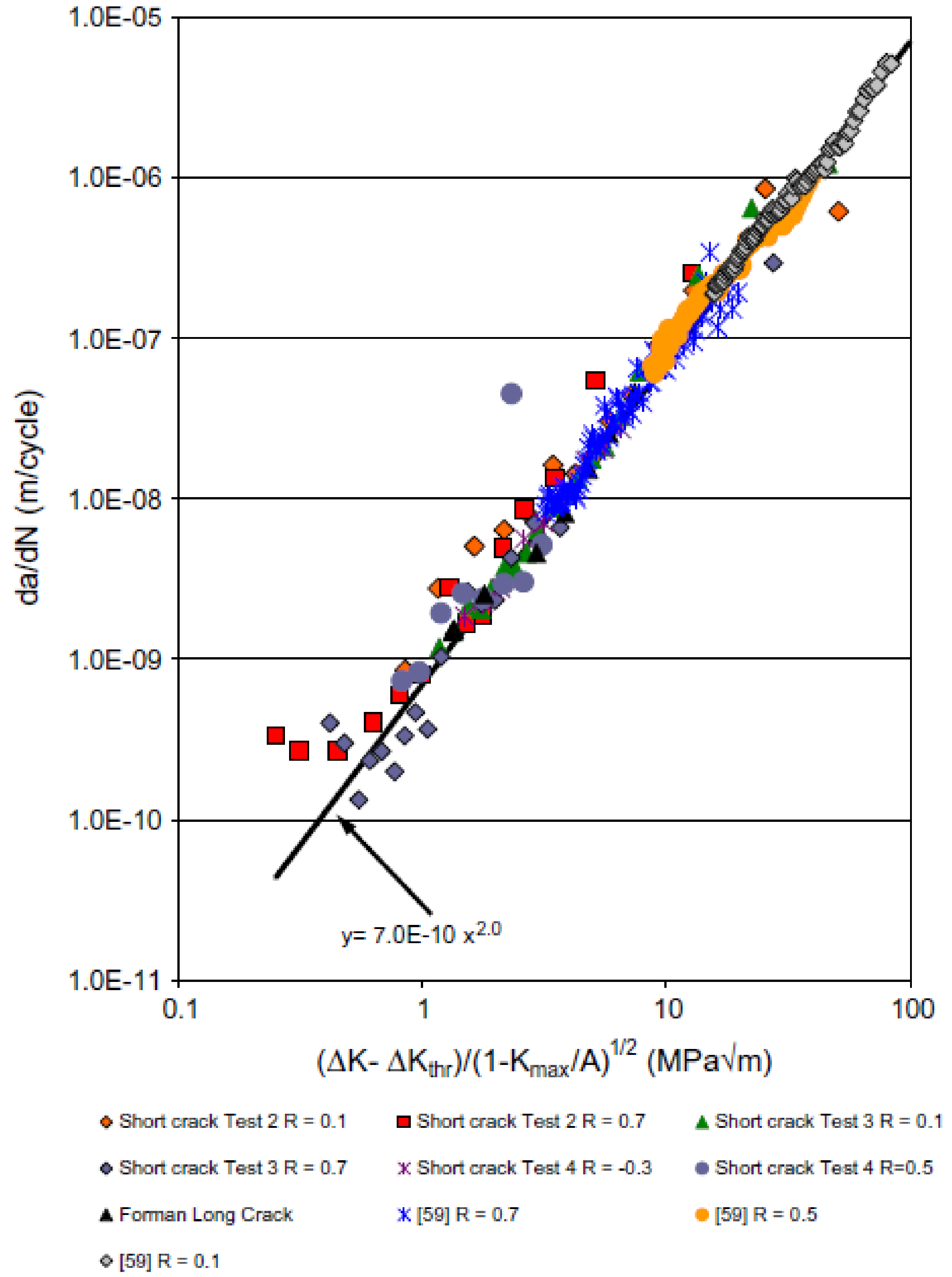

Figure 2.5 Comparison of short and long crack growth rates for 7050-T7451 at different R ratios [54].

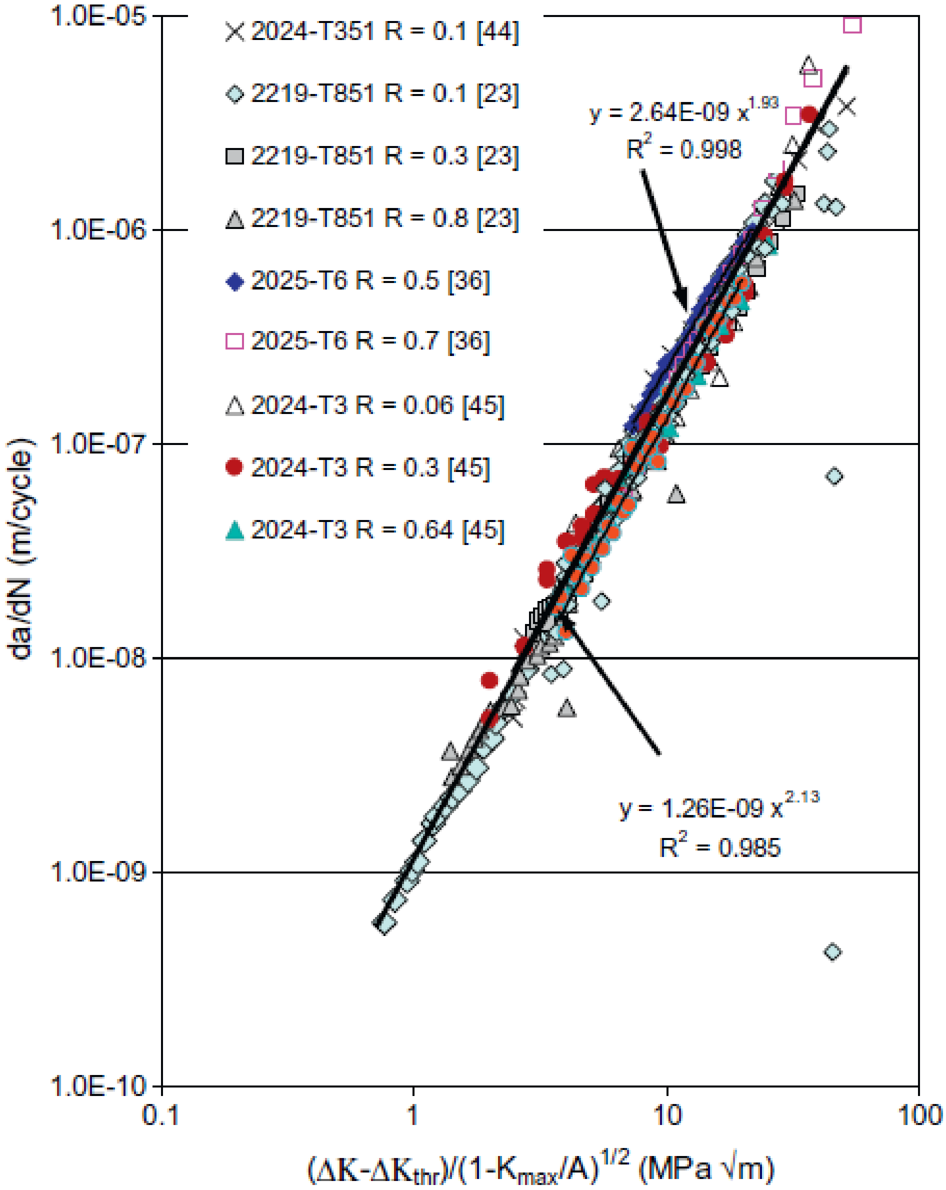

Figure 2.6 Comparison of crack growth rates for different aluminium alloys in 2000 series [54].

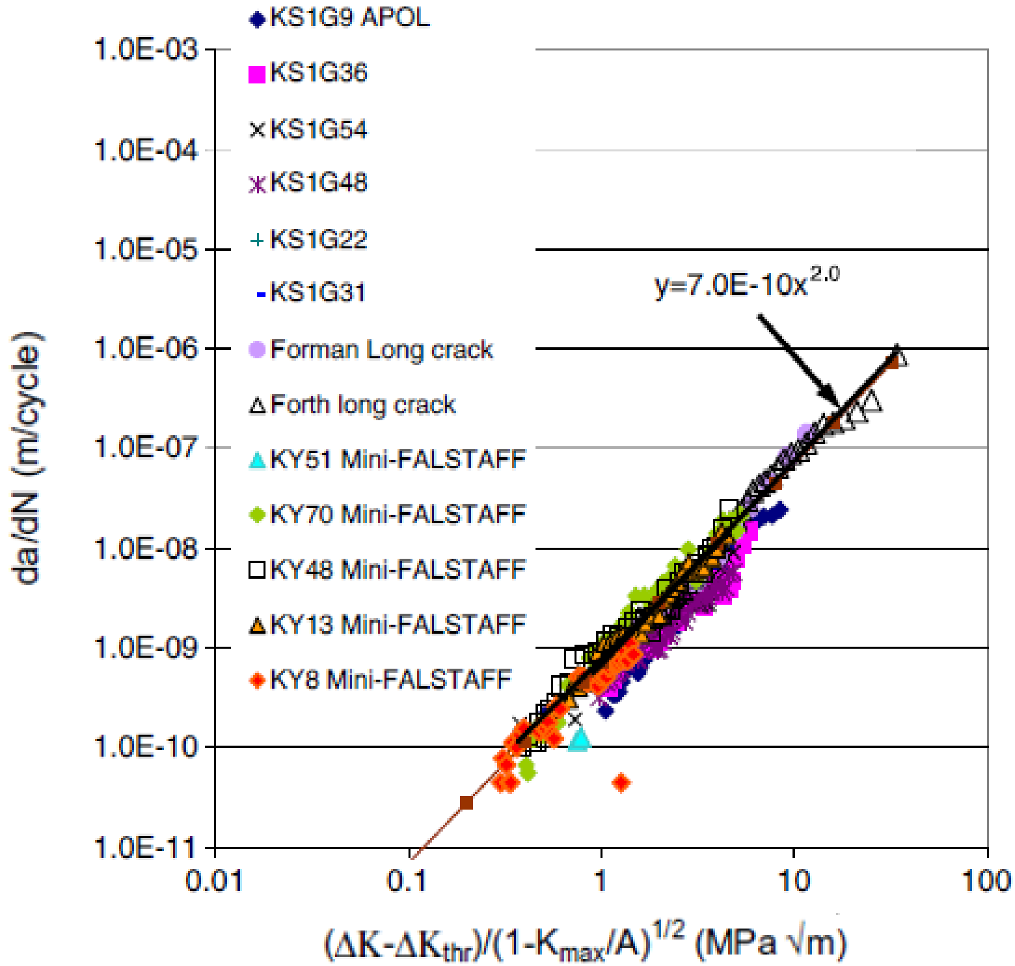

Figure 2.7 Comparison of NASA test under Mini-FALSTAFF and RAAF operational load spectrum [55].

2.3 Stress Methods for Predicting Fatigue Growth

Apart from fracture mechanics approach, stress approaches are also used to predict the fatigue crack growth. The work by Shanley [56] was possibly the first to characterise the crack growth with stress and noted that the crack growth is a relationship of exponential form, see Equation (2.16).

$$a = Ae^{f(\sigma)n} \tag{2.16}$$

where a is the crack depth, A is a constant, n is number of cycles of reversed loading and f (σ) a function of the nominal applied stress. Frost and Dugdale [57] propose a crack growth equation in 1958 which was similar to that of Shanley [56]. See Equation (2.17),

$$\frac{da}{dN} = \beta a \sigma^n \tag{2.17}$$

where a is the crack length, σ is the applied maximum stress and β is an apparent constant which is dependent on material and geometry. Based on Frost and Dugdale's research, n was equal to 3 for mild steels and aluminium alloys irrespective for the mean stress. Numerous researchers from Australian Defence Science and Technology Group (DSTG) [39, 58, 59, 60, 61, 62] have subsequently reported that length or depth of the crack growth versus flight hours/cycles/blocks curve can be approximated by a near-exponential crack growth curve. These findings conform to the Frost-Dugdale relationship, because Equation (2.17) can be rearranged as follows:

$$\frac{da}{a} = \beta \sigma^n dN \tag{2.18}$$

$$\ln(a) = \beta \sigma^n N + \ln(a_0) \tag{2.19}$$

$$a = a_0 e^{\beta \sigma^n N} \tag{2.20}$$

where N represents the fight hours/cycles/blocks. a_o is the equivalent pre-crack size which may be obtained by back-extrapolating FCG data for cracks in the same area or location using an exponential crack growth model. One example is shown in Figure 2.8. The sizes of cracks from surface discontinuities are growing exponentially against load blocks/flight hours. There are two specimens, i.e. KS1G3 and KS1G66, whose cracks were initiating at subsurface. Hence their starting points of fatigue data were delayed by around 26,000 and 10,000 flight hours respectively.

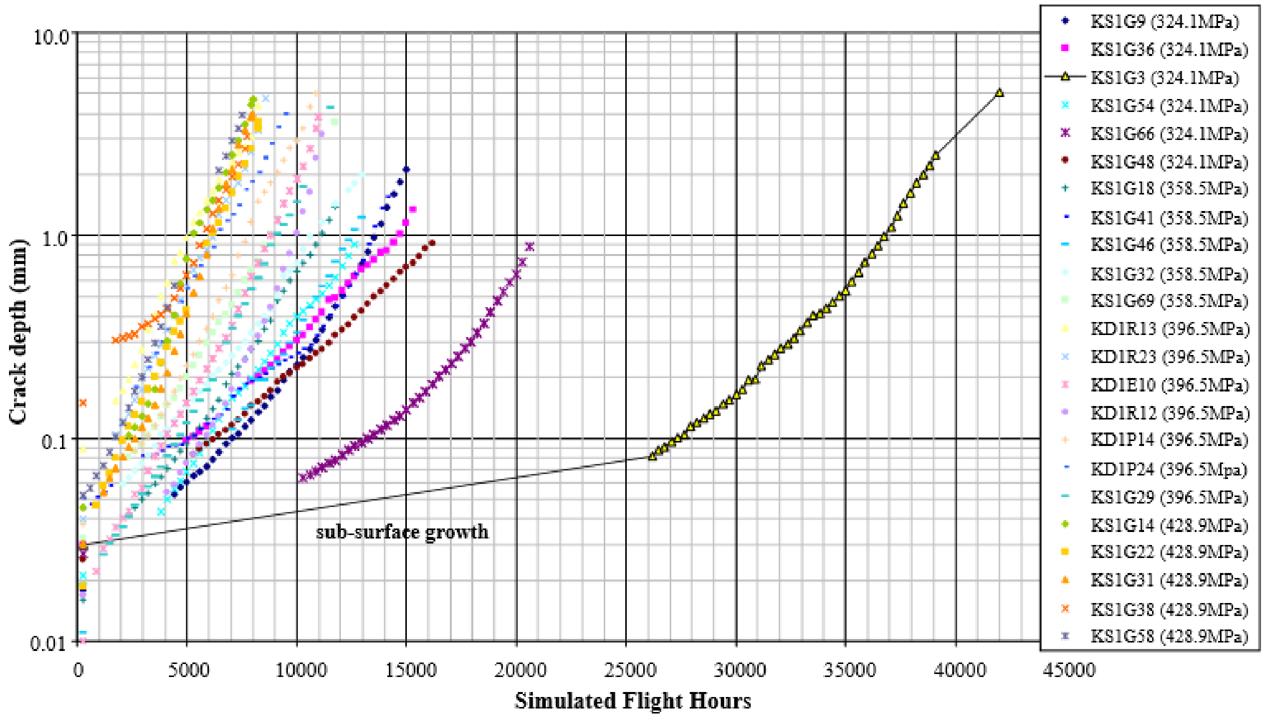

Figure 2.8 Fatigue data for AA7050-T7451 under combat aircraft flight-by-flight block loading. Each block represents about 300 airframe hours [39].

In 2016, Molent and Jones [63], extended the Frost-Dugdale relation [54] together with the concept of lead crack [39] and then proposed the Cubic rule. The lead crack concept has been developed based on observing experiment test results. Key characteristics for lead crack s are [39]:

- *Lead cracks start to grow shortly after testing begins or the aircraft is introduced into service and subjected to flight loads*
- *Lead cracks start growing from material production discontinuities*
- *Lead cracks grow approximately exponentially with time*
- *The small fraction of FCG life influenced by quasi-static fracture close to final failure is insignificant.*

The Cubic rule is a very handy tool for the preliminary estimation of the fatigue life for specimens due to stress change. If the reference fatigue test condition (β and σ) is known, the unkown test condition can be obtained by comparing the ratio of stress of two conditions, see Equation (2.21) [63].

$$(\beta\sigma^n)_{unkown} = \left(\frac{\sigma_{unknown}}{\sigma_{ref}}\right)^n (\beta\sigma^n)_{ref} \tag{2.21}$$

where the subscription of unknown and ref represents the rest conditions that are wanted and already known respectively. Researchers [57, 63, 64] discovered that for aluminium alloys the FCG rate is (approximately) linearly proportional to the cube of the stress. Consequently, Molent and Jones [63] proposed the Cubic rule where n=3 in Equation (2.21) and they used AA7050-T7451 data from [64] to illustrate the considerably accuracy of Cubic rule. Two tests conditions were performed, one was under 155 MPa and another one was 250 MPa. The lead crack growing under 155 MPa can be represented as Equation (2.22) which has the exponential constant of 0.123. The exponential constant for test under 250 MPa can be simply calculated with Equation (2.21) which obtains 0.516, see Equation (2.23).

$$a = 0.0247e^{0.123N} \tag{2.22}$$

$$(\beta\sigma^3)_{250} = \left(\frac{250}{155}\right)^3 0.123 = 0.516 \tag{2.23}$$

The results of the Cubic rule prediction are illustrated in Figure 2.9 and Figure 2.10. The preliminary calculation shows a considerably good agreement with AA7050-T7451 fatigue crack growth results.

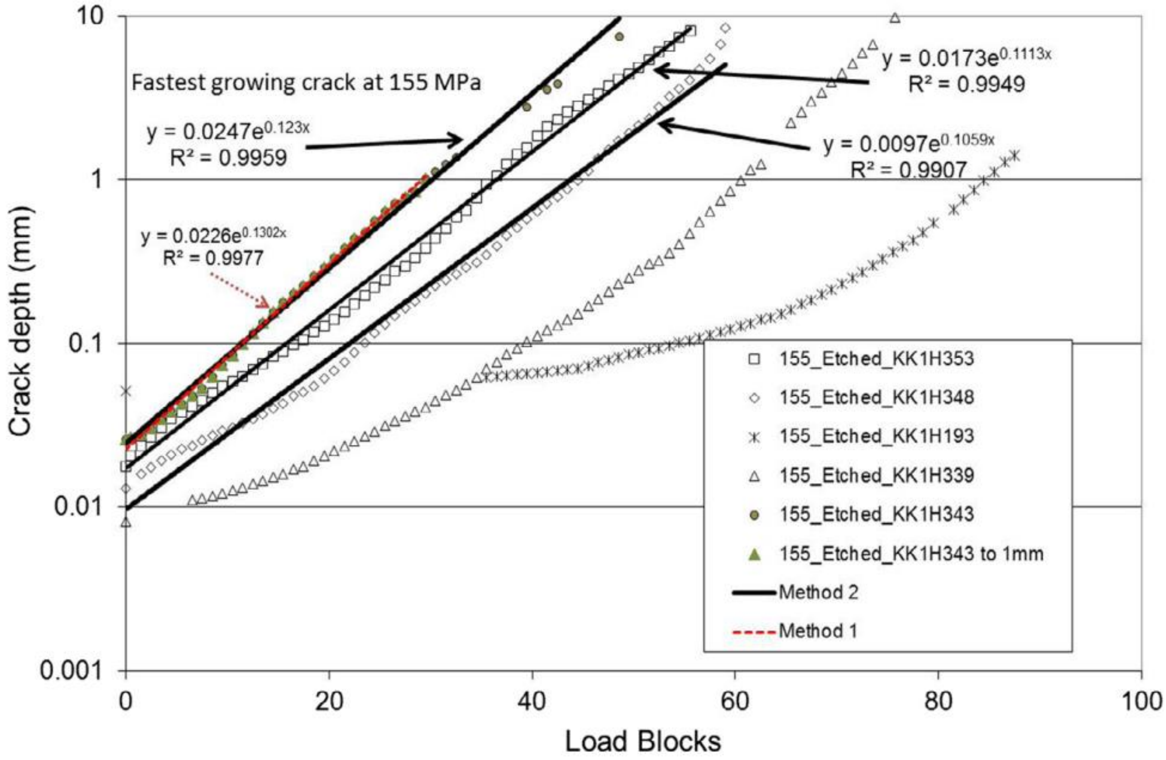

Figure 2.9 Crack growth histories associated with the 155 MPa etched tests [63].

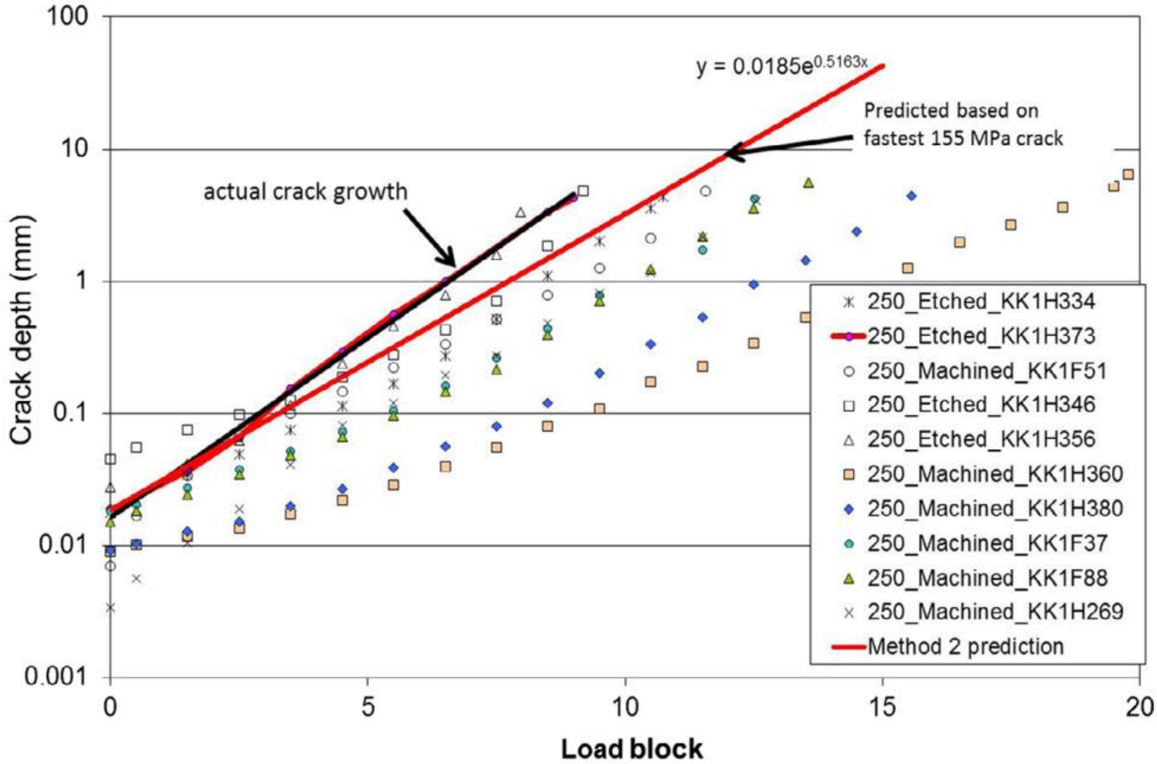

Figure 2.10 Crack growth histories associated with the 250 MPa etched tests [63].

2.4 Quantitative Fractography

Quantitative fractography (QF) is a method that can observe and measure the fracture surface. Crack length or depth and the number of load cycles or blocks can be obtained by measuring striation marks on fracture surface which produced as the result of crack propagation under cyclic fatigue loading [65]. A schematic diagram of the striations seen on a surface fatigue crack is shown in Figure 2.11. It illustrates how a typical crack grows from a_0 to a depth of a_N after N cycles/blocks. In this approach the crack depth is generally measured at the deepest point of the crack propagating direction [66]. Hence, the measurement of the crack depth may not always be a straight line.

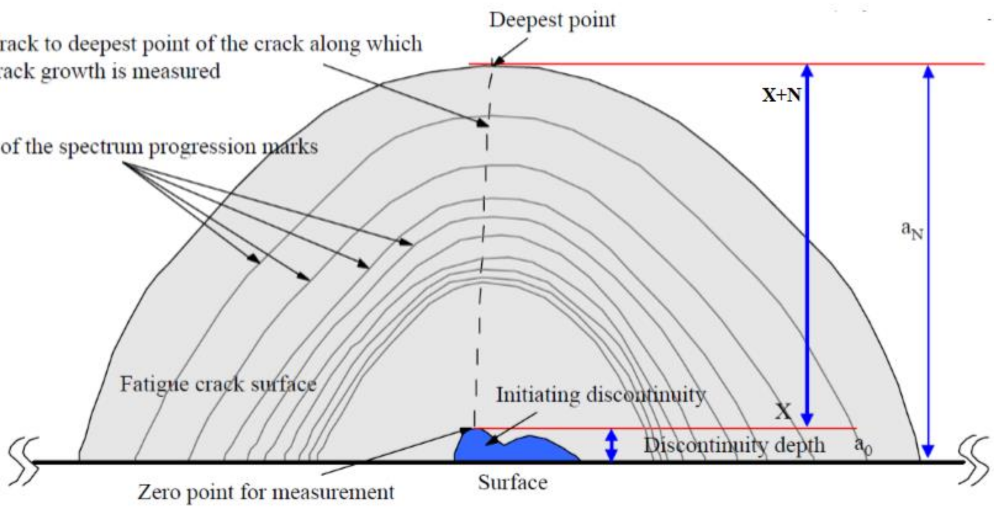

Figure 2.11 The schematic diagram of quantitative fractography [66].

As measuring the beach marks associated with crack propagation for a constant amplitude loading is quite difficult, the used of load blocks which can produce marker bands are preferred. Here the hope is that the used of load blocks can enhance the ability to measure the fatigue crack growth history. In order to distinguish different marker bands and improve detectability, several types of load blocks are using, e.g. changing R-ratio and maximum load stress. Figure 2.12 illustrates the marker bands associated with a simple marker load spectrum.

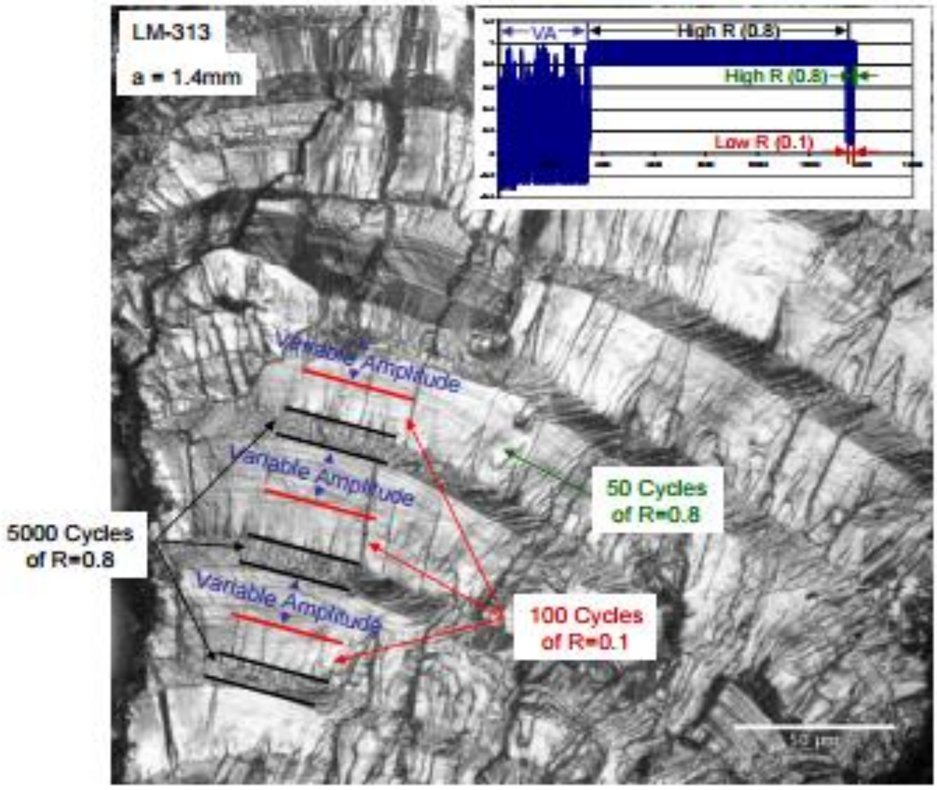

Figure 2.12 Marker bands associated with a simple marker load spectrum [67].

2.5 Fatigue in Composite and Adhesively Bonded Structures

The next question discussed is the stress singularity. Wang et al. [68] found that for cracks in a thin layer of adhesive between two relatively rigid composite or metallic substrates, the region that is dominated by the $r^{-1/2}$ singularity in the stress field is exceptionally small. From their finite element analysis results, Wang et al. [68] concluded that after a distance of less than one layer of adhesive thickness from the crack tip the stress field in the adhesive layer essentially becomes uniform. As a result, G is generally used instead of K when employing fracture mechanics to investigate the failure of anisotropic bodies, i.e. fibre reinforced composite and structural adhesives [69, 70]. Consequently, when a Paris power relation is used to describe the FCG rate for composites and structural adhesives, it is common to plot da/dN versus ΔG, see Equation (2.24).

$$\frac{da}{dN} = D(\Delta G)^m \tag{2.24}$$

where D and m are experiment constants for cohesive failures in adhesively bonded structures.

2.5.1 Mixed mode fatigue propagation parameters for delamination

A few of commonly used equations that have been developed to characterise Mode I and II cracking or delamination growth are shown in Table 2.1. The subscript I and II represent Mode I and Mode II respectively. In these equations the G_c refers to the critical value of G or the fracture toughness of the composite or adhesive.

Table 2.1 Several equations used to characterise Mode I, II and Mixed Mode growth.

Reference	Expression of Power relation	Equation
Brussat et al. [71, 72]	$\frac{da}{dN} = D\left[\left(1 + \frac{2G_{II}}{G_I + G_{II}}\right)\Delta G_I\right]^m$	2.25
Mall et al. [73, 74]	$\frac{da}{dN} = D[\Delta(G_I + G_{II})]^m$	2.26
Gustafson and Hojo [75]	$\frac{da}{dN} = D_I(\Delta G_I)^{m_I} + D_{II}(\Delta G_{II})^{m_{II}}$	2.27
Benzeggagh and Kenane [76, 77]	$\frac{da}{dN} = D\left[\Delta(G_I + (G_{II} - G_I)\left(\frac{G_{II}}{G_I + G_{II}}\right)^{\gamma})\right]^m$	2.28*
Cheuk et al. [78]	$\frac{da}{dN} = D\left[\Delta(G_I + \frac{G_{I,C}}{G_{II,C}} G_{II})\right]^m$	2.29
Quaresimin and Ricotta [79, 80]	$\frac{da}{dN} = D\left[\Delta(G_I + \frac{G_{II}}{G_I + G_{II}} G_{II})\right]^m$	2.30
Rans et al. [81]	$\frac{da}{dN} = D_I\left[(\Delta\sqrt{G_I})^2\right]^{m_I} + D_{II}\left[(\Delta\sqrt{G_{II}})^2\right]^{m_{II}}$	2.31

* γ in Equation (2.28) is an experimentally determined constant that depends on the mode mix.

There is presently no accepted, or universal, equation for describing Mixed Mode I and II fatigue crack growth in anisotropic materials. Sih et al. [69] were the first to develop a fracture mechanics solution for a crack in an anisotropic body and revealed that the crack the near tip stress field was governed by $\sqrt{G}$. As such the logical extension of the Paris equation for metals to express da/dN as a function of $\Delta\sqrt{G}$, i.e. $\sqrt{G_{max}}$ - $\sqrt{G_{min}}$ [81, 82], rather than ΔG.

2.5.2 Discussion of FCG parameters in composite structures

Until recently the SEER range, ΔG, was a generally accepted parameter for describing FCG in composite and adhesively bonded structures. However, in 2011 Rans et al. [81] declared that by using ΔG as the FCG parameter can cause two problems. The first is an inappropriate R ratio effect, see Figure 2.13. This Figure presents experiment data from Hojo et al. [83] and infers that for the same value of ΔG, the FCG rate is greater for low R ratio tests than for high R ratio tests. This means that a lower mean stress will give rise to faster delamination/disbond growth rates. However, for a fixed ΔG increasing the R ratio represents an increase in both the G_{max} and the mean value of ΔG. For example, a value of ΔG = 80 J/m^2 and R = 0.2 means G_{max} = 100 J/m^2 and G_{min} = 20 J/m^2. On another hand for ΔG = 80 J/m^2 and R = 0.5 we obtain G_{max}= 160 J/m^2 and G_{min} = 80 J/m^2. Logic suggests that a test with G_{max}= 160 J/m^2 and G_{min} = 80 J/m^2 should be more severe, rather than less severe, than a test performed with G_{max}= 100 J/m^2 and G_{min} = 20 J/m^2. This conclusion contradicts the curves shown in Figure 2.13.

The second problem that Rans et al. [81] mentioned is that ΔG does not account for the residual stress caused during the curing and cooling stage due to the mismatch of thermal expansion coefficients of different materials in fibre reinforced composites or adhesively bonded structures. To illustrate this effect, consider the test data presented by Lin and Kao [84]. In this test, they presented data associated with three as-cured specimens and three specimens that were post-stretched so as to eliminate the thermal residual stress in the specimen. It is clear from Figure 2.14 that for specimens without residual stress the da/dN against ΔG curves are almost aligned. In the contrast, for three as-cured specimens the da/dN rates are differing significantly. As a result, Rans et al. [81] suggested that the use of ΔG can result in misinterpreting the role of residual stresses.

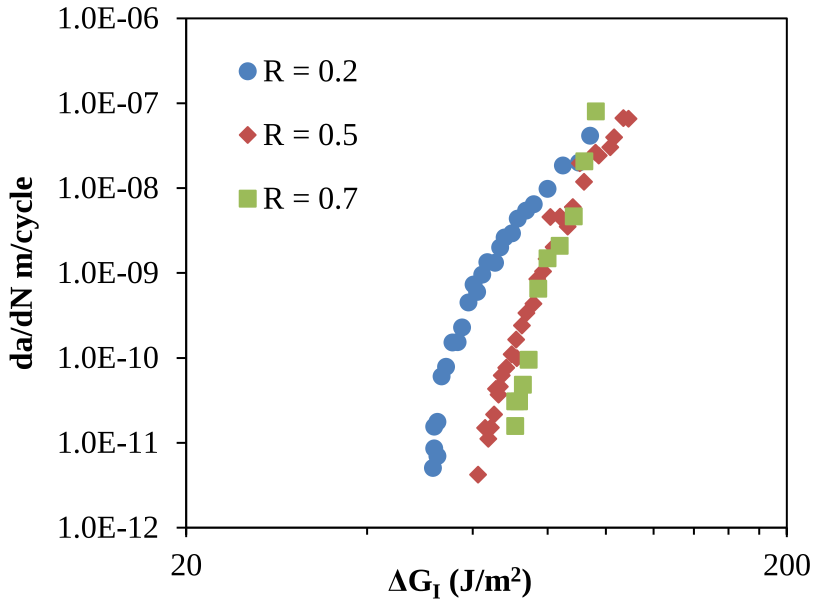

Figure 2.13 The FCG behaviour for P305 laminates in terms of ΔG [83].

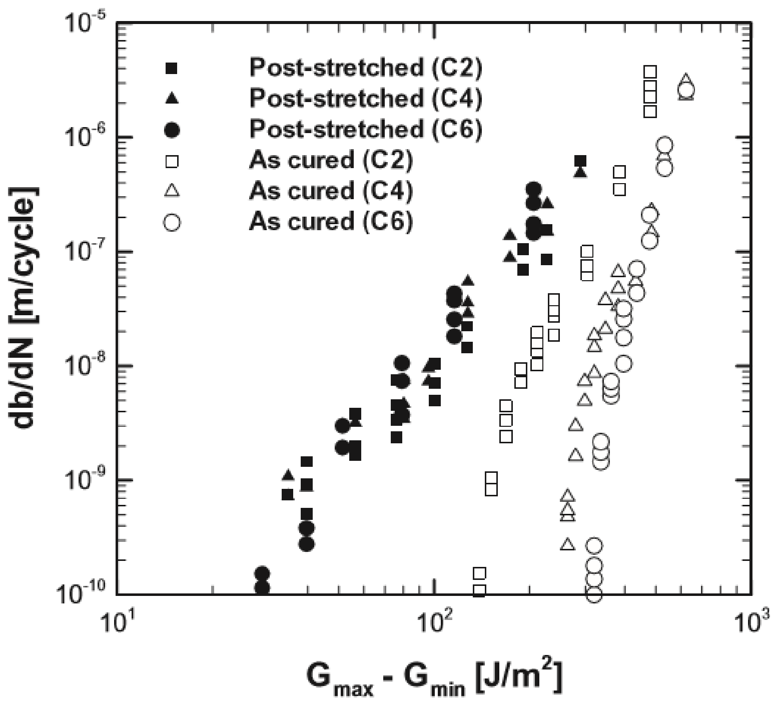

Figure 2.14 Comparison of residual stress on delamination growth when using ΔG [84].

To overcome these problems, Rans et al. [81] proposed expressing da/dN as a function of $\Delta\sqrt{G}$. Table 2.2 shows that both ΔK and $\Delta\sqrt{G}$ are linearly proportional to 1-R. In contrast ΔG is proportional to $1\text{-}R^2$. In addition, because $\sqrt{G}$ is linearly proportion to stress, $\sqrt{G}$ is able to be broken up into an effective SEER, $\sqrt{G_{eff}}$, and the SEER caused by residual strength, $\sqrt{G_{rs}}$, see Equation (2.32). Thus, the residual stress can be automatically eliminated when using $\Delta\sqrt{G}$ as the FCG parameter. With this in mind Rans et al. [81] replotted the data shown in Figure 2.13 and Figure 2.14 as a function of $\Delta\sqrt{G}$, see Figure 2.15 and Figure 2.16. When plotted in this form the anomalies associated with the R ratio effect and the residual stress effect were disappeared, see Figure 2.15 and 2.16.

Table 2.2 Comparison of different FCG parameters.

Parameter	Expression	Functional dependence on the R ratio
ΔK	K_{max} - K_{min}	(1-R) K_{max}
ΔG	G_{max} - G_{min}	$(1\text{-}R^2)$ G_{max}
$\Delta\sqrt{G}$	$\sqrt{G_{max}}$ - $\sqrt{G_{min}}$	(1-R) $\sqrt{G_{max}}$

$$\begin{aligned} \Delta\sqrt{\mathrm{G}} &= \sqrt{\mathrm{G}}_{max} - \sqrt{\mathrm{G}}_{min} \\ &= \left(\sqrt{\mathrm{G}}_{eff,max} + \sqrt{\mathrm{G}}_{rs}\right) - \left(\sqrt{\mathrm{G}}_{eff,min} + \sqrt{\mathrm{G}}_{rs}\right) \\ &= \sqrt{\mathrm{G}}_{eff,max} - \sqrt{\mathrm{G}}_{eff,min} \end{aligned} \tag{2.32}$$

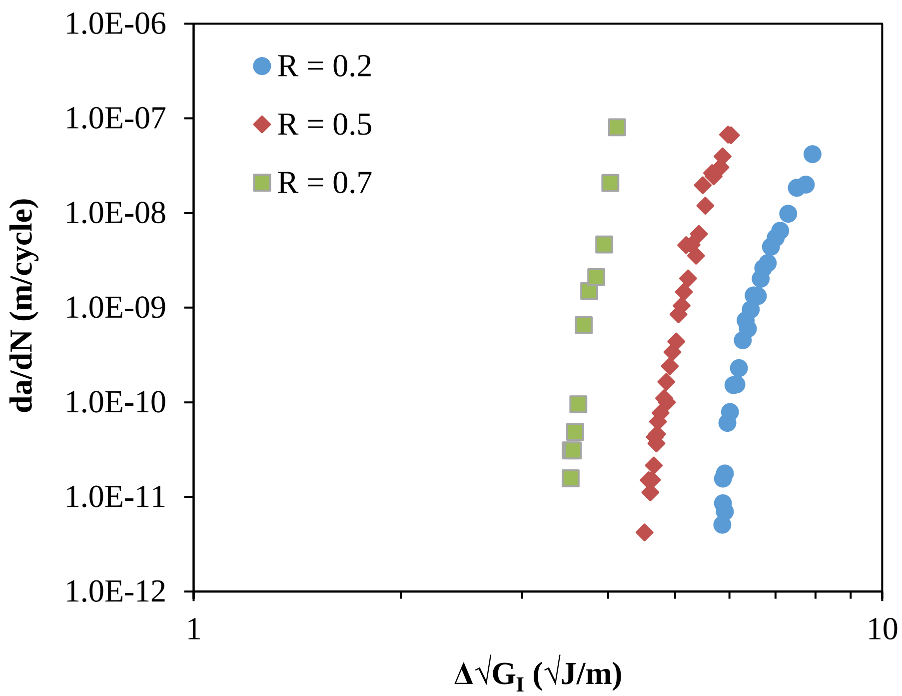

Figure 2.15 Relation between delamination rate and Δ√G for the P305 laminate [81].

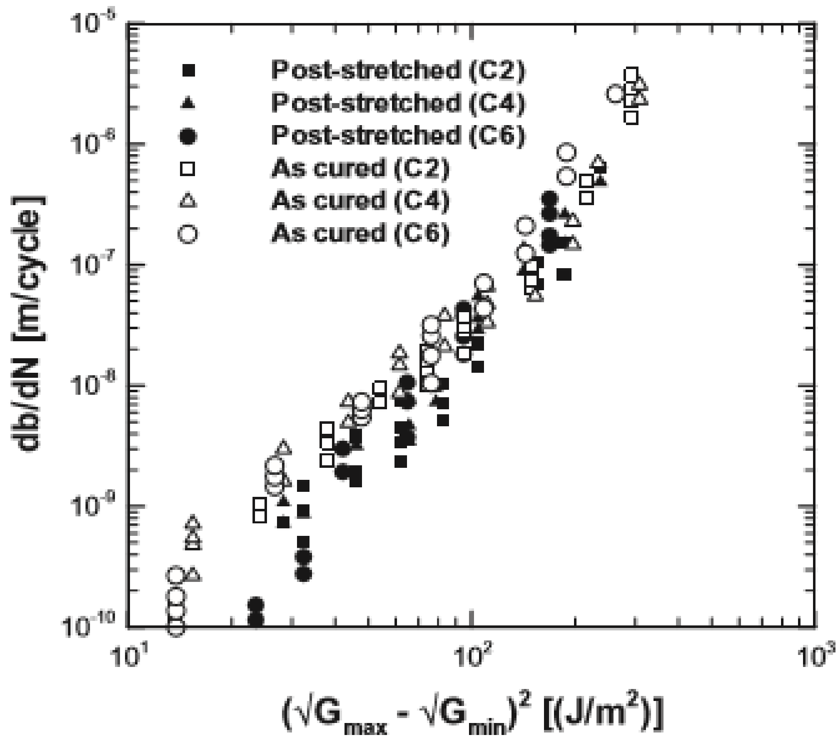

Figure 2.16 Comparison of the residual stress effect on delamination growth when using Δ√G [81].

2.5.3 Hartman-Schijve equation for composite structures

In Section 2.2.4, it was remarked that for metals the Hartman-Schijve equation [55], see Equation (2.15), is able to account for:

- both short and long cracks.
- R ratio effects.
- different materials.
- different load types, e.g. constant and variable amplitude load.

Jones et al. [70] extended the Hartman-Schijve equation based on the fact that as first shown by Sih et al. [69] the near tip stress field for a composite laminate is described by $\sqrt{G}$. As such Equation (2.15) was re-written in terms of $\sqrt{G}$, see Equation (2.33).

$$\frac{da}{dN} = D\left(\frac{\Delta\sqrt{G} - \Delta\sqrt{G_{thr}}}{\sqrt{1 - \sqrt{\frac{G_{max}}{A}}}}\right)^m \tag{2.33}$$

where $\Delta\sqrt{G_{thr}}$ is the apparent threshold term for $\Delta\sqrt{G}$ and A is the critical SERR. As previously $\Delta\sqrt{G_{thr}}$ and A are best interpreted as parameters chosen to fit the measured da/dN data [18]. Hojo et al. [85] and Jones et al. [86] revealed that the threshold was not a constant value in a G_{max} decreasing test. Furthermore, Simon et al. [87] suggested that if $\Delta\sqrt{G}$ is used as the crack driving force, the threshold value of tests with different R-ratio will converge, see Figure 2.17. However, given the large scatter seen in delamination and disbond tests [74, 85], it is unclear if this finding will hold in general.

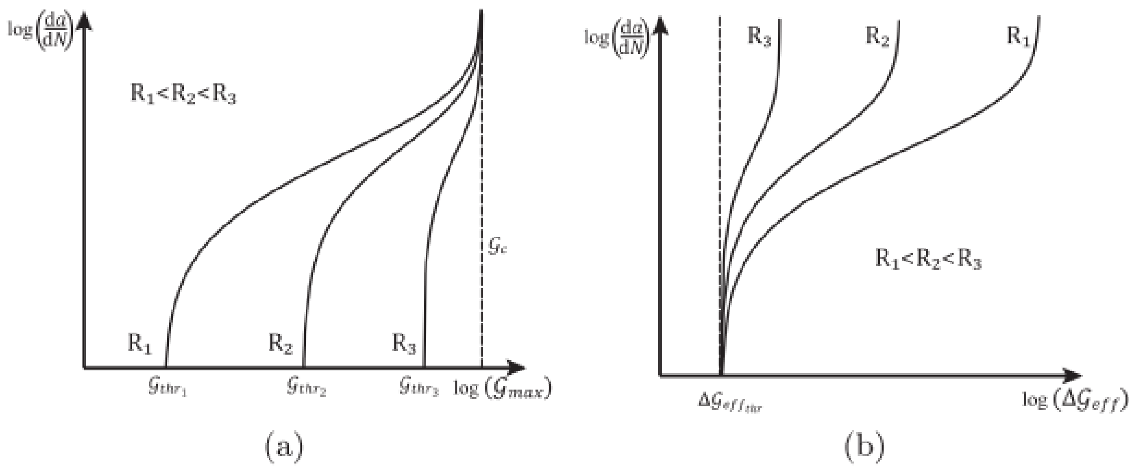

Figure 2.17 A schematic representation of R-ratio effects on the fatigue delamination growth rate curves as a function of (a) G_{max} and (b) ΔG_{eff} (=$(\Delta\sqrt{G})^2$) [87].

Jones and co-workers [70, 88] have presented several examples of how the Hartman-Schijve approach can be used to characterise delamination damage in composites. One example examined the data obtained by Brunner et al. [89] as part of the Technical Committee on Fracture of Polymers, Composites and Adhesives of the European Structural Integrity Society (ESIS). This was a Mode I double cantilever beam (DCB) test with specimens were made from unidirectional carbon–fibre epoxy (IM7/977-2) [89]. The original da/dN against G_{Imax} plot is shown in Figure 2.18. The threshold term, G_{Ith} is approximately 100 J/m^2 and da/dN is approximately proportional to $(G_{max})^{14.7}$. However, at this point it should be noted that Martin and Murri [90] stated that: *"the exponents of these power laws were too large for them to be adequately used as a life prediction tool. A small error in the estimated applied loads could lead to large errors in the delamination growth rates"*. Jones et al. [70] replotted da/dN data against $(\Delta\sqrt{G_I} - \Delta\sqrt{G_{Ithr}})/\sqrt{(1-\sqrt{(G_{Imax}/A)})}$, see in Figure 2.19. The exponential term has decreased to around 2.1. The parameters, i.e. $\Delta\sqrt{G_{Ithr}}$ and A, used in Figure 2.19 are listed in Table 2.3.

Table 2.3 Mode I delamination threshold and critical SEER range [70].

Specimen	A (J/m^2)	$\Delta\sqrt{G_{Ithr}}$ ($\sqrt{J}/m$)
DCB 1	134	8.18
DCB 2	170	9.27
DCB 3	220	9.04
DCB 4	180	8.08
DCB 5	190	9.31

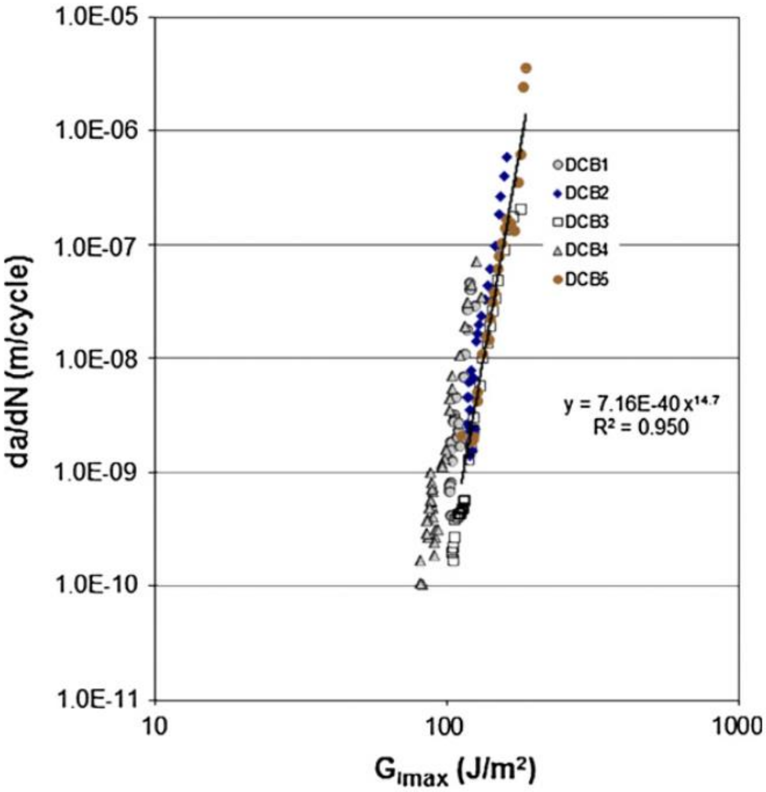

Figure 2.18 A power relation representation of the ESIS TC4 round robin data on IM7/977-2 [89].

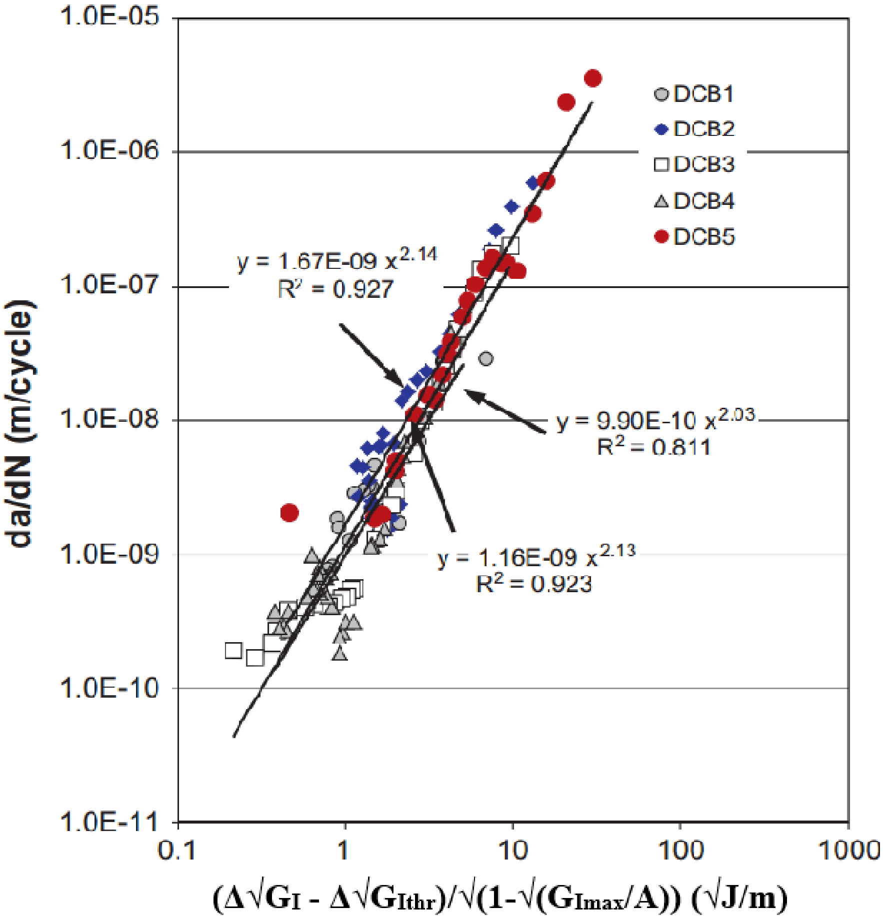

Figure 2.19 Hartman–Schijve representation of the ESIS TC4 round robin data [70].

A second example presented in [91] was the end notched flexure (ENF) Mode II delamination test done by Matsubara et al. [91] for a unidirectional T-glass fibre in a 180 °C cure Toray #3651 epoxy resin. This test was conducted under three different R-ratios, i.e. -0.5, 0.1 and 0.3. The Hartman–Schijve equation again yields lower exponential when plotted against da/dN. The parameters, i.e. $\Delta\sqrt{G_{IIthr}}$ and A, used in Figure 2.21 are listed in Table 2.4. These two examples illustrate that the Hartman–Schijve equation is capable of accounting for the different R ratios for both Mode I and Mode II FCG.

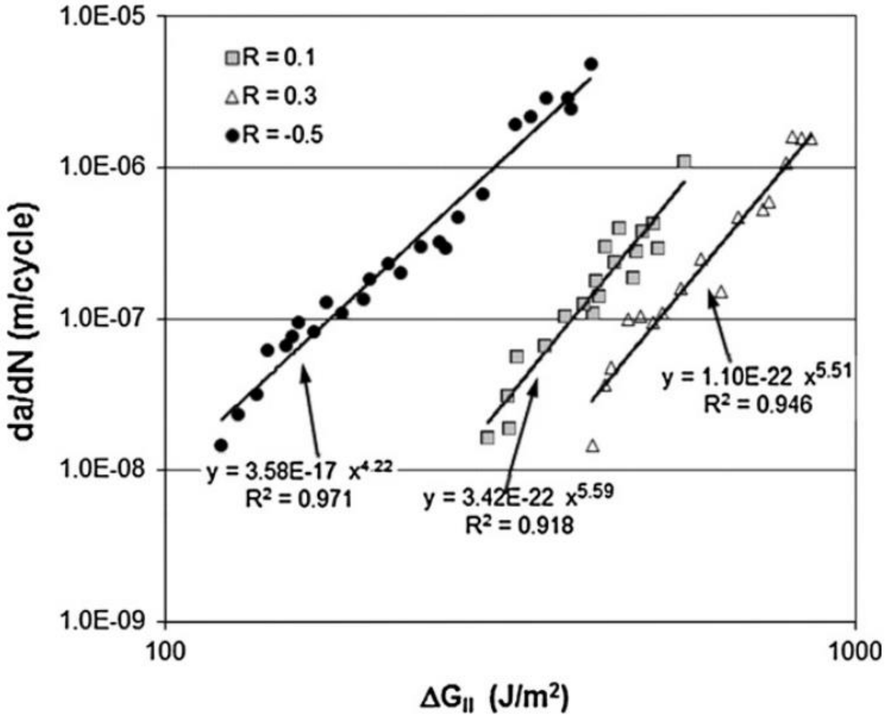

Figure 2.20 Paris representation of Mode II delamination growth in T-glass #3651 [91].

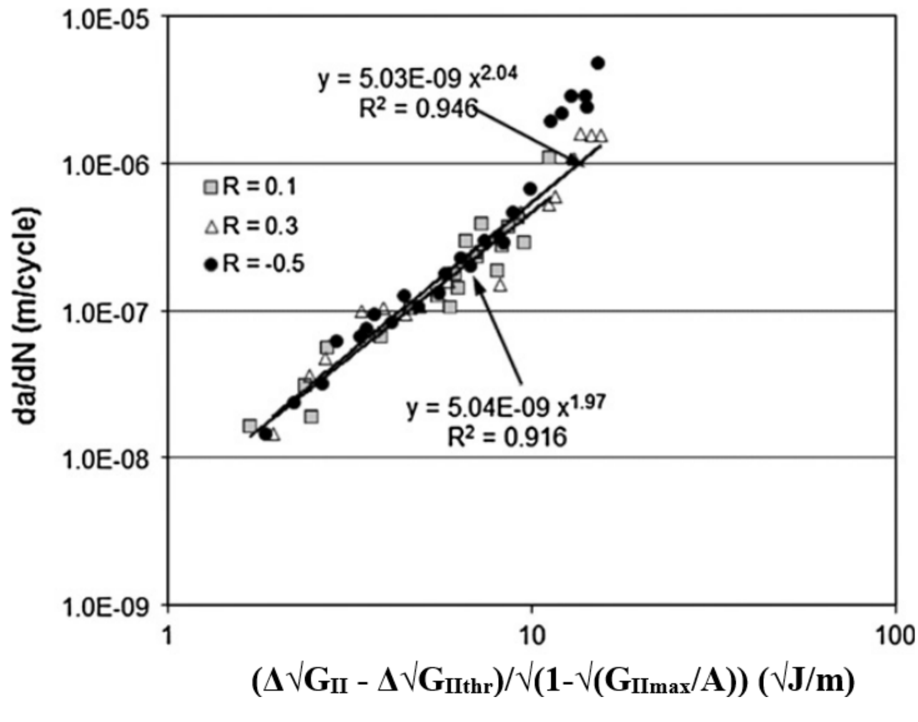

Figure 2.21 Hartman-Schijve representation of Mode II delamination growth in T-glass #3651 [70].

Table 2.4 Mode II delamination threshold and critical SEER range for in T-glass #3651 [70].

R ratio	A (J/m^2)	$\Delta\sqrt{G_{IIthr}}$ ($\sqrt{J/m}$)
-0.5	1750	9.40
0.1	1750	13.6
0.3	1750	14.2

The Hartman-Schijve equation approach for characterizing delamination growth in composites was also discussed in [87, 92] and questioned by researchers that its threshold term, $\Delta\sqrt{G_{thr}}$, was arbitrary and determined by plot fitting. In this context, it would appear that the large scatter in the threshold value is inherent in delamination growth.

2.5.4 Analysis in adhesively bonded joint and composite repairs

Roach and Rackow summarised a method of bonded composite doubler repairs for Boeing DC-10 and MD-11 in 2007 [93]. Such a cost-effective method can safely extend the lives of their aircraft. The primary goal of this study was to demonstrate the routine use of this repair technology. In this study, they validated the lower bound fatigue thresholds for bonded joints/repairs with Equations (2.34) and (2.35) which were proposed by Jones et al. [94]. This methodology is based on the findings of Heart-Smith [95] that the adhesive is uniquely characterised by the strain energy density in the adhesive and that fatigue damage is a function of the inelastic work. As such Jones et al. [94] proposed that fatigue damage will not arise if both load and strain are below the fatigue threshold load, P_f, and the fatigue threshold strain, ε_f.

$$P_f = 2(tW_f ET)^{\frac{1}{2}} \tag{2.34}$$

$$\varepsilon_f = 2(tW_f E/T)^{\frac{1}{2}} \tag{2.35}$$

where t and T are thickness of the adhesive and the adherend (skin) respectively, E is the Young's modulus of the skin and W_f is the threshold value of the strain energy density of the adhesive which can be determined experimentally [96]. W_f is determined from a point where the adhesive film experiences a transition between purely linear elastic behaviour with essentially no energy dissipation. This approach is more suitable than the designed method suggested in the Primary Adhesively Bonded Structure Technology (PABST) program [97] where was suggested that the adhesive should not to be loaded beyond 50% of yield strength. This limit was arbitrarily chosen. The approach suggested in [94] is more general. That said for the structural film FM 73 discussed in [94, 97], these two approaches gave very similar values.

In 2015, Pascoe et al. [98] proposed a new crack driving force, the release of strain energy, to characterize the fatigue disbond growth in bonded structures, see Equation (2.36).

$$\frac{da}{dN} = D\left(-\frac{dU_{cyc}}{dN}\right)^m \tag{2.36}$$

where D and m are material constants and Ucyc is the cyclic strain energy. They declared that in this model, during the loading half of the fatigue cycle the test machine will supply energy to the specimen, which is stored in the form of strain energy. This energy will be returned during unloading and the amount of energy that is released is not necessarily equal to the amount of energy supplied, as dissipation of energy may occur due to processes, e.g. crack growth and plastic deformation. See the schematic plot in Figure 2.23 which defines the monotonic strain energy, cyclic strain energy and total strain energy.

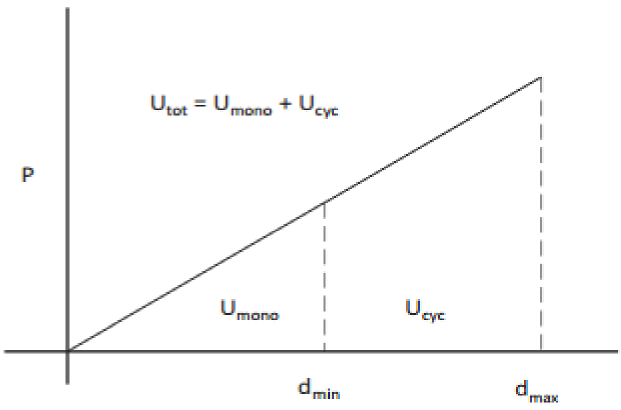

Figure 2.22 Schematic force (P) – displacement (d) diagram, showing the definition of U_{mono}, U_{cyc} and U_{tot}.

2.6 Summary

This chapter has presented a brief history of fatigue and how scientists and engineers have focused their efforts on understanding and predicting fatigue crack growth. In this context it should be noted that, despite its simplicity, the Paris crack growth equation with fracture mechanics approach is extensively used to predict FCG in metallic materials and that this formulation appears to be well suited to cracks that initiate and grow from small naturally occurring material discontinuities. Elber's crack closure effect concept is widely used for long cracks that have grown from large artificially induced notches. However, it is generally recognised that for a given ΔK the FCG rate of short cracks is faster than that seen by long cracks and that the fatigue threshold associated small naturally occurring cracks in metal is very small. Consequently, as explained in ASTM E647-13a the use of long crack data to predict the short crack propagation rate can lead to significantly non-conservative estimates.

Based on the Hartman and Schijve's research, Jones and co-workers have proposed an empirical formula, named the Hartman-Schijve equation, which can account the crack growth for both short and long cracks. This approach also appears to be able to account for R ratio effect and different load types.

As previously noted the first mathematical representation of crack growth in metal suggested crack growth was exponential. Frost and Dugdale subsequently suggested that the FCG rate had a power relation to the remote stress. Based on their research, the exponential constant in such power relation was found to be approximately 3 for both mild steels and aluminium alloys irrespective of the mean stress. This finding was subsequently validated by researchers with the USAF and this exponential growth law is built into the USAF approach to Structural Assessment Manual. Researchers from Australian DSTG adopted this concept and proposed a so-called Cubic rule. The Cubic rule combines with quantitative fractography which is a method that can observe and measure the fracture surface can provide a good first approximation to estimate the crack growth and life expectation when the remote stress amplitude is changed.

The crack growth in anisotropic materials, i.e. composites and adhesively bonded structures, is also discussed in this Chapter. In practical situations, anisotropic bodies are more likely to experience both tension and in-plane shear. Consequently, Mixed Mode I and II problems attracted attentions from researchers and many different parameters are used to tackle the mixed mode problems. Rans and his co-workers proposed $\Delta\sqrt{G}$ as the crack driving force, because it has the ability to resolve the of R ratio anomaly and account the residual stress effect. Jones and co-workers have extended the Hartman-Schijve equation to composite structure by using $\sqrt{G}$ as the crack driving force. Consequently, the next chapter will discuss the applicability of the Hartman-Schijve equation to adhesively bonded structures.

Chapter 3

The Hartman–Schijve Equation For Adhesively Bonded Structures

3.1 Introduction

Adhesively bonded structures and bonded repairs are widely used in the aerospace industry. However, as explained in MIL-STD-1530 [13], which delineates the certification requirements for damage tolerance assessment and analysis of military aircrafts [99], it is imperative to understand their cyclic-fatigue behaviour. Further, it is important to have a sound, and validated, means for accounting for the effects of test conditions, such as R ratio, test temperature and the inherent variability, and hence scatter, seen in the fatigue performance of structural adhesives. In this context, it should be noted that Pascoe et al. [100] has provided an excellent review of the methods available for predicting fatigue crack growth in both adhesively bonded components and polymeric-matrix fibre composites. Hence it should be noted that the measurement and predictive methods developed so far, for example, Pascoe et al. [100], Azari et al. [101], Ripling et al [102] Jethwa and Kinloch [103] and Curley et al. [104] have been largely based upon the principles of linear-elastic fracture mechanics (LEFM).

Current fracture mechanics approaches to crack growth in adhesive joints (and also in the polymeric matrix in fibre-composite materials) are predominated by variants of the Paris crack-growth equation, where the rate of crack growth per cycle, da/dN, is assumed to be linearly related to $(\Delta G)^m$. Here, ΔG is the range of the applied strain energy release rate in the fatigue cycle, i.e. G_{max} - G_{min}, and m is a material constant. However, several problems are found to arise with this approach.

- Whether ΔG is a valid crack driving force (CDF) which can be used to represent fatigue crack growth in adhesively bonded structures;
- How to account for the load ratio effect in Mode I, Mode II and Mixed-Mode I and II fatigue tests;
- How to account for typical scatter that is observed in the experimental fatigue tests is a challenge;
- The value of the exponent, m, in this relationship tends to be relatively large for structural adhesives (and fibre-composite materials);
- How to account for the effects of the particular test conditions, such as the test temperature which can have significant influence on the mechanical properties of structural adhesives;
- Fatigue crack growth may be initiated from relatively small naturally occurring material discontinuities and be more rapid than is predicted from experimental data obtained from relatively 'long-crack' tests.

This Chapter discusses the ability of the Hartman–Schijve equation to model fatigue crack growth in structural adhesives and so hopefully offers a solution to several of the shortcomings outlined above. The first step in investigating whether this approach can be used for predicting disbond growth in adhesives is to establish whether it can represent crack growth reported in experimental test data taken from the existing literature in structural adhesive joints, where the crack is propagating through the adhesive layer.

3.2 The Validation of Crack Driving Force in Structural Adhesives

3.2.1 Stress intensity factor and load ratio in metal

The ‘similitude hypothesis’, also referred to as the ‘similarity principle’, plays a central role in aircraft design, certification and sustainment. For metals the starting point for the basic ‘similitude hypothesis’ can be expressed [47] as:

“*Two different cracks growing in two specimens of the identical material with the same thickness and the same crack driving force, and with the same value of K_{max}, will grow at the same crack-growth rate per cycle, da/dN.*”

For metals, the CDF is generally taken to be the range of the stress intensity factor, ΔK (= K_{max} – K_{min}), where K_{max} and K_{min} are the maximum and minimum values of K in a fatigue cycle respectively. At this stage, it should be noted that, for a constant ΔK, the mean stress increases as the load ratio increases. As such, for a constant ΔK the value of da/dN should be faster for higher load ratio cyclic-fatigue tests.

The effect of the load ratio, R (= σ_{min} / σ_{max}), where σ_{max} and σ_{min} are the maximum and minimum values of σ in a fatigue cycle respectively, is shown in Figure 3.1 from [54], which presents the da/dN versus ΔK curves for a AA7050-T7451 tested at load ratios of R = 0.1 and 0.7. A feature of this plot is that for a given CDF, i.e. a given value of ΔK, an increase in the R-ratio increases the mean stress and thereby increases the crack growth rate, da/dN. Another way of saying this is that as the R ratio increases then the da/dN versus ΔK curves move to the left. Thus, the basic ‘similitude hypothesis’ stated above needs the following corollary:

“For two different cracks growing in two specimens of the identical materials with the same thickness and the same crack driving force, then the crack in the specimen subjected to a higher R ratio will grow at a faster da/dN value.”

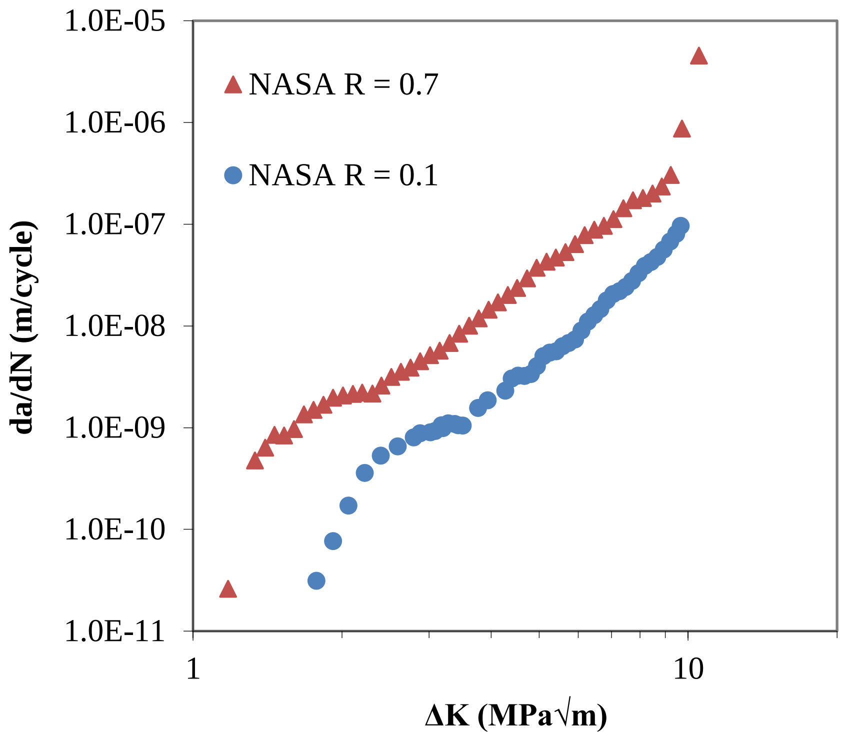

Figure 3.1 Fatigue crack growth in AA7050-T7451, tested at R = 0.1 and 0.7 [54].

3.2.2 Load ratio effect in composite and adhesively bonded structures

Consider Figure 3.2 which presents two tests, ‘Test 1’ and ‘Test 2’, with the same value of ΔG. Assume that ‘Test 1’ is subjected sinusoidal loading of P_{1max} and P_{1min} and that ‘Test 2’ is subjected sinusoidal loading of P_{2max} and P_{2min}, where P_{1max} is greater than P_{2max}. The tests are such that for a given crack length, a, the values of the ΔG are the same in both ‘Test 1’ and ‘Test 2’.

The value of ΔG is proportional to P_{max}^2 - P_{min}^2. As such, at a crack length, a, the value of ΔG issame in both tests.

$$P_{1max}^2 - P_{1min}^2 = P_{2max}^2 - P_{2min}^2 \tag{3.1}$$

As a result:

$$\frac{(1-R_1^2)}{(1-R_2^2)} = \frac{P_{2max}^2}{P_{1max}^2} \tag{3.2}$$

Since P_{2max} is less than P_{1max} then:

$$(1-R_1^2) < (1-R_2^2) \tag{3.3}$$

So that:

$$R_1 > R_2 \tag{3.4}$$

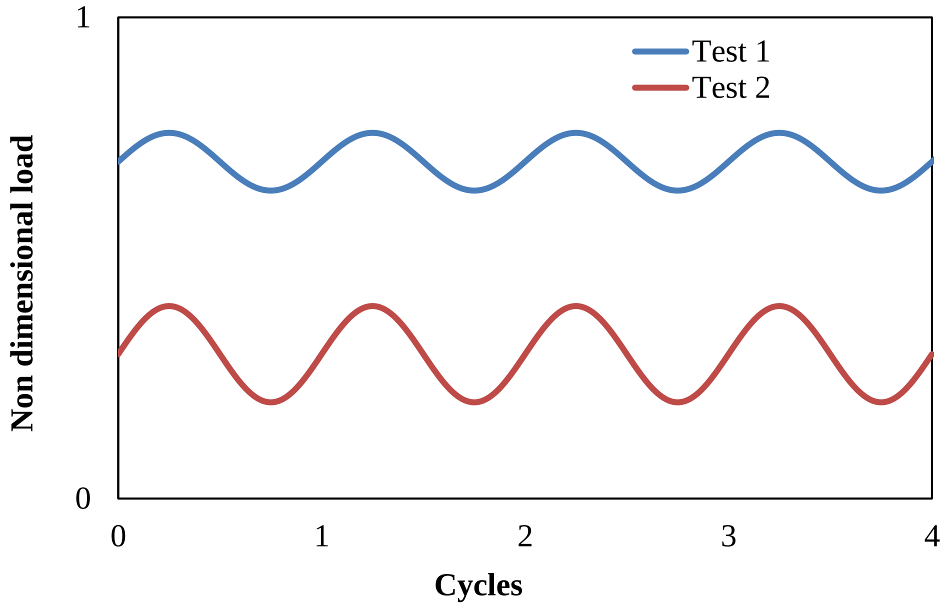

Figure 3.2 Schematic diagram of two tests.

Thus, if the two tests have the same ΔG and 'Test 1' has a maximum load greater than 'Test 2', then the R ratio associated with 'Test 1' will be greater than the R ratio associated with 'Test 2'. Since, 'Test 1' gives rise to a higher R ratio and so it should exhibit a more rapid rate of fatigue crack growth for a given value of the ΔG. However, as can be seen from Figure 3.3 - 3.6, when express da/dN in ΔG the opposite occurs, viz tests with the higher mean stress (higher R ratios) appear to show slower crack growth.

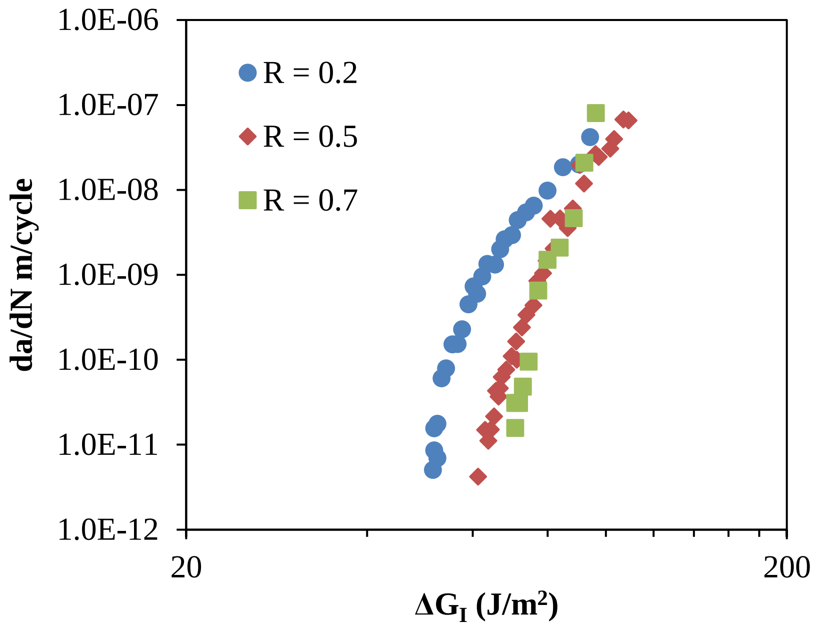

Figure 3.3 Plot of da/dN versus ΔG given in for delamination growth in P305 laminate [83].

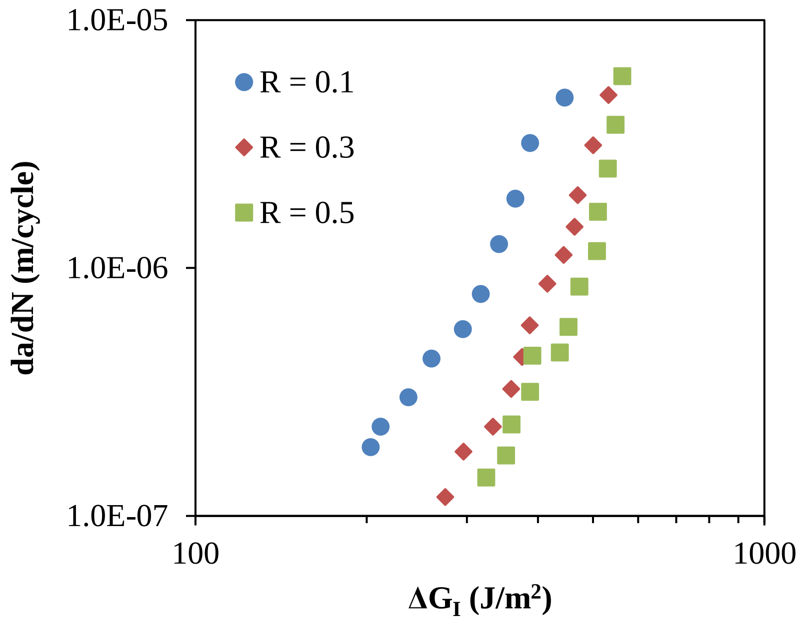

Figure 3.4 Plot of da/dN versus ΔG given in for disbond growth in DCB tests [74].

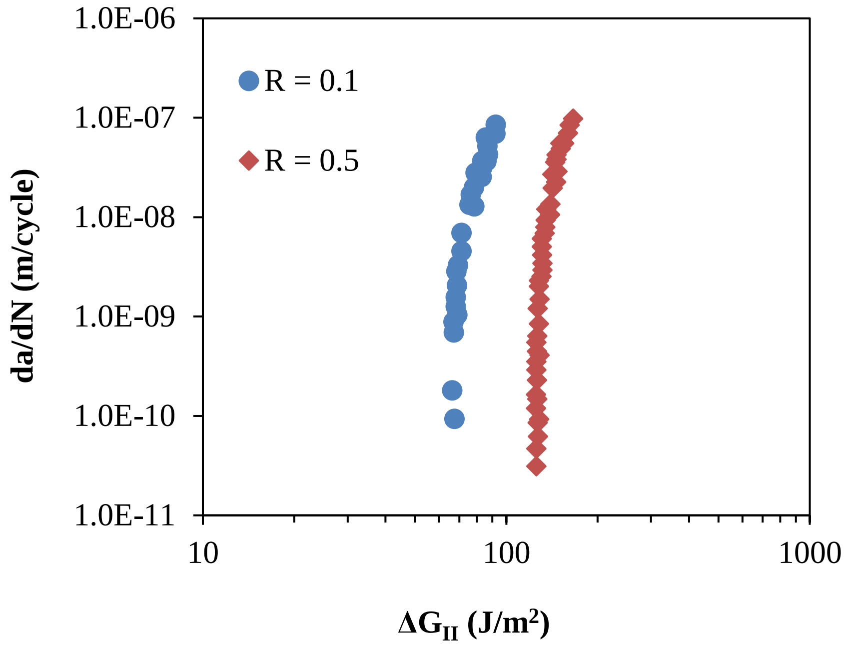

Figure 3.5 Plot of da/dN versus ΔG given in for disbond growth in end notched flexure (ENF) [85].

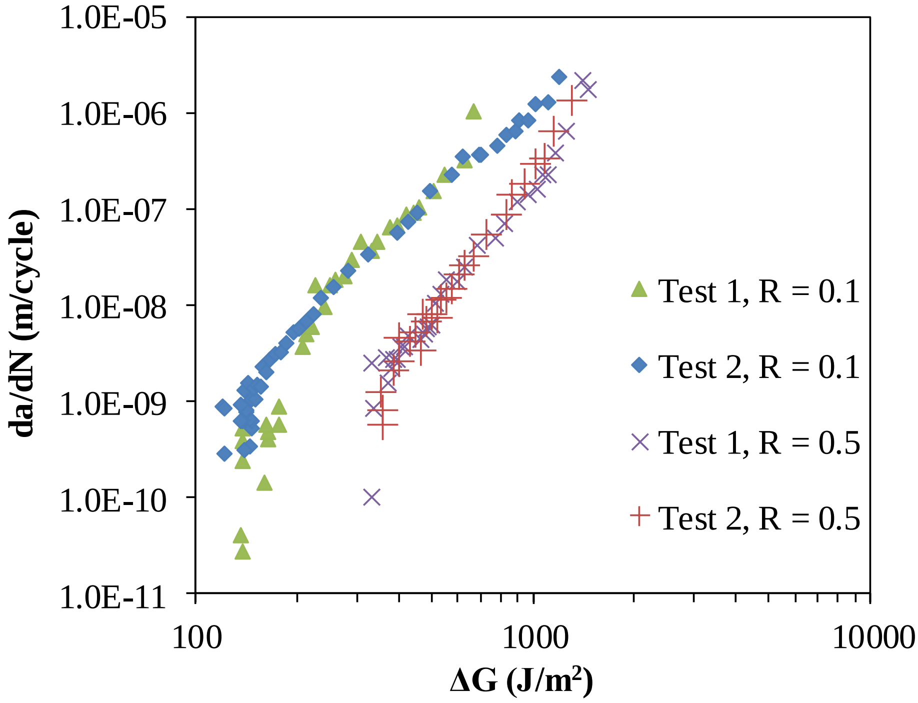

Figure 3.6 Plot of da/dN versus ΔG data given in for disbond growth in asymmetric double-cantilever beam (ADCB) specimens [101].

3.2.3 Resolving the similitude hypothesis anomaly

Rans et al. [81] and Khan et al. [105] have suggested that this R ratio anomaly vanishes if da/dN is plotted against $\Delta\sqrt{G}$ ($=\sqrt{G_{max}} - \sqrt{G_{min}}$). Whereas [81, 105] only presented a few examples, this observation is now confirmed in Figure 3.7 - Figure 3.10 where Figure 3.3 - Figure 3.6 have been replotted against $\Delta\sqrt{G}$. In these examples, it may indeed be seen that for two different cracks growing in two specimens of the identical materials with the same thickness and the same $\Delta\sqrt{G}$, then the crack in the specimen subjected to a higher R ratio grows faster. Thus, the anomaly seen when plotting da/dN against ΔG is resolved when da/dN is expressed as a function of $\Delta\sqrt{G}$.

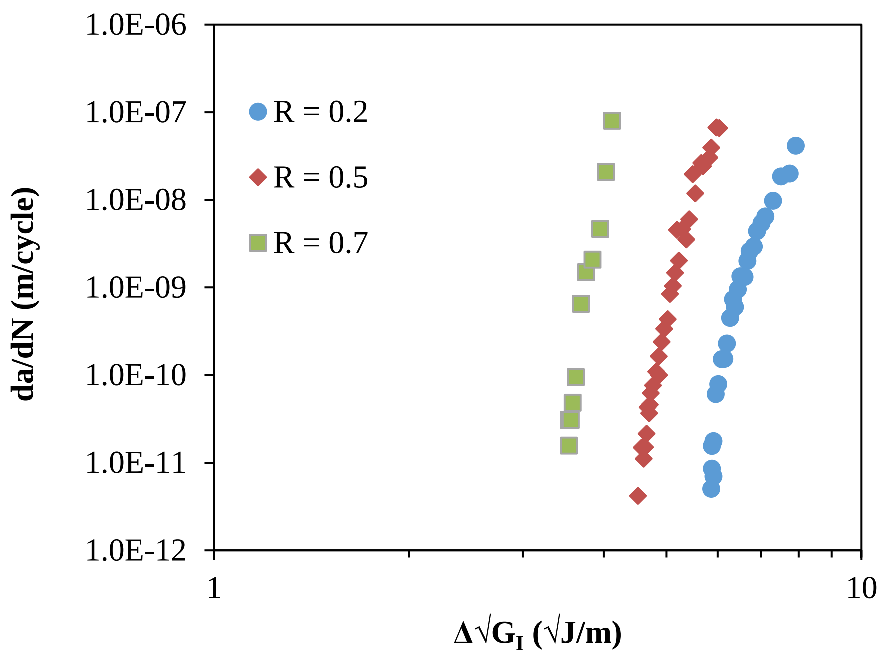

Figure 3.7 Plot of da/dN versus $\Delta\sqrt{G}$ given in for delamination growth in P305 laminate. Data is from [83].

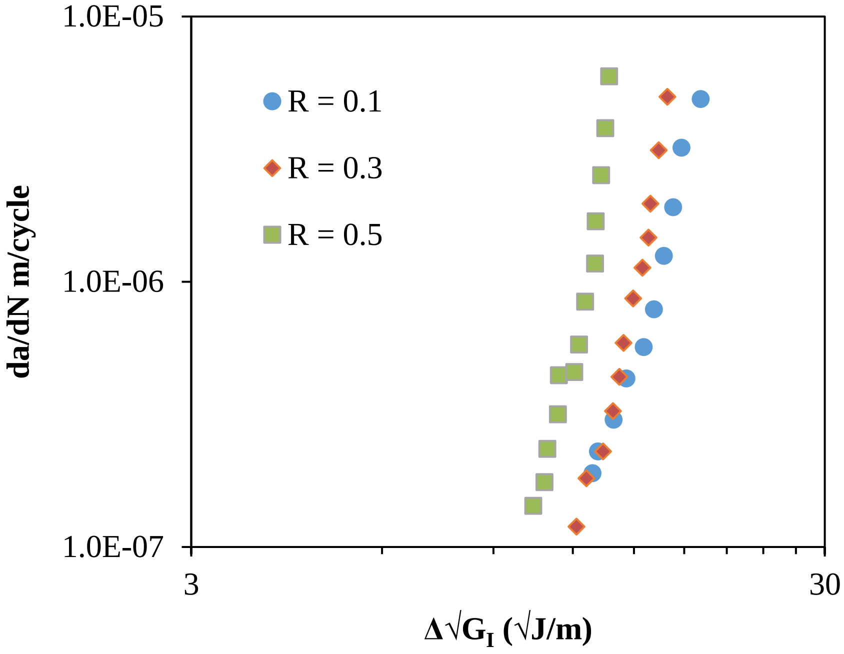

Figure 3.8 Plot of da/dN versus Δ√G given in for disbond growth in adhesively bonded DCB. Data is from [74].

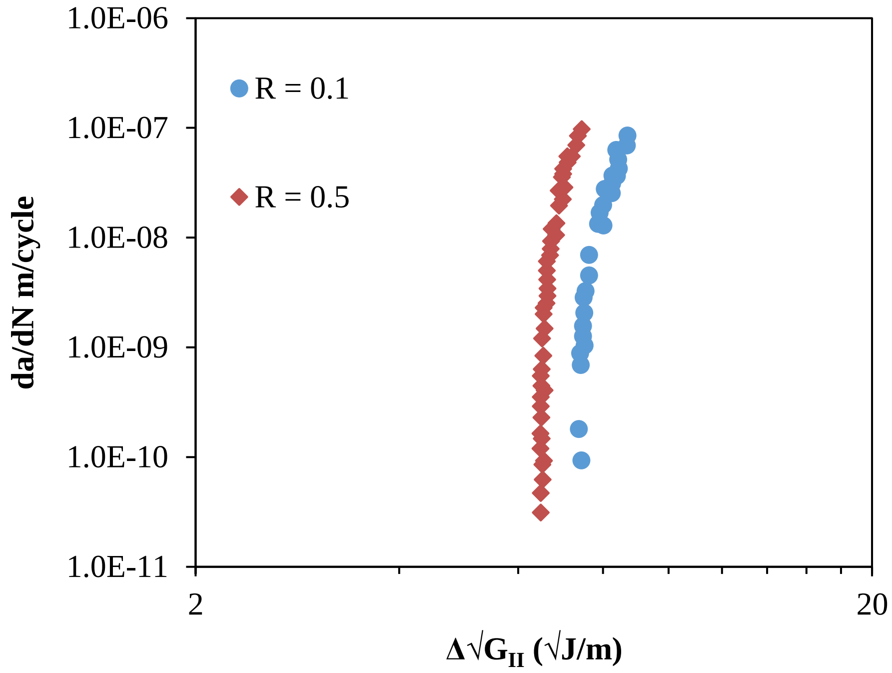

Figure 3.9 Plot of da/dN versus Δ√G for disbond growth in in adhesively bonded ENF. Data is from [85].

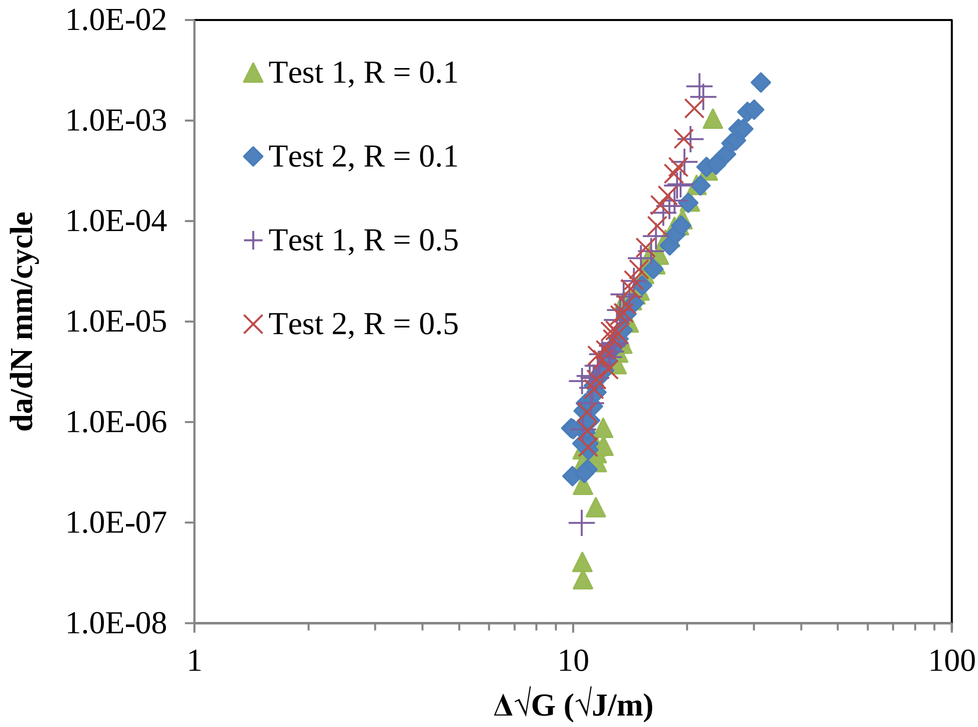

Figure 3.10 Plot of da/dN versus Δ√G for disbond growth in adhesively bonded ADCB specimens. Data is from [101].

3.3 Hartman–Schijve Equation for Adhesively Bonded Structures

Previously shown that it is best to plot da/dN against Δ√G rather than against ΔG, the rest of this Chapter attempts to take a first step to study whether cyclic fatigue crack growth in structural adhesive joints can be represented by a form of the Hartman-Schijve crack growth equation. Particular attention is given to:

- Whether the Hartman-Schijve equation can collapse test data with different load ratio onto a “master” curve for Mode I, Mode II and Mixed-Mode I and II fatigue tests;
- If the variability seen in the fatigue crack growth in adhesive joints can indeed be represented using the Hartman-Schijve equation via allowing for variations in the associated threshold term $\sqrt{G_{thr}}$;

- Whether the experimental fatigue crack growth data may be represented by the Hartman-Schijve equation with a relatively low value for the exponential term;
- Whether the Hartman-Schijve approach will allow the reconciliation of the effects of the test conditions, such as test temperature and initial crack size.

3.3.1 Development of Hartman–Schijve equation

A review of fatigue crack growth and damage tolerance [55] has revealed that in metals the effects of changing the R ratio and the growth of both long cracks and short cracks, can be captured using a form of the Hartman-Schijve approach. This approach aims to evaluate the potential of Hartman-Schijve equation to represent disbond growth in adhesively bonded structures.

At first sight, the most obvious and corresponding parameter against which to plot the rate of fatigue crack growth, da/dN, is the range of applied strain energy release rate, ΔG. However, as shown by Sih et al. [69], the near tip stress filed around the crack tip in anisotropic bodies can be characterized by √G. Δ√G should be employed as the CDF term in the extension of Hartman-Schijve approach to describe the cyclic fatigue behaviour of adhesive joints and polymeric fibre composites [106]. Thus, the form of the Hartman-Schijve equation now becomes:

$$\frac{da}{dN} = D\left(\frac{\Delta\sqrt{G} - \Delta\sqrt{G_{thr}}}{\sqrt{1-\sqrt{\frac{G_{max}}{A}}}}\right)^{m} \tag{2.33}$$

where D and m are material constants for adhesive film, $\Delta\sqrt{G_{thr}}$ is the apparent threshold range of SERR and A is the apparent cyclic fracture energy. The value of $\Delta\sqrt{G_{thr}}$ is experimentally measured for those adhesives where a clearly defined threshold value exists, below which little fatigue crack growth occurs. If this is not the case, then the concepts described in the ASTM standard [35], which are widely used by the metals community, may be employed. This standard defines a threshold value that the value of $\Delta\sqrt{G}$ at a value of da/dN of 10^{-10} m/cycle. The value of $\Delta\sqrt{G_{thr}}$ is given by rearrangement of Equation (2.33):

$$\Delta\sqrt{G_{thr}} = \Delta\sqrt{G_{th}} - \sqrt{1 - \sqrt{\frac{G_{max}}{A}}}\left[\frac{10^{-10}}{D}\right]^{1/m} \tag{3.5}$$

where $\Delta\sqrt{G_{th}}$ is the value of $\Delta\sqrt{G}$ at a da/dN of 10^{-10} m/cycle. As discussed in Jones [55] the value of A is best interpreted as a parameter chosen so as to fit the experimentally measured data. To do this, A is taken to be the quasi-static value of the fracture energy, G_c, or any reasonable first estimate.

The detailed aims of this chapter are to explore the validity of the Hartman–Schijve equation, as embodied in Equation (2.33), when applied to cyclic fatigue crack growth in structural adhesive joints. There is a special emphasis on exploring in detail, for a given adhesive, several important aspects of the Hartman–Schijve approach, namely whether:

- A 'master' linear representation for the fatigue data may be obtained when the experimentally measured data, even with different R ratio, are conveniently plotted according to the Hartman–Schijve representation;
- The Hartman–Schijve equation may readily account for the degree of variability, and hence the scatter caused by manufacturing process, test temperature and initial crack length;
- The slope, n, of this 'master' linear relationship has a relatively low value, ideally of the order of approximately two to three. Consequently, this raises the possibility that the Hartman–Schijve equation is suitable for enabling engineers to allow for some

(limited) fatigue crack growth to be permitted when designing with structural adhesives, as opposed to imposing the rigidly implemented ‘no crack growth’ or ‘slow crack growth’ criterion.

3.3.2 A ‘master’ line in fatigue crack growth

The Hartman–Schijve equation for composite and adhesively bonded structures is able to collapse disbond and delamination data onto a single curve and account the variability in the crack growth data, as is shown in [17, 70]. The ability to represent the variability seen in delamination growth is a major advance, since delamination growth in composites generally exhibits a high degree of scatter [17, 90]. Further, the ability to represent the scatter associated with delaminations and disbonds that grow from naturally occurring material discontinuities in operational aircraft is essential both for certifying new designs and also for fleet management purposes.

The ability of Hartman–Schijve equation to collapse the delamination and disbond data, shown in Figure 3.7 - Figure 3.10, onto a single linear curve with a value of n of approximately two, is shown in Figure 3.11 - Figure 3.14. The da/dN values which are less than 1E-10 are ignored as suggested by ASTM E647-13a [35]. The values of D, m, $\Delta\sqrt{G_{thr}}$ and A used in Figure 3.11 - Figure 3.14 are given in Table 3.1. Figure 3.11 - Figure 3.14 demonste the ability of Hartman-Schijve equation to collapse all data, with different load ratios, onto a ‘master’ line by keeping D, m and A constant and slightly changing the threshold term $\Delta\sqrt{G_{thr}}$. In addition, values of A in this instance were kept unchanged from respective literatures.

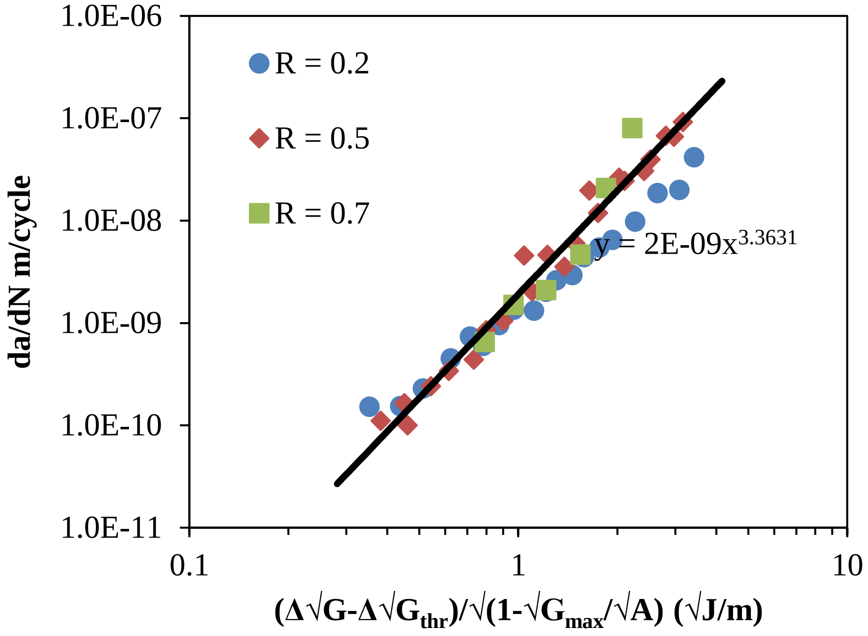

Figure 3.11 Hartman-Schijve representation of delamination growth in DCB tests using an unidirectional CFRP laminate. Data is from [83].

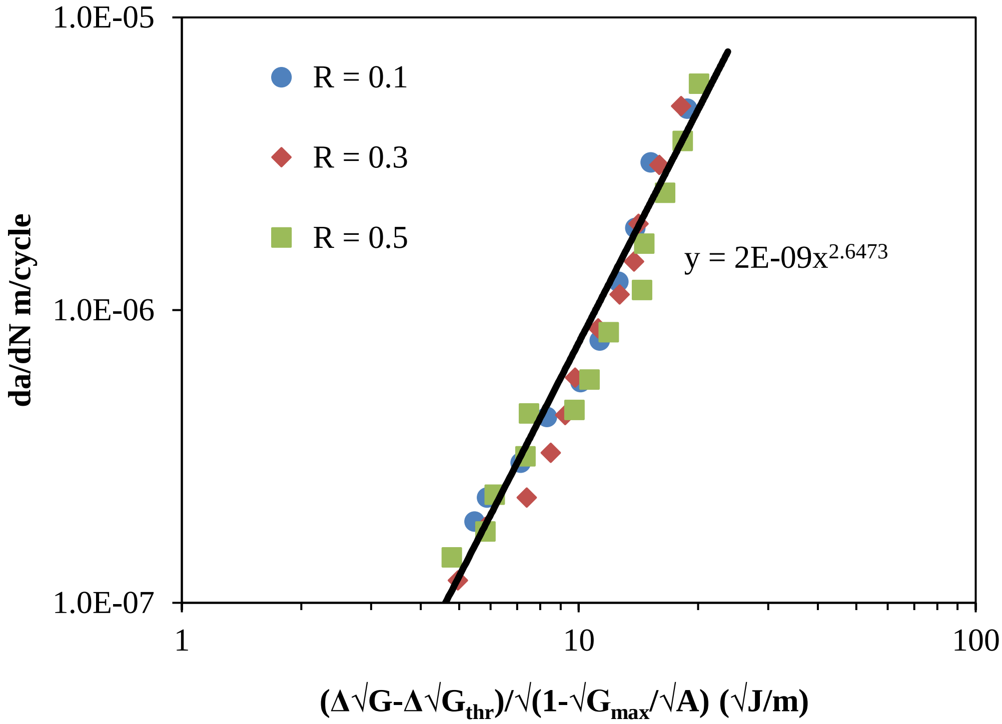

Figure 3.12 Hartman-Schijve representation of disbond growth in adhesively bonded DCB. Data is from [74].

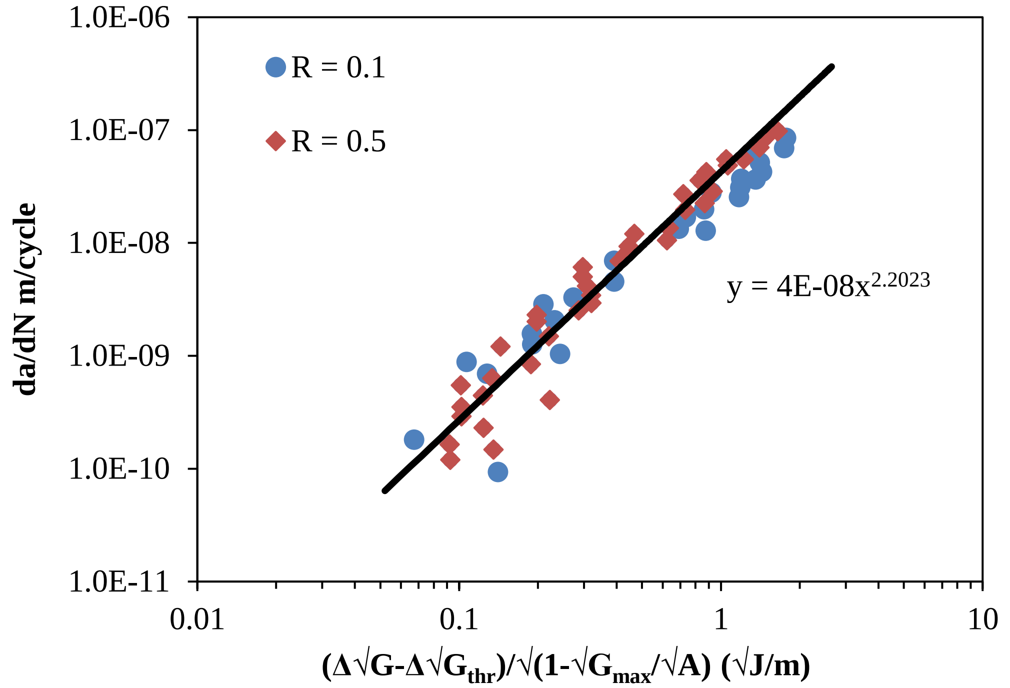

Figure 3.13 Hartman-Schijve representation of disbond growth in adhesively bonded ENF. Data is from [85].

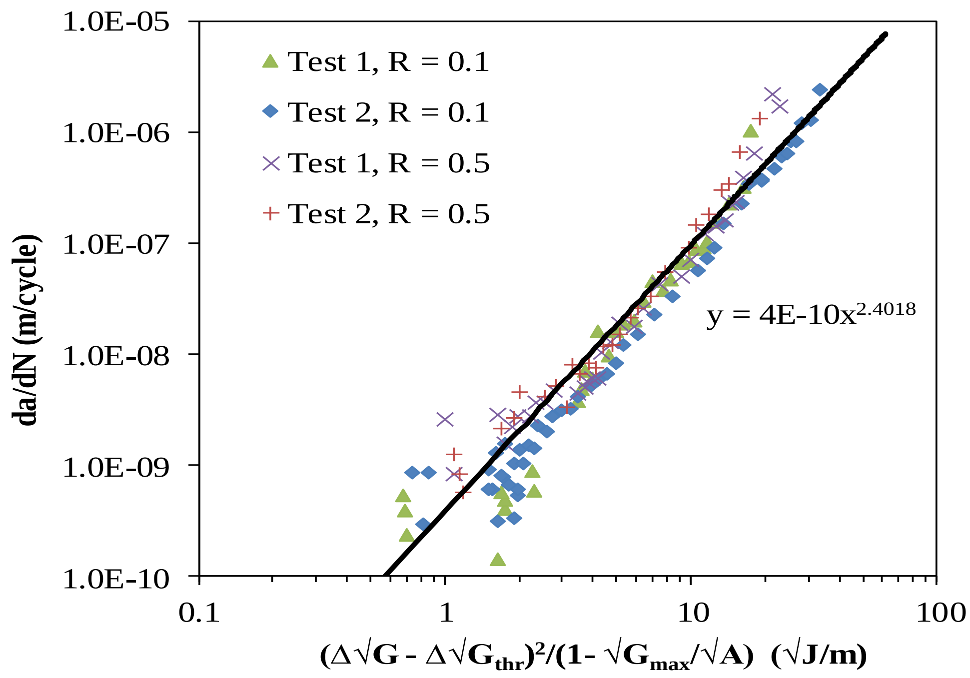

Figure 3.14 Hartman-Schijve representation of disbond growth in ADCB. Data is from [101].

Table 3.1 The values of D, m, $\Delta\sqrt{G_{thr}}$ and A used in Figures 3.11-14

Figure	D	m	$\Delta\sqrt{G_{thr}}$ ($\sqrt{J/m}$)	A (J/m^2)
Figure 3.11	2E-9	3.36	3.3 – 5.8	250 [83]
Figure 3.12	2E-9	2.65	7.7 – 8.9	900 [73]
Figure 3.13	4E-8	2.20	6.4 – 7.3	610 [85]
Figure 3.14	4E-10	2.40	9.2 – 10	3860 [107]

The values of A in Table 3.1 are the fracture toughness of the tested materials. Table 3.1 indicates the range of $\Delta\sqrt{G_{thr}}$ associated with various R ratio tests.

3.3.3 Scatter in the fatigue crack growth data

One of the phenomena seen in the growth of small naturally occurring cracks in metallic airframes under representative operational loading is the relatively large scatter observed in the crack depth versus flight time relationships. However, as explained by Jones [55], one of the advantages of the Hartman–Schijve approach is that this scatter can be captured by allowing for the variability in the fatigue threshold term. It has also been shown that, when the initial crack length was held constant, the variability in the resultant crack length versus cycles/hours could be captured by allowing the fatigue threshold term to vary [55].

Azari et al. [108] conducted a study of the fatigue behaviour of structural adhesive joints when subjected to Mixed-Mode I and II loading. Specimens were from different adhesive batches. Those adhesives had the same nominal formulation, but manufactured in different facilities at different time. Such experimental results have been reported for a toughened-epoxy structural adhesive tested at room temperature and an R = 0.1. In this work, asymmetric DCB tests were undertaken. The results of these replicated tests demonstrated some degree of variability in the measured data, especially in threshold region, see Figure 3.15. The scatters diminish as replotted the data with Hartman-Schijve equation, see Figure 3.16. The detail of Figure 3.16 is shown in Table 3.2. Again, with only slightly change of threshold term, the variation of fatigue crack growth collapses onto a ‘master’ line.

Table 3.2 The values D, m, $\Delta\sqrt{G_{thr}}$ and A used in Figure 3.16.

Patch	D	m	$\Delta\sqrt{G_{thr}}$ ($\sqrt{J/m}$)	A (J/m^2)
1	5E-10	2.25	11.8	3860
2			9.7	
3			8.7	

It should be noted that the variabilities in the values of D, m and $\Delta\sqrt{G_{thr}}$ is consistent with the ADCB test which used the same material [101] that shown in Table 3.1.

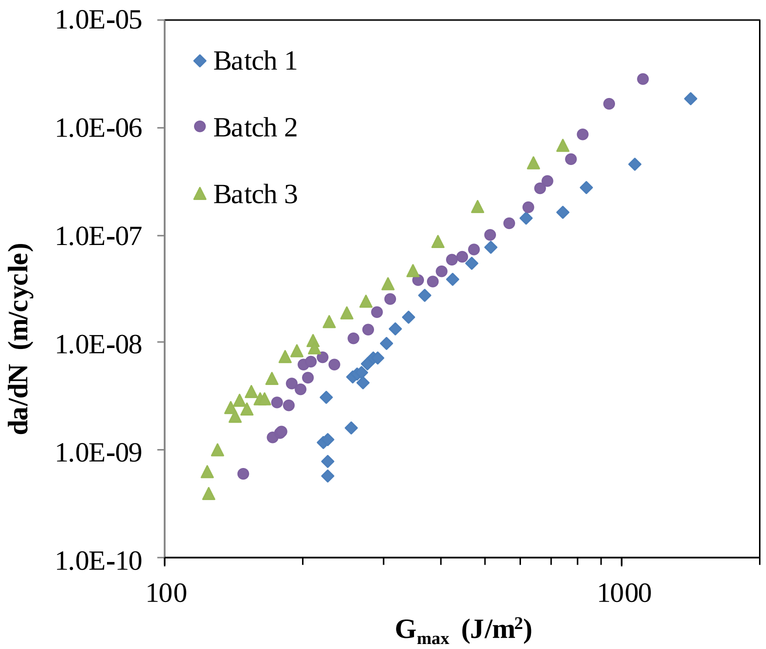

Figure 3.15 The measured data [108] for the Mixed-Mode I and II fatigue behaviour for a toughened-epoxy adhesive of different patches.

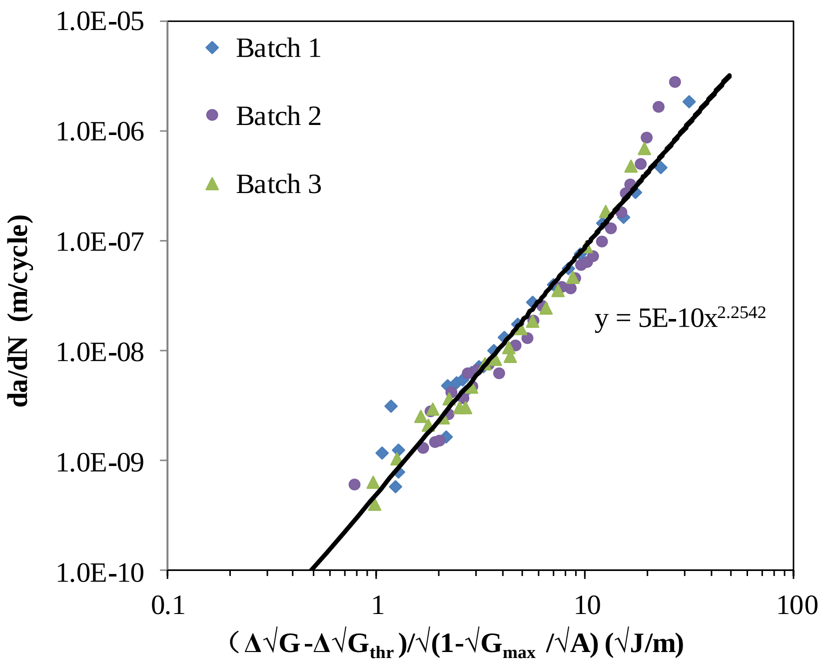

Figure 3.16 Hartman-Schijve representation for the Mixed-Mode I and II fatigue behaviour for a toughened-epoxy adhesive of different patches. Data is from [108].

3.3.4 The value of the exponent

As commented earlier, in the Paris crack growth equation, the rate of crack growth per cycle, da/dN, is assumed to be linearly related to either $(G_{max})^m$ or $(\Delta G)^m$ where the exponent m is a constant that is determined experimentally. Unfortunately, for structural adhesives and fibre-composite materials, many researchers [101, 102, 103, 104, 109] discovered that the value of the exponent, m, in this relationship tends to be relatively high. As a result, Martin and Murri [90] concluded:

For composites, the exponents for relating propagation rate to strain-energy release rate have been shown to be high especially in Mode I. With large exponents, small uncertainties in the applied loads will lead to large uncertainties (of at least one order of magnitude) in the predicted delamination growth rate. This makes the derived power-law relationships unsuitable for design purposes.

This shortcoming has led to the aerospace industry adopting a 'no-growth' design philosophy for adhesively bonded components and composite structures; that is, designs are such that there would be no disbond or delamination crack growth allowed during the lifetime of the aircraft [110].

The same situation holds for fatigue crack growth in structural adhesives. This can be seen in Figure 3.17 where we present the da/dN versus G_{Imax} relationship obtained by Kinloch et al. [111] for a series of (nominally identical) tests on a typical rubber-toughened epoxy-film adhesive ('EA9628' from Hysol, USA) that is used widely in aerospace applications, where the subscript 'I' indicates Mode I loading. In this instance, the exponent, m, varies from 6.92 to 7.97, see Figure 3.17. Thus, as noted earlier, this makes the derived power-law relationships unsuitable for design purposes. However, when Figure 3.17 is replotted with Hartman–Schijve equation, the exponential term m is only about 3.16. Its fracture energy is 1700 J/m^2 [111] and the threshold varies between 6.7 and 8.1, see Figure 3.18.

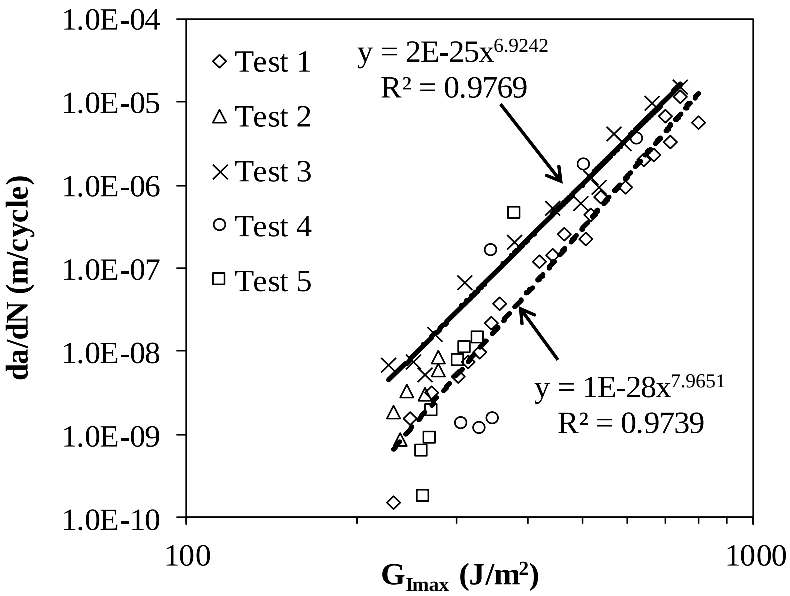

Figure 3.17 The measured [111] Mode I fatigue behaviour for tapered DCB with the rubber-toughened epoxy-film adhesive (Hysol 'EA9628').

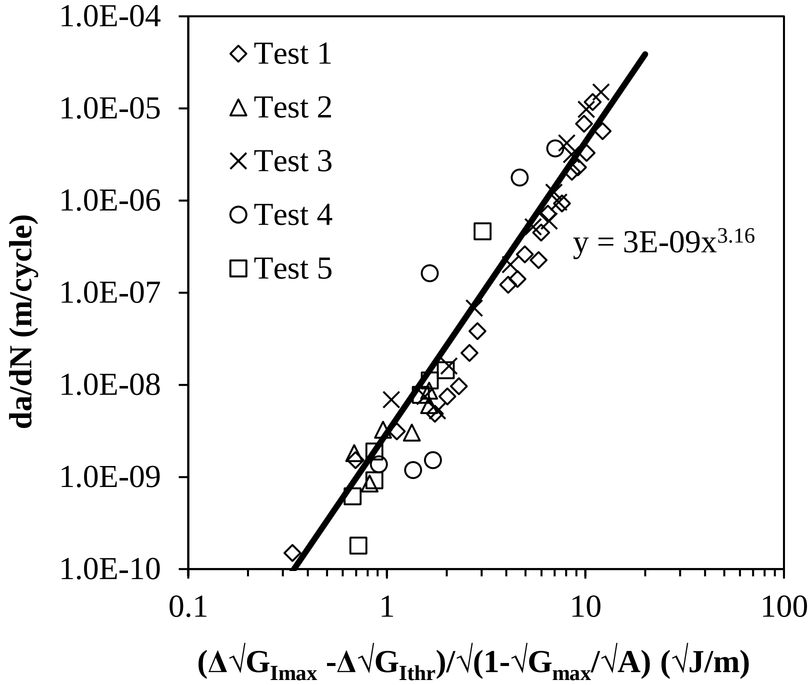

Figure 3.18 Hartman-Schijve representation of disbond growth in tapered DCB. Data is from [111].

3.3.5 Fatigue crack growth under different test conditions

Unlike metal, the performance of composite and adhesively bonded structures varies significantly with test conditions, as the mechanical properties of adhesives and polymers are strongly correlated to temperature. This can be seen in Russell's report [112] which demonstrated that the fatigue performance of Mode II for FM 300K varies at -50 ^{o}C, 20 ^{o}C and 100 ^{o}C, see Figure3.19. The fatigue tests were conducted under Mode II loading using the end-loaded split test specimen with R = -1. The frequency of the test was varied from 0.1 to 4 Hz, and no significant of effect of the test frequencies was observed. The data from Figure 3.19 is replotted as per the Hartman-Schijve representation, see Figure 3.20. The values of constants of Figure 3.20 are shown in Table 3.3.

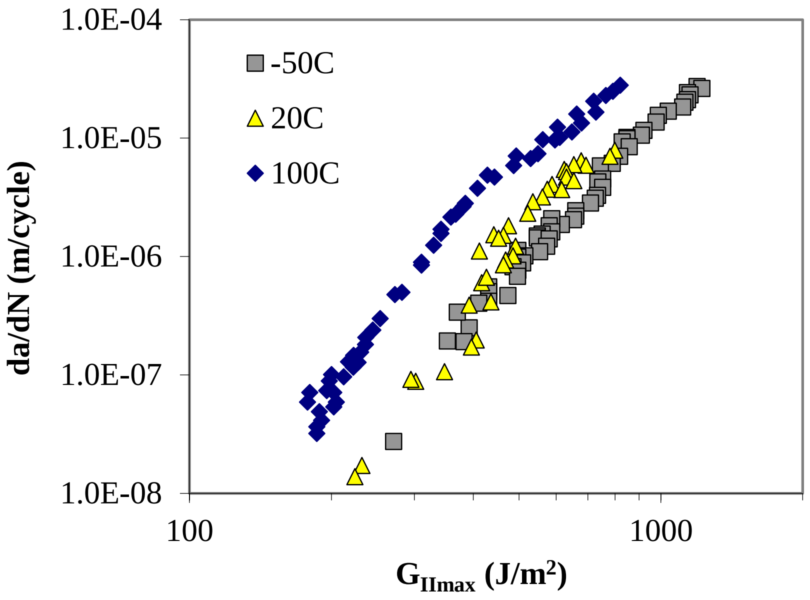

Figure 3.19 The measured curves for the Mode II fatigue behaviours for the FM 300K at different test temperature [112].

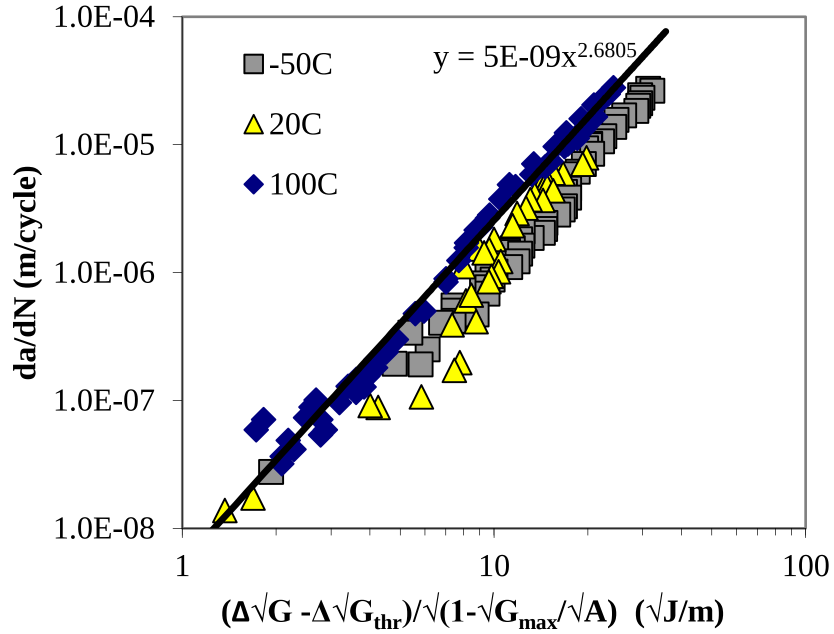

Figure 3.20 Hartman-Schijve representation for the Mode II fatigue behaviours for the FM 300K at different test temperature. Data is from [112].

Table 3.3 The values D, m, $\Delta\sqrt{G_{thr}}$ and A used in Figure 3.20.

Test Temperature	D (m/cycle)	m	$\Delta\sqrt{G_{thr}}$ ($\sqrt{J}$/m)	A (J/m^2)
-50 ^oC	5E-9	2.68	14.8	3280
20 ^oC			13.8	3680
100 ^oC			11.8	3060

Figure 3.20 reveals that the various temperature-dependent curves essentially collapse onto a single ‘master’ linear plot when the Hartman-Schijve representation is employed to represent the fatigue data. The values of A in each test are unchanged from literature [112]. The value of exponent term, m, in the Hartman-Schijve equation is 2.68. Thus, the Mode II cyclic-fatigue behaviour of the FM 300K structural adhesives can be represented using the Hartman-Schijve equation.

3.3.6 Fatigue crack growth from short cracks

For crack growth in metallic airframes, the life and inspection intervals are determined by the fastest growing cracks, which Molent et al. [113] referred as ‘lead cracks’. In such cases, Wanhill [114] stated that ‘*it appears that fatigue crack growth thresholds are largely irrelevant for short/small→long/large fatigue crack growth*’. In operational aircraft, where cracking generally starts from small naturally occurring material discontinuities, it therefore follows that the threshold term in the Hartman–Schijve equation is very small. As such, when assessing the variability in the life associated with lead cracks that grow from small naturally occurring material discontinuities in operational aircraft, the effect of the variability in the threshold term can essentially be ignored, and the scatter in the lives can be described by the probability distribution associated with the size of the initiating defect [115]. It is currently unclear if a similar approach could be used to assess the scatter seen in crack growth associated with adhesively bonded structures

Notwithstanding the previous statement, Jones et al. [17] has presented a number of examples, viz: in the ‘F-111’, ‘A-320’, ‘F/A-18’ and Canadian ‘CF-5’ aircraft, where fleet data and data obtained from full-scale fatigue tests [110] revealed that small sub-millimetre initial delaminations or disbonds can grow when subjected to operational flight loads. As such, the inability of the ‘no-growth’ design approach to ensure that there is no in-service disbond or delamination crack growth has led to the realisation that there is a need to allow for some slow crack growth in the initial design and thereby determine the appropriate inspection intervals. This approach to certifying adhesively bonded and composite structures was introduced in the 2009 US Federal Aviation Administration Airworthiness Advisory Circular [12]. To manage the growth of disbonds and delaminations in operational aircraft, it is necessary to be able to account for the growth of such disbonds or delaminations from small naturally occurring material discontinuities. For metals, it is essential to use a da/dN versus ΔK curve that represents growth from such naturally occurring material discontinuities. This conclusion was echoed in [55]. Therefore, the present challenge is how to determine a representation with a small exponent that has the potential of assessing sustainment problems associated with such small naturally occurring debonds and delaminations.

The ASTM E647-13a states that standard tests on ‘long cracks’ should not be used for assessing the growth of small naturally occurring cracks [35]. A strength of the Hartman–Schijve approach [55] is that, it has potential to be used to determine the appropriate ‘small cracks’ relationship from such ‘long crack’ test data, as well as accounting for other aspects of fatigue test data such as the effect of the R-ratio on the crack-growth rate and the scatter that is frequently observed in the data especially at low values of crack-growth rate.

To illustrate this effect in a composite laminate, an experiment was conducted with delamination growth in CFRP specimens at R = 0.5 by Yao et al. [116]. The DCB test specimens consisted of 32-ply unidirectional CFRP laminates with a nominal cured thickness of 5 mm. Various lengths of initial delaminations were tested and the resultant da/dN versus $\Delta\sqrt{G_I}$ curves, which show a strong dependency on the size of the initial delamination which was 4.1, 12.7 or 20.5 mm, are given in Figure 3.21. It is obvious that for shorter initial crack length, less crack driving force is needed to achieve the same delamination growth rate.

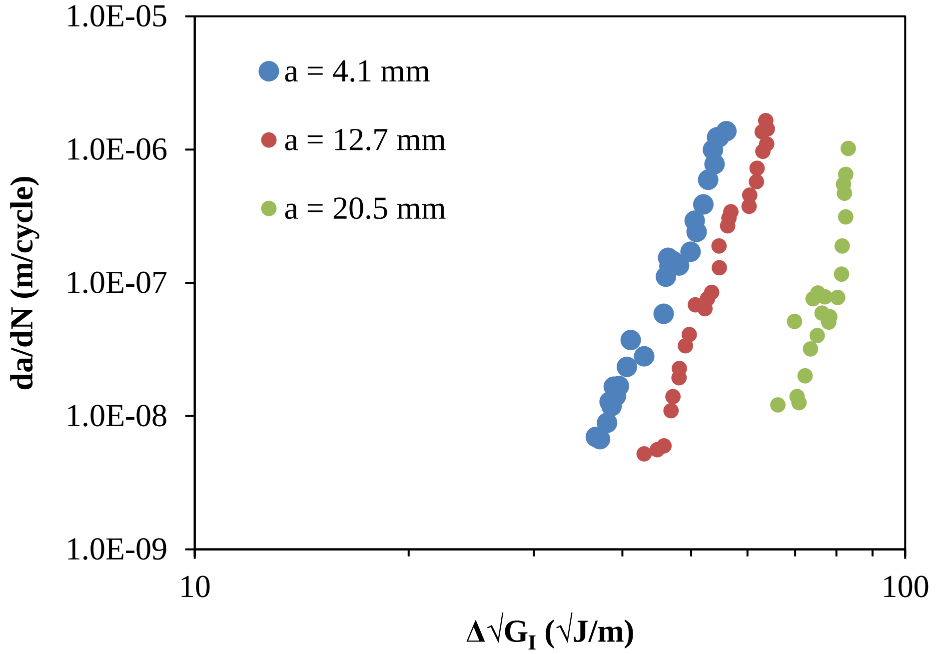

Figure 3.21 Plot of da/dN versus $\Delta\sqrt{G}$ for delamination growth in DCB tests using a unidirectional CFRP laminate for three different initial sizes of delamination [116].

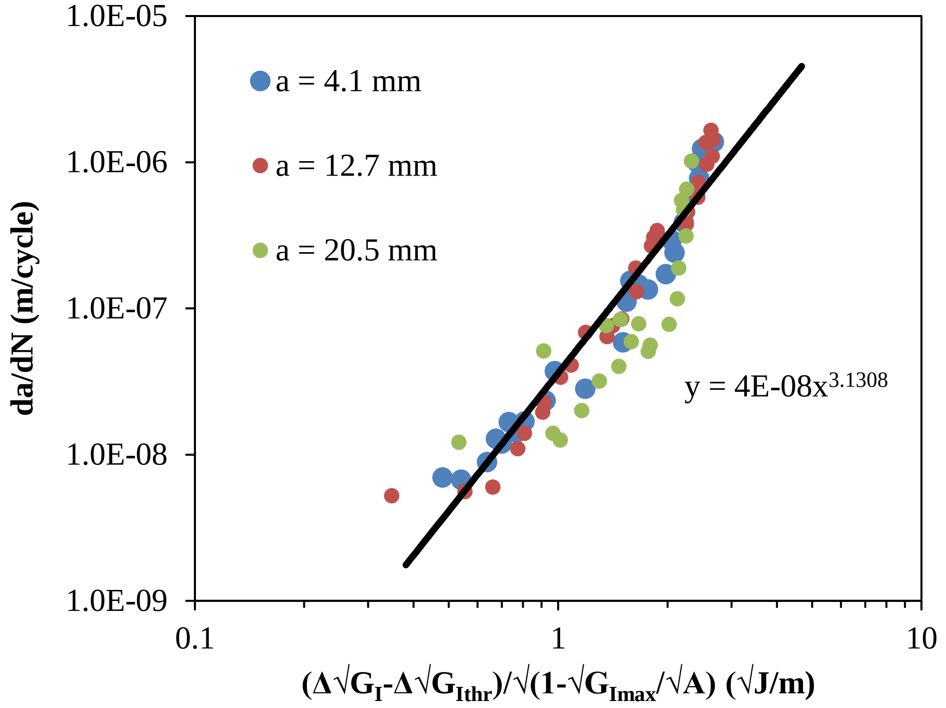

Figure 3.22 Hartman–Schijve representation for delamination growth in DCB tests with three different initial sizes of delamination. Data is from [116].

When Figure 3.21 is replotted with the Hartman–Schijve equation, it not only collapses the three curves which associated with different initial crack lengths together, see Figure 3.22, but also suggests that for smaller initial defects the threshold is smaller, see Table 3.4. This finding is consistent with fleet experience and the results of full-scale tests [17]. It also raises the potential for the Hartman–Schijve approach to be employed to use long-crack growth data to predict the growth of smaller or naturally-occurring, delamination and disbond.

Table 3.4 The values D, m, $\Delta\sqrt{G_{thr}}$ and A used in Figure 3.22.

Initial crack length (mm)	D	m	$\Delta\sqrt{G_{Ithr}}$ ($\sqrt{J/m}$)	A (J/m^2)
4.1	4E-8	3.13	5.3	720 [117]
12.7			6.3	
20.5			7.8	

3.4 Summary

For the US FAA slow crack growth approach to certifying composite and adhesively bonded structures to be viable, it requires for translating laboratory coupon test data on delamination and disbond growth to real delamination and disbond growth as seen in full-scale aircraft structures. This, in turn, requires invoking a 'similarity hypothesis' and determining a valid CDF together with standards for determining the relationship between the CDF and the rate of fatigue crack growth, da/dN. Unfortunately, this chapter suggests that the term ΔG cannot be employed as a valid CDF. It thus follows that for composites and adhesively-bonded structures the ability to use da/dN versus ΔG data determined from laboratory test coupons to assess and certify designs in accordance with the FAA approach is questionable.

Fortunately, unlike ΔG, the term $\Delta\sqrt{G}$ appears to have the potential to fulfil the requirements of a valid CDF. We have also shown that the Hartman-Schrive equation shows promise for modelling both delamination and disbond growth in composite and adhesively bonded structures. Hence, this approach would appear to have the potential to meet the FAA requirements for translating laboratory coupon test data on delamination and disbond growth to real delamination and disbond growth as seen in full-scale aircraft structures.

This Chapter also shows that the exciting potential for the Hartman-Schijve approach to unify many aspects of the cyclic fatigue crack growth behaviour that have been observed in structural adhesive joints. For example, we have illustrated several noteworthy features for a wide range of structural adhesives:

- A 'master' linear representation for the fatigue data points, if plotting in log-log form, has always been observed when such data are plotted according to the Hartman-Schijve equation.

- The slope, m, of this ‘master’ linear relationship has a relatively low value of approximately two to three.
- The Hartman-Schijve equation was found to be applicable to Mode I, Mode II and Mixed-Mode I and II of fatigue crack grwoth. Indeed, it has been demonstrated that all three modes of fatigue behaviour may be described by a ‘master’ line via the Hartman-Schijve representation.
- This approach accounts for, and unifies, the typical degree of scatter seen from testing nominally identical specimens. Indeed, the typical scatter from such duplicate tests were all found to lie on a ‘master’ linear plot when plotted using Hartman-Schijve equation.
- This equation appears to account for both R ratio and test temperature effects, again yielding a ‘master’ linear relationship which can capture these effects.
- The Hartman-Schijve equation also appears to have the potential to collapse the delamination growth curves obtained for different initial delamination lengths onto a ‘master’ line.
- Finally, it is noteworthy that the constants, i.e. D, m and A, used in the appropriate Hartman-Schijve equation were held constant for a given adhesive, and hence were taken to be independent of the test conditions and the degree of variability observed in the experimental tests.

This conclusion means that the values of the constants, i.e. D, n and A, for a given adhesive which are ascertained from a limited set of experimental results. These values may then be used to predict the fatigue behaviour of the adhesive when the structural adhesive joints are subjected to different fatigue test conditions. It would appear that the Hartman-Schijve equation has the potential to predict the degree of variability in the fatigue behaviour that might be expected to occur. Consequently, in next chapter, we discuss the use of the Hartman-

Schijve approach for designing and predicting the lifetime of structural adhesive joints subjected to cyclic fatigue.

Chapter 4

Computing The Growth Of Naturally Occurring Disbond For Adhesively Bonded Joints

4.1 Introduction

Adhesively bonded joints are commonly used in the aerospace industry both in the fabrication of new aircraft and in the repair of both metallic and composite structures [118, 119]. The adhesives are typically based upon thermosetting epoxy polymers which are highly crosslinked and amorphous in nature. As with all materials, such epoxy polymers undergo failure under cyclic fatigue loading more rapidly than under the equivalent applied statically loads. However, little work has been reported on gaining a fundamental understanding of the mechanisms involved [120]. Nevertheless, it is clear that the fatigue mechanisms which are operative in epoxy polymers at relatively low frequencies below about 10–20 Hz are broadly similar to those in other materials [121]. They involve the creation of a plastic damage zone at the crack tip as the polymer is subjected to repeated loading–unloading cycles. This causes disruption of the plastic zone and rupture of the polymeric molecular chains, and thus more readily enables crack advance under such applied fatigue loads. Nevertheless, significant advances have been made in accurately measuring the fatigue crack behaviour of epoxy polymers, especially via applying a fracture mechanics approach [120].

Until 2009 certification of adhesively bonded aircraft structures was based on a ‘no growth’ design philosophy which means there should be no any form of disbond growth within the designed life. However, there have been a number of in service instances and full-scale fatigue tests where there has been extensive delamination/disbonding [17, 122, 123]. In each case the disbonds grew from small naturally occurring sub mm material defects. To address this problem the US FAA introduced a slow growth approach to certify composite and adhesively bonded structures and adhesively bonded repairs

Unfortunately a lack of understanding of and an inability to predict disbond growth, especially for disbonds that arise from small naturally occurring material discontinuities, is an obstacle which hampers the use of the slow growth approach for certification. As such Jones et al. [18] revealed how the Hartman-Schijve variant of the NASGRO equation derived for delamination/disbond growth associated with large artificial initial disbonds, could be used to compute the growth of disbonds that grow from small naturally occurring sub mm material defects. It is also shown that the constants of the Hartman-Schijve equation can be determined from tests using specimens associated with large artificial initial disbonds.

Whilst this approach has been shown to be able to represent both delamination and disbond growth [18, 70] associated with large initial defects, this Chapter addresses the growth of small sub-millimetre initial disbonds. To this end two examples are studied where naturally occurring disbonds have been allowed to initiate and grow in:

1. a symmetrical double over lap adhesively bonded specimen [124]
2. an asymmetrical adhesively bonded doubler joint, typical of a bonded repair [118].

These two examples revealed that the Hartman–Schijve equation is able to predict the growth histories of disbond length versus number of fatigue cycle and the predictions are in good agreement with the experimental measurements. This finding highlights the potential to estimate the necessary inspection intervals needed to certify composite and adhesively bonded structures and bonded repairs.

4.2 Preliminary Work on Life Prediction

4.2.1 Accounting for the variability in crack growth

Virkler et al. [125] recognised the variability seen in FCG. Consequently, Virkler and his co-workers carefully prepared sixty-eight, nominally identical, 2.54 mm thick aluminium alloy 2024-T3 centre notched specimens and tested them under constant amplitude loading. The number of cycles it took for the centre cracks to reach pre-specified lengths was determined. Care was specifically taken to ensure that the initial crack length, 2a, was 18.0 mm. This study revealed the degree of scatter in the FCG that can be expected in ASTM E647-13a tests on long cracks, see Figure 4.1. Jones [55] illustrated that, with the values of A = 70 MPa√m, C = 1.2 10^{-9} m/cycle and n = 2 (taken from [54]), the variability in the measured FCG rates was captured to a relatively high degree of accuracy by merely allowing for changes in the value of ΔK_{thr}, i.e. using vales between 2.9 and 4.2 MPa√m in Equation (2.15). Also shown in Figure 4.1 is the conservative nature of the computed crack growth curve for the case when ΔK_{thr} = 0.0 MPa√m. Molent and Jones [126] subsequently revealed that this finding, i.e. that variability in crack growth seen in crack growth under both constant amplitude and variable amplitude loading could be captured by allowing for small changes in the term ΔK_{thr}, held for both large cracks and for cracks that initiated and grew from small naturally occurring material discontinuities.

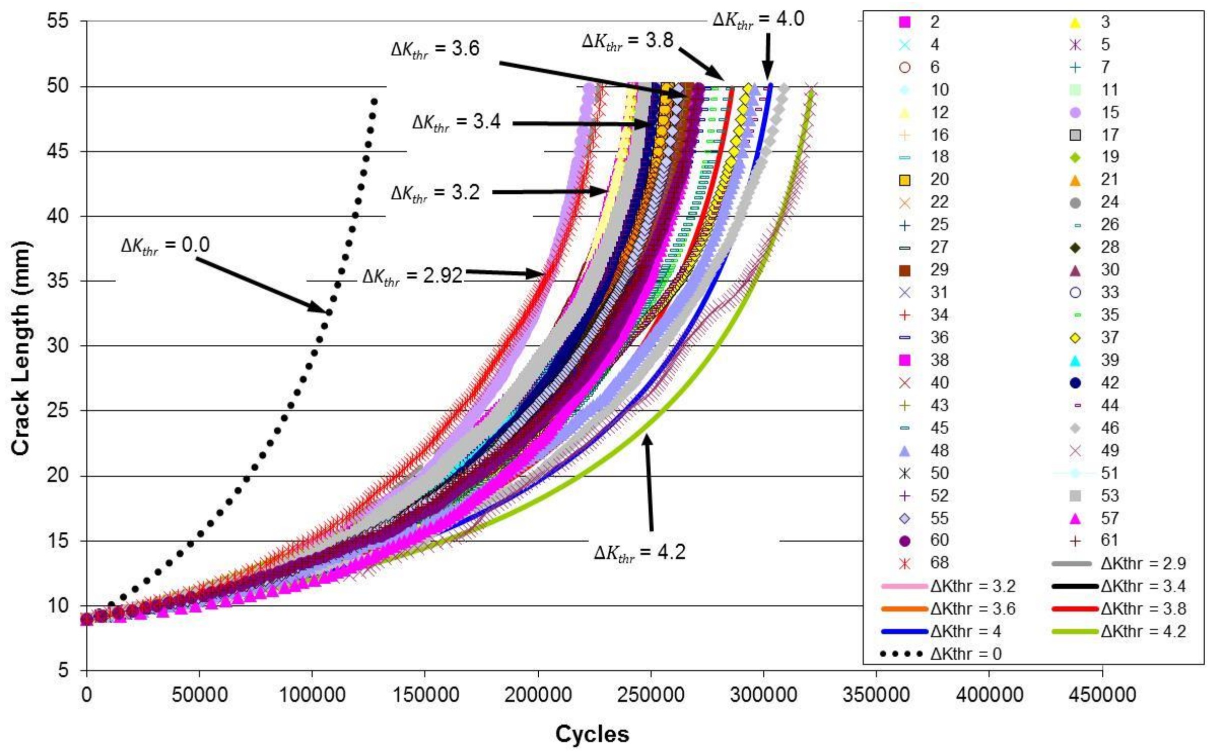

Figure 4.1 Crack growth data from Virkler et al. [125] and the computed variability [55] for an aluminium alloy 2024-T3. The curve computed using $\Delta K_{thr} = 0$ is also presented.

Jones et al. [18] extended this finding, i.e. that the variability in crack growth could be captured by allowing for variability in the threshold, to the growth of relatively large, through-thickness, initial disbonds in adhesively-bonded joints. One such example involved FCG data measured for an epoxy-film aerospace structural adhesive [111], namely EA9628 adhesive (Hysol Dexter, USA). This test data set was examined, see Figure 4.2, where was shown that the scatter in the data was captured by allowing for changing the $\Delta\sqrt{G_{thr}}$, see Table 4.1.

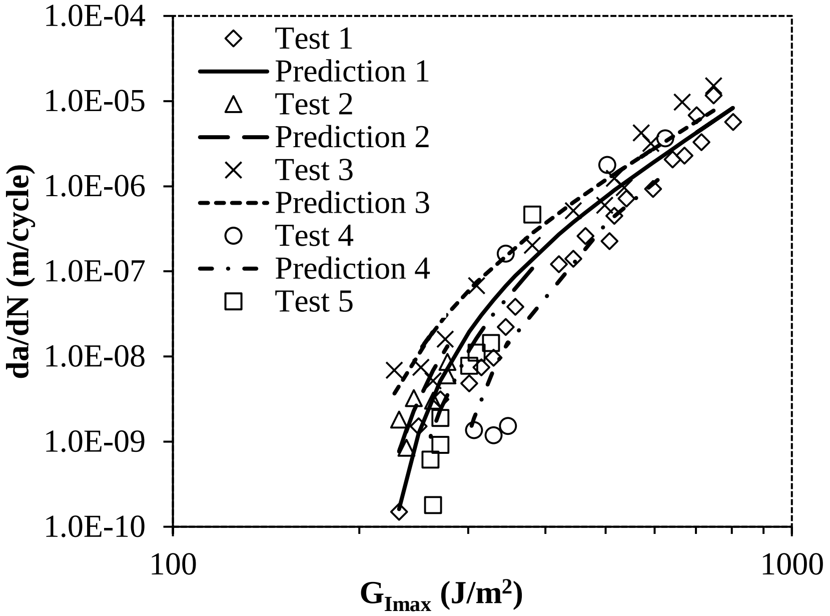

Figure 4.2 The measured and computed curves for the EA9628. Data is from [111].

Table 4.1 Values of the constants employed in the Hartman-Schijve euqation for fatigue crack growth in the EA9628 epoxy adhesive.

Test Number	D	m	A (J/m2)	$\Delta\sqrt{G_{thr}}$ ($\sqrt{J/m}$)
1	3E-9	3.16	1700	7.3
2	3E-9	3.16	1700	7.1
3	3E-9	3.16	1700	6.7
4	3E-9	3.16	1700	8.1
5	3E-9	3.16	1700	7.5

4.2.2 Accounting for different fracture modes

The most popular laboratory experiments were preferred to use double cantilever beam (DCB) or tapered DCB for Mode I fatigue crack growth and the end notched flexure (ENF) for Mode II fatigue crack grwoth. However, those artificial tests with their delaminations/disbonds are not particularly represented of those structures and joints in real airframes, which are usually subjected to a Mixed Mode I and II fracture mode and where the delaminations/disbonds arises naturally. In order to predict the fatigue life of such structures and joints, it is necessary to investigate the mode mixity, i.e. the ratio between Mode I and Mode II fracture. Numerous researchers [68-78] have proposed methodologies to account for the Mixed Mode I and II fracture mode with different proportion of mode mixity, see Section 2.5.1. However, there is no accepted test geometry for Mixed Mode I and II fatigue crack growth in composite or bonded structures.

It is a delight finding that the Hartman-Schijve variant of the NASGRO equation is capable of collapsing the mixed model data given by Hafiz et al. [127] onto a master line. In this work, Hafiz et al. [127] tested 200 mm long and 15 mm wide mild steel DCB adherends which were bonded by 0.16 mm thick FM73 adhesive film, see Figure 4.3. The test setup is shown in Figure 4.4. The experiment was performed under an initial load ratio, R, equals to 0.1 with different mode mixities (GII/GI), i.e.0, 0.22, 0.72, 1.29 and 6.62. The SERR was calculated with Equations (4.1) and (4.2).

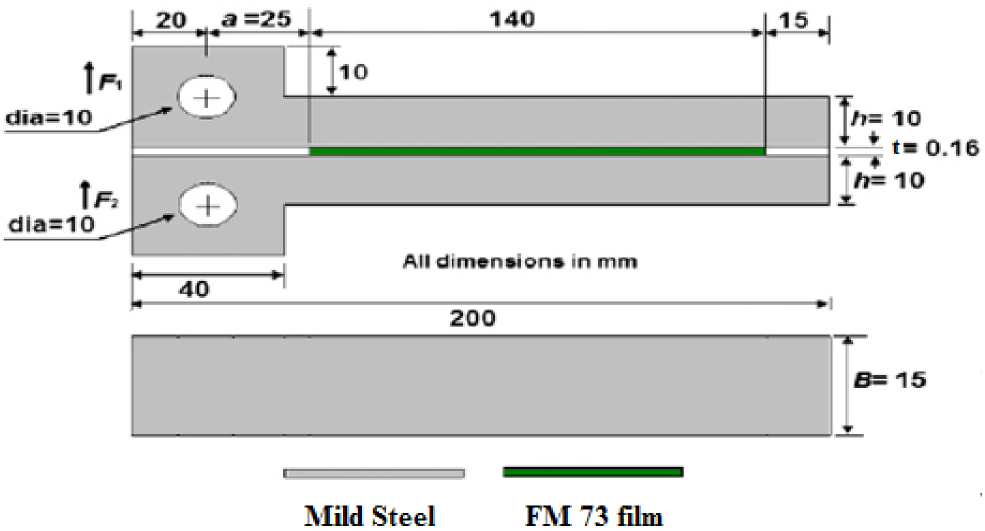

Figure 4.3 Bonded DCB specimen geometry [127].

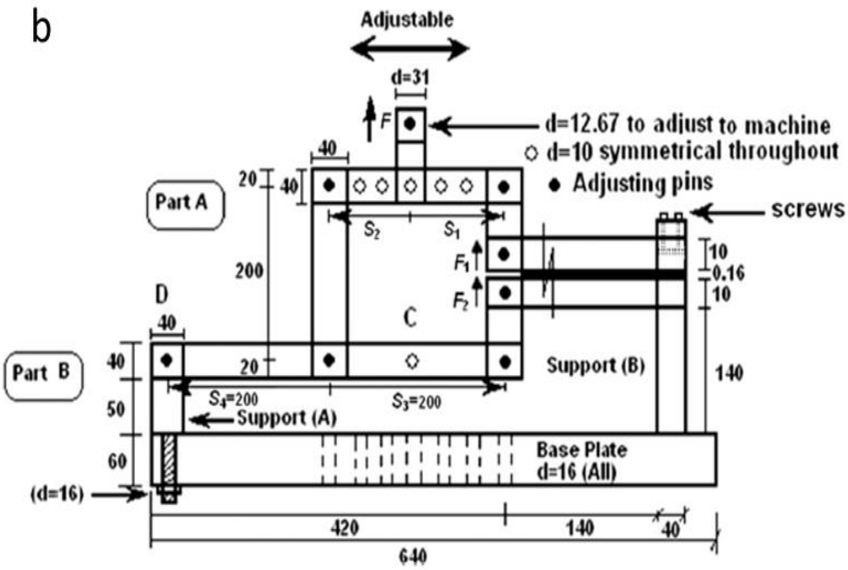

Figure 4.4 a) Experimental setup. b) Schematic diagram of the load jig (in mm) [127].

$$G_I = \frac{12M_I^2}{B^2Eh^3}\left(1 + \frac{(1+\upsilon)}{5}\left(\frac{h}{a}\right)^2\right)\left(1 + \frac{1)}{\lambda a}\right)^2 \tag{4.1}$$

$$G_{II} = \frac{9M_{II}^2}{B^2Eh^3}\left(1 + \frac{1)}{\lambda a}\right)^2 \tag{4.2}$$

where

$$M_I = \frac{F_1a - F_2a}{2}$$

$$M_{II} = \frac{F_1a + F_2a}{2}$$

$$F_1 = F\left(\frac{S_2}{S_1 + S_2}\right)$$

$$F_2 = F\left(\frac{S_1}{S_1 + S_2}\right)\left(\frac{S_4}{S_3 + S_4}\right)$$

$$\lambda^4 = \frac{6}{h^3t}\frac{E_a'}{E}$$

where a is the disbond length, F is the applied load and F_1, F_2 are the loads on upper and lower adherends respectively. S_1, S_2, S_3 and S_4 are the shown in Figure 4.4 b. B, h, E and υ are the width, height, elastic modulus and Poisson's ratio of the adherend respectively. E'_a is the elastic modulus plain strain modulus of the adhesive FM73. The maximum total SERR and crack driving force, i.e. $\Delta\sqrt{G_{total}}$, for Mixed Mode I and II in the Hartman-Schijve variant of the NASGRO equation are defined as Equation (4.3) and (4.4) respectively.

$$G_{total,max} = G_{Imax} + G_{IImax} \tag{4.3}$$

$$\Delta\sqrt{G_{total}} = (1 - R)\sqrt{G_{Imax} + G_{IImax}} \tag{4.4}$$

A plot of fatigue disbond growth rate versus $\Delta\sqrt{G}$ is given in Figure 4.5. This data set is re-plotted against the Hartman-Schijve representation with A = 2800 J/m^2 [128] and with the of threshold term, i.e. $\Delta\sqrt{G_{thr}}$ is between 6 and 17, see Figure 4.6. All fatigue data is collapsed onto the master line, linear constant $D = 1.2\times10^{-9}$ and exponential constant m = 2.3. The Hartman-Schijve variant of the NASGRO equation shows its potential capability of accounting for different mode mixities with the same values of D, m and A. Hence it should be noted in the absence of knowing the mode dependent values of A, it was decided to use the Mode I toughness for FM 73 given by Johnson and Butkus [128]. The fit to the data could have been improved had the values of A chosen so as to best fit the data. Consequently, it is possible to use the fatigue data from Mode I test to predict the fatigue performance of Mixed Mode I and II.

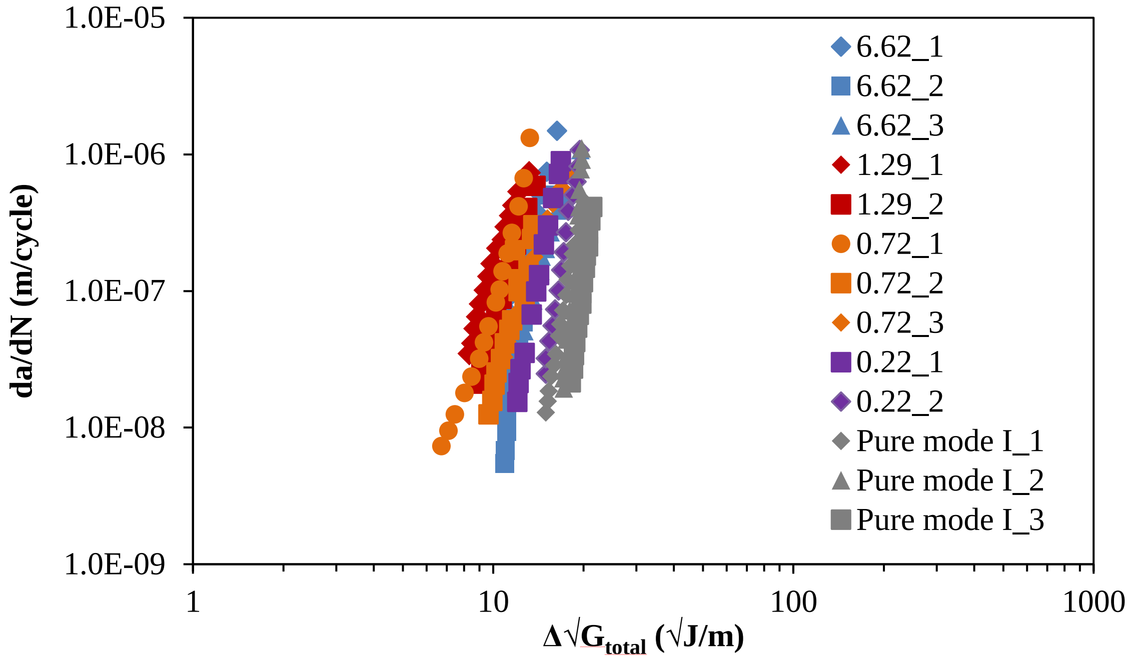

Figure 4.5 Plot of disbond growth rate against $\Delta\sqrt{G}_{total}$ for FM73 in different mode mixitie. Data is from [127].

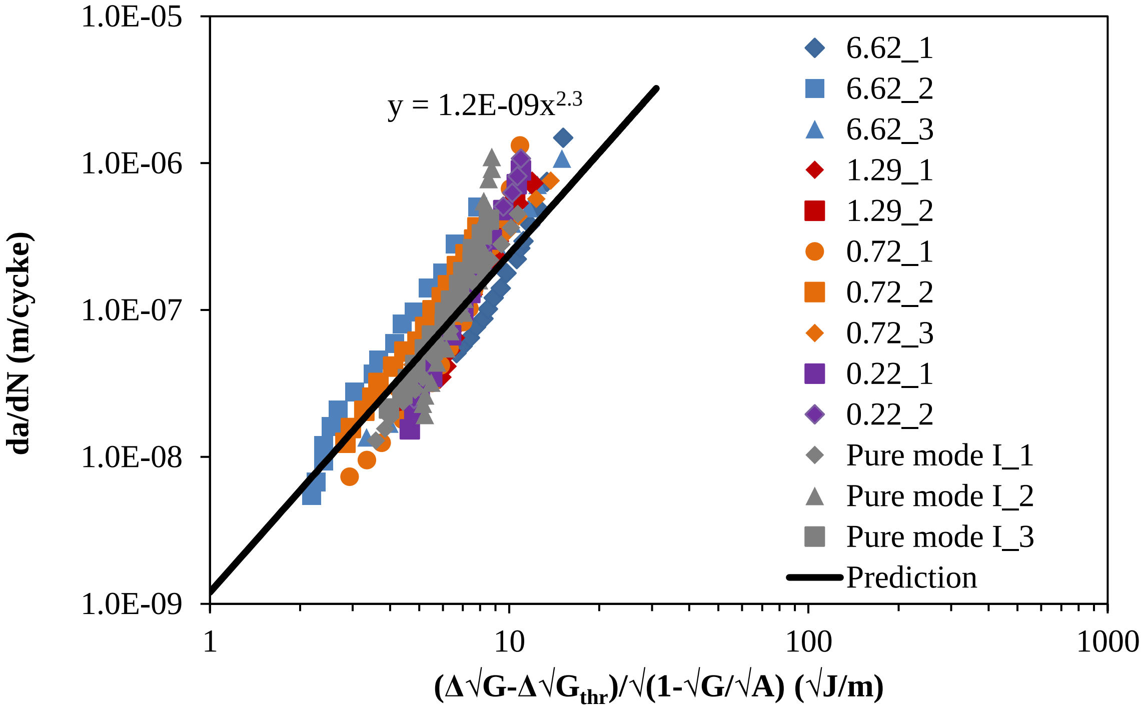

Figure 4.6 Plot of disbond growth rate against Hartman–Schijve representation for FM73 in different mode mixities. Data is from [127].

4.3 Experimental Data for FM73

The papers by Pascoe et al. [118] and Cheuk et al. [124] have presented the disbond histories associated with tests employing an asymmetrical adhesively-bonded joint and a symmetrical double overlap adhesively-bonded joint respectively, when they are subjected to cyclic fatigue tests. For each type of specimen the substrates were bonded using an aerospace epoxy-film adhesive (i.e. FM73 from Cytec, UK). Further, in both cases, the fatigue crack growth, that grew through the adhesive layer, was recorded from relatively small naturally-occurring discontinuities.

Prior to predicting the disbond growth histories associated with these test specimens, information on the fatigue performance of the FM73 adhesive is needed. The paper by Johnson and Butkus [128] has presented the results of fracture mechanics tests using the FM73 adhesive to bond aluminium-alloy 7075-T651 substrates to form double cantilever beam specimens. In all cases the locus of joint failure was via cohesive crack growth through the adhesive layer, which is the same type of failure as observed by Pascoe et al. [118] and Cheuk et al. [124] in their test specimens. Johnson and Butkus [128] plotted their results in the form of a log da/dN versus log ΔG_I relationship, as shown in Figure 4.7.

The experimental data given in Figure 4.7 is replotted with Hartman–Schijve representation with values of the various parameters employed are given in Table 4.2, see Figure 4.8. The values of A, m and A used in this analysis were those determined in Section 4.2. This log-log linear curve has a relatively low slope of value of 2.3 and there is an excellent agreement between the measured and the computed relationships.

Table 4.2 The constants employed in the Hartman-Schijve representation for FM 73.

D	m	A (J/m2)	$\Delta\sqrt{G_{thr}}$ ($\sqrt{J/m}$)
1.2E-9	2.3	2800	8.1

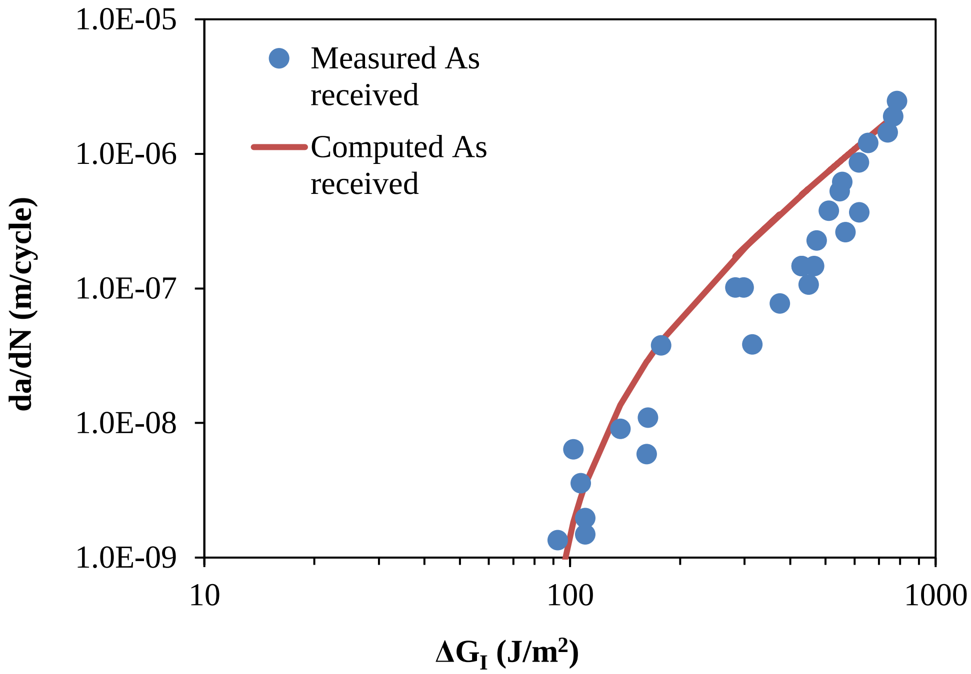

Figure 4.7 The measured data points and computed curve for the fatigue behaviour for the rubber-toughened epoxy-film adhesive FM73. Data is from [128].

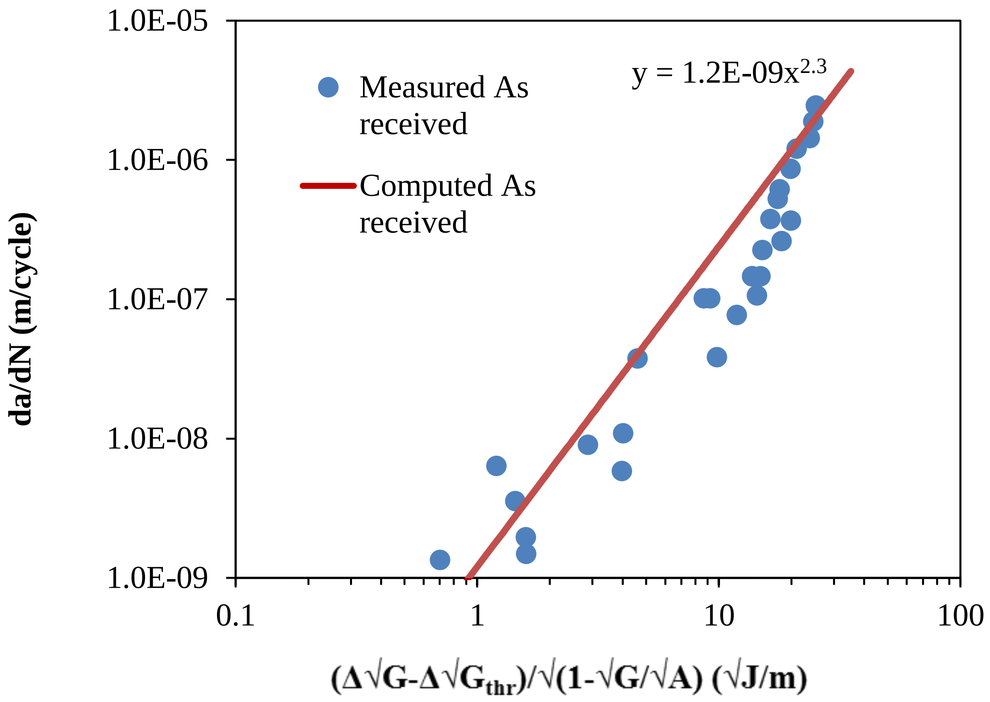

Figure 4.8 The Hartman–Schijve representation of the fatigue behaviour for the rubber-toughened epoxy-film adhesive FM73. Data is from [128].

These results from relatively short-term fracture-mechanics tests are next employed to predict the long-term crack growth histories from naturally-occurring disbonds in the test specimens studied by Pa Pascoe et al. [118] and Cheuk et al. [124].

4.4 Predicting the Fatigue Behaviour of Adhesively Bonded Joints

4.4.1 The bonded-joint configuration from Cheuk et al.

Cheuk et al. [124] have presented disbond length versus number of fatigue cycles data for a symmetrical double over-lap adhesively-bonded specimen, see Figure 4.9. The inner and outer substrates were 2024-T3 aluminium-alloy and the adhesive was FM73. The fatigue crack was observed to grow cohesively through the adhesive layer from naturally-occurring defects which were present in the adhesive layer. The Young's modulus and the Poisson's ratio associated with the aluminium-alloy substrates and the FM73 adhesive are shown in Table 4.3.

Table 4.3 Mechanical properties of the AA 2024-T3 and FM73 adhesive [124].

Properties/Units	Aluminium 2024-T3	FM73 adhesive
Elastic modulus, *E* (GPa)	72	2.295
Poisson's ratio, *υ*	0.33	0.35

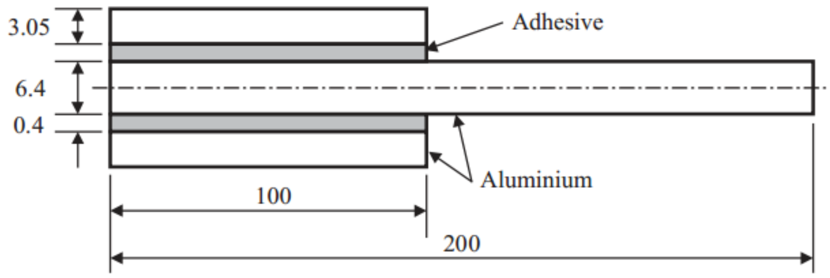

Figure 4.9 Schematic of the right-hand side of the symmetrical double over-lap adhesively-bonded specimen [124].

The inner aluminium-alloy substrate was 400 mm long and 6.4 mm thick. The outer aluminium-alloy substrate was 200 mm long and 3.05 mm thick. The FM73 adhesive layer was 0.4 mm thick. The specimen was symmetrical with a width of 20 mm. The right-hand side of the specimen is shown in Figure 4.9. The specimen was subjected to variable amplitude loading. As explained by Cheuk et al. [124], the test spectrum consisted of a series of constant amplitude (sub) spectra, i.e.:

(i) (i) Sub-spectra 1: 18,000 cycles, at a frequency of 3 Hz, of constant amplitude loading where the load was varied from 0 to 25 kN.

(ii) (ii) Sub-spectra 2: 62,000 cycles, at a frequency of 3 Hz, of constant amplitude loading where the load was varied from 0 to -25 kN.

(iii) Sub-spectra 3: 25,000 cycles, at a frequency of 3 Hz, of constant amplitude loading where the load was varied from 0 to 25 kN.

(iv) Sub-spectra 4: 26,000 cycles, at a frequency of 3 Hz, of constant amplitude loading where the load was varied from 0 to -25 kN.

(v) Sub spectra 5: 50,000 cycles, at a frequency of 3 Hz, of constant amplitude loading where the load was varied from 0 to 25 kN.

However, it should be noted that Cheuk et al. [124] observed that the disbond did not propagate under compression, i.e. sub-spectra (ii) and (iv). Therefore, these two sub-spectra were ignored in the analyses later on.

Before we can predict the disbond growth, the SERR versus disbond (crack) length relationship is needed. This relationship was obtained by using finite element analysis (FEA) [124]. In this two-dimensional full model, the length of the crack was placed within the adhesive layer and its length was varied from 0.25 mm to 10 mm and the virtual crack-closure technique (VCCT) was implemented. The calculated values of the total SERR, G, as a function of the crack length, a, from the FEA study are shown in Figure 4.10. The empirical relationships between the total SERR, G, and the disbond length, a, from Figure 4.10 is given in Equation (4.5) which indicates that the SERR is constant if the crack length is greater 8 mm, i.e. G_{total} = 470 J/m^2.

$$G_{total} = \begin{cases} 51.468ln(a) + 363.66, & 0.25 \leq a \leq 8 \\ 470 \qquad , & a \geq 8 \end{cases} \tag{4.5}$$

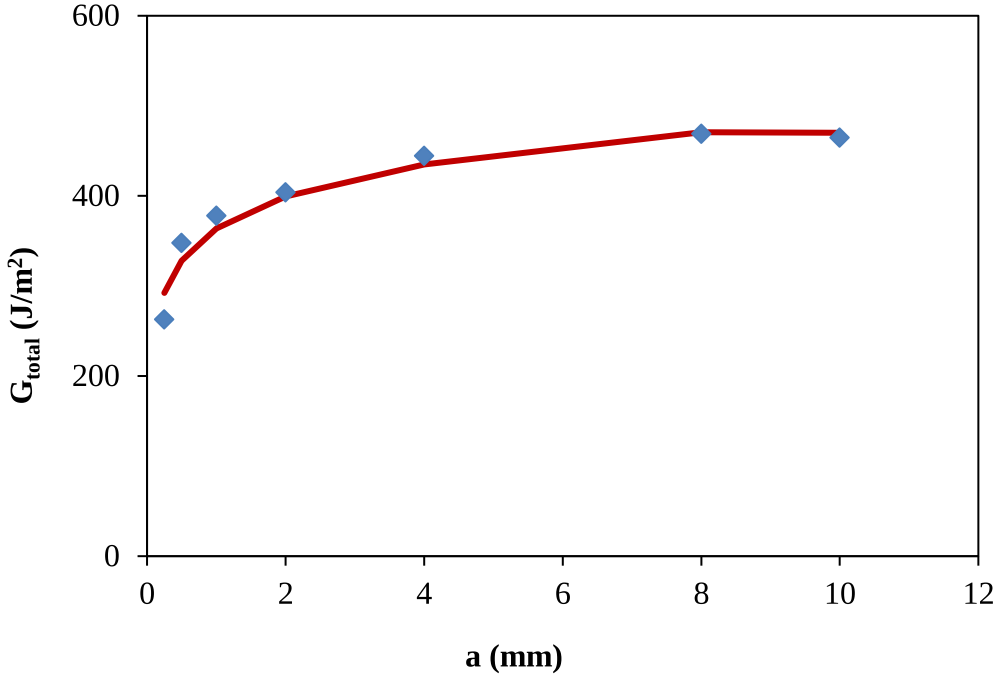

Figure 4.10 The calculated values of the total SERR, G_{total}, as a function of the crack length, a. The FEA results from Cheuk et al. [124].

The disbond length history versus number of fatigue cycles was now computed using the procedure outlined in Figure 4.11. In this procedure the values of the constants A, D, m and $\Delta\sqrt{G_{thr}}$ used in Hartman–Schijve representation were as given in Table 4. 2, i.e. A = 2800 J/m^2, D = 1.2×10^{-9} m/cycle, m = 2.3 and $\Delta\sqrt{G_{thr}}$ was adjusted to 10~11 √J/m. Equation (2.33) was integrated using the simple forward integration procedure outlined in Figure 4.11 and the G_{max} versus a relationship shown in Figure 4.10.

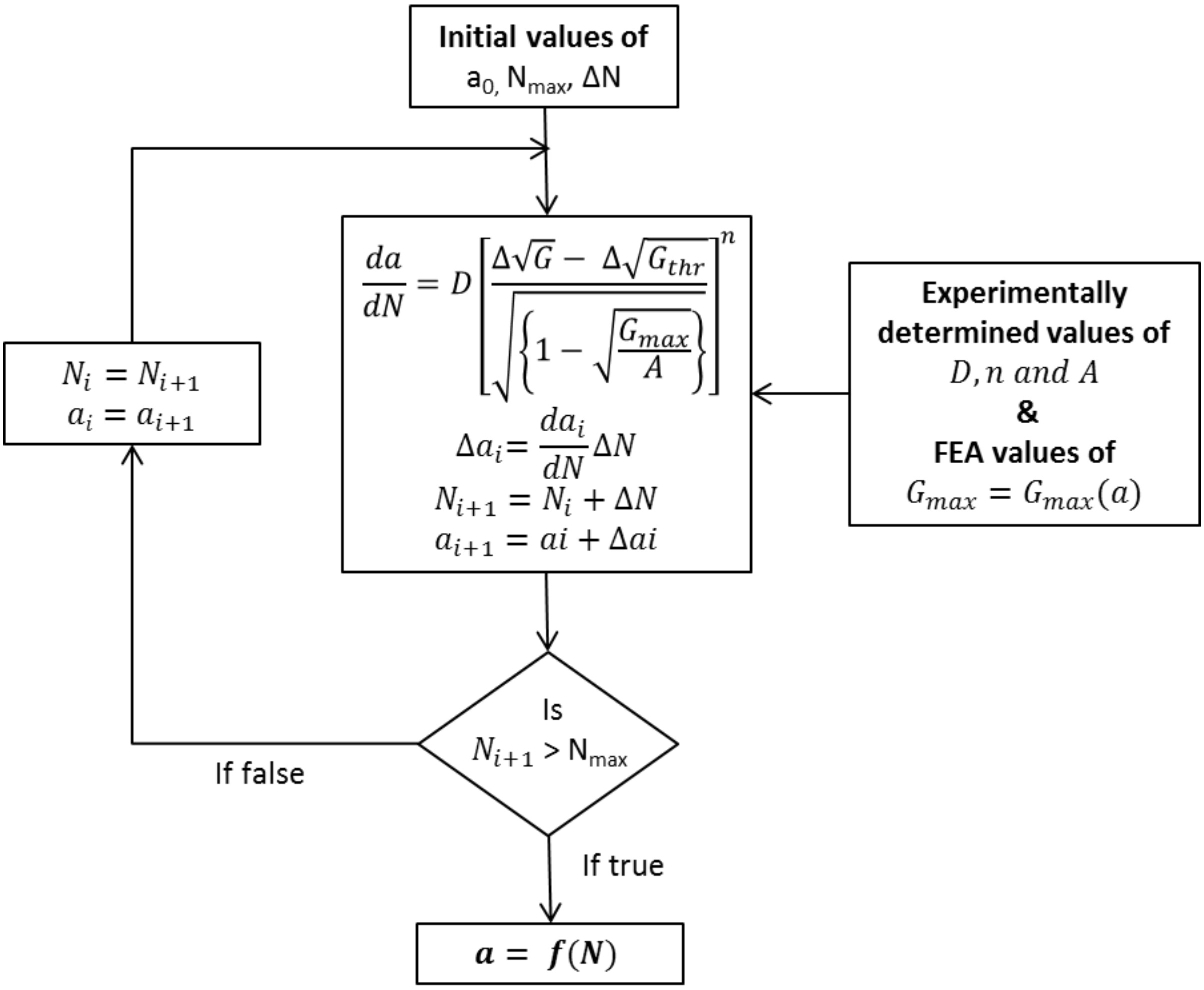

Figure 4.11 The flowchart of the procedure to compute the disbond growth as a function of the number, N, of fatigue cycles.

The measured and predicted disbond histories for the naturally-occurring defects in the double over-lap adhesively bonded specimens growing under the cyclic fatigue loads are shown in Figure 4.10. There is good agreement between the measured and predicted results.

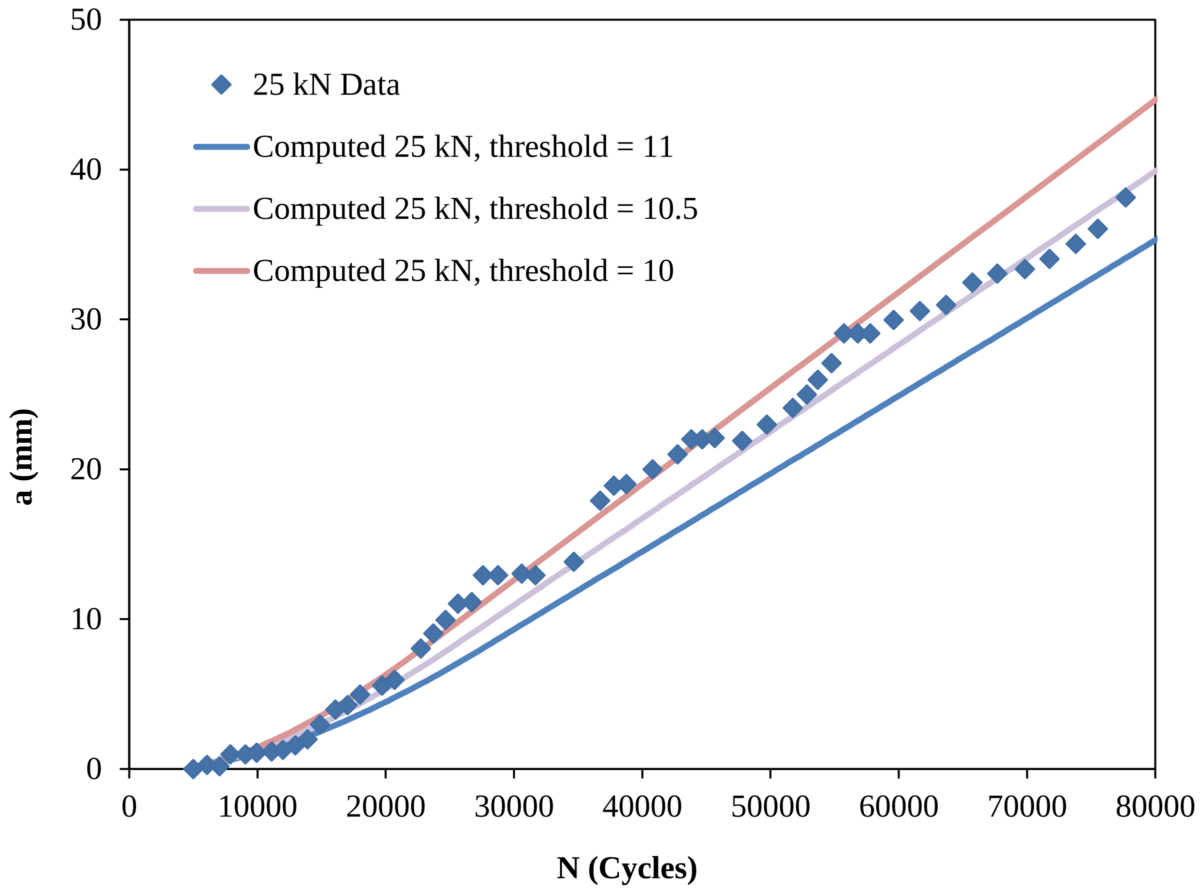

Figure 4.12 The measured [124] and predicted disbond histories for the double over-lap adhesively-bonded specimens.

Next, it was considered to be a valuable exercise to try and also predict the typical scatter observed in the crack growth histories of the adhesively-bonded double over-lap joints. As discussed in Section 4.2.2, it is considered that the variability in the observed disbond growth may be captured by allowing for variability in the threshold value, $\Delta\sqrt{G_{thr}}$. Unfortunately, Johnson and Butkus [128] did not undertake sufficient replicate fracture-mechanics tests to enable the scatter on their reported data to be accurately assessed. However, the epoxy-film adhesive FM73 is very similar in chemical and mechanical properties to the EA9628 epoxy-film adhesive discussed in Section 4.2.2. Thus, it is not unreasonable to apply the degree of scatter observed for this adhesive to the values of the threshold for the FM73 adhesive. This proposal leads to lower- and upper-bound values of $\Delta\sqrt{G_{thr}}$ of 10 and 11 $\sqrt{J/m}$, respectively, for the FM73 adhesive. Using these values of $\Delta\sqrt{G_{thr}}$ to account for the variability in the predicted crack growth. Thus, Figure 4.12 reveals that in these bonded joints the growth and associated variability of a disbond from small naturally-occurring material discontinuities in the FM73 adhesive may be accurately captured using the Hartman–Schijve variant of the NASGRO equation.

4.4.2 The bonded joint configurations from Pascoe et al.

The second problem studied involved disbond growth in the adhesive layer of an asymmetric joint consisting of an adhesively-bonded doubler as shown in Figure 4.13, where the adhesive was again the epoxy-film FM73 adhesive [118]. The test specimens consisted of a tapered aluminium-alloy 7175 adhesively-bonded to a 0.4 mm thick aluminium-alloy 7475 plate, which was bonded to a high static-strength (HSS) Glare plate. The aluminium-alloy 7475 plate extended beyond the edge of the patch. Two tests were performed under load control with an R-ratio of 0.1. The initial, naturally-occurring, disbond grew in the adhesive layer which bonded the aluminium-alloy 7475 plate to the Glare substrate and the length of the growing disbond was measured from the edge of the lower aluminium-alloy 7475 plate. For each test the length of the growing disbond was independently measured from both sides of the test specimen, so resulting in two sets of crack growth histories for each test. The maximum applied stress on the Glare plate employed for the cyclic fatigue tests was 150 and 170 MPa.

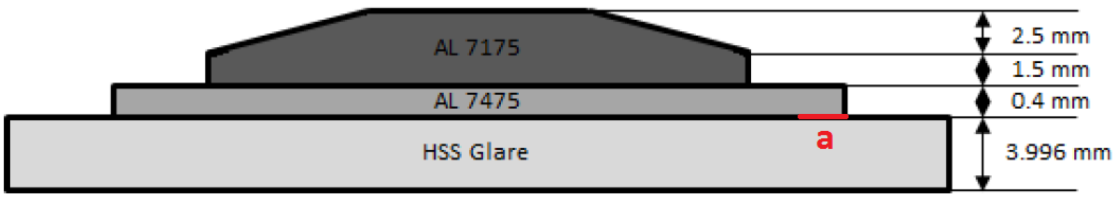

Figure 4.13 The asymmetric joint consisting of an adhesively-bonded doubler and the location of the disbond [118].

Pascoe et al. [118] used FEA with a remote stress on the Glare substrate plate of 160 MPa tensile stress to obtain the relationship between total SERR, G_{total}, and disbond length, a. The results are given in Figure 4.14. The analytical approximation for the total SERR versus disbond length relationship, G_{160}, is also shown in Figure 4.14. The SERR is proportional to square of remote load or stress, i.e. G linearly proportional to P^2 for linear elastic fracture mechanics. Therefore, total SERR of tests subjected to150 MPa and 170 MPa tensile stress was obtained via Equation (4.6).

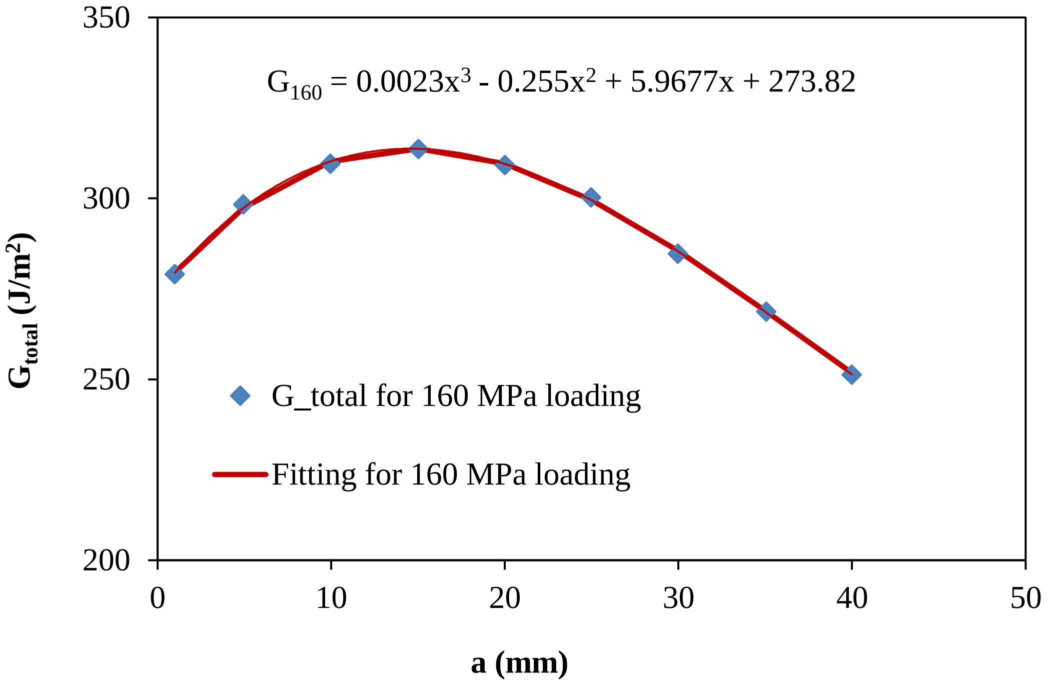

Figure 4.14 The calculated values of the total SERR as a function of the crack length for applied stresses of 160 MPa for the asymmetrical adhesively-bonded doubler joint [118] (The FEA results and the polynomial fitting).

$$G_{total} = \begin{cases} \left(\dfrac{150}{160}\right)^2 G_{160}, & for\ \sigma = 150 \\ \left(\dfrac{170}{160}\right)^2 G_{160}, & for\ \sigma = 170 \end{cases} \tag{4.6}$$

The Hartman-Schijve variant of the NASGRO equation together with the relationship between G_{total} and a, given in Equation (4.6), and the associated constants given in Table 4.2 (i.e. n = 2.3, D = 1.2 $\times 10^{-9}$ m/cycle and A = 2800 J/m^2) were used to compute the disbond growth histories associated with each of the tests, as explained in the procedure outlined above and in Figure 4.11. The measured and the computed histories of the disbond length versus the number of fatigue cycles are shown in Figure 4.15. As may be seen, the agreement between the measured and predicted crack growth histories, for both levels of applied maximum load, are in good agreement.

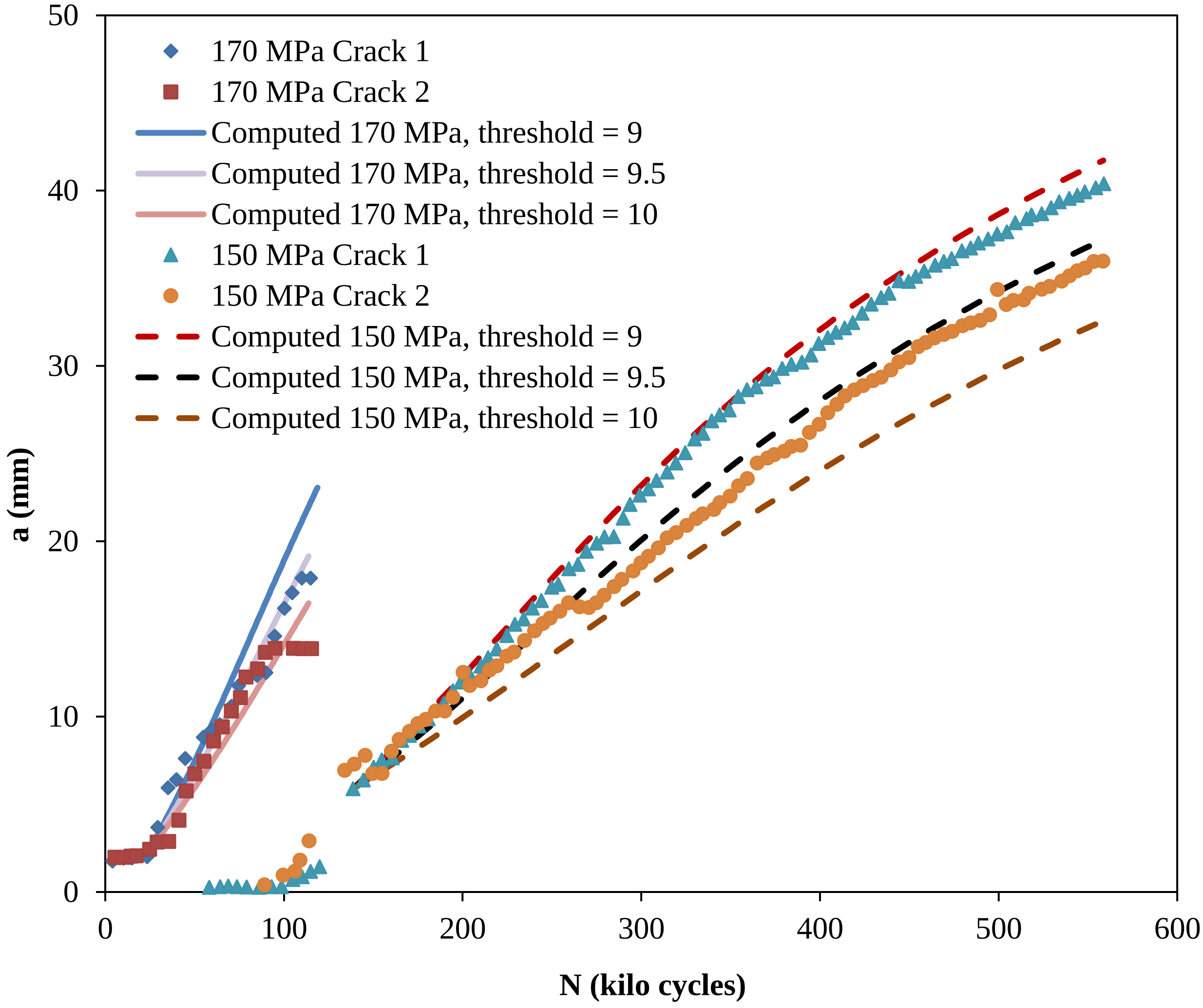

Figure 4.15 The measured [118] and predicted disbond histories for the asymmetric bonded joint consisting of an adhesively-bonded doubler.

As above, it was considered to be a valuable exercise to try and also predict the typical scatter observed in the crack growth histories of the asymmetrical adhesively-bonded doubler joints. As discussed in Section 4.2.2, it is considered that the variability in the observed crack growth may be captured by allowing for variability in the threshold value, $\Delta\sqrt{G_{thr}}$. Thus, lower- and upper-bound values of $\Delta\sqrt{G_{thr}}$ of 9 and 10 J/m^2 respectively for the FM73 adhesive were employed. Using these values of $\Delta\sqrt{G_{thr}}$ to account for the variability in the predicted crack growth. Figure 4.15 thus reveals that in these bonded joints the growth and associated variability of a disbond from small naturally-occurring material discontinuities in the FM73 adhesive may be reasonably accurately captured using the Hartman–Schijve variant of the NASGRO equation.

4.5 Summary

This Chapter has shown that the Hartman-Schijve equation can reasonably accurately compute the fatigue disbond growth associated with small naturally-occurring discontinuities in adhesively bonded joints. It also illustrates that like tests involving large artificial initial cracks, the scatter in the disbond growth histories may also be captured by allowing for small changes in the threshold term, $\Delta\sqrt{G_{thr}}$. Another finding of this Chapter is that the Hartman-Schijve equation has the potential to represent the crack growth of different mode mix with the critical energy release rate obtained from Mode I. These findings suggest that the Hartman-Schijve equation has the potential to address the 'slow growth' approach to certify adhesively bonded structures and adhesively bond repairs outlined in the US FAA Airworthiness Advisory Circular No: 20-107B [12]. These findings also raise the possibility of designing bonded composite repairs to metallic airframes to ensure that they meet the current damage tolerant design criteria.

Chapter 5

Experimental Studies In The Use Of Composite Patches To Repair Metallic Structures

All life is an experiment. The more experiments you make the better.

Ralph Waldo Emerson

5.1 Introduction

One challenge of managing airworthiness of operational aircrafts is the issue of aging aircraft. An example is the AP-3C Orion fleet which was first introduced to the Royal Australian Air Force (RAAF) fleet in 1978 and which as of late 2017 is still flying. In late 1998, the RAAF completed their negotiations with the US Navy, Canadian Forces and the Royal Netherlands Navy for a Service Life Assessment Program (SLAP). The goal of SLAP was to extend the service life of AP-3C to at least 2019 [129]. This service life extension is far beyond its original design life and requires highly sophisticated inspection and maintenance plan. When discussing the risk analysis associated with aging aircraft fleets the USAF [130] explained that:

“*The operational life of individual airframes is seldom equal to the design life of the fleet and that the life of an aircraft fleet tends to be determined more by its inherent operational capability and maintenance costs rather than by the number of flight hours specified at the design stage*.”

The need for different tools and methodologies for ab initio design and aircraft sustainment was also highlighted by Jones [55].

The use of adhesively bonded fibre reinforced composite patch to extend the service lives of metallic airframes was pioneered by the Australian DSTG in the 1970s [131, 132, 133, 134, 135, 136, 137, 138, 139, 140]. It is first applied in ensuring the safe operation of RAAF C130 Hercules aircraft and led DSTG to develope a number of successful boron fibre patch repairs on a range of RAAF aircraft, e.g. Mirage, F111, Orion, etc. According to Baker [136], adhesively bonded repair has following advantages compared to mechanical methods, i.e. riveting or bolting:

- Provide very efficient load transfer into the patch from the cracked component;
- Produce a sealed interface that can reduce the possibility of being exposed under corrosive environment;
- Since no additional holes are created, it does not introduce additional stress concentration into the structure.

However, one disadvantage of composites is their relatively low thermal expansion coefficient compared to metals such as aluminium alloys. This thermal mismatch can lead to problems of thermal residual stress, bending and distortion.

Unfortunately, there have been few studies on the effect of composite patch on small near micron initial cracks. To overcome this the present Chapter addresses cracks that were growing from two different crack initiators, viz: laser induced notches and corrosion pits. Both tests allowed the specimens to grow cracks from sub millimetre lengths to a length scales of the order of a mm. Once the cracks had reached this length scale they were patched on both sides with a boron epoxy patch. This test configuration was used to ensure that unwanted bending effects were eliminated. In this context it should be noted that when evaluating a repair to a wing skin of thickness ‘‘t”, it is common to test a specimen with a ‘‘2t” thickness and with patches on both sides [119].

5.2 Materials Selection

The unidirectional boron/epoxy 5521/4 prepreg was used as the patch material and its mechanical properties are shown in Table 5.1.

Table 5.1 Mechanical properties of unidirectional boron/epoxy 5521/4 prepreg [141, 142].

E_1 (GPa)	E_2 (GPa)	E_3 (GPa)	υ_{12}	υ_{13}	υ_{23}	G_{12} (GPa)	G_{13} (GPa)	G_{23} (GPa)
210	19	19	0.21	0.21	0.37	6.89	6.89	6.89

For the ease of field application the adhesive should ideally cure at relatively low temperature and pressure and should also provide a high level of bond durability with simple surface treatment procedures. The adhesive film used to bond the metallic adherend and boron patches was FM 300-2K which is the thickest variant of FM 300-2 series. FM 300-2 film adhesive is a 121 °C cure version of Cytec Engineered Materials' widely used FM 300 film adhesive. It delivers the same superior high temperature performance, toughness and stress/strain properties of FM 300 film adhesive without requiring a 177 °C cure cycle [143]. FM 300-2 series was specifically developed for co-cure and secondary composite bonding applications. Consequently, the residual stress caused by different thermal expansion rates of metal adherend and patches is reduced. The mechanical properties of FM 300-2K are shown in Table 5.2.

Table 5.2 Mechanical properties of FM 300-2K [143, 144, 145, 146].

E (GPa)	G (GPa)	υ	G_{IC} (J/m^2)	G_{IIC} (J/m^2)	Uncured nominal thickness (mm)
2.4	0.84	0.4	1300	5000	0.41

Prior to patching an additional layer of FM300-2K adhesive film (from Cytec-Solvay, Australia) was co-cured with the unidirectional boron/epoxy 5521/4 prepreg (from Textron, USA) in autoclave under the manufacture's specified cure cycle, i.e. 1 hour at 120°C with 450 kPa positive pressure. The DSTG standard surface treatment [119] was employed, viz:

1. An initial abrasion using 'Scotch Brite' (from 3M, Australia) pads;
2. Solvent clean with methyl ethyl ketone;
3. Grit blast;
4. Application of the coupling agent (a solution of the silane 'Silquest A-187').

The co-cured unidirectional boron/epoxy 5521/4 prepreg was assembled with adherend which has another layer of FM 300-2K film. The patched specimen was cured at 121˚C for 120 minutes. The entire patching process was completed by Fortburn, a contractor for DSTG.

The material chosen as the metallic adherend was aluminium alloy AA7050-T7451 which is one of the main aluminium alloys used in the F/A-18 Classic Hornet [147]. AA7050-T7451 is often used in highly stressed aircraft components such as upper wing surfaces, spars, stringers, pressure bulkheads, framework and carry-throughs [148]. Table 5.3 shows the mechanical properties of AA 7050-T7451.

Table 5.3 Mechanical properties of AA 7050-T7451 [149].

E (GPa)	υ	Yield Strength (MPa)	Ultimate Tensile Strength (MPa)	K_C (MPa√m)
71.7	0.33	469	524	32

5.3 Specimen Specification

5.3.1 Dog-bone shaped specimen with laser induced notches

The dog-bone shaped metallic adherends were cut from a 6.35 mm thick AA 7050-T7451 plate. The specimen had a working area that was 25 mm wide and 74 mm long, see Figure 5.1. Both sides of the adherend contained 29 columns (in the length direction) of small laser induced notches. The number of notches in any given column alternated between five and six. In each column, the notches were 4 mm apart and the distance between each column was 1 mm. This array of notches was located in the centre of the working section, see Figure 5.2. To minimize crack interaction the array was staggered as per Figure 5.2. Each laser induced notch has a typical dimension of 0.2 - 0.3 mm deep and 0.04 - 0.07 mm wide. A view of a typical laser notch is shown in Figure 5.3.

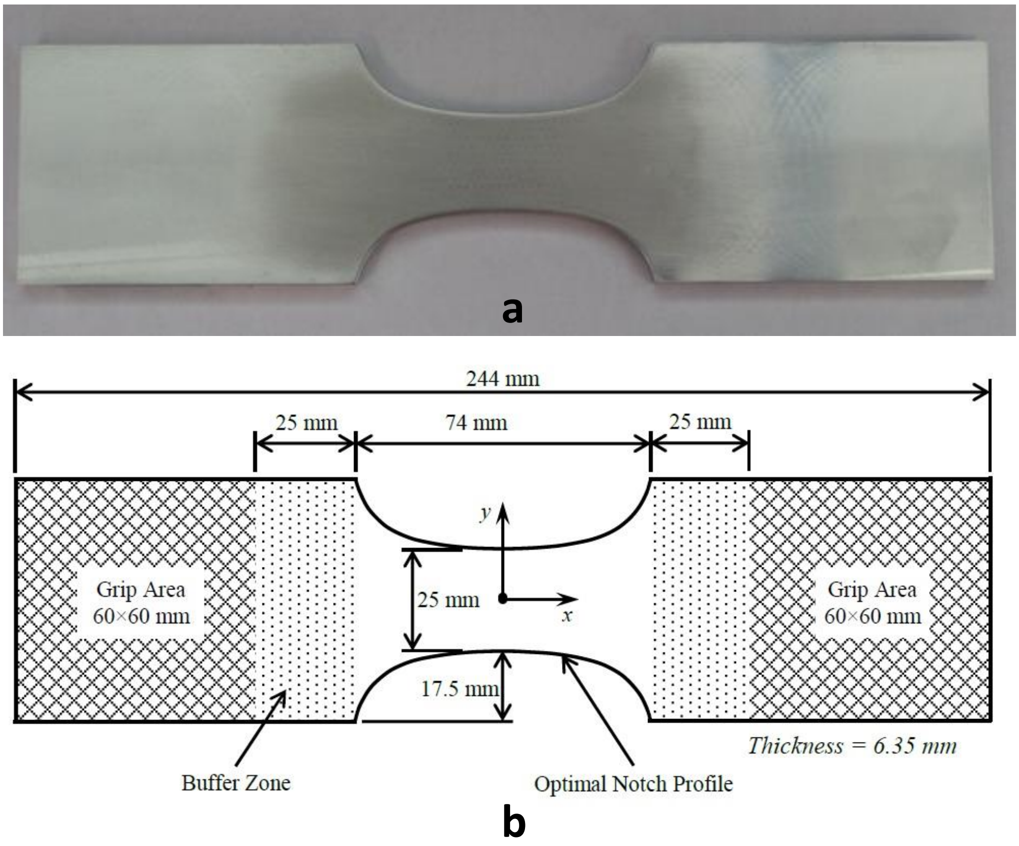

Figure 5.1 (a) Photograph and (b) sketch of the geometry of the metal adherend.

Figure 5.2 The staggered nature of the laser induced notches which can initiate fatigue crack(s).

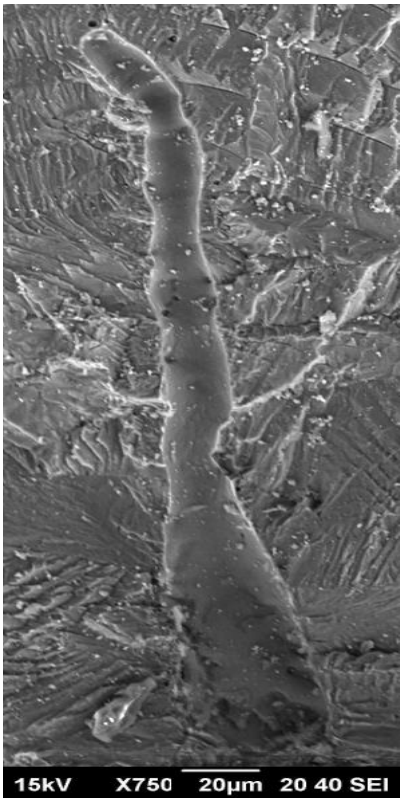

Figure 5.3 A scanning-electron microscope image of a typical laser induced notch and the subsequent fatigue crack radiating from this notch.

Twelve metallic specimens were prepared, namely Specimen 1 to 12. Two tests were performed without any patches. Six specimens had a 5-ply unidirectional boron epoxy patch on both sides. Two specimens had a 5-ply unidirectional boron patch on both sides. In these two specimens a 6 mm disbond that was created by locating a teflon film in the centre of the working area, see Figure 5.4. The final two specimens tested had a 2-ply boron epoxy patch on both sides. The nominal thickness of each boron epoxy ply was 0.13 mm. There was 3 mm drop off for each ply at both ends of the patch, see Figure 5.4. The patch was rectangular and had the dimension of 100 mm long and 25 mm wide. This was done to fully cover the narrowest working area, see Figure 5.4. The details of the various patch configuration is shown in Table 5.4. A photograph of composite patched dog-bone specimen is presented in Figure 5.5.

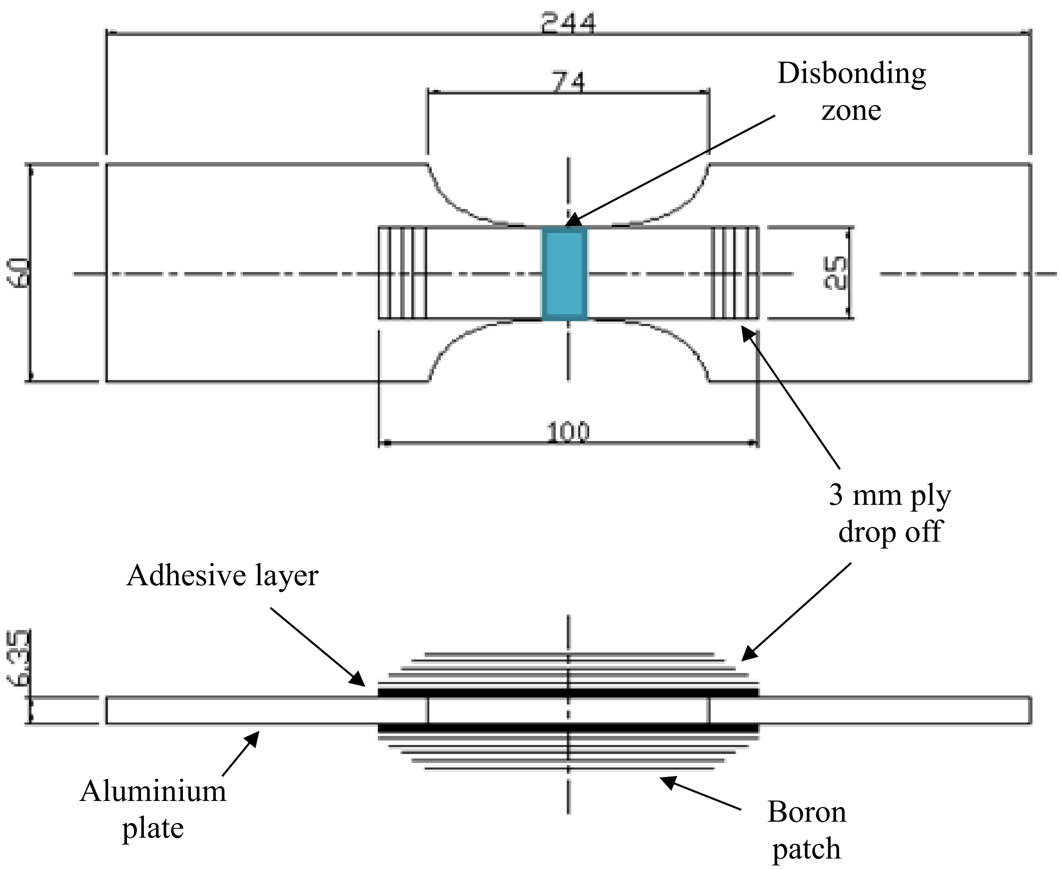

Figure 5.4 Schematic diagram of dog-bone patch system.

Table 5.4 List of specimen configerations.

Specimen number	Number of plies	Patch thickness (mm)	Disbonding zone
1	N/A	N/A	N/A
2			
3	5	0.65	N/A
4			
5			
6			
7			
8			
9	5	0.65	6 mm wide
10			
11	2	0.26	N/A
12			

Figure 5.5 The dog-bone specimen after patching. (The brown-coloured material is the spew from the FM300-2K adhesive. The green-coloured layer is a film that limits the adhesive spreading out from the bonded area.)

5.3.2 Dog-bone shaped specimen with corrosion pits

To continue this study, another test program was performed on dog-bone shaped specimens which contained corrosion pits. In these specimens the thickness of the metal adherend was 11 mm and the narrowest width of the working section was 42 mm, see Figures 5.6 and 5.7. Both sides of the specimen contained 13 columns (in the length direction) of surface corrosion pits which were generated by exposure of the surface to 3.5% NaCl solution droplets, see Figure 5.8. The number of pits in any given column alternated between five and six. In each column the corrosion pits were approximately 7 mm apart and the distance between each column was approximately 7 mm. This array of pits was located in the centre of the working section, see Figure 5.8. The size of corrosion pit which initiated the "lead crack" was approximately 0.6 mm wide and 0.1 mm deep. A typical corrosion pit is shown in Figure 5.9.

Two metallic adherends were prepared, namely Specimens 13 and 14. Both of them were patched on both sides with a 5-ply unidirectional boron epoxy patch. Each boron epoxy ply was approximately 0.13 mm thick. As previously the boron epoxy patch had a 3 mm drop off per ply, at both ends. This was the same as the laser notched specimen. The shape of the patch was rectangular with dimension of 160 mm long and 42 mm wide. The shape of the patch was chosen so as to could fully cover the narrowest working area, see Figure 5.7c.

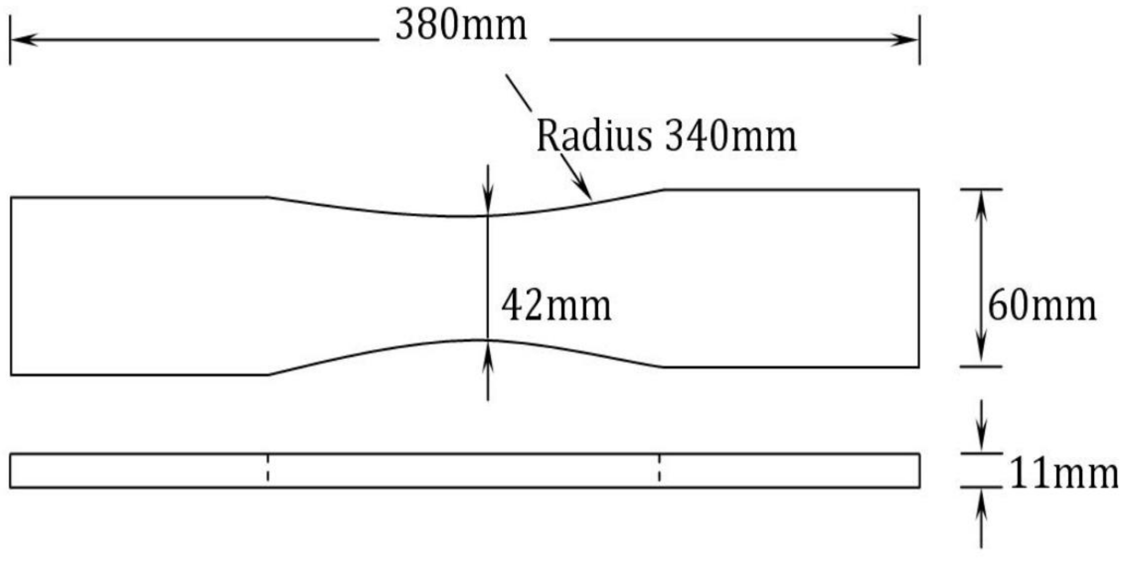

Figure 5.6 The geometry of adherend of corrosion pits specimen (Not to scale).

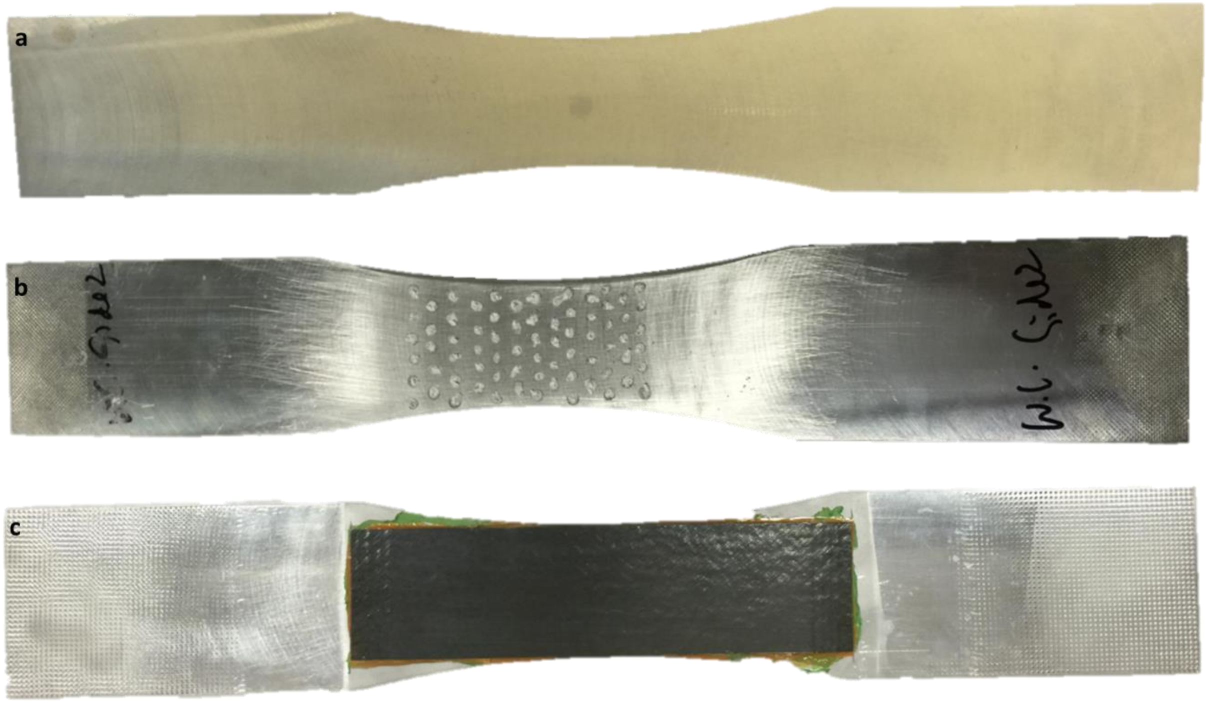

Figure 5.7 Photos of (a) the AA 7050-T7451 adherend, (b) the adherend with corrosion pits, (c) the corroded specimen with boron patches.

Figure 5.8 Top: NaCl solution droplets applied on metal adherend. Bottom: The array of dried corrosion pits on the surface of the metal adherend.

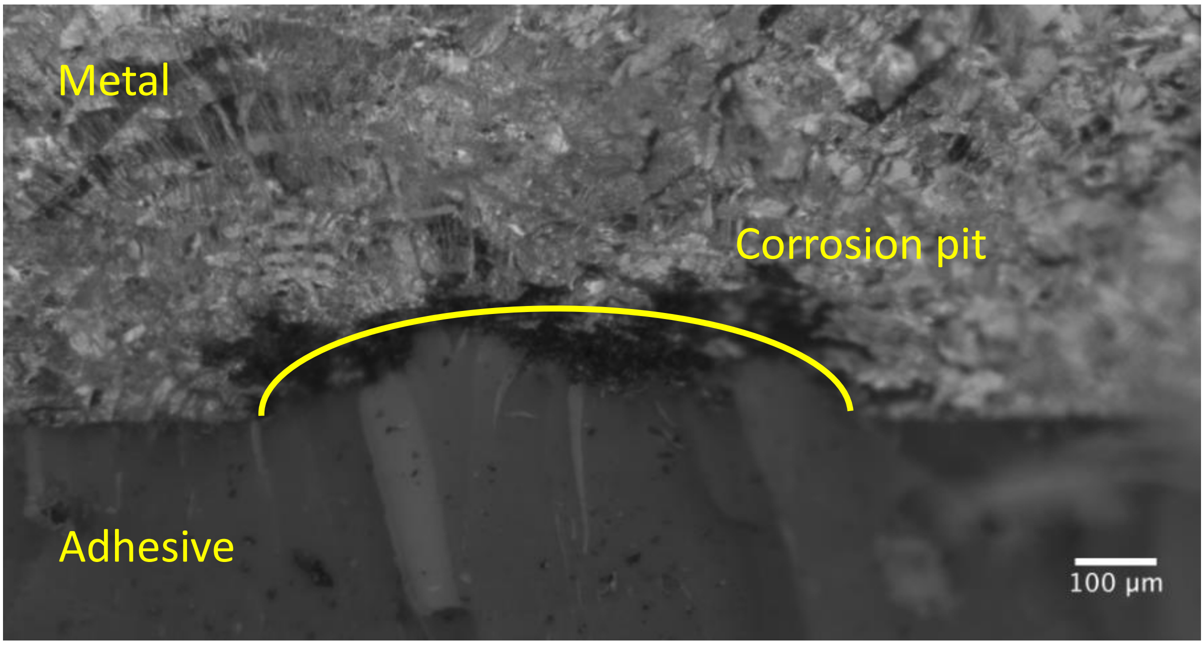

Figure 5.9 A typical corrosion pit.

5.4 Test Procedure

5.4.1 Dog-bone shaped specimen with laser induced notches

A MTS 100 kN hydraulic fatigue testing machine was used to test the laser notched dog-bone specimens. The frequency of the test was fixed as10 Hz and the test was performed under load control. Each specimen was subjected to cyclic loading with a repeated load block that was designed so as to mark the fracture surface with a repeating pattern. The loading block had 300 cycles at R = 0.1 and 10,000 cycles at R = 0.8, see Figure 5.10. Load cycles for both R ratios had the same peak load of 50 kN. This enabled fatigue marker bands to be seen on the surface of the fatigue crack. These marker bands enabled quantitative fractography to be used to determine the crack growth history.

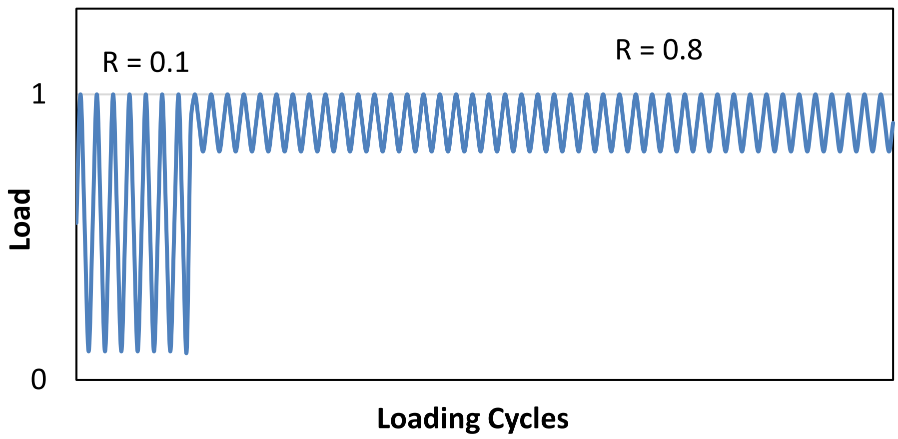

Figure 5.10 A typical block loading spectrum.

Prior to patching the laser notched specimens were subjected to fifty-eight load blocks. This was done so as to grow fatigue crack(s) from the laser induced discontinuities to a scale of approximately 1 mm. To help distinguish between the marker bands before and after patching, just before patching each specimen was subjected to an additional 900 cycles of R = 0.1. After that, specimens were subjected to the same load block with reverse loading sequence, i.e. 10,000 cycles at R = 0.8 first and then 300 cycles at R = 0.1. Consequently, the different fatigue patterns between R = 0.1 and R = 0.8 could be used to determine the crack size at any point in the test. Table 5.5 presents details of the load spectrum used for laser notched dog-bone specimens.

Table 5.5 Details of the block load spectrum used for the Laser notched dog-bone specimen.

Peak Load	50 kN	
Load Spectrum	Up to 58 Blocks	300 cycles at R = 0.1
		10,000 cycles at R = 0.8
	900 cycles at R = 0.1	
	Since Blocks 59	10,000 cycles at R = 0.8
		300 cycles at R = 0.1

Thermoelastic stress analysis (TSA) was employed both as an NDI tool to identify crack growth as well as a means to identify patch delamination or disbond. In this test the CEDIP infrared camera system was used, see Figure 5.11. The relationship given in [150] between the measured infra-red signal and the surface stress field was used to convert the infra-red signal to stresses on the surface of the patch.

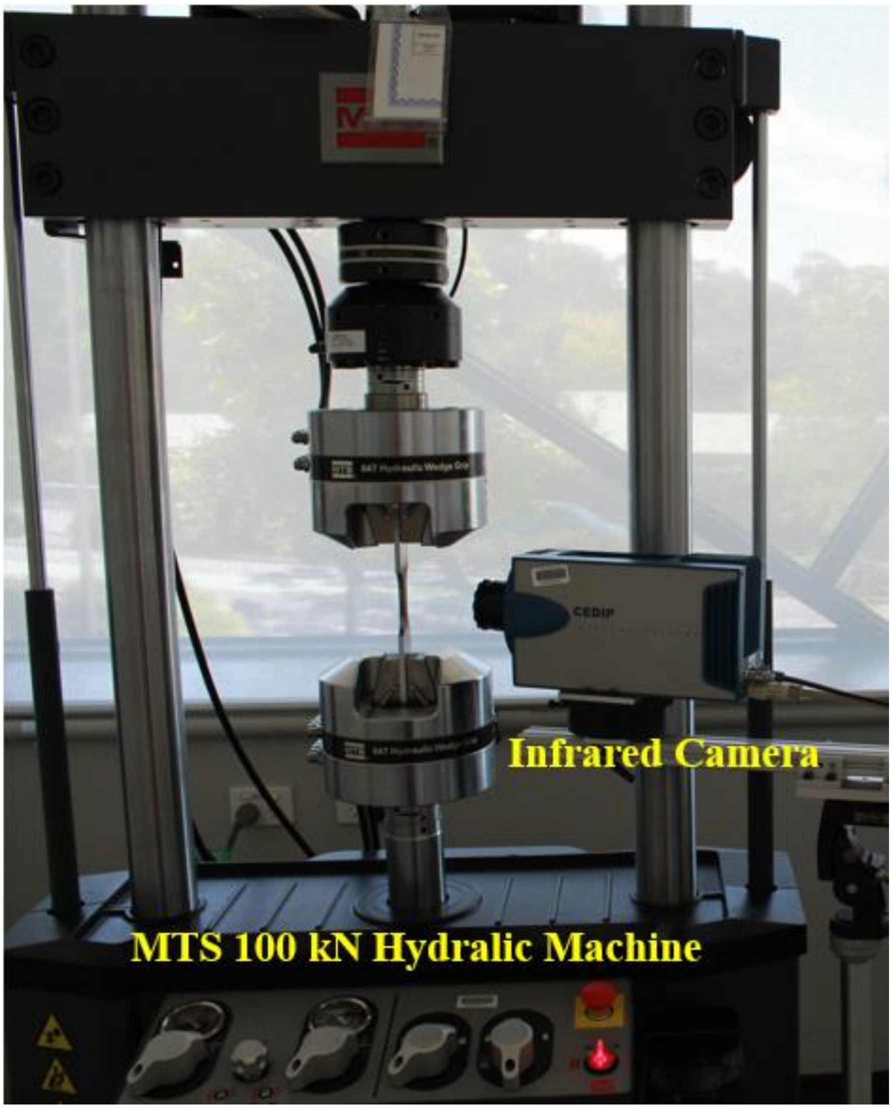

Figure 5.11 Laser notched dog-bone specimen test set up with Infrared camera.

5.4.2 Dog-bone shaped specimen with corrosion pits

The corroded dog-bone specimens were tested under a similar block loading spectrum to that described above for the laser notched dog-bone specimens, except that the peak load was increased to 148 kN. The increase in the load meant that the corroded dog-bone specimens were tested on a MTS 500 kN hydraulic fatigue testing machine rather than on the 100 kN machine. The frequency of the test was 5 Hz and the test was performed under load control. In this test the number of load blocks prior to patching was twenty. This was due to large size of the corrosion pits, which were typically approximately 0.6 mm wide and 0.1 mm deep. The load spectrum used for the corroded dog-bone specimens is detailed in Table 5.6.

Table 5.6 Detail of the marker load blocks used in the corroded dog-bone specimen test.

Peak Load	148 kN	
Load Spectrum	Up to 20 Blocks	300 cycles at R = 0.1
		10,000 cycles at R = 0.8
	900 cycles at R = 0.1	
	Since Blocks 21	10,000 cycles at R = 0.8
		300 cycles at R = 0.1

5.5 Test Results and Analysis

A summary of the fatigue life of the various specimens is shown in Table 5.7. Once the specimens failed they were taken to DSTG for photography and for quantitative fractography. The number of major crack(s) found in each specimen is presented in Table 5.7. The major cracks which includes the lead crack are the cracks that have grown to a significant scale and contributed to the final failure of the specimen.

The crack depth history was determined using the marker bands produced by the repeating block loading spectrum. A typical example that illustrates how the measurement of the crack depth history, in this case for Specimen 11, is shown in Figure 5.12. The white dots indicated the locations where the crack depth was measured. In this specimen the fatigue crack propagated as a semi-elliptical shaped crack until it reached the side edge and became a corner crack. The corner crack then grew through the thickness of the aluminium adherend. It subsequently rapidly propagated through the repaired specimen and resulted in the complete failure of the specimen.

Table 5.7 Fatigue test results of specimens.

Specimen type	Specimen	Life in cycles	Life in blocks	major cracks
No Patch	1	865319	84	1
	2	578728	56	1
5-ply patch	3	2040358	198	1
	4	989716	96	2
	5	1473895	143	1
	6	2040276	198	1
	7	2174387	211	4
	8	1104394	107	2
5-ply patch with 6 mm disbond	9	1772657	172	1
	10	1082332	105	1
2-ply patch	11	1213914	118	1
	12	1381225	134	3
Corrosion pit specimens	13	679663	66	5
	14	720944	70	1

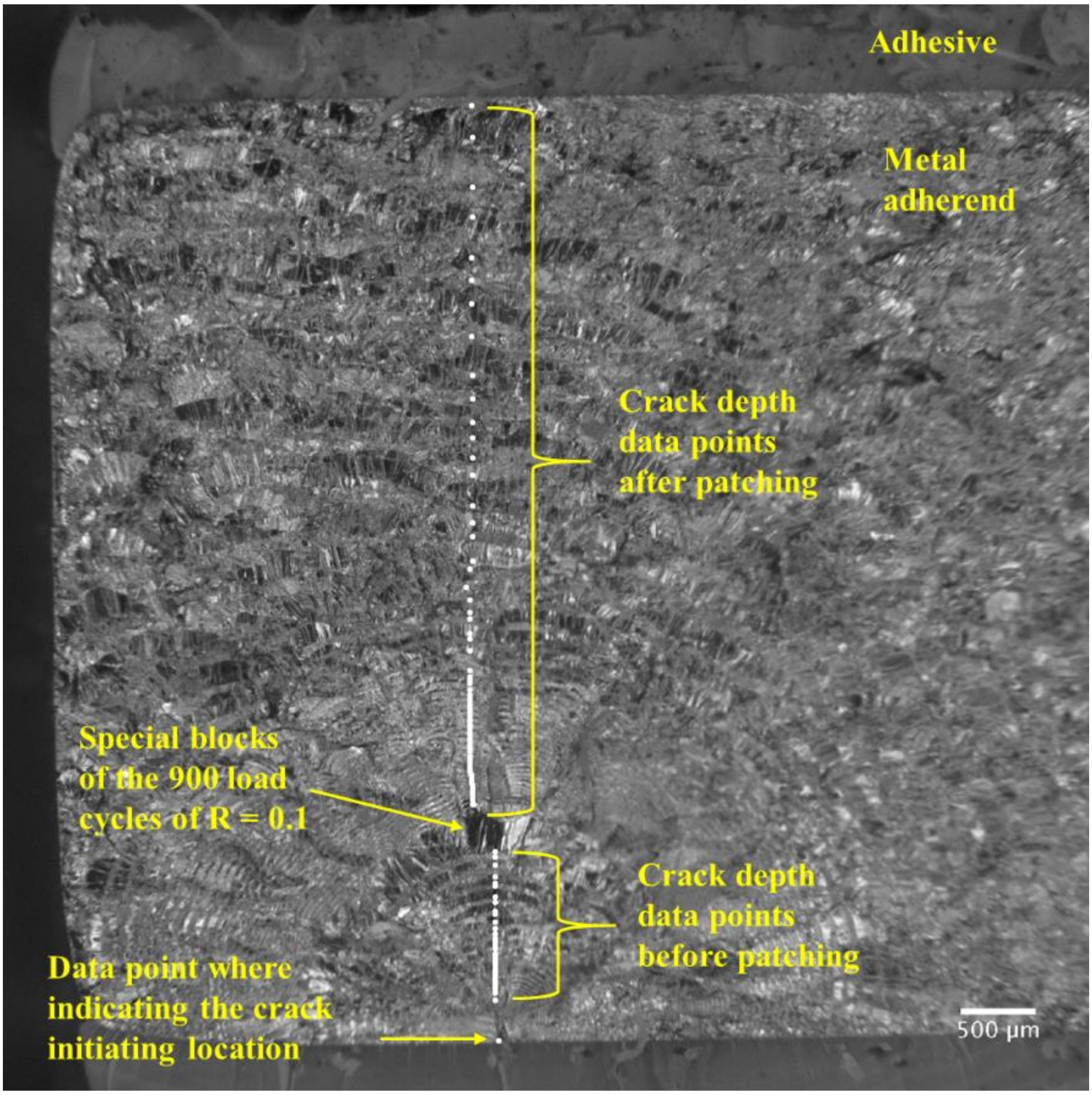

Figure 5.12 The quantitative fractography of laser notched specimen 11.

The fatigue crack growth histories associated with the various specimens are illustrated in Figures 5.13-17. The boundary before and after patching was easy to identify. This was due to the special maker band produced by the 900 cycles of R = 0.1, see Figure 5.12. Furthermore, the slope of crack propagation curve decreased after boron patches were applied. The measurement of the crack depth histories did not go beyond 4 mm for laser notched specimens or beyond 5 mm for corrosion pit specimens as after these depths the crack(s) grew too fast and under microscope the marker bands became too rough to identify.

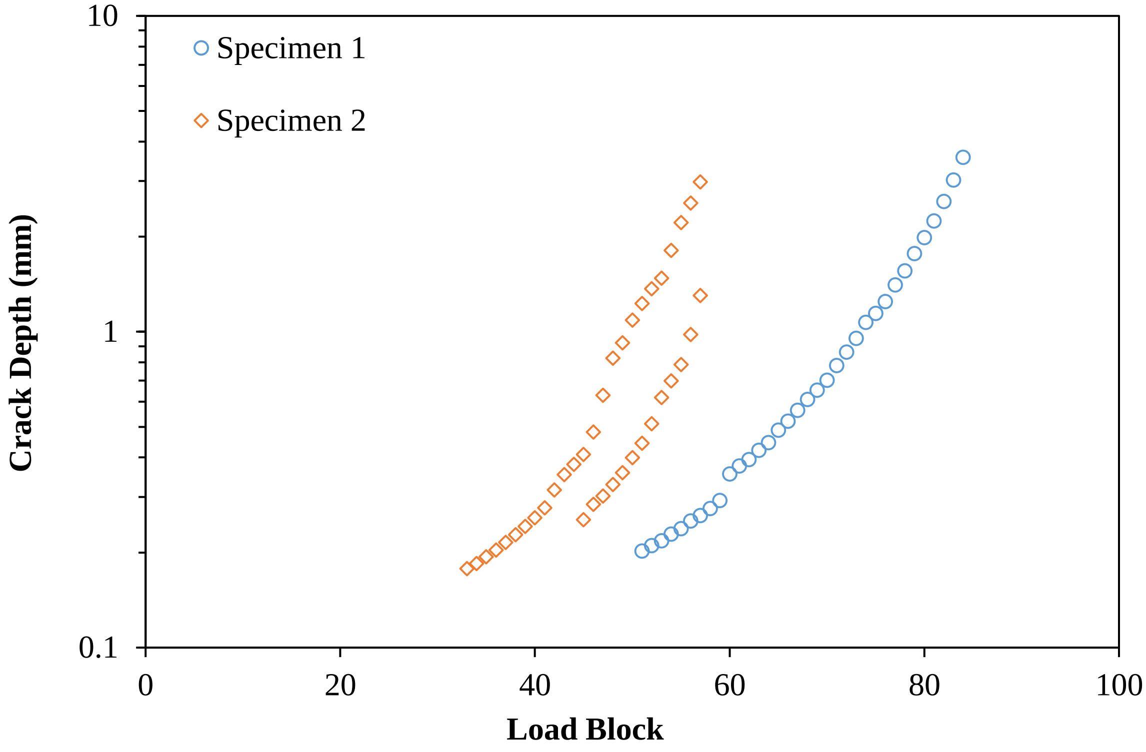

Figure 5.13 Crack depth histories for non-patched laser notched specimens.

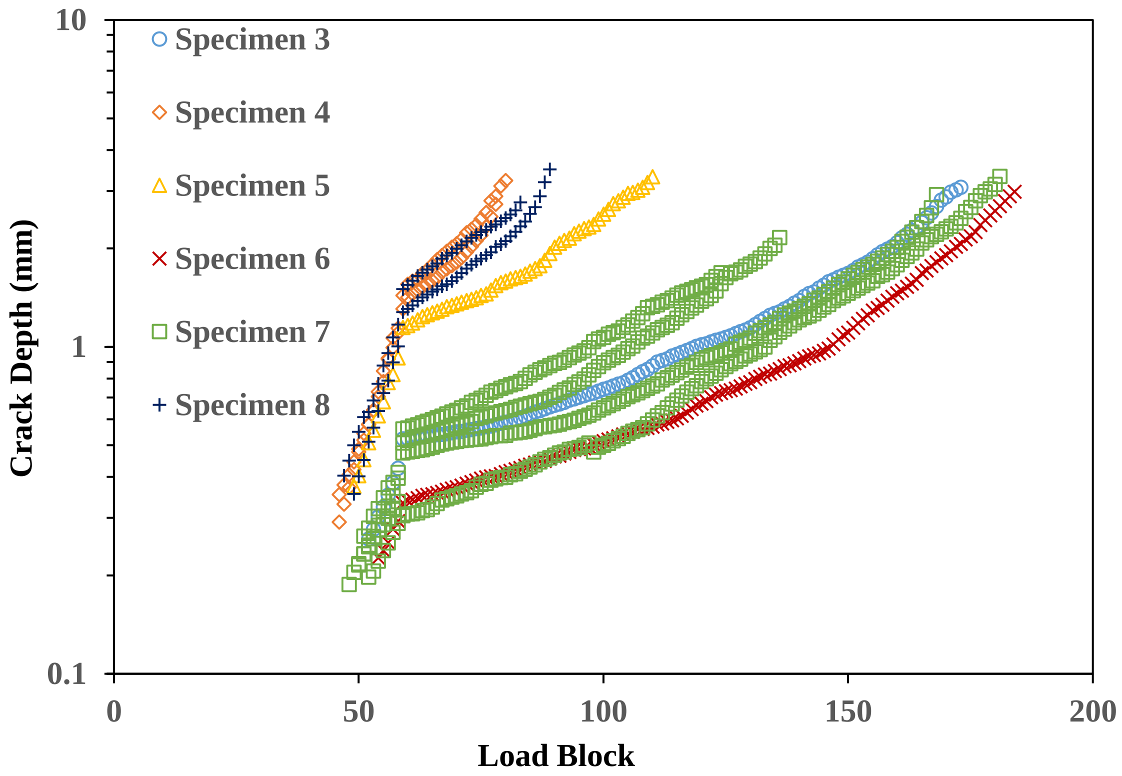

Figure 5.14 Crack depth histories for 5-ply patched laser notched specimens.

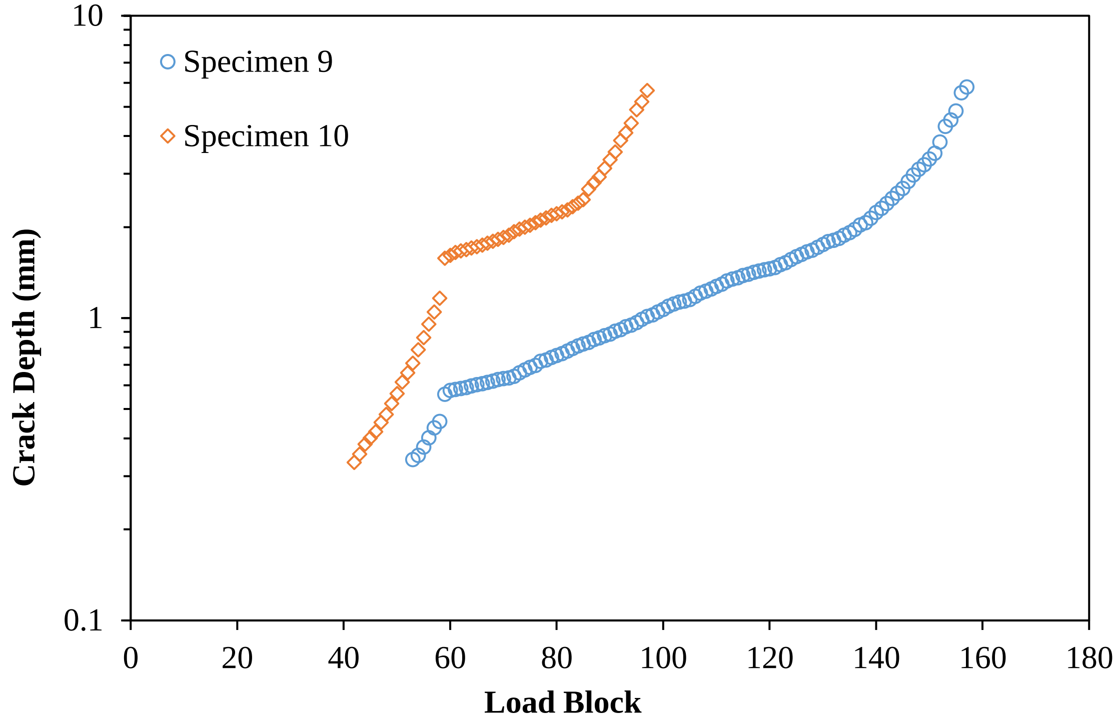

Figure 5.15 Crack depth histories for 5-ply patched laser notched specimens with 6 mm disbonding zone.

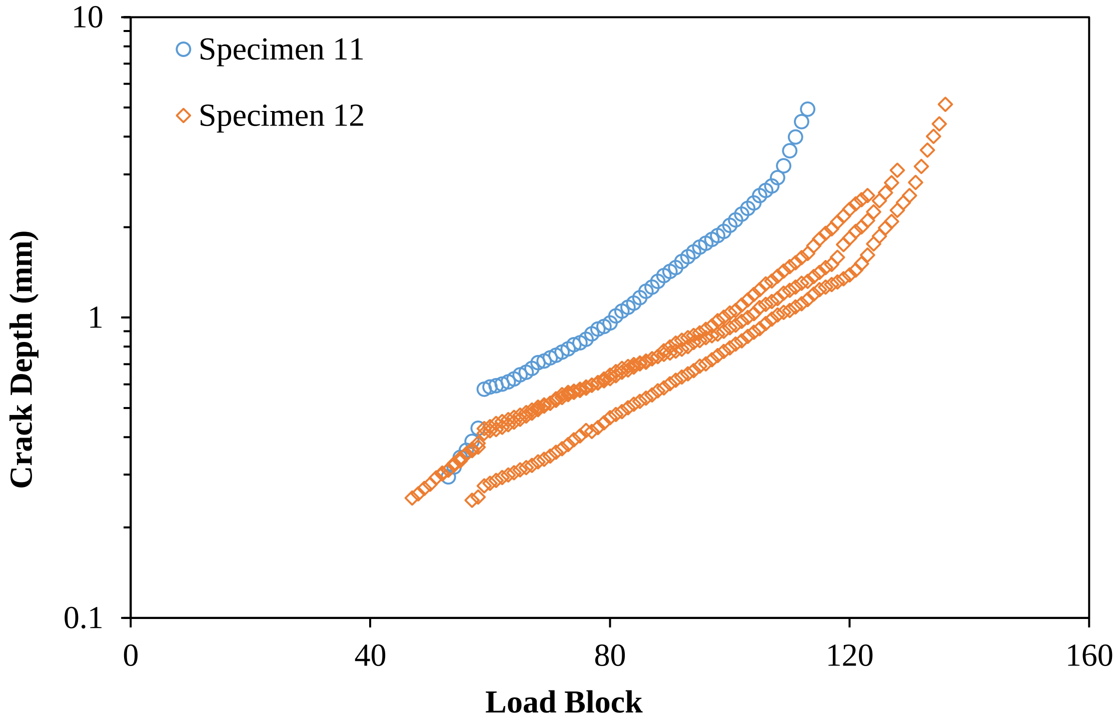

Figure 5.16 Crack depth histories for 2-ply patched laser notched specimens.

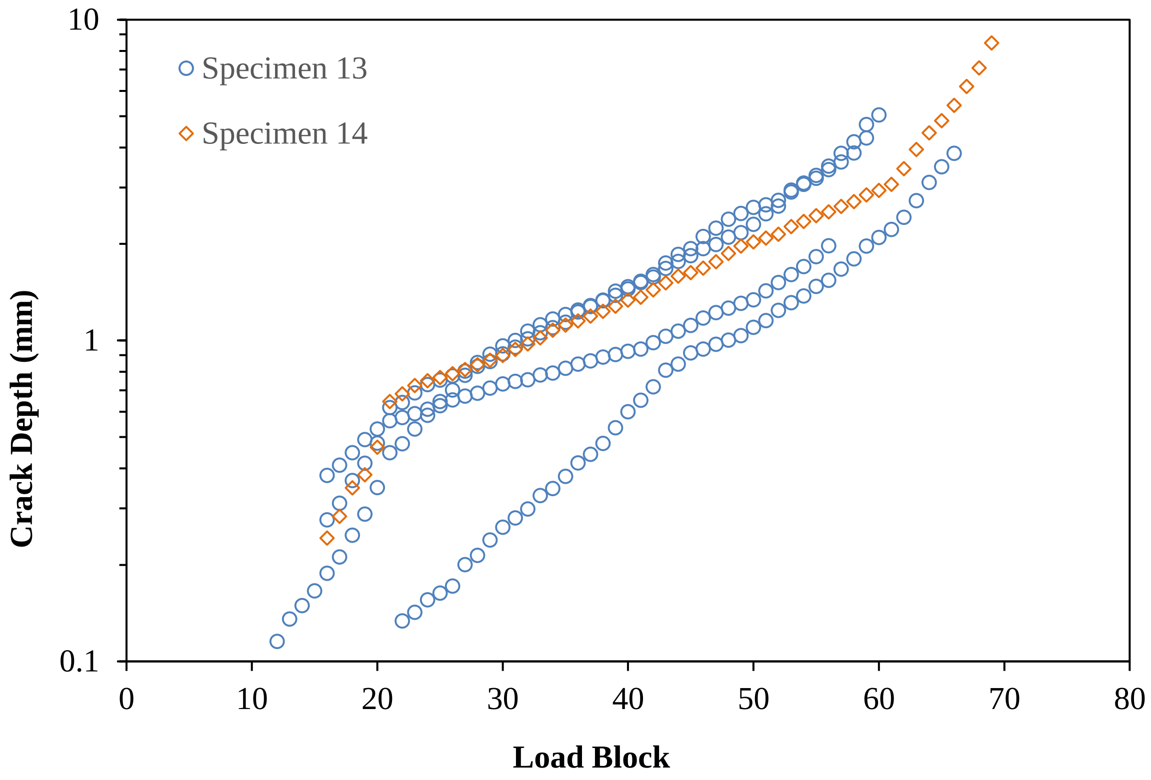

Figure 5.17 Crack depth histories for 5-ply patched corroded specimens.

5.5.1 Scatter

An important problem for fatigue is that, for nominally identical specimens, there can be significant scatter in the crack growth histories particularly those associated with cracks that grow from small sub mm material discontinuities [126]. Virkler et al. [125], Stelzer et al. [151] and Hafiz et al. [127] performed cyclic fatigue tests on metal, fibre reinforced composites and adhesive bonded joints respectively. They used identical specimens and performed tests under the same procedures. However, in each case the growth rates exhibited significant scatter. Figure 4.1 illustrated the relatively large scatter for 9 mm long initial cracks in the aluminium alloy AA2024-T3. In metals the scatter associated with small naturally occurring cracks is even generally greater than that seen for long initial cracks [152]. Hence, it was essential to account for the scatter associated with these sub millimetre cracks.

The idea of creating an array of laser induced notches, or corrosion pits, on specimens was to investigate the scatter associated with short cracks, i.e. less than 1 mm, after patching. The majority of those artificial discontinuities did not grow. Figure 5.18 shows the fatigue life for specimens with different configurations. Figure 5.19 shows the crack depth of lead cracks prior to patching for Specimen 3 to 14 (Specimens 1 and 2 did not have patch). The crack depth of laser notched specimens prior to patching varied between 0.33 mm and 1.44 mm. For the corroded specimens crack depth of prior to patching varied between 0.45 mm and 0.58 mm.

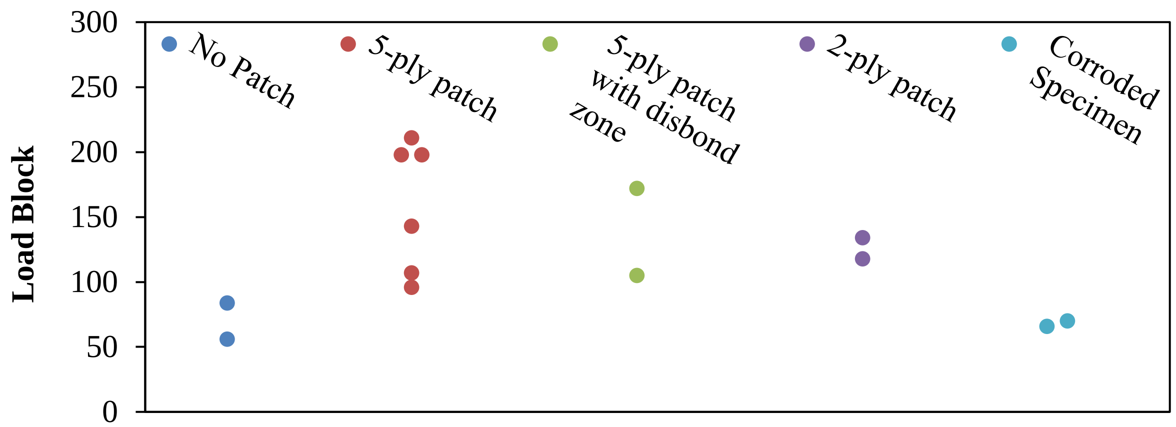

Figure 5.18 Fatigue life for specimens with different configurations.

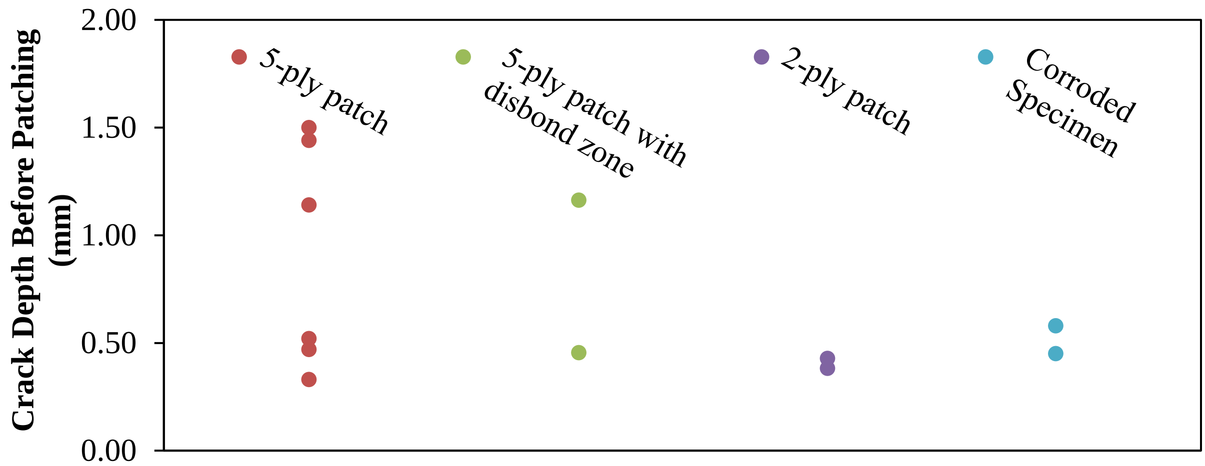

Figure 5.19 The crack depth of lead cracks before patching for Specimen 3 to 14.

If the question of scatter is not taking into consider, Figure 5.20 suggests that for specimens without a patch the life of a specimen was dominated by the time spent in the short crack regime, i.e. when the crack was smaller than approximately 1 mm. For laser notched specimens, almost 90% of the total life was consumed in growing the lead crack to a 1 mm deep fatigue crack.

For the patched laser notched specimens the average percentage of the life when the lead crack was 1 mm deep were approximately 56% for a 5-ply patch, 55% for a 5-ply patch with a disbonded zone and 74% for a 2-ply patch. Increasing the thickness of of the patch extended the fatigue life of the specimens. The disbonding zone appears to have had little influence on the life of specimens.

For the patched pre-corroded specimens the average percentage of life spended in growing to a 1 mm crack was approximately 46%. However, drawing cnclusion about the percentage of the life is dangerous with such small number of specimens

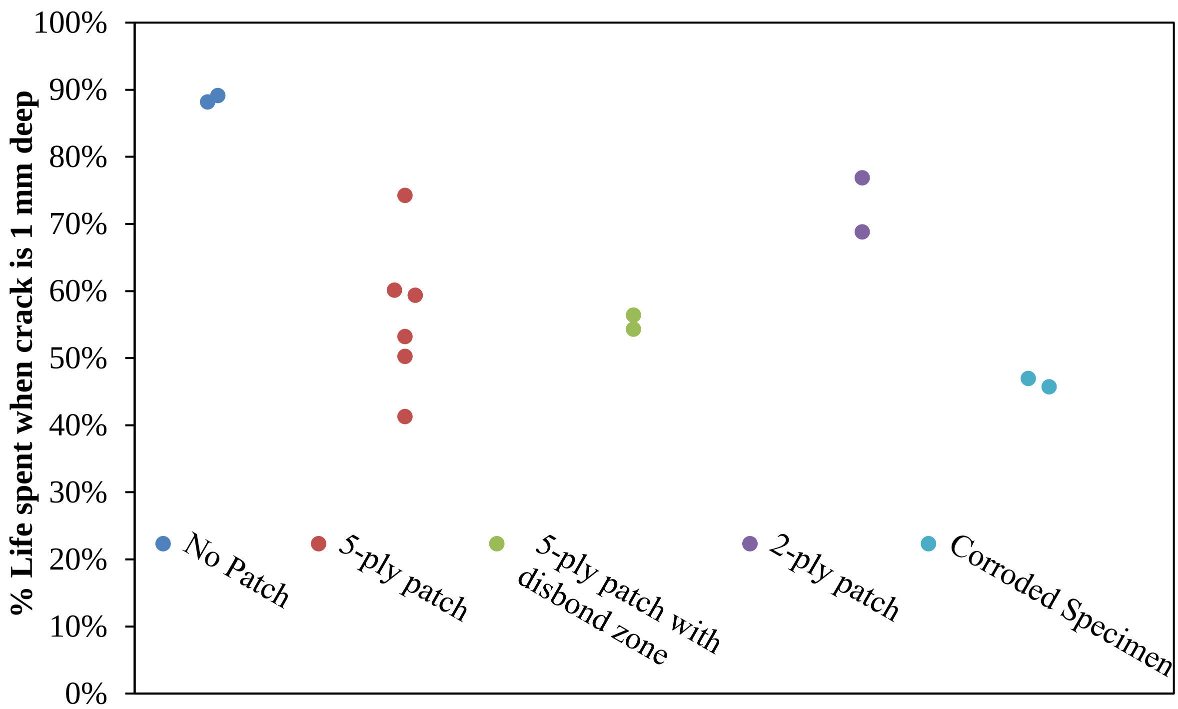

Figure 5.20 Percentage of life when crack is 1 mm deep.

Although there were other small fatigue cracks that arose and grew they did not appear to significantly contribute to the final failure of the specimen.

5.5.2 Fracture surface analysis

Examining the fracture surfaces of the specimens revealed that the most specimens had only a single major crack. That said there were specimens that contained between two to five significant cracks. For example specimens 1 and 2 had two obvious cracks, see Figure 5.21. However, in both instances one crack was significantly bigger than the other.

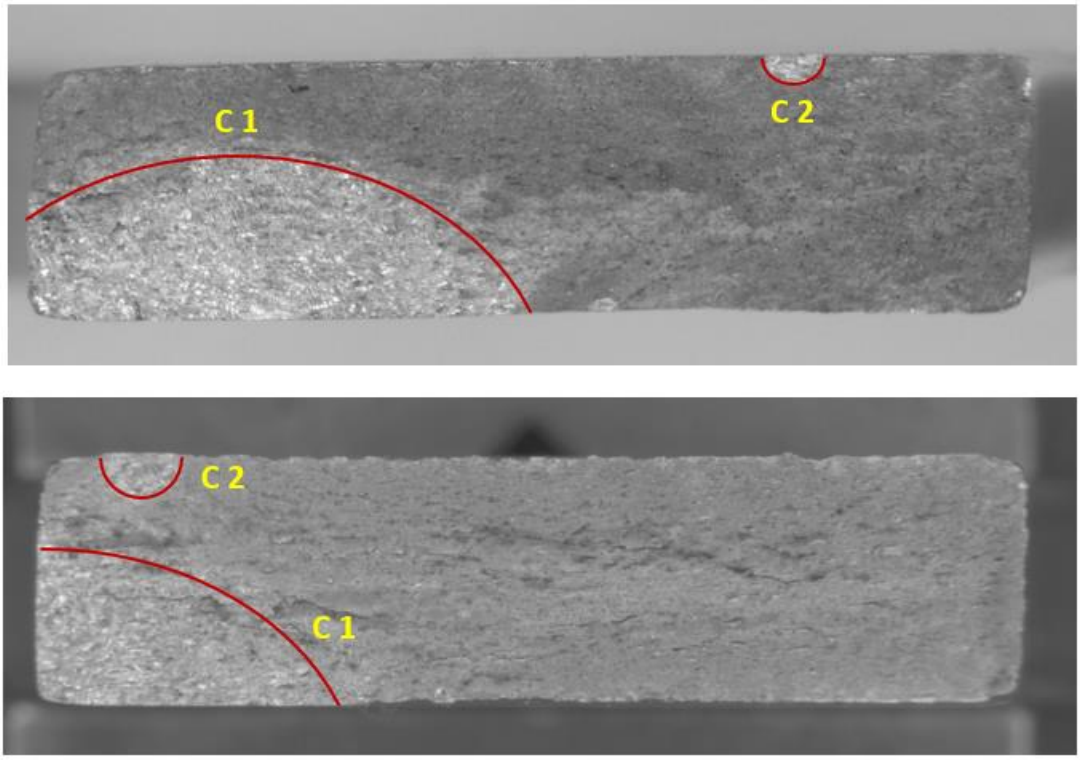

Figure 5.21 Fracture surfaces of Specimen 1 (top) and 2 (bottom). C represents Crack.

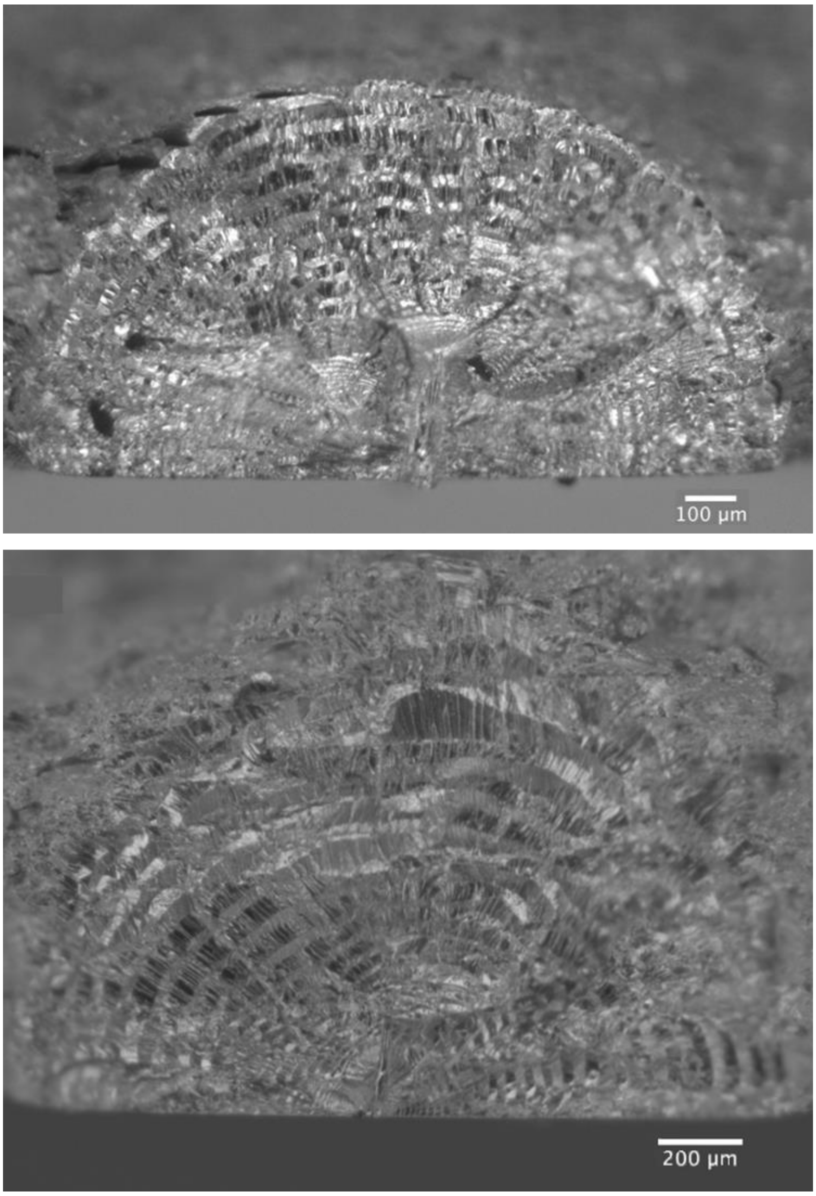

Figure 5.22 Crack 2 in Specimen 1 (top) and Crack 2 in Specimen 2 (bottom).

As shown in Table 5.7, Specimens 3, 5, 6, 9, 10, 11 and 14 also had one dominant fatigue crack. These dominant cracks propagated through the entire thickness of the specimen. If the initial location was near an edge the crack first grew to become a corner crack, see Figure 5.23. It then grew to become a through crack. Specimens with 2-ply patches failed immediately after the crack became a through-the–thickness crack. Specimens with 5-ply patches did not, see Figure 5.23. However, once a crack has become a though crack the remaining life is a small fraction of the total fatigue life.

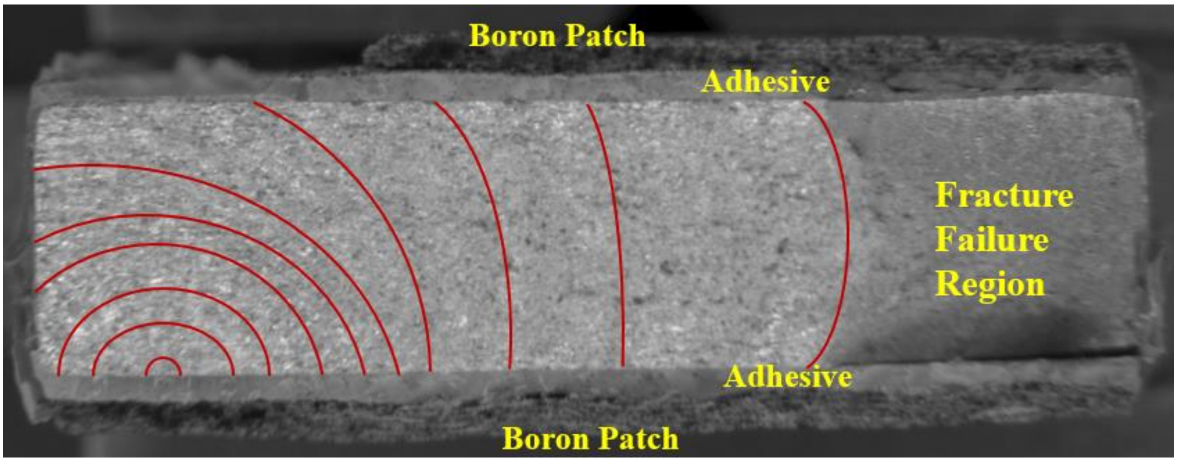

Figure 5.23 The path of crack growth on Specimen 6. Red lines are crack path.

For those specimens with two or more dominant cracks, i.e. Specimens 1, 2, 4, 7, 8, 12 and 14, fatigue cracks would first join to form a through crack. The crack then propagated rapidly throughout the specimen horizontally, see Specimen 8 in Figure 5.24. The fracture surface of Specimen 8 contained two major cracks which grew from opposing sides. One crack initiated at the middle of one surface and initially grew as a near semi-elliptical surface crack. The other major crack initiated close to a side edge and grew to a corner crack. These two cracks merged together just prior to failure.

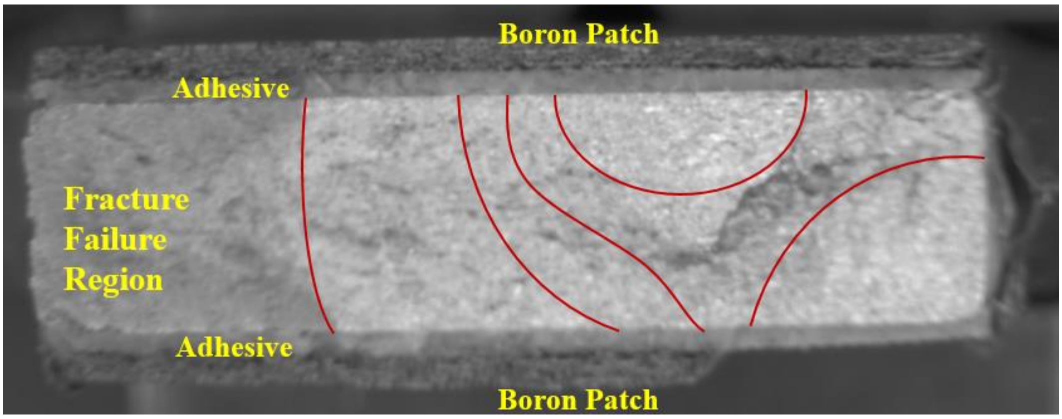

Figure 5.24 The path of crack growth on Specimen 8.

Another interest finding was that for specimens with a 6 mm disbond, the failure was not associated with the metal beneath the disbond, see Specimen 10 in Figure 5.25. This could explain why for the 5-ply patched specimens the fatigue performances were similar for specimens with or without disbonding zone. Consequently, the disbonded zone had limited influence on the fatigue crack growth.

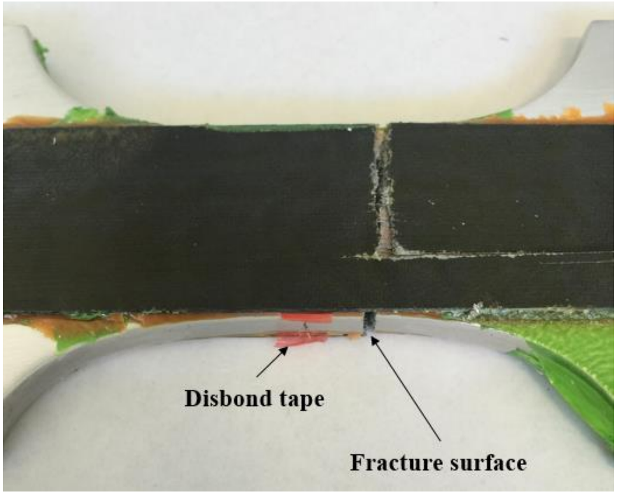

Figure 5.25 The photo of working area in Specimen 10.

5.5.3 Patch failure modes

Adhesively bonded structures can exhibit four different fracture failure modes [10]:

- Adherend failure: failure in metallic adherend or fibre failure in the composite patch
- Adhesive failure: disbond between interface of two different materials
- Cohesive failure: failure within the adhesive layer
- First ply failure: Interlaminar failure between the first and second plies in the patch [141].

Adherend failure is often caused by the defects induced during manufacturing or during operational usage, surface pitting during operation or by inappropriate design. Adhesive failure is likely to be the result of poor surface treatment or by the adhesive stress exceeding their fatigue allowable. For cohesive failure in this experiment, the surface typically appeared rough and contained voids, see Figure 5.26.

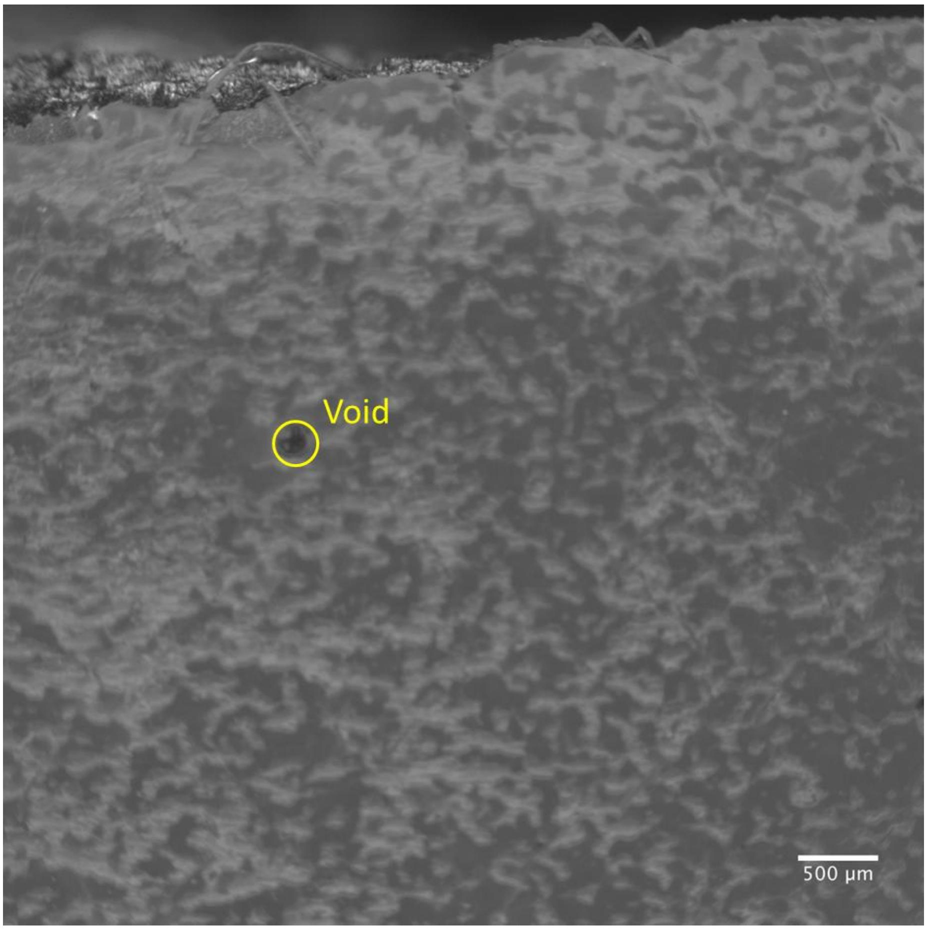

Figure 5.26 Surface of bondline failure in Specimen 5.

Many researchers [153, 154, 155] have reported that fibre reinforced composites can experience failure at the first ply which is adjacent to the adhesive layer. In another word, the first ply of composite remains attached to the adhesive film and the rest part of the patch delaminates from it. In this experiment the term, first-ply failure, will be used for both the adhesive failure and for what has been termed (above) first-ply failure. This is because it was very difficult to distinguish the boundary between the composite patch and the adhesive film. All four modes of patch failure were encountered in this test program. Furthermore, three laser notched specimens also experienced a combination of first-ply failure and cohesive failure, see Figure 5.27. Details of patch failure modes are summarised in Table 5.8.

Table 5.8 Summary of patch failure mode for laser notched specimens.

Patch configuration	Adherend failure	Cohesive failure	First-ply failure	First-ply failure & Cohesive failure
5-ply	1	1	1	3
5-ply with disbond			2	
2-ply	2			
Corroded Specimen	1		1	

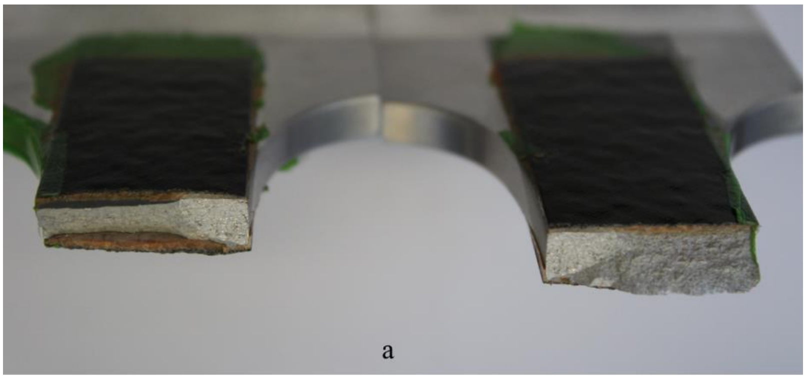

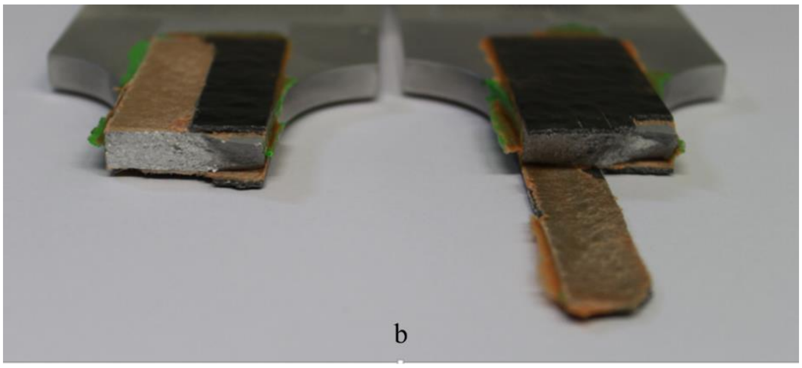

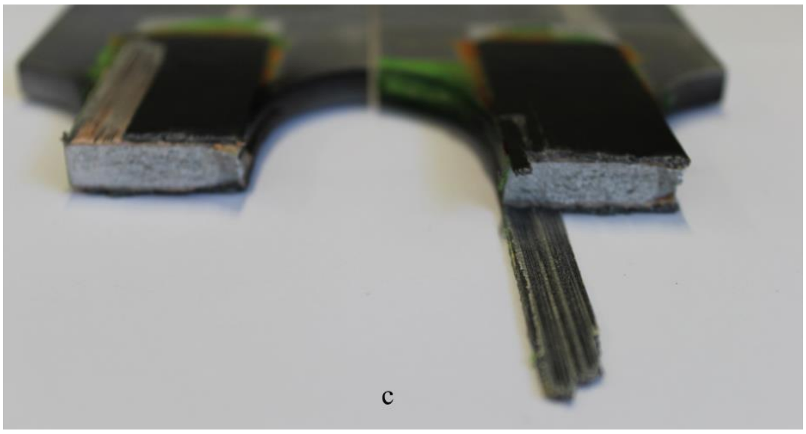

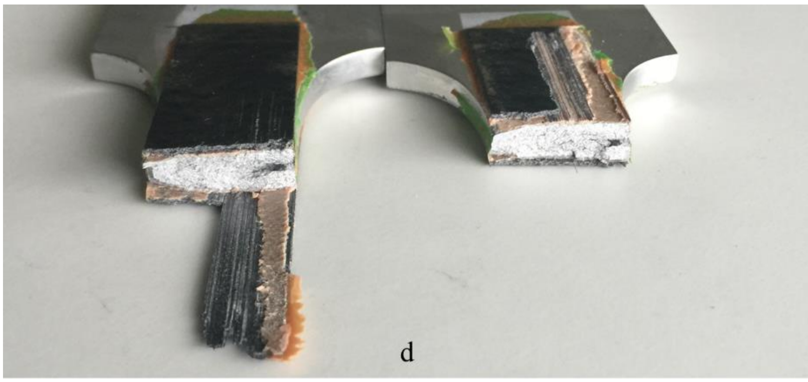

Figure 5.27 Photographs of atch failure modes. (a) Adherend failure, (b) Cohesive failure, (c) First-ply failure, (d) the combination of First-ply failure and Cohesive failure.

5.5.4 Adhesive failure mechanism

Prior to testing, one assumption made by the author was that delamination or disbond of the composite patch would only grow along the same direction as the load. This assumption was based on tests performed by Cheuk et al. [78] who declared cracks were found to initiate in spew fillet and then propagate through the entire first ply of composite patch in an adhesively bonded composite-metal double lap joint, see Figure 5.28. The double lap joint specimen configuration was very similar to the patch repaired specimen except the metallic adherend was rectangular shaped and did not have any initial cracks.

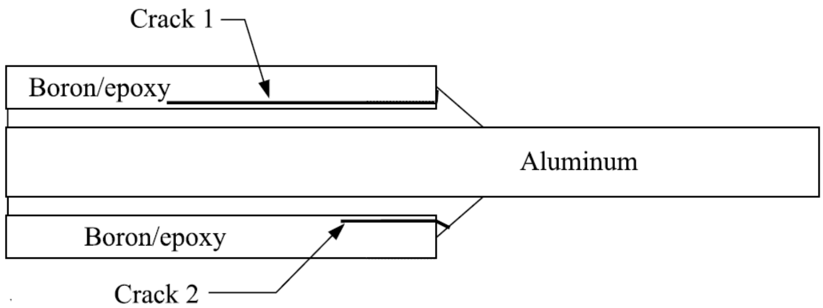

Figure 5.28 Geometry and dimensions of the double-lap joint, from [78].

However, delamination or disbonding was only found at only one side of fracture surface in this experiment, e.g. left-hand side of Specimens 4 and 10, see Figure 5.29 On the contrary, even after specimen failure the interface between the patch and the adhesive at another side, i.e. the right-hand side, remained intact.

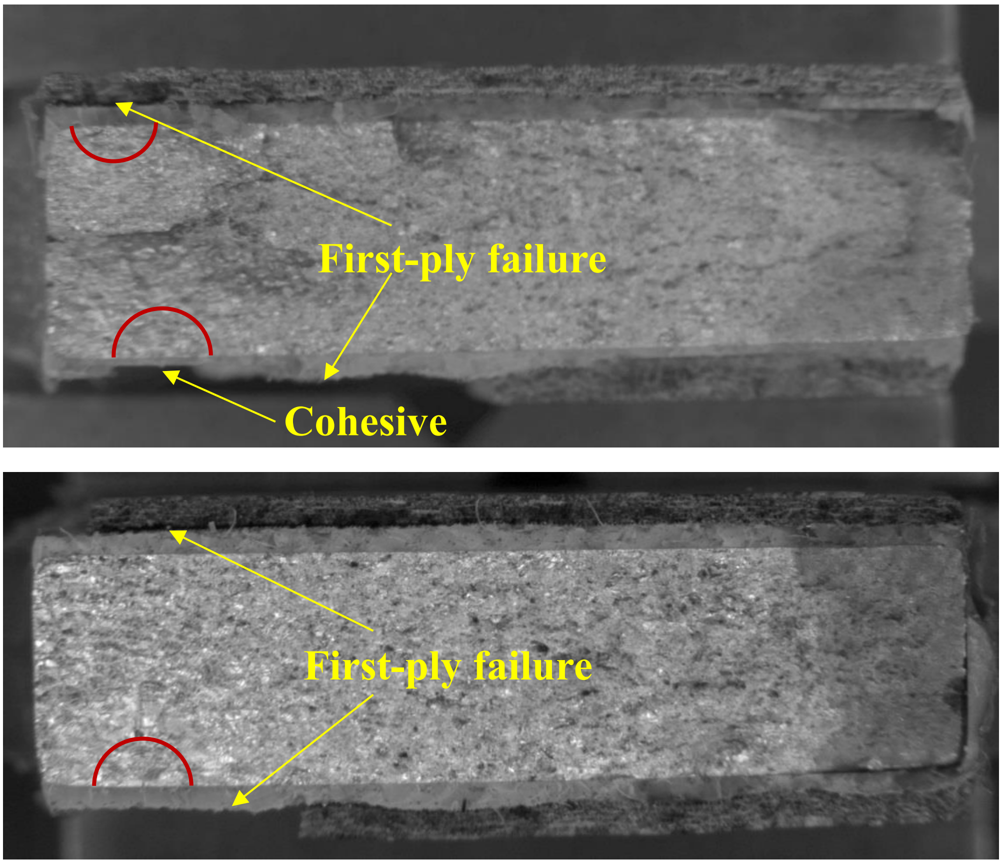

Figure 5.29 Fracture surfaces of Specimen 4 (top) and 10 (bottom). The red semicircles indicate where the locations of crack initiation.

It was subsequently found that delamination, or disbond, occurred after the crack in adhesive film grew through the adhesive and reached the composite, see Figure 5.30. The marker bands on fracture surface of adhesive were clear and they were associated with, i.e. linked with, cracks that had grown in the metallic adherend. This suggests that there is no or little time for adhesive film to initiate cracks even it is not observable.

In the horizontal direction the crack in the adhesive could be "matched up with" crack growth in the metal. As a result there were the wide maker bands close to the interface Figure 5.30. However, marker bands in the depth direction were squeezed together. This indicated a slow growth rate through the adhesive. Delamination/disbonding only occurred once the crack in the adhesive reached the composite patch. These adhesive maker bands could potentially become a tool to predict when the delamination or disbond occurred.

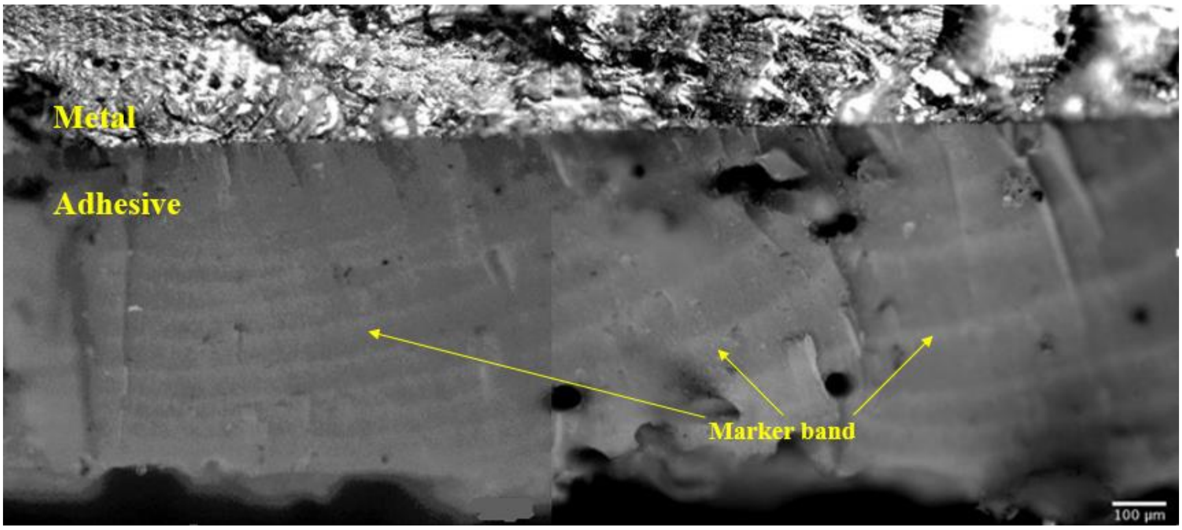

Figure 5.30 Marker bands on FM 300-2K of Specimen 10.

As mentioned above that there was no delamination or disbond in specimens with a 2-ply patch. The fracture surface of Specimen 12 is shown in Figure 5.31 which illustrates that prior to failure the maker bands had not reached the composite patch. Figure 5.31 also shows the first maker band which can be seen was 0.25 mm deep and 1.54 mm away from laser notch.

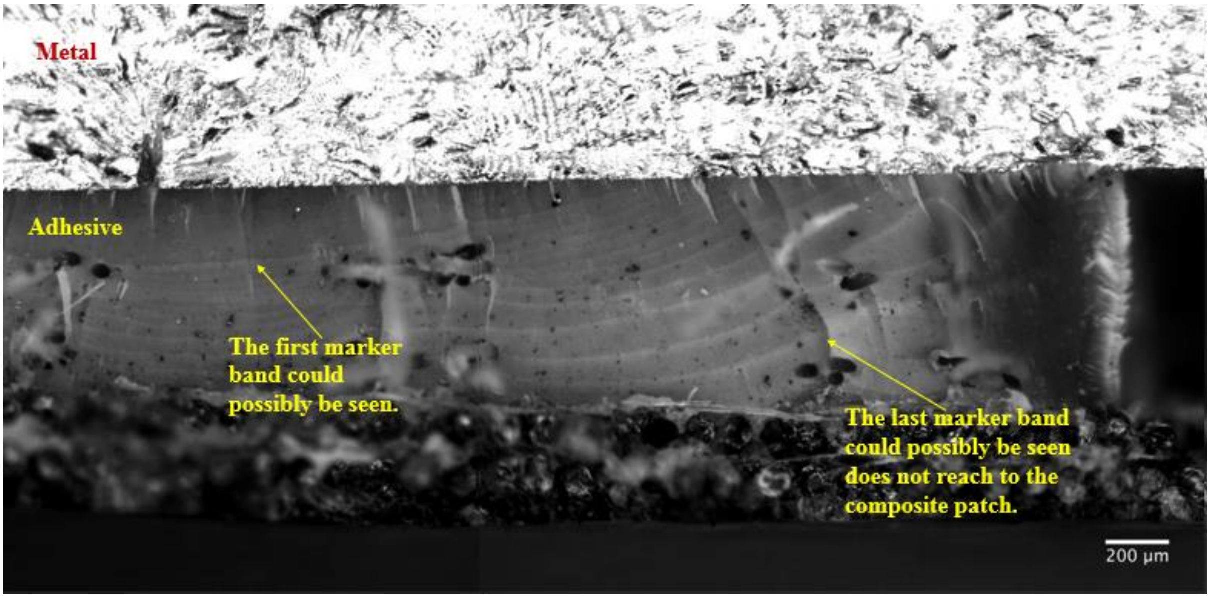

Figure 5.31 Marker bands on FM 300-2K of Specimen 12.

5.5.5 Thermography analysis

Thermoelastic Stress Analysis (TSA) can be used to measure the stress field associated with a dynamically loaded structure and thus has the potential to detect the growth of discontinuities. TSA has long been used to assess the effectiveness of composite repairs [156]. Choi and Rajic [157] declared that TAS was a promising full-field strain/stress measurement technique. All scales of TSA in this Section were arbitrary and only indicating the relative stress and strain. Australian DSTG applied TSA to a number of full-scale fatigue test (FSFT) programs, i.e. C-130J wing fatigue test and F/A-18 Hornet centre barrel fatigue test. Figure 5.32 illustrates the TSA applied to the Y488 bulkhead and a computational model validation. The agreement between the thermoelastic response and the prediction model was seen to be excellent [157].

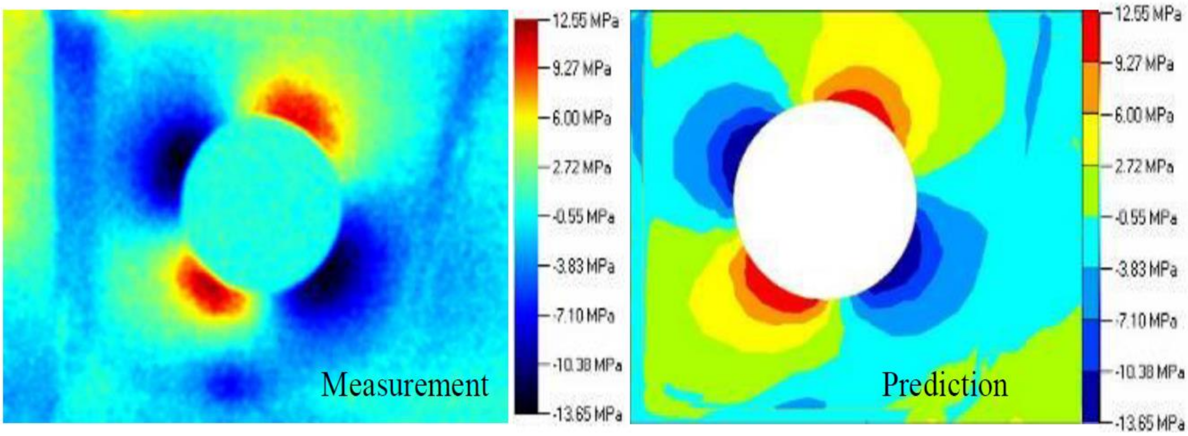

Figure 5.32 Measurement and prediction of bulk stresses around a circular hole in the Y488 bulkhead [157].

As a result TSA was used to investigate crack growth in Specimen 1. Figure 5.33 shows the fracture surface of Specimen 1 and Figure 5.34 shows thermal images of the surface where the lead crack can clearly be seen. The left image in Figure 5.34 was taken at the 70th load block. At this stage there was no sign of a crack. The middle image was taken at the 80th load block. This image revealed a crack which had a surface length of approximately a quarter of the width of the specimen. Due to the existence of the crack, the regions above and below the crack had a low stress level whereas the left and right sides of the crack had a higher stress level. The result of the thermal image were similar to the results from Lo [38]. The right image was taken at the 83th load block, which was only one block before the complete failure of the specimen. At this stage the crack had reached the right-hand edge and had become a corner crack. Consequently, the stress field at right hand side of the specimen was reduced and the stress field the left hand side of the crack increased dramatically.

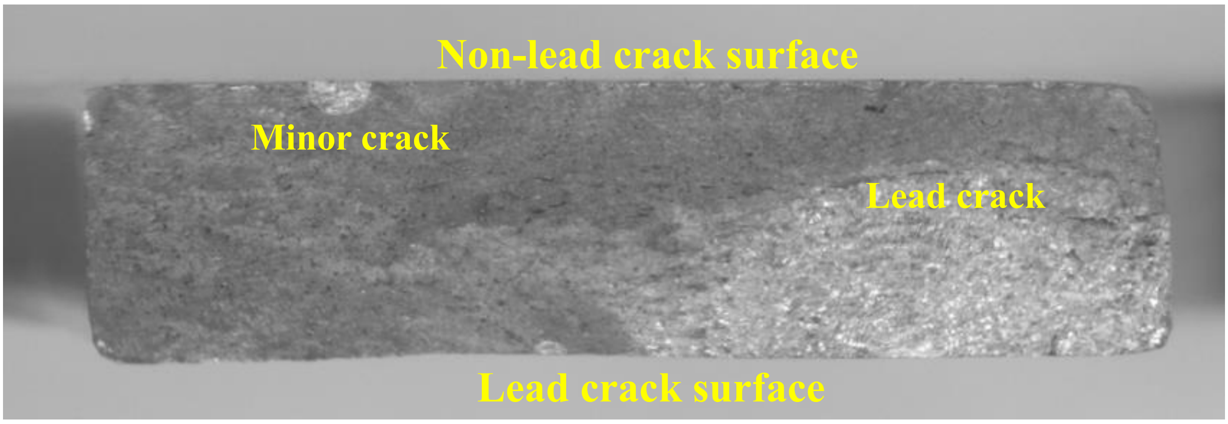

Figure 5. 33 Fracture surface of Specimen 1.

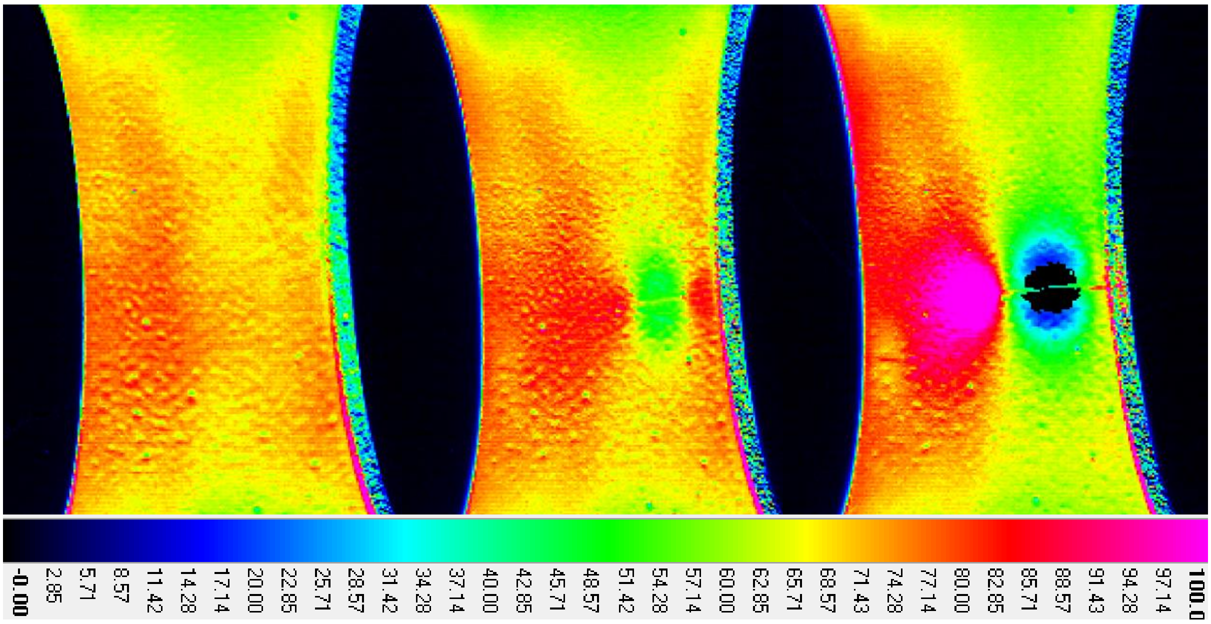

Figure 5.34 Thermal images of the lead crack surface on Specimen 1. Left: taken at the 70th load block. Middle: taken at the 80th load block. Right: taken at the 83th load block.

Unfortunately, the thermal images were only useful for large cracks, i.e. bigger than 1 mm. Figure 5.35 presents the thermal image of a non-lead crack on Specimen 1. The image was taken at the 82th load block which is only two blocks before final failure. The minor crack on fracture surface shown in Figure 3.33 can't be seen in Figure 5.35. The surface length of the minor crack at the 82th load block was approximately 1.3 mm. In addition, there was an obvious stress reduction on the top right side in Figure 5.35. This was caused by two corner cracks which were not on the fracture surface, see Figure 5.36. The surface length of two cracks after the specimen had failed were approximately 4.9 and 3.8 mm respectively.

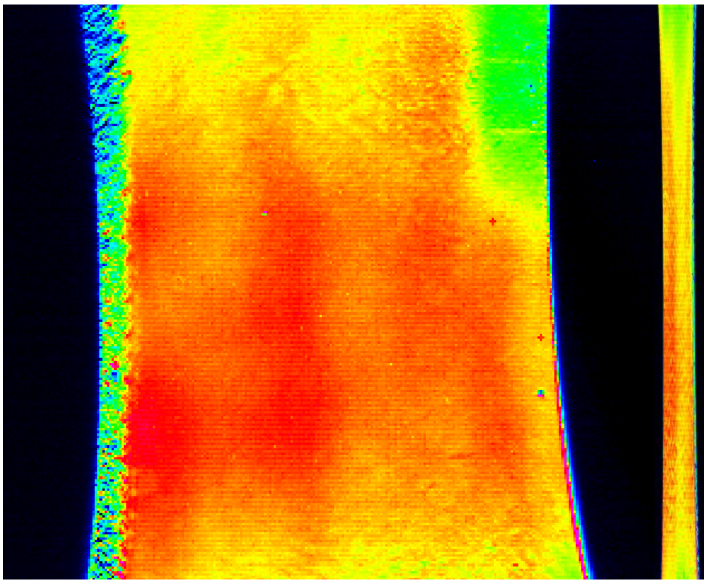

Figure 5.35 Thermal image of the minor crack surface on Specimen 1. Taken at the 82th load block.

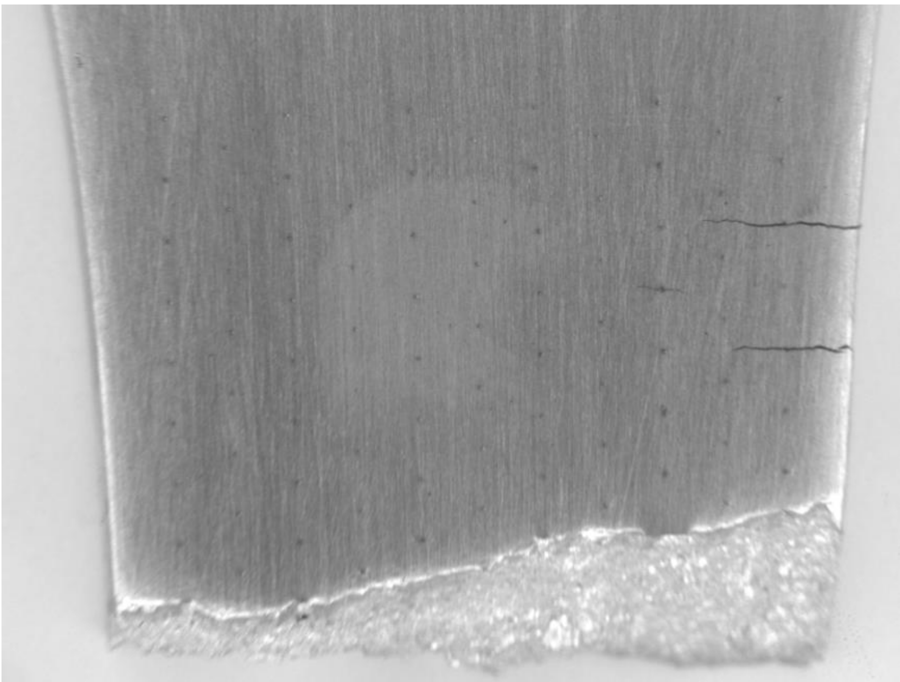

Figure 5.36 Two corner crack on the non-lead crack surface of Specimen 1.

Thermal images of Specimen 6 which had a 5-ply patch were also taken. Figure 5.37 presents the fracture surface associated Specimen 6. It reveals a lead crack initiated at bottom left of the fracture surface, see Figure 5.37, which subsequently forms a corner crack before becoming a through thickness crack. The lead crack surface represented the surface where the lead crack initiated. Figure 5.38 shows the thermal images associated with both surfaces at the 88th load block, which was 30 load blocks after patching. There were no prior indications of any form of defects, e.g. crack, disbond or delamination. However at the 186th load block a stress concentration appeared on the left part of lead crack surface, but not on the non-lead crack side, see Figure 5.39. At the 196th load block, which was two blocks before the final failure, both the lead crack surface and the non-lead crack surface revealed a large stress concentration at the middle left hand side of the working area, see Figure 5.40. This is because at this stage the specimen now contained a through crack.

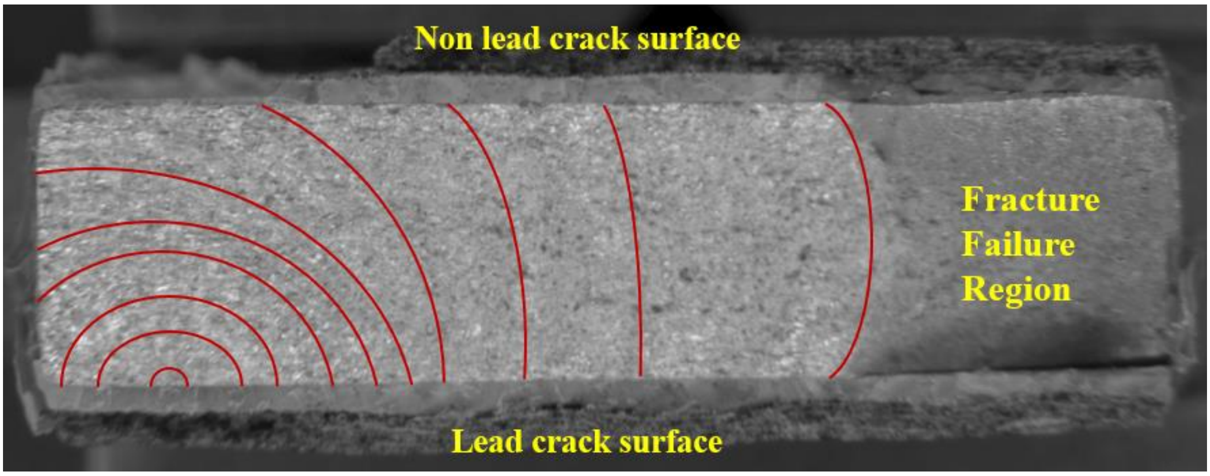

Figure 5.37 Fracture surface of Specimen 6.

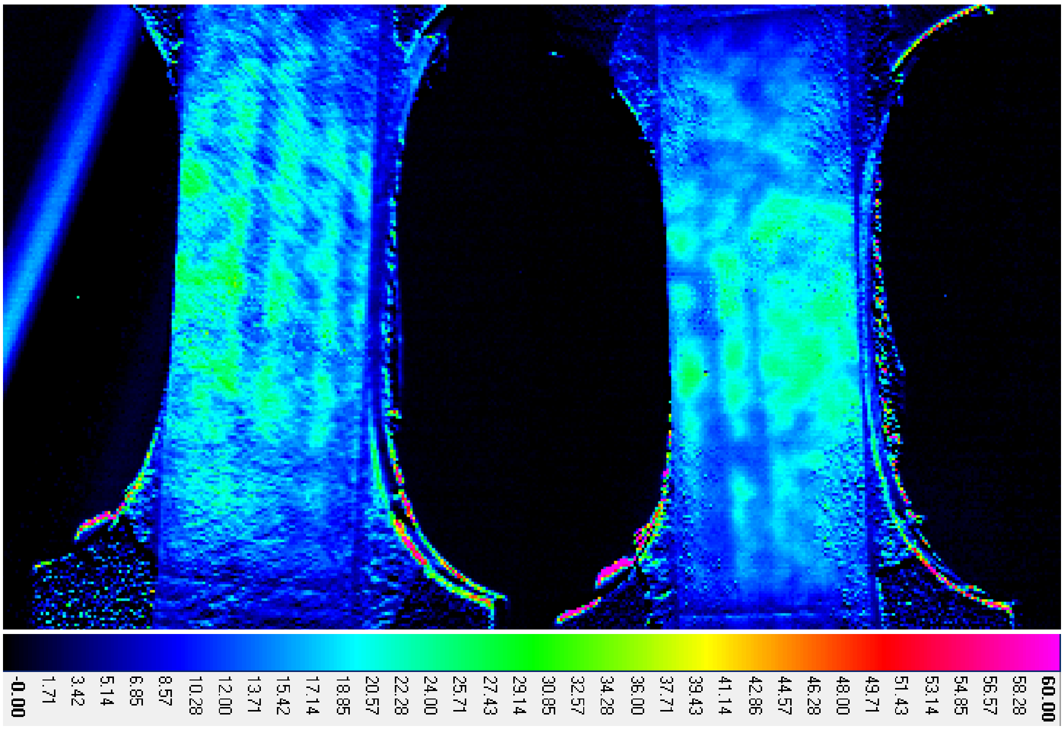

Figure 5.38 Thermal images of Specimen 6 at the 88th load block. Left: lead crack surface. Right: non-lead crack surface.

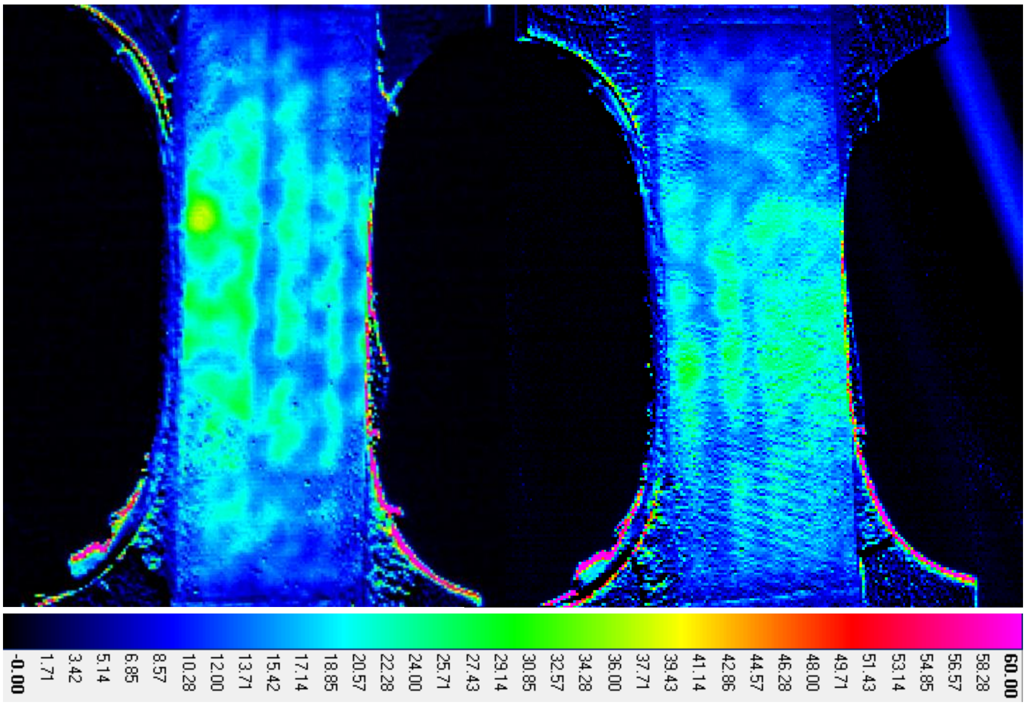

Figure 5.39 Thermal images of Specimen 6 at the 186th load block. Left: lead crack surface. Right: non-lead crack surface.

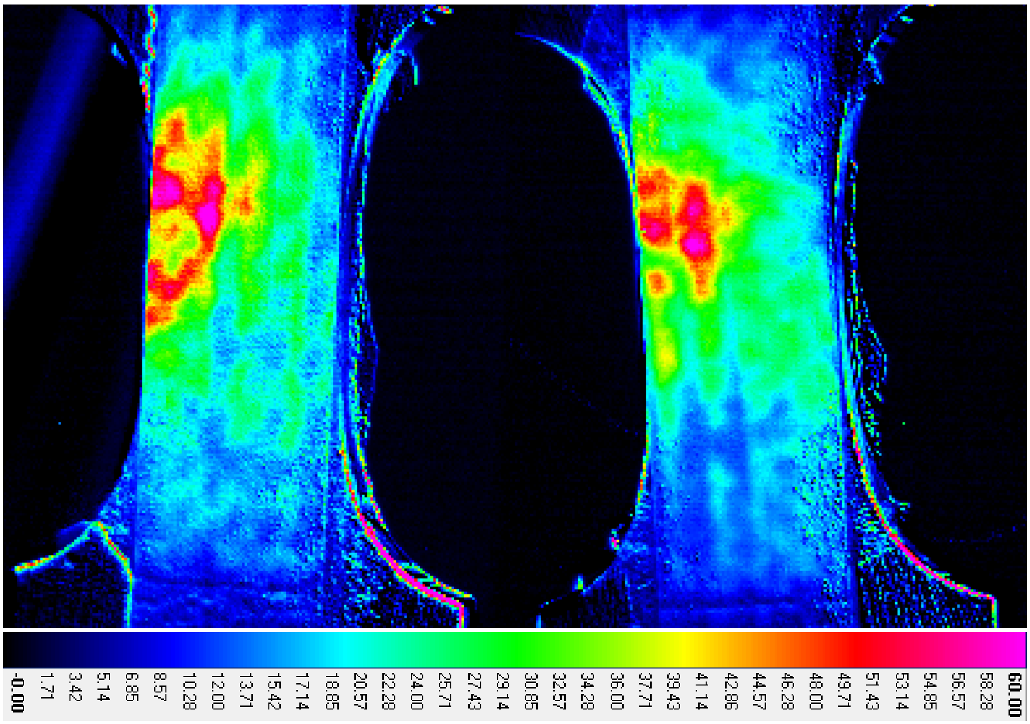

Figure 5.40 Thermal images of Specimen 6 at the 196th load block. Left: lead crack surface. Right: non-lead crack surface.

5.6 Summary

Two fatigue test programs were performed. Both programs used the same materials, viz: AA 7050-T7451, FM 300-2K and a unidirectional boron epoxy composite patch. The differences between the two programs were the specimen geometries and methods used to introduce sub millimetre initial notches, i.e. laser induced notches and NaCl solution induced corrosion pits. Both test programs resulted in a large scatter in the life to failure.

The majority of specimens, i.e. eight out of fourteen, contained only one major crack in the metal. If its location of initiation was away from the side edge the fatigue crack in the metal tended to grow from a semi elliptical crack to a though crack. Otherwise, the crack would reach the edge and then form a corner crack before becoming a through crack. Multiple cracks, if closed to each other, tended to merge together and subsequently form a through crack which would then propagate horizontally before the specimen failed.

Specimens also experienced different types of patch failure. These included adherend failure, cohesive failure, first-ply failure of composite patch and a combination of cohesive and first-ply failures. It was also found that not only did the metal adherend had crack, but that the crack in the metal led to cracking that grew in the adhesive film that subsequently led to either disbond or first-ply failure. The crack in adhesive, as the author believed, was the major mechanism which caused either cohesive failure or first-ply failure in patches. In addition, thermography established patch failure only occurred near the very end of the fatigue test.

A patch repaired specimen with a 6 mm disbonded zone across the width in the central working area was designed to test the effect of disbond on the fatigue crack growth of short cracks. Unfortunately, no cracks beneath this disbonded zones grew to any significant extent. A test program to further investigate this effect is recommended.

Chapter 6

Prediction Of Patch Repaired Structures

6.1 Introduction

The USAF report on the risk analysis of aging aircraft fleets [130] stated that "*the operational life of individual airframes is seldom equal to the design life of the fleet and that the life of an aircraft fleet tends to be determined more by its inherent operational capability and maintenance costs rather than by the number of flight hours specified at the design stage*". Consequently, different tools and methodologies are needed for ab initio design and aircraft sustainment [55]. Implicit in these findings is the fact that, as explained in ASTM E647-13a Annex X3 [35], crack growth data obtained using ASTM E647-13a like specimens, where the cracks have been grown from long artificial notches, are inappropriate for assessing aircraft sustainment related issues. This leads us to conclude that tests that use ASTM E647-13a like specimens, where prior to patching the cracks have been grown from long artificial notches, are inappropriate for assessing the effect of composite repairs to operational aircraft [50, 158] where the cracks have initiated and grown from small naturally occurring material discontinuities.

In this context, it should be noted that to date the vast majority of studies into the effect of composite repairs to cracked structures have used ASTM E647-13a like specimens where prior to patching the crack was grown from large artificial notches [119, 137]. However, as explained in ASTM E647-13a, such specimens do not reflect how a crack in an operational structure will grow. This is because the fatigue threshold associated with such specimens is significantly greater than that seen by cracks that have grown from small naturally-occurring material discontinuities typical of those found in operational aircraft [55]. This is aptly illustrated in Figure 6.1 which presents the da/dN versus ΔK curves associated with the growth of small cracks in AA 7050-T7451, which is a commonly used aerospace aluminium alloy.

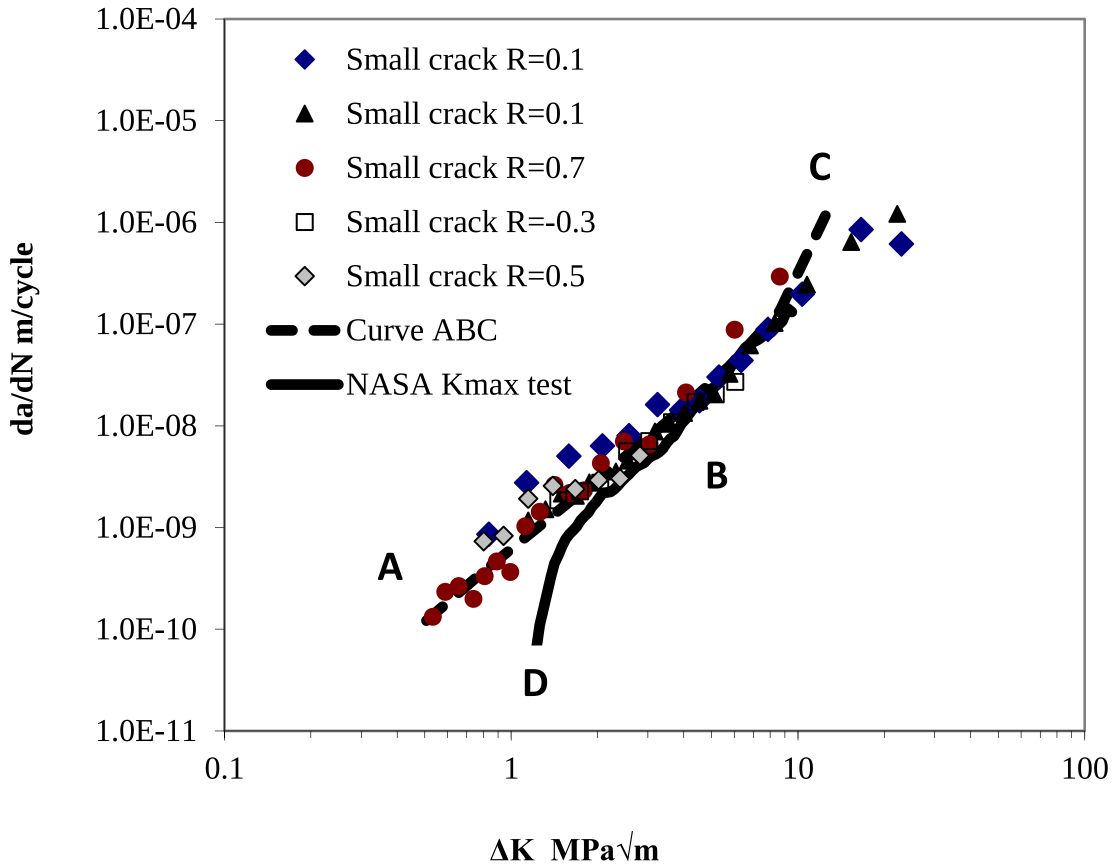

Figure 6.1 Comparison of da/dN versus ΔK curves associated with naturally-occurring cracks for 7050-T7451 [55].

The sigmoidal shape seen for the da/dN versus ΔK curve as determined in accordance with the fatigue test standard ASTM E647-13a is represented as the curve DBC in Figure 6.1. The da/dN versus ΔK curve associated with small naturally-occurring cracks is represented by curve ABC. This curve has a lower threshold than curve DBC and reflects a Paris crack growth equation with a low value apparent threshold. In the mid-ΔK and below region, this curve has little (if any) R-ratio dependency. An example of the need to use the curve ABC, rather than the curve DBC, is given in [159], which discusses how to assess the operational life of critical locations in the Lockheed Martin F-22. In this context the present Chapter illustrates two methods for predicting the life of patch repaired metallic structures with cracks that have grown from small surface damage states.

6.2 Life Prediction of Patch Repaired Structure with the Hartman–Schijve Equation

As mentioned in Section 2.2.4 the Hartman–Schijve equation, i.e. Equation (2.15), can be used to predict the growth of short cracks, i.e. cracks are less than 1 mm. To this end, Finite Element (FE) analysis is employed to obtain the detailed information on the laser notched specimens and to compute the associated stress intensity factor solutions. The commercial package, Abaqus version 6.13, is used in this research. In all standard FE models, the reduced 3D quadratic element is employed. In Abaqus, the code of this element is C3D20R which contains 20 nodes. Every middle node around the crack tip were adjusted to its quarter position to create quarter-point elements. All FE models were passed the convergence check in order to obtain reliable results.

6.2.1 FE analysis of undamaged specimens

3D models of uncracked laser notched specimens both before and after patching were created, see Figures 6.2 and 6.3. In this analysis, only a half of the specimen was modelled. The specimen geometry is as given in Figure 5.1. Laser notches were ignored in this model, so there was no surface damage in this initial analysis. The elastic modulus and Poisson ratio of the AA 7050-T7451 was taken to be is 71.7 GPa and 0.33 respectively. The mechanical properties of the boron epoxy patch are shown in Table 5.1. A tensile stresses equivalent to 50 kN was applied at the end of AA 7050-T7451 adherend. Constraints were applied at the grip area to simulate test condition, so that in the grips the models could only move alone the same direction as tensile stress.

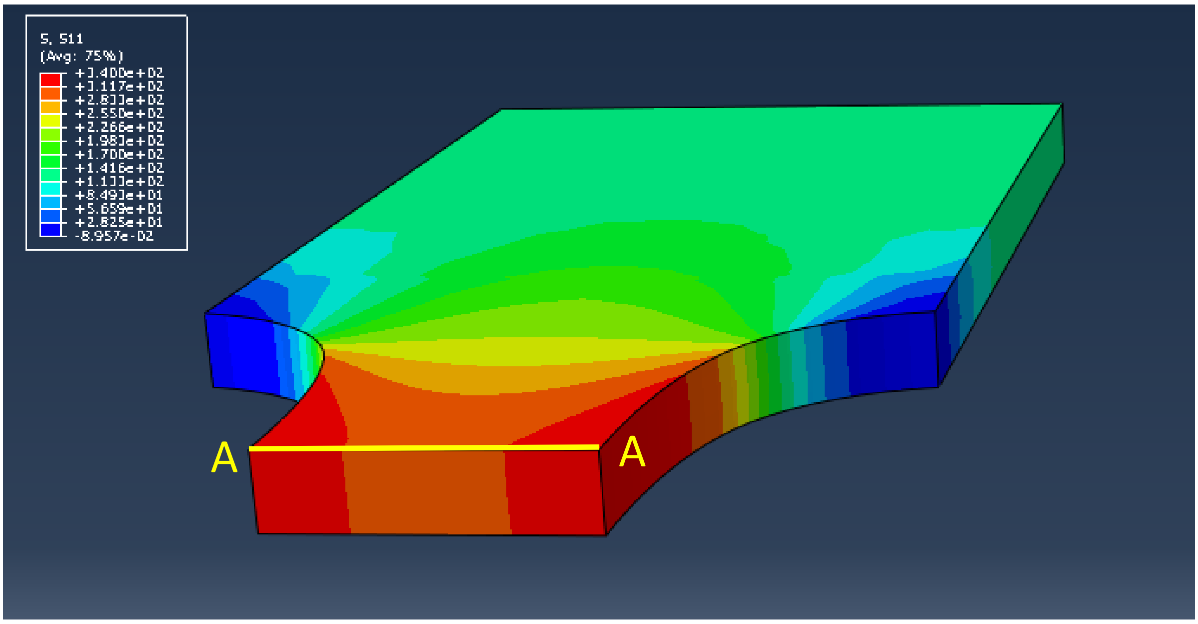

Figure 6.2 FE model of unpatched laser notched specimen.

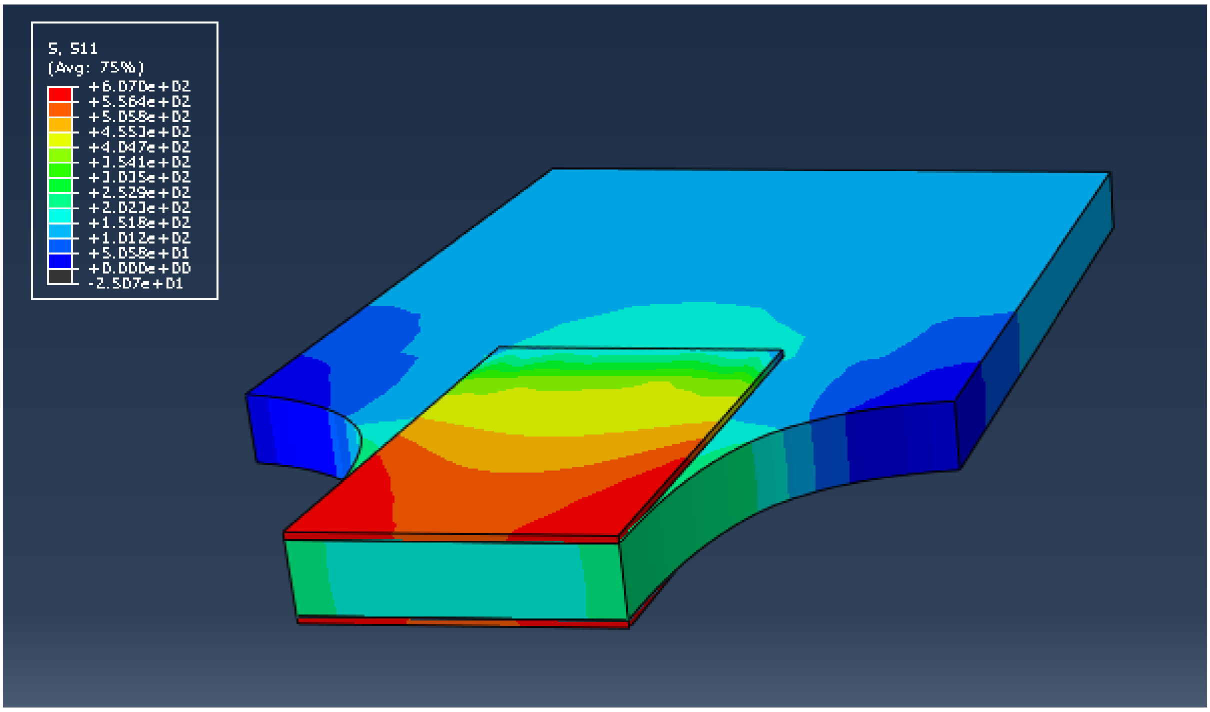

Figure 6.3 FE model of 5-ply patched laser notched specimen.

Figure 6.4 shows the stress field in the metallic adherend in the patched model. It indicates that the stress distribution on the cross-sectional area are similar before and after patching, see Figures 6.2, 6.4 and 6.5.

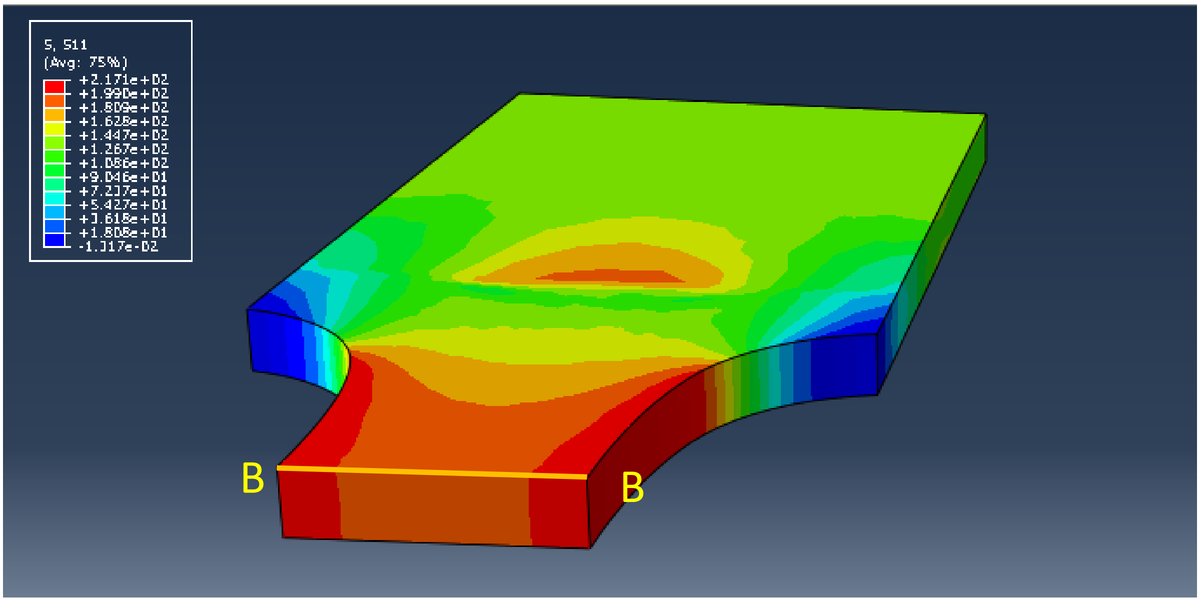

Figure 6.4 Stress field of the metallic adherend in Figure 6.3.

The stress fields that along Lines AA in Figure 6.2 and BB in Figure 6.4 are plotted in Figure 6.5. The 5-ply patch reduced the stress by approximately 37%. This reduction arose for patches both with and without a centrally located 6 mm wide disbonded zone. The 2-ply patch only resulted in a 19% reduction. For both the patched and the unpatched models, it was found that the stress in the centre of the working section is approximately 7% lower than the stress at the edges, see Figure 6.3, 6.4 and 6.5.

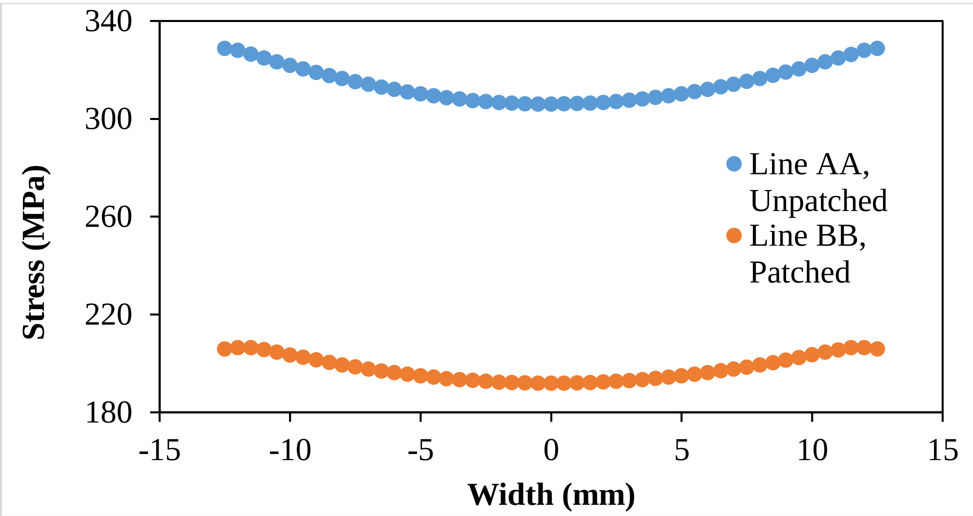

Figure 6.5 Stress field along Lines AA and BB of the metallic adherend.

6.2.2 FE analysis of specimens with single crack

A simple unpatched FE model which only had one major crack was created. The fracture surface was assumed to lie on the median plane of the specimen. A semi-circular crack was located at a distance of 6.25 mm away from the side edge, see Figures 6.6 and 6.7. This is because in experiment mentioned in Chapter 5 most lead cracks initiated at this position. A number different cracks sizes were analysed. The crack depth was varied between 0.5 and 3.5 mm with increments of 0.5 mm. A model with a crack size of 0.5 is shown in Figure 6.6 and 6.7. The associated stress field is shown in Figure 6.8.

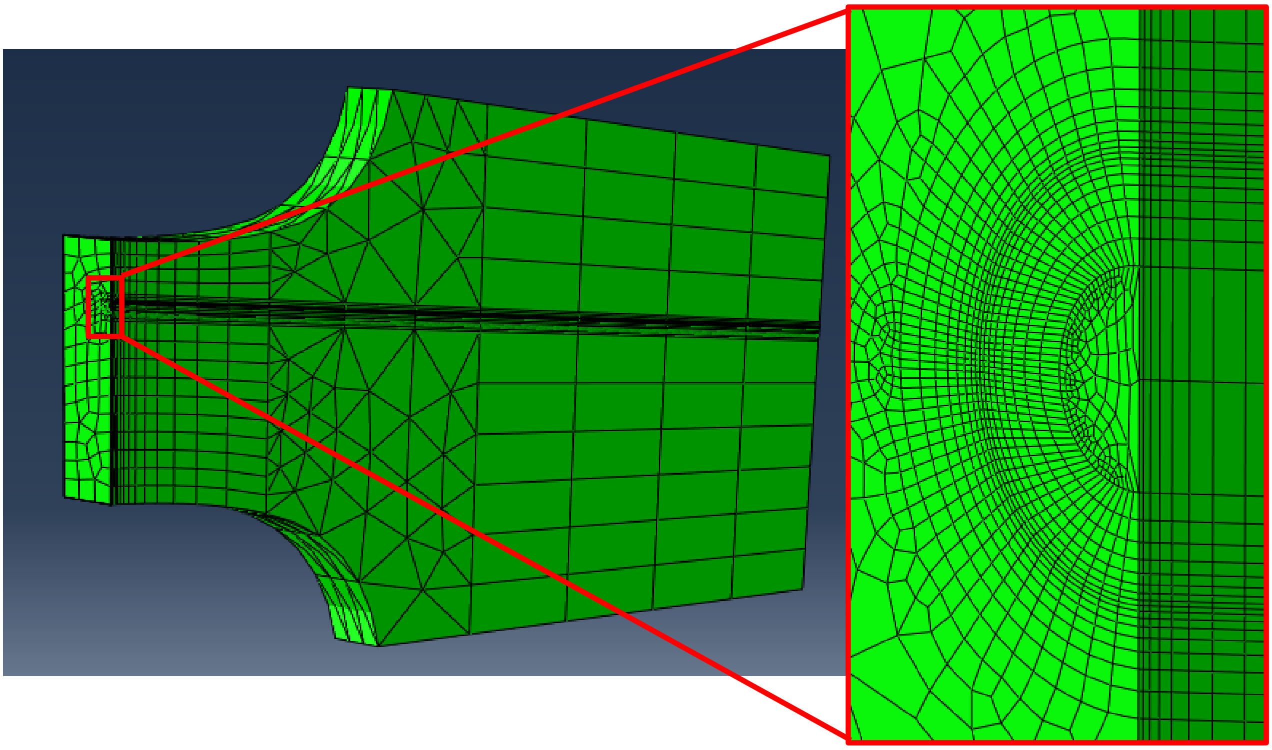

Figure 6.6 A FE model of laser notched dogbone with 0.5 mm crack used to calculate K for the deepest point (90°).

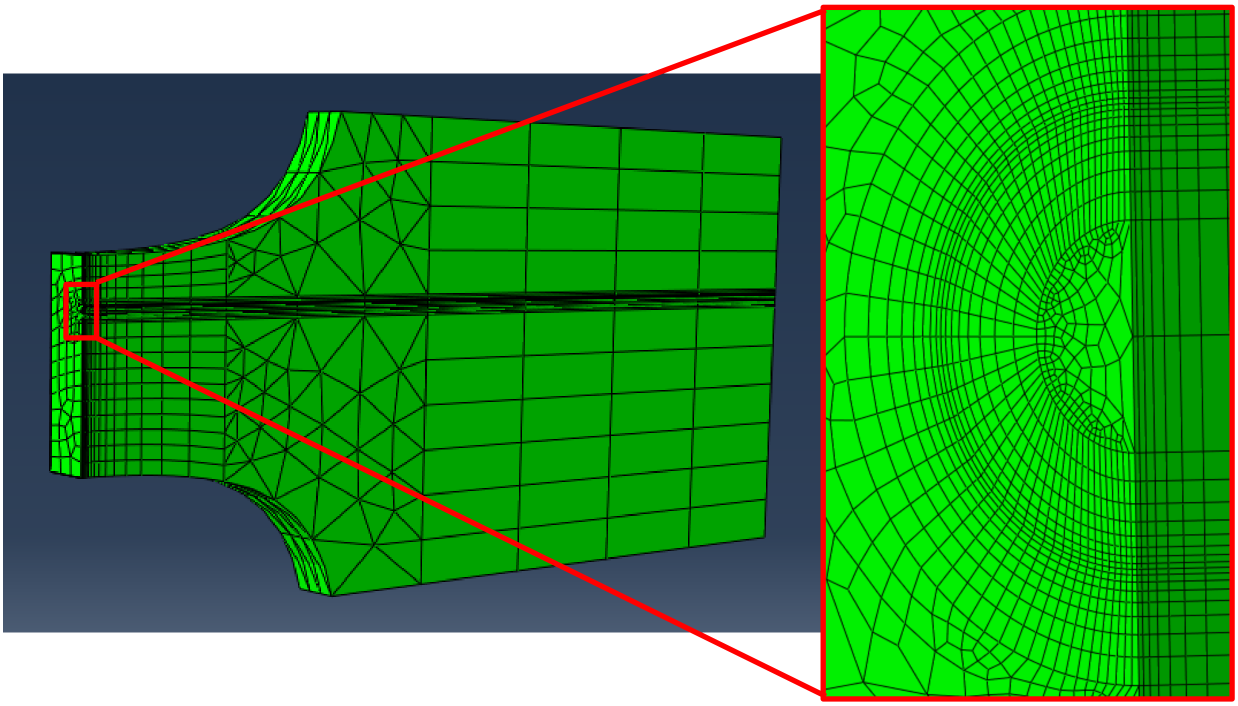

Figure 6.7 A FE model of a notched dogbone with a 0.5 mm crack used to calculate K for free surface (0°).

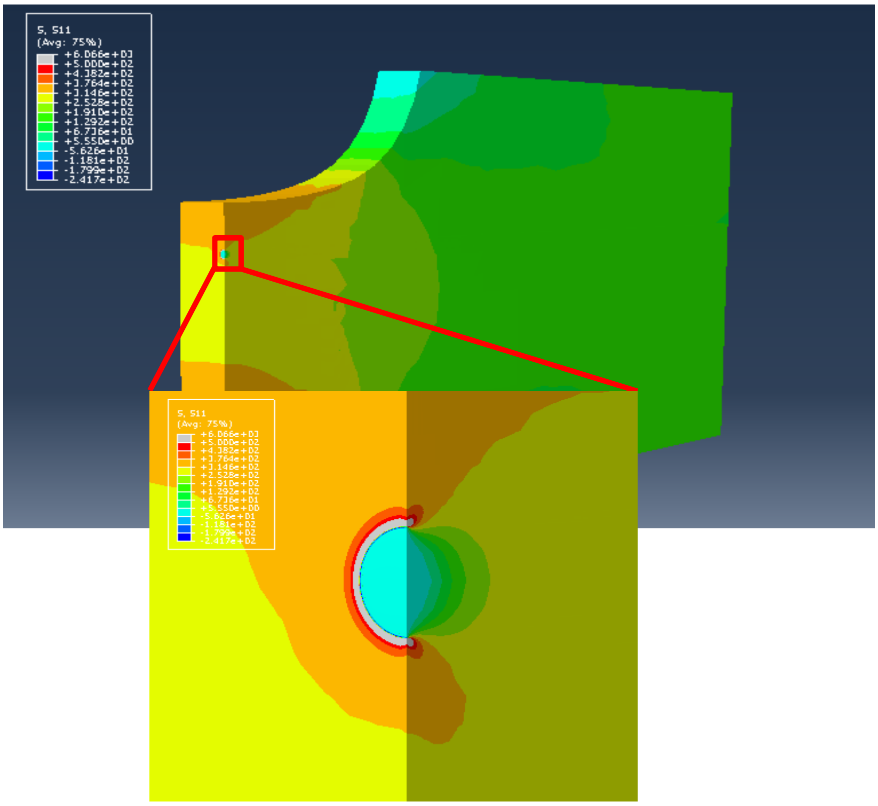

Figure 6.8 Stress fields of the notched dogbone specimen with 0.5 mm semi-circular crack.

6.2.3 Life prediction of specimens with single crack

For each crack size, the SIFs of the deepest point (90°) and at the free surface (0°) were calculated using a crack opening displacement (COD) method, see Equation (6.1) [160].

$$K_I = \frac{E' \mathrm{v}}{4} \sqrt{\frac{2\pi}{l\left(1 - \frac{l}{2a}\right)}} \tag{6.1}$$

where E' = E for plane stress and E/(1-υ^2) for plane strain, v is the crack opening displacement, *l* is the distance between node and crack tip and a is the crack length.

For a 3D crack, the value of K at the deepest point was calculated assuming plane strain conditions whilst at the free surface plane stress was assumed. To simulate the near tip stress singularity the mid-side nodes around the crack tip were moved towards to the quarter position of elements, see Figure 6.9.

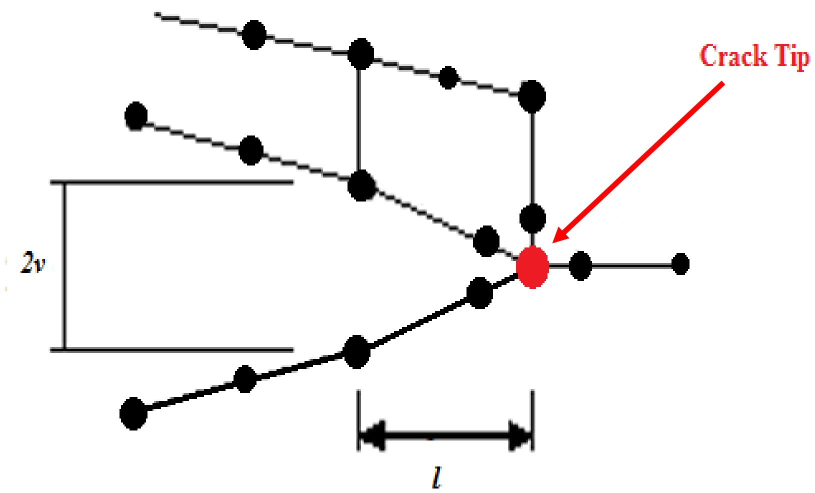

Figure 6.9 Schematic diagram of crack tip.

Estimates of K were obtained for four different values of *l*. The final value of K at the crack tip was then obtained by extrapolating these values to a value associated with *l* = 0. An example of this for K crack depth of 0.5 mm is given in Figure 6.10. These values of K were then compared to those computed using the values obtained via the J-integral method that is built into Abaqus 6.13. Here the value of K was computed from the value of the J-integral by using Equation (2.2). An alternative semi-analytical method, Fatigue Analysis of Structure (FAST) [161], was also used to obtain the value of K both at the point of maximum depth and at the upper surface. FAST is a computational program developed by Jones et al. [161] that can automatically calculate FCG history and its corresponding SIF with the stress field data of intact model (no crack) from FEA. The values obtained by these three different methods at the depth and at the surface point closer to the edge are shown in Table 6.1 and 6.2 respectively.

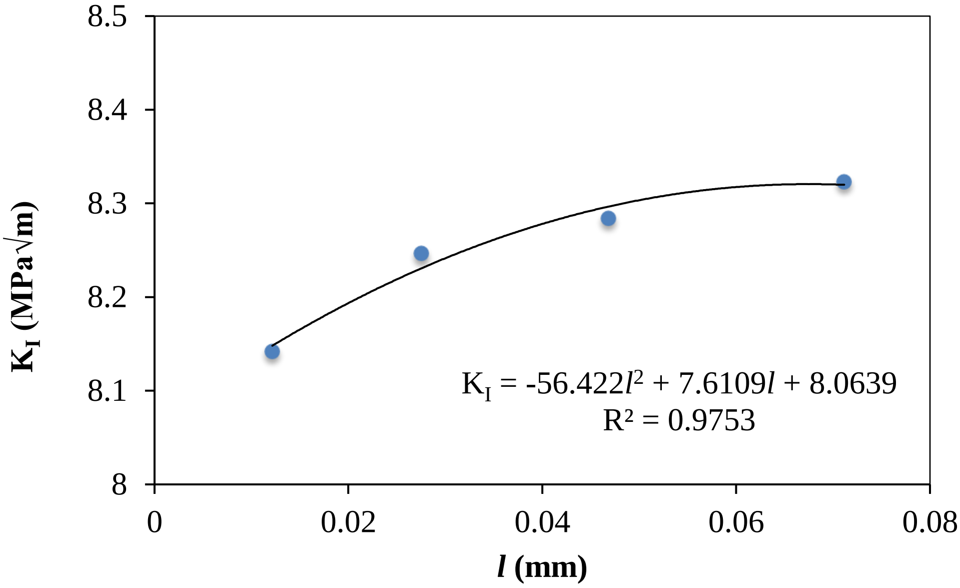

Figure 6.10 Relationship between K and *l* for a crack depth of 0.5 mm.

Table 6.1 The relationship between K (at the deepest point) and crack depth.

Crack Depth (mm)	0.5	1	1.5	2	2.5	3	3.5
COD (MPa√m)	8.1	11.6	14.2	16.6	18.9	21.2	23.5
J-integral (MPa√m)	8.2	11.7	14.4	17.2	19.4	22.1	24.1
FAST (MPa√m)	7.4	10.6	13.1	15.5	17.7	20.1	23.2

Table 6.2 The relationship between K at the surface and surface crack length.

Crack Length (mm)	0.5	1	1.5	2	2.5	3	3.5
COD (MPa√m)	8.1	11.6	14.2	16.6	18.9	21.2	23.5
J-integral (MPa√m)	7.7	11.2	14.0	16.7	19.5	22.4	25.9
FAST (MPa√m)	7.4	10.7	13.2	15.8	18.3	21.1	24.7

The relationships between K_I and crack depth/length are ploted in Figures 6.11 and 6.12. The results obtained from the different methods are in a reasonably good agreement. The values of K obtained using the COD method were used to predict the growth of crack depth for the experiment of ptached specimens sicnce. The reason to only use crack depth to predict the fatigue life is that it was the crack depth which determined the life of the specime.

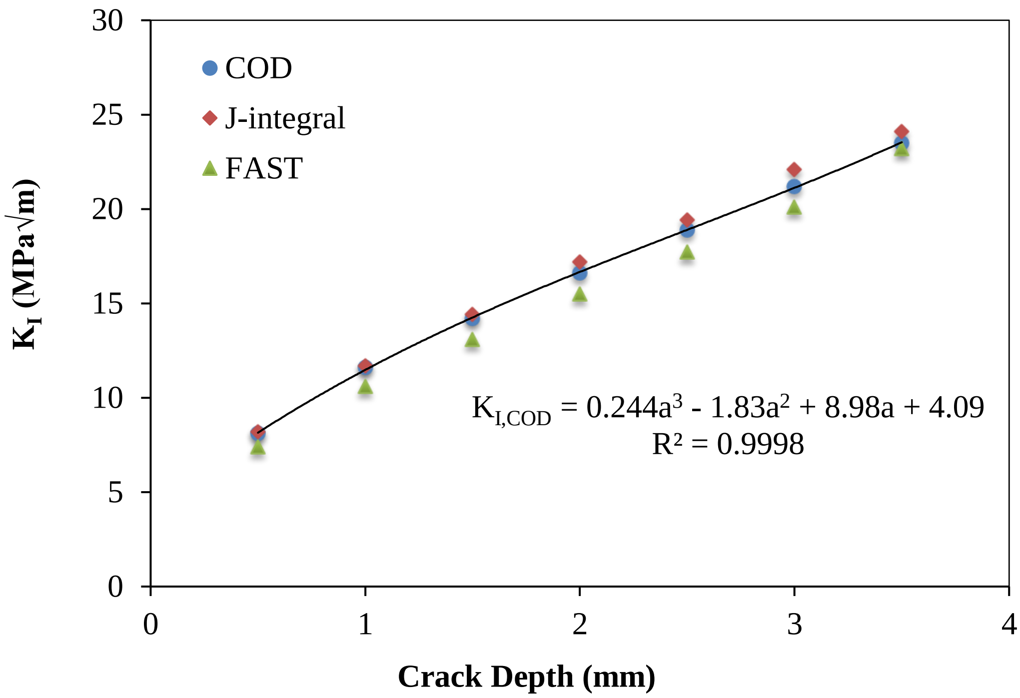

Figure 6.11 The relationship between SIF and crack depth.

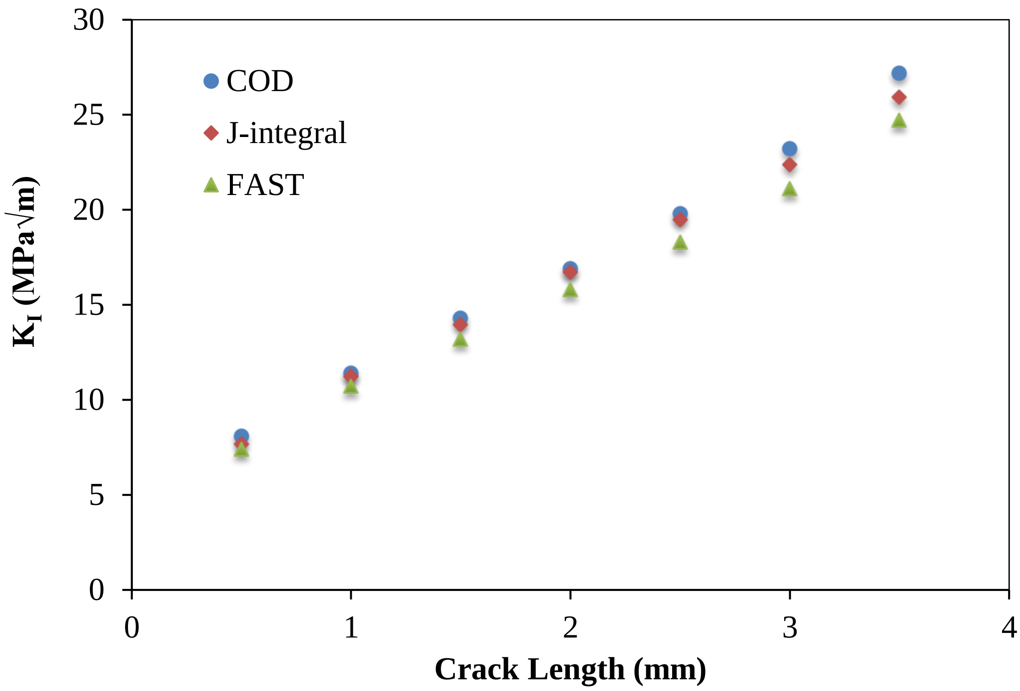

Figure 6.12 The relationship between SIF and surface crack length.

The crack growth history of aluminium alloy 7050-T7451 was then predicted as per [50] by using the Hartman-Schijve equation. The values of constants, i.e. C, n, A, used were taken from [50] so that the crack growth equation for this material can be expressed as Equation (6.2).

$$\frac{da}{dN} = 7 \times 10^{-10} \left(\frac{\Delta K - \Delta K_{thr}}{\sqrt{1 - \frac{K_{max}}{32}}} \right)^2 \tag{6.2}$$

The value of K, at the point of maximum depth, was calculated via Equation (6.3) which was obtained by fitting to the values obtained using COD method, see Figure 6.11, viz:

$$K_{I,COD} = 0.244a^3 - 1.83a^2 + 8.98a + 4.09 \tag{6.3}$$

However, it should be stressed that this approximation should only be used for crack depth between 0.5 to 3.5 mm. As discussed in Section 6.1, for cracks that grow from small naturally occurring material discontinuities the fatigue threshold is very low. This is reflected in the

ASTM Fatigue Test Standard E647-13a [35], "*It is not clear if a measurable threshold exists for the growth of small fatigue cracks*". As a result in this analysis the small crack growth equation was obtained, as recommended in [55, 126], by setting the threshold term in Equation (6.2) to a small value, in this instance to zero. The resultant predicted and measured crack growth histories for both Specimens 1 and 2 are shown in Figure 6.13. Considering the complex nature of the fracture surface, the predicted and measured crack depth histories are in reasonably good agreement.

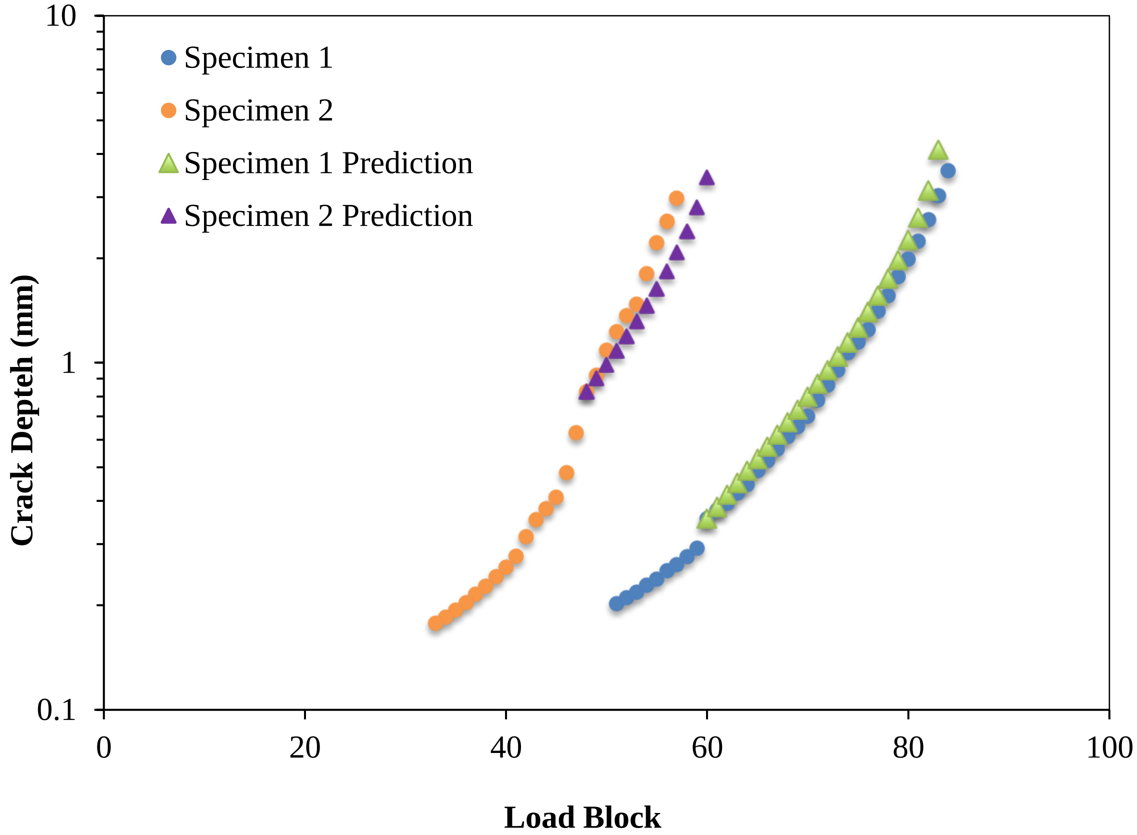

Figure 6.13 Measured and predicated crack growth history of lead cracks in unpatched laser notched specimens.

The same procedure was then used to predict crack growth in the patched laser notched specimens. As mentioned in Section 6.2.1, the stress level was reduced by 19% for specimens with 2-ply patches and by 37% for specimens with 5-ply patches. Hence, since as explained by

Jones [162] the effect of the fibres bridging the crack is generally a second order effect the values for K for the patched specimens were calculated via Equation (6.4) and (6.5) for 2-ply and 5-ply patched specimens respectively by merely allowing for this stress reduction. The results of measured and predicted crack depth histories are shown in Figures 6.14-16. As explained by Molent and Jones [126] the variability in the growth of small cracks can be captured by allowing for variability in the threshold term. In the present study to capture the variability in the crack growth rates post patching the threshold terms varied between 0 and 0.8, see Table 6.3. this level of variability is consistent with that reported in [152] for the same aluminium alloy. The predicted and measured crack growth histories are in good agreement.

$$K_{2-ply\ patch} = 0.81 K_{unpatched} \tag{6.4}$$

$$K_{5-ply\ patch} = 0.63 K_{unpatched} \tag{6.5}$$

Table 6.3 Threshold terms for Specimens 3-12.

Specimen type	Specimen	ΔK_{thr} (MPa$\sqrt{m}$)
5-ply patch	3	0.7
	4	0
	5	0.7
	6	0.5
	7	0.65
	8	0.3
5-ply patch with 6 mm disbond	9	0.5
	10	0.7
2-ply patch	11	0.75
	12	0.8

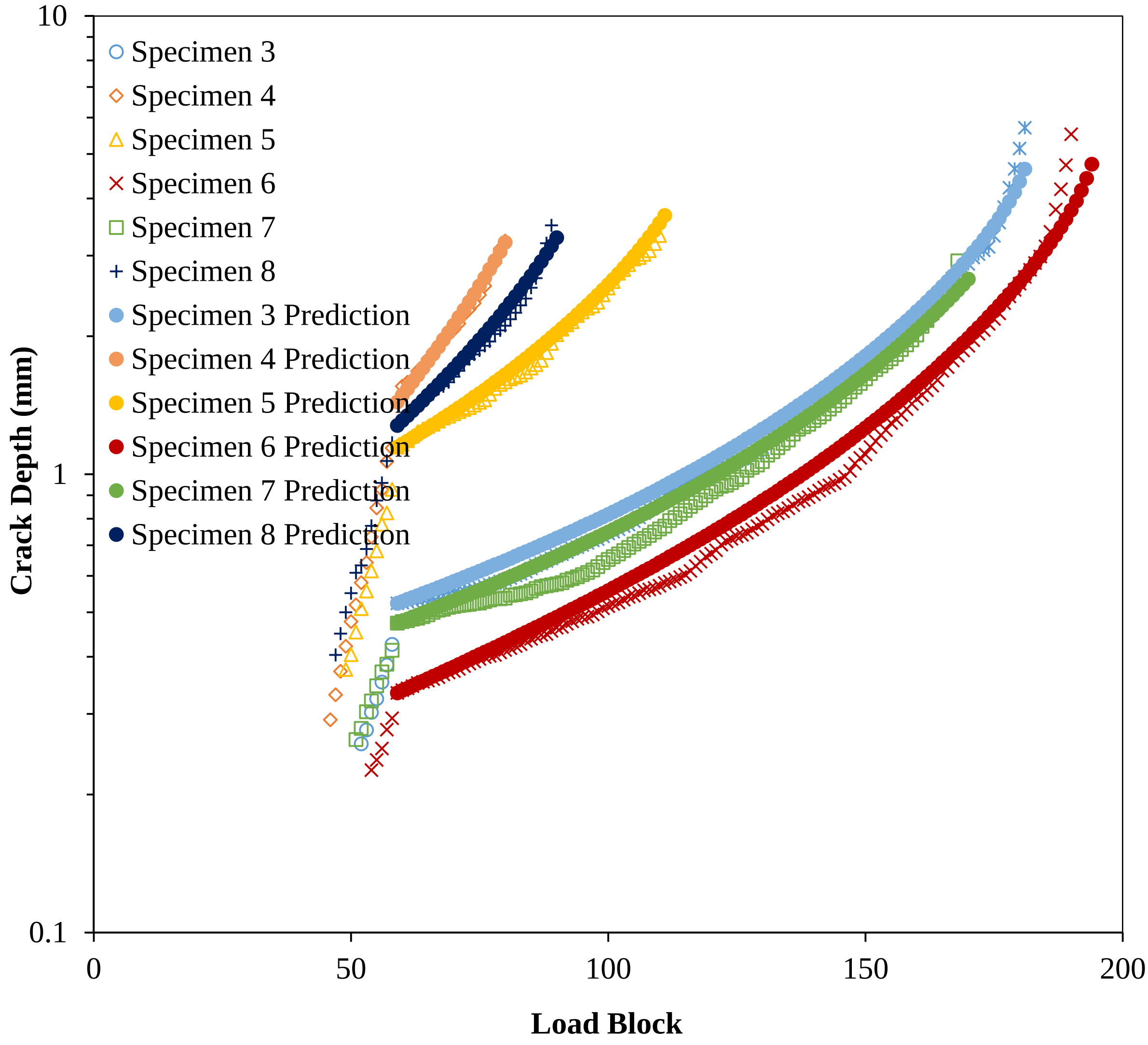

Figure 6.14 Measured and predicated crack growth history of lead cracks in 5-ply patched laser notched specimens.

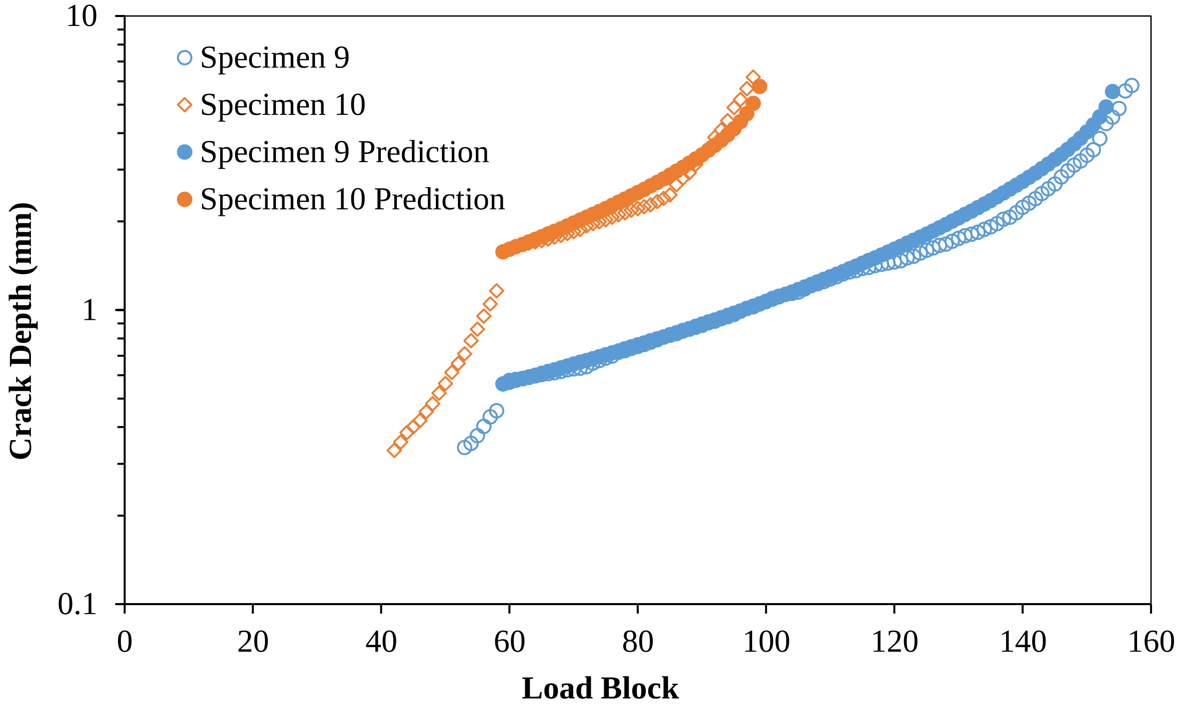

Figure 6.15 Measured and predecited crack growth history of lead cracks in 5-ply patched laser notched specimens with disbonding zone.

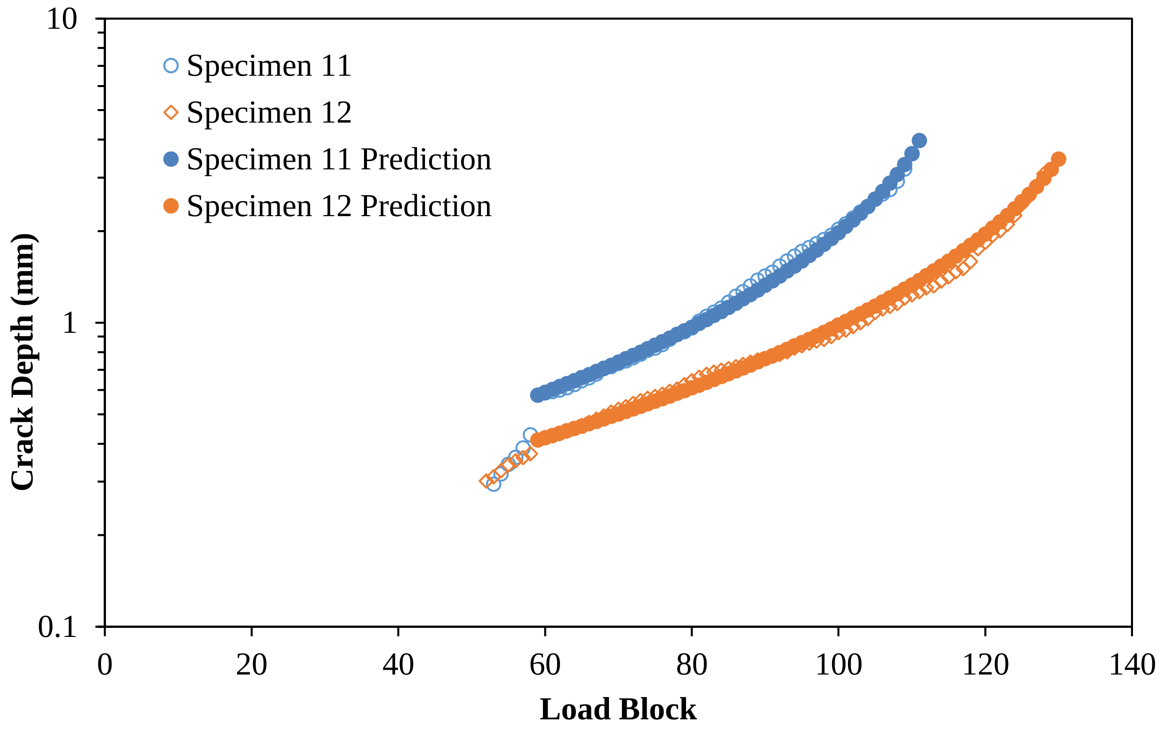

Figure 6.16 Measured and predicated crack growth history of lead cracks in 2-ply patched laser notched specimens.

6.3 Application of the Cubic Rule to Predict Crack Growth in Patched Specimens

As previously mentioned the experimental data analysed in [162] suggested that for composite repairs to cracks in operational structures, i.e. cracks that have arisen and subsequently grown from small naturally occurring material discontinuities, the effect of the fibres bridging the crack is generally a second-order effect. From this it follows that the growth of small naturally-occurring cracks repaired with a composite patch should be near exponential albeit with a reduced growth rate due to the patch repair. As can be seen in Figures 6.13-16 the results of this test program support this statement. This is an important finding since the experimental data presented [162] revealed that the growth of "long" cracks, with initial lengths of 5 mm or greater, repaired with a bonded composite patch is also exponential. This means that the growth of both long and short cracks repaired with a composite patch essentially exhibit approximately exponential crack growth. This, in turn, means that the risk assessment tools and the associated computer code (PROF) developed by the USAF [163] are equally applicable to composite repairs as to aging airframes.

To further investigate this phenomenon, the crack depth histories are shown in Figures 6.17-20. In some specimens there are more than one crack, but only the lead cracks are taken into consideration. The growth of the lead cracks was essentially exponential and could be expressed as Equation (6.6).

$$a = a_0 e^{\omega N} \tag{6.6}$$

where a_0 is the equivalent pre-crack size (EPS), ω is a material, loading and geometric dependent parameter and N is the fatigue life. (As previously noted, exponential crack growth is common for both cracks growing in operational aircraft and for the growth of small naturally-occurring cracks in laboratory tests.) For cracks that exhibit exponential growth, the Cubic rule is used by the Royal Australian Air Force in the Hornet Structural Analysis Methodology (SAM) and in the P3C Repair Assessment Methodology (RAM), to predict the crack growth [63].

When using the Cubic rule, the value of exponential term ω after patching is denoted as $\omega_{patched}$, and the value of ω prior to patching is denoted as $\omega_{unpatched}$. The exponential term ω is proportional to the cube of applied stress. The crack growth history of lead cracks in Specimens 3-14 were fitted with the exponential model, i.e. Equation (6.6). The value of ω were determined for each specimen, both before and after patching, are shown in Table 6.4. The $\omega_{unpatched}$ and $\omega_{patched}$ for Specimen 9 are 0.0613 and 0.0168 respectively. This is shown in Figure 6.18.

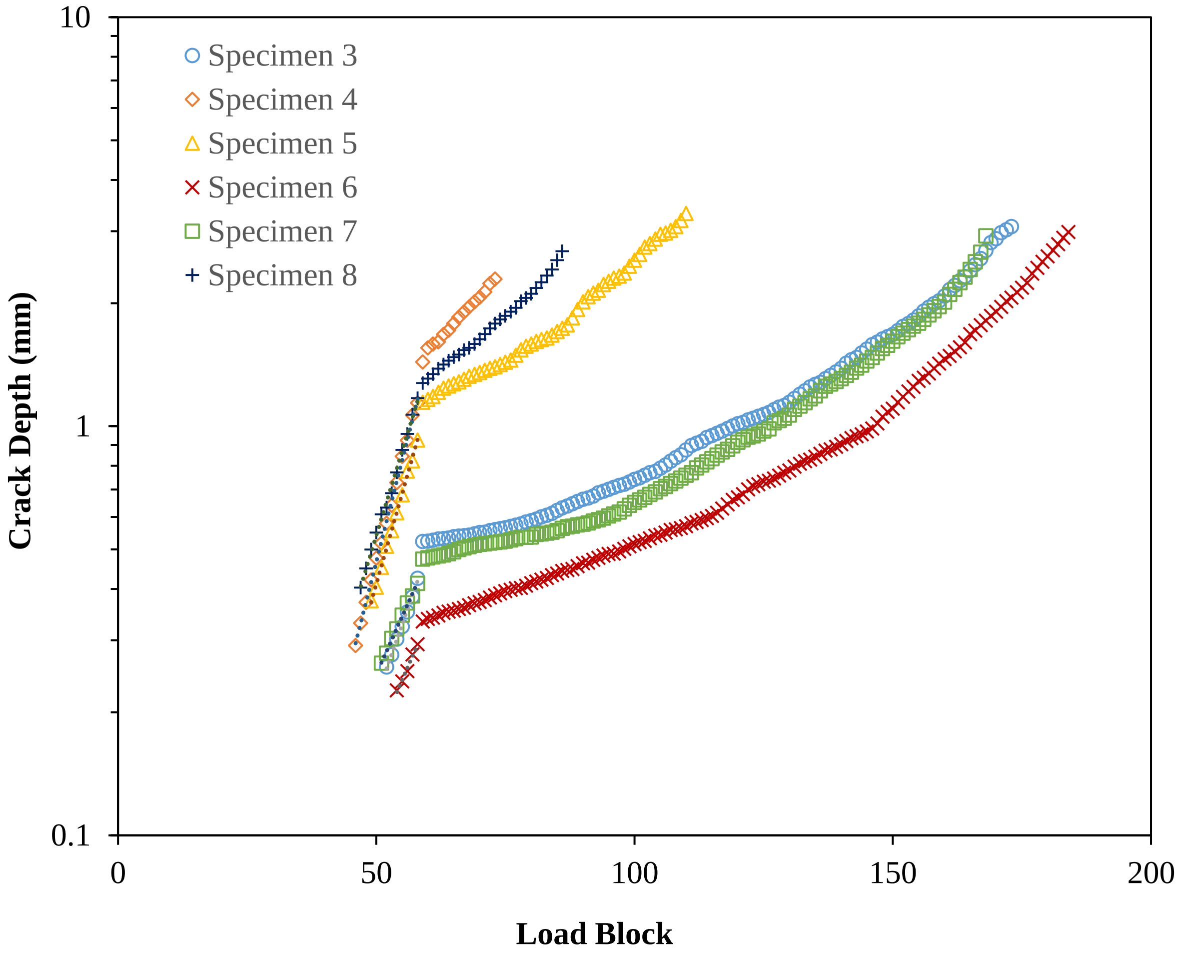

Figure 6.17 Crack growth history of 5-ply patched specimens.

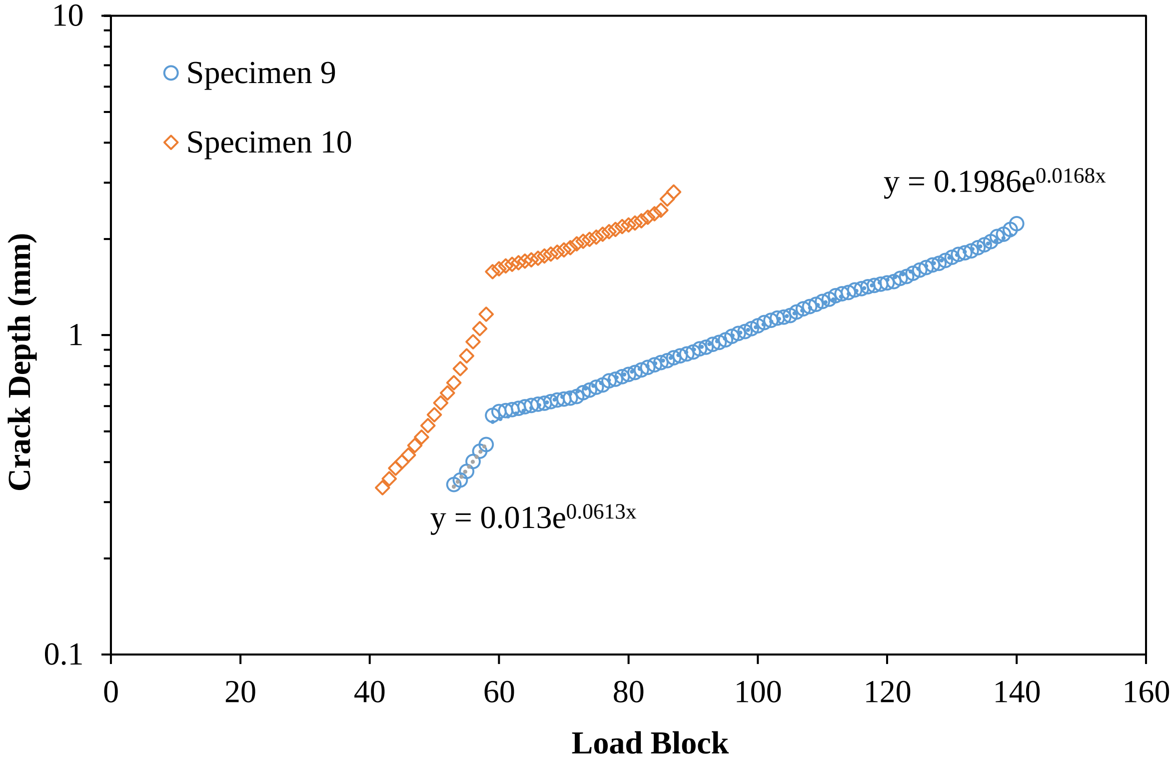

Figure 6.18 Crack growth history of 5-ply patched specimens with disbonding zone.

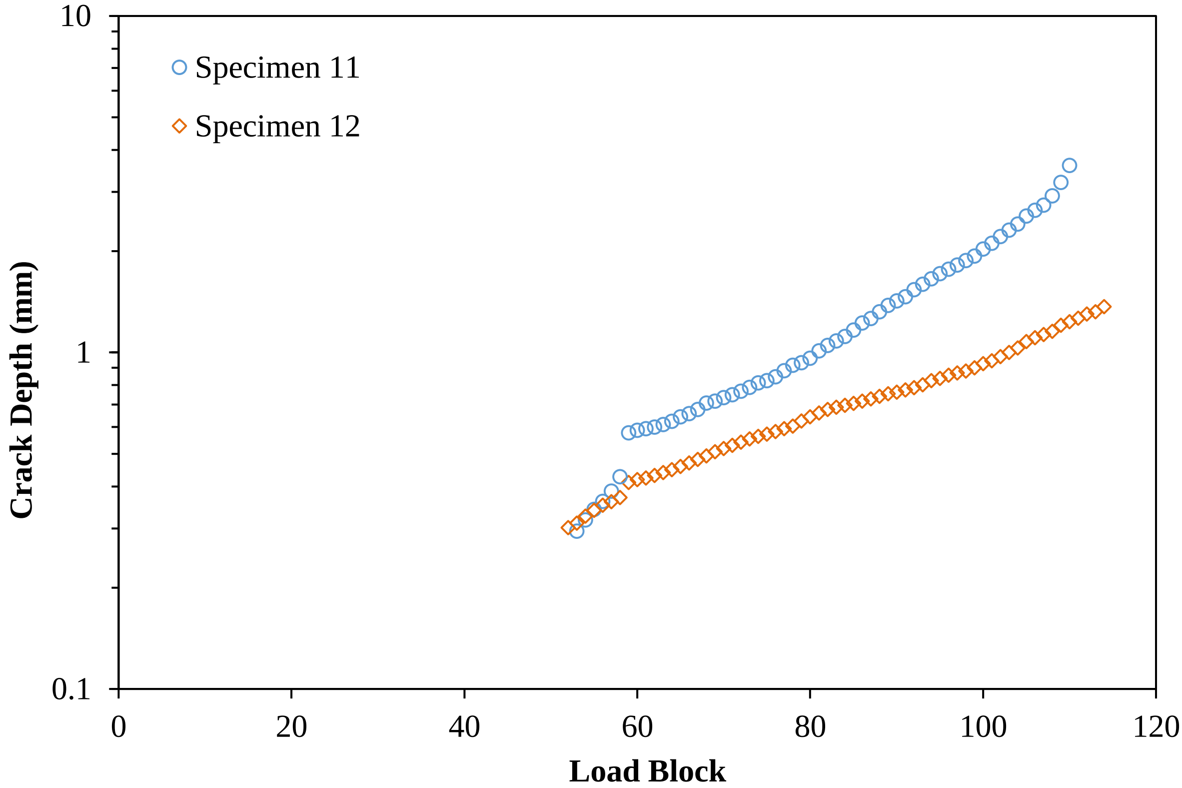

Figure 6.19 Crack growth history of 2-ply patched specimens.

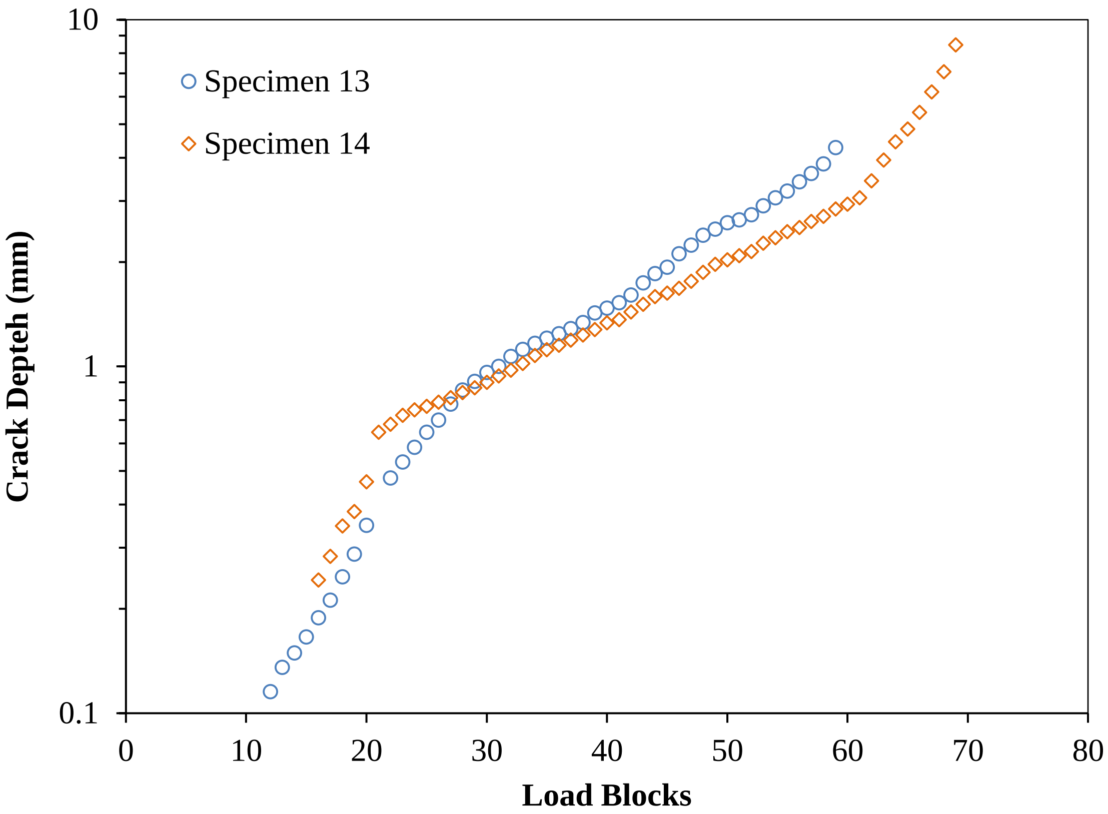

Figure 6.20 Crack growth history of 5-ply corroded specimens.

Table 6.4 Values of ω, both before and after patching, for Specimens 3-14.

Specimen	$\omega_{unpatched}$	$\omega_{patched}$	Specimen	$\omega_{unpatched}$	$\omega_{patched}$
3	0.0822	0.0153	4	0.1145	0.0314
5	0.1018	0.0208	6	0.0671	0.0164
7	0.0647	0.0155	8	0.0951	0.0257
9	0.0613	0.0168	10	0.0773	0.0179
11	0.0718	0.0344	12	0.0352	0.0211
13	0.1348	0.0533	14	0.1602	0.0469

In accordance with the exponential rule the value ω for a patched specimen can be predicted from ω of unpatched specimen via Equation (6.7), viz:

$$\omega_{predicted} = \omega_{unpatched} \left(\frac{\sigma_{patched}}{\sigma_{unpatched}} \right)^3 \tag{6.7}$$

The ratio of the stress ($\sigma_{patched}$ / $\sigma_{unpatched}$) can be determined using Equation (6.8).

$$\frac{\sigma_{patched}}{\sigma_{unpatched}} = \frac{E_{al} T_{al}}{E_{al} T_{al} + E_b T_b} \tag{6.8}$$

where E is the elastic modulus and T is the thickness of material. The subscript al and b are corresponding to the values associated with the aluminium alloy and the boron composite patch respectively. The stress ratio for the various specimen configurations is shown in Table 6.5. The results are promising as both the 5-ply and 2-ply cases give approximately the same reduction rate as results of FE analysis in Section 6.2.1.

Table 6.5 Values of $\omega_{patched}/\omega_{unpatched}$ for different specimen configurations.

Specimen configuration	E_{al} (GPa)	E_b (GPa)	T_{al} (mm)	T_b (mm)	$\frac{\sigma_{patched}}{\sigma_{unpatched}}$
5-ply	71.7	210	6.35	1.3	0.625
2-ply			6.35	0.52	0.807
Corroded			11	1.3	0.743

Table 6.6 presents a comparison between the predicted and measured values of $\omega_{patched}$ for the lead cracks in Specimens 3-14. The crack growth histories of Specimens 4, 10, 11 and 13 are plotted in Figures 6.21-24 as they have the shortest fatigue life among its own type, i.e. 5-ply, 5-ply with disbonding zone, 2-ply and corroded specimens. For those specimens with the fastest crack growing rate, the error is around approximately ± 12%. In the cases where this is not true the predicted crack growth curve is conservative. The reasonably good prediction further supports the conclusion that for specimens repaired with a composite patch fibre bridging is a second order effect.

Table 6.6 Measured and predicted values of ω and their percentage in some specimens for Specimens 3 to 15.

Specimen	$\omega_{patched}$	$\omega_{predicted}$	Error %
3	0.0153	0.0201*	31.2%
4	0.0314	0.0280	-11.0%
5	0.0208	0.0249*	19.5%
6	0.0164	0.0164	-0.1%
7	0.0155	0.0158	1.9%
8	0.0257	0.0232	-9.7%
9	0.0168	0.0150	-10.9%
10	0.0179	0.0189	5.4%
11	0.0344	0.0377	9.7%
12	0.0211	0.0185	-12.3%
13	0.0533	0.0553	3.7%
14	0.0469	0.0657*	40.1%

* Crack growth predictions are conservative.

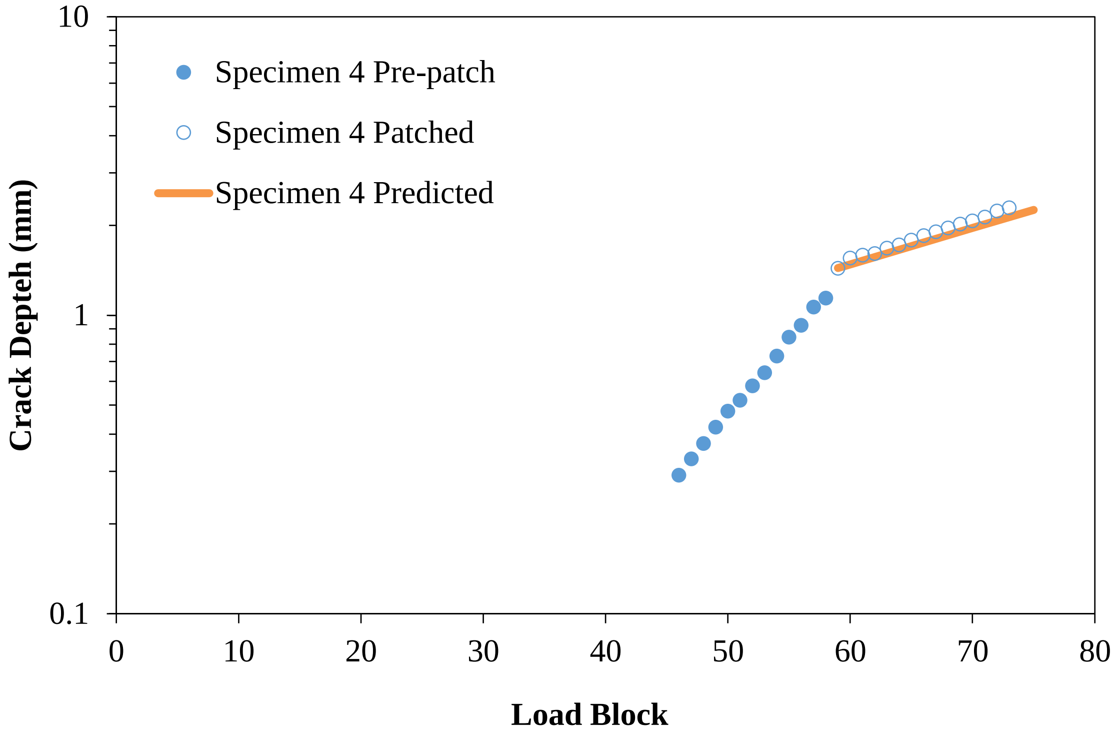

Figure 6.21 Prediction of Specimen 4 with Cubic rule.

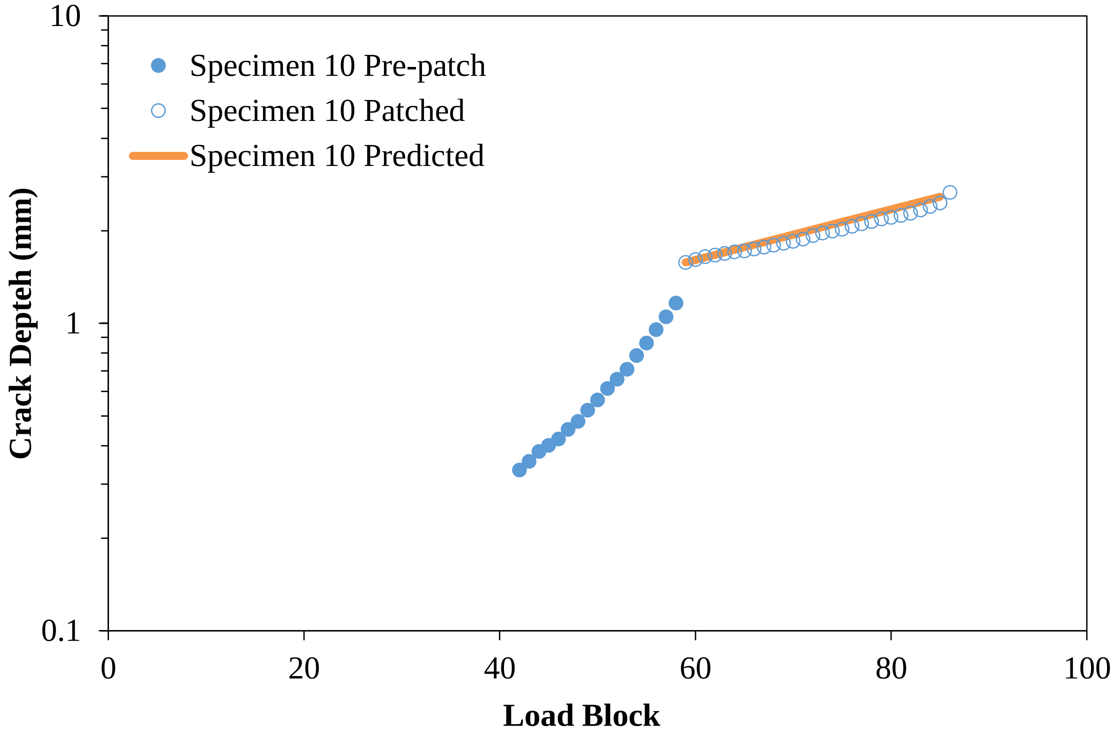

Figure 6.22 Prediction of Specimen 10 with Cubic rule.

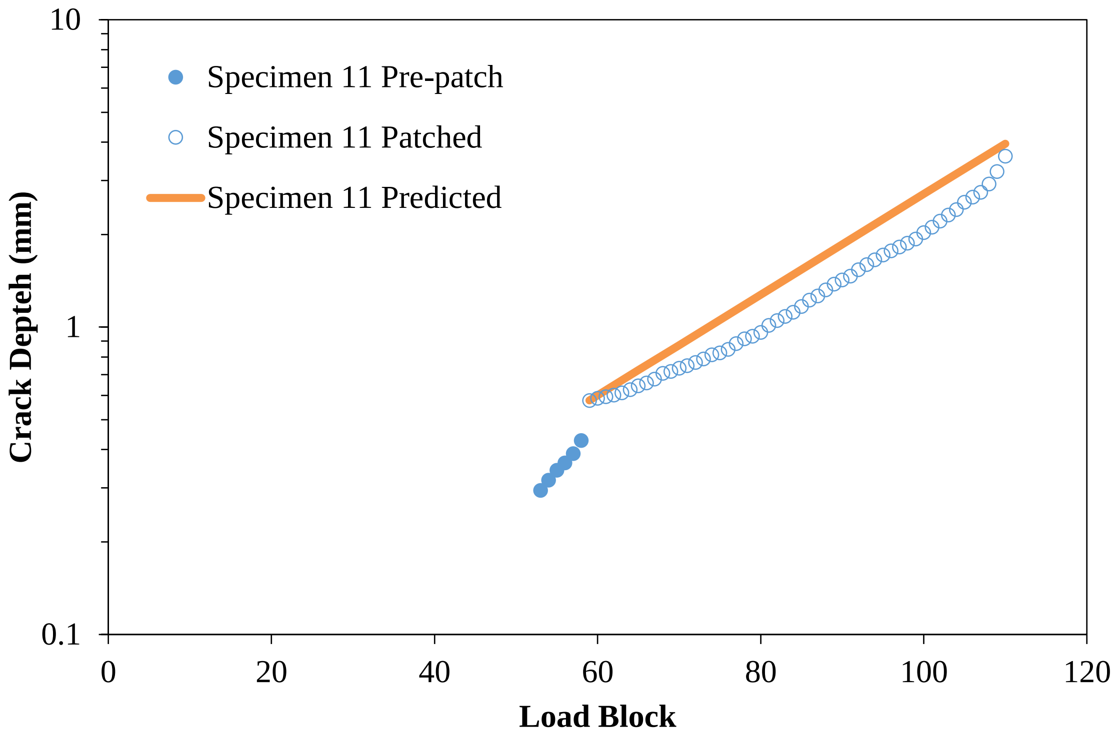

Figure 6.23 Prediction of Specimen 11 with Cubic rule.

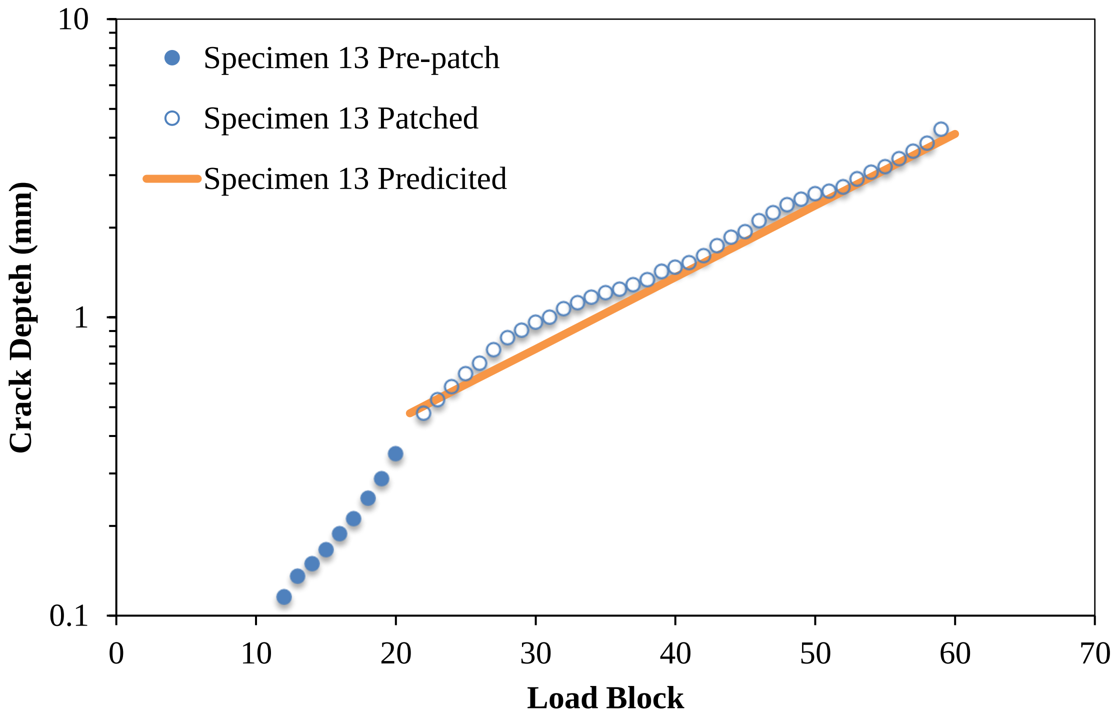

Figure 6.24 Prediction of Specimen 13 with Cubic rule.

6.4 Summary

This Chapter presents two methods which use information obtained from unpatched specimens to predict the crack growth history in patch repaired specimens. The change in the stress, for uncracked specimens, due to patching is simulated using FE analysis. FE models of unpatched specimens with a crack on the median plane were used to obtain the stress intensity factors. In the first method the Hartman-Schijve equation was used to compute crack growth in both patched and unpatched structures. The scatter in the growth histories was captured by allowing for changes in the threshold term.

In the second method the Cubic rule is used to predict crack growth in the patch repaired specimen used information associated with crack growth in the unpatched specimen. Both approaches yielded crack growth histories that were in good agreement with the measured data. The analysis also supports the conclusion that for composite repairs to naturally occurring cracks the effect of the fibres bridging is a second order effect and that the primary effect of patching specimen is due to the reduction in the net cross-section stress in the structure beneath the patch.

Chapter 7

Conclusion And Recommendation

7.1 Conclusions

In 2009 the US FAA introduced a slow growth approach for certifying composite and adhesively bonded structures. A prerequisite to adopting this approach is to establish that the growth of cracks/disbonds is slow, stable and predictable. This thesis provides evidence that the Hartman-Schijve equation has the potential to predict the delamination/disbond with several structural adhesives. The experimental study performed in conjunction with the Australian DST Group established that the growth of cracks, that prior to patching were allowed to initiate and grow naturally, was predictable. In this test program fatigue cracks were grown from surface damage, i.e. laser notches or corrosion pits. These cracked specimens were subsequently patched with boron/epoxy doublers that were bonded to both sides of the specimens. This was done so as to ensure that unwanted bending effects were eliminated. Two prediction methods were developed. One was based on the Hartman-Schijve equation. The second method used the approach delineated in the USAF approach to assessing the Risk of Failure together with the RAAF Cubic Rule as outlined in the F/A-18 Structures Assessment Manual.

7.1.1 The Hartman-Schijve variant of NASGRO equation

This thesis has shown that for composite and adhesively bonded structures, plotting the strain energy release rate range, ΔG, against crack growth rate, da/dN, can cause an anomaly of R ratio effect. A new formulation, called the Hartman-Schijve equation which is based on $\Delta\sqrt{G}$, is then proposed and this formulation can eliminate this anomaly. The Hartman-Schijve equation, which was first proposed to predict crack growth in metal, is extended to adhesively bonded structures. The Hartman-Schijve approach has revealed several noteworthy features for a wide range of structural adhesives:

- A 'master' line for the fatigue data points is produced by the Hartman-Schijve approach.
- The slope, m, of this 'master' linear has a relatively low value.
- The Hartman-Schijve approach is found to be applicable to Mode I, Mode II and Mixed-Mode I and II types of fatigue loading.
- This approach can capture the scatter that results from testing multiple nominally identical specimens.
- This approach collapses the crack growth curves associated with different R ratios, temperature and initial delamination lengths onto a single 'master' curve with the same D, m and A.

7.1.2 Prediction of disbond of undamaged adheive

Since the Hartman-Schijve variant of NASGRO equation is capable of collapsing disbond growth data with different degrees of mode mixity, the constants obtained for pure Mode I test, e.g. double cantilever beam, can be sued to predict Mixed Mode I and II disbond growth in a double over-lap joint and a patch repaired joint. The constants, i.e. D, m and A, in the Hartman-Schijve equation are held constantly and the scatter in the fatigue tests is captured by allowing for changes in the threshold term, $\Delta\sqrt{G_{thr}}$. The simulation of disbond growth in FM 73 in both a bonded joint and a patch repair is shown be in reasonable agreement with experiment data.

7.1.3 Experiments of bonded patch repair to metallic structures

In the experimental fatigue tests, only a few fatigue cracks grow to any significant extent, even though there were hundreds of surface damage states in each specimen. This illustrates the large scatter that is associated with short cracks. After fatigue cracks had initiated and had grown to a length of approximately 1 mm, the unidirectional boron/epoxy patches were applied to both sides of each specimen. It is interesting to note that cracks initiated in adhesive layer grew through the adhesive, i.e. on the same plane as cracks in metal adherend. Disbonding and subsequent failure of the composite only occurred after the crack in the adhesive had grown through the film and reached the composite patch. Furthermore, the disbonds in the patch had little influence on crack growth in the metal adherend in this experiment.

7.1.4 Prediction of patch repaired structures

Two methods were used to simulate the crack growth in the composite repaired specimens. The first involves FE analysis to obtain the stress field and thus the stress intensity factors. The Hartman-Schijve equation is then used to predict the crack growth of patched laser notched and corrosion pitted specimens using the Ks obtained from an analysis of the unpatched specimens and the stress change due to patching. The results of the predicted and measured crack growth histories were in a good agreement.

The second method is the Cubic rule which predicts the crack growth after patching using the information of crack growth prior patching and the change in the stress due to patching. This method also illustrates that the fibre bridging is the second order effect in the composite repair of cracked structures.

7.2 Recommendations for Future Works

This thesis has shown that the Hartman-Schijve variant of NASGRO equation is able to be used for several structural adhesives under constant amplitude loading. However, studies into the ability to compute representative operational flight load spectra are needed.

In the experimental work discussed in this thesis, one patch configuration had a 6 mm disbonded zone across its entire width. Unfortunately, cracks did not initiate beneath the disbonded zone. Consequently, a new specimen should be designed so that fatigue cracks can only initiate and grow beneath the disbonded zone. The purpose of this study should be to investigate of the effect of size, shape and location of the disbonded zone on the fatigue crack growth.

Since the marker bands were found in the adhesive film of patched specimens, it is clear that there are fatigue cracks growing in the fracture surface of adhesive film. It was found that if the marker bands in the adhesive did not reach the composite patch, then the patch would generally fail cohesively or break into half instead of delaminating. Consequently, it is interesting to investigate whether patch failure can be delayed by increasing the time for the marker bands to reach the patch. There are two thoughts which may achieve such purpose:

- Increase the local adhesive thickness.
- Look for a structural adhesive with an improved fatigue resistance.

References

[1] J. C. Newman, X. R. Wu, S. L. Venneri and C. G. Li, “Small-Crack Effects in High-Strength Aluminium Alloys,” NASA-RP-1309, Langley Research Center, Hampton, Virginia, 1994.

[2] C. F. Tiffany, J. P. Gallagher and C. A. Babish IV, “Threats To Aircraft Structural Safety, Including A Compendium Of Selected Structural Accidents/Incidents,” ASC-TR-2010-5002, Aeronautical Systems Centre, Engineering Directorate, Wright-Patterson Air Force Base, 2010.

[3] R. J. Wanhill, “Milestone Case Histories in Aircraft Structural Integrity,” NLR-TP-2002-521,Structures and Materials, National Aerospace Laboratory NLR, 2002.

[4] G. Negaard, “The History of the Aircraft Structural Integrity Program,” Aerospace Structures Information and Analysis Center (ASIAC), Wright-Patterson AFB, OH, 1980.

[5] J. R. Gebman, Challenges and Issues with the Further Aging of U.S. Air Force Aircraft – Policy Options for Effective Life-Cycle Management of Resources, Santa Monica, CA: Rand Corporation, 2009.

[6] US Military, “Airplane Damage Tolerance Requirements,” MIL A 83444 Notice 1, US Military, 1974.

[7] Federal Aviation Administration, “Establishing and Implementing Limit of Validity to Prevent Widespread Fatigue Damage,” Advisory Circular No: 20-104, 2011.

[8] C. A. Babish IV, “USAF ASIP: Protecting Safety for 50 Years,” in *ASIP conference*, San Antonio, TX, 2008.

[9] J. A. Pascoe, *Characterisation of fatigue crack growth in adhesive bonds*, PhD Thesis, Delft University of Technology, 2016.

[10] M. H. Davis and D. A. Bond, “The Importance of Failure Mode Identification in Adhesive Bonded Aircraft Structures and Repairs,” in *ICCM 12 Conference,* Paris, 1999.

[11] Federal Aviation Administration, “Composite Aircraft Structure,” Advisory Circular No: 20-107A, 1984.

[12] Federal Aviation Administration, “Composite Aircraft Structure,” Advisory Circular No: 20-107B, 2009.

[13] US Department of Defense, “Military Standard: Aircraft Structural Integrity Program, Airplane Requirements, MIL-STD-1530A,” 1975.

[14] DEPARTMENT OF DEFENSE, “COMPOSITE MATERIALS HANDBOOK: VOLUME 3. POLYMER MATRIX COMPOSITES MATERIALS USAGE, DESIGN, AND ANALYSIS,” 2002.

[15] P. Chalkley and R. Geddes, “Service History of the F-111 Wing Pivot Fitting Upper Surface Boron/Epoxy Doublers,” DSTO-TN-0168, DSTO, 1998.

[16] A. A. Baker, R. J. Chester, M. J. Davis, J. D. Roberts and J. A. Retchford, “Reinforcement of the F-111 Wing Pivot Fitting with a Boron/Epoxy Doubler System—Materials Engineering Aspects,” *Composites,,* vol. 24, no. 6, pp. 511-521, 1993.

[17] R. Jones, S. Stelzer and A. J. Brunner, “Mode I, II and Mixed Mode I/II delamination growth in composites,” *Compostie Structrues,* vol. 110, pp. 317-324, 2014.

[18] R. Jones, W. Hu and A. J. Kinloch, “A Convenient Way to Represent Fatigue Crack Growth in Structural Adhesives,” *Fatigue and Fracture of Engineering Materials and Structures,* vol. 38, no. 4, pp. 379-391, 2015.

[19] W. Schutz, “A History of Fatigue,” *Engineering Fracture Mechanics,* vol. 54, no. 2, pp. 263-300, 1996.

[20] O. H. Basquin, “The Exponential Law of Endurance Tests,” *American Society for Testing and Materials Proceedings,* vol. 10, pp. 625-630, 1910.

[21] A. A. Griffith, “The Phenomena of Rupture and Flow in Solids,” *Philosophical Transactions of the Royal Society,* vol. 221, pp. 163-198, 1921.

[22] G. R. Irwin, “Analysis Of Stresses And Strains Near The End Of A Crack Traversing A Plate,” *ASME Journal of Applied Mechanics,* vol. 24, pp. 361-364, 1957.

[23] P. C. Paris, “Brief History of the Crack Tip Stress Intensity Factor and Its Application,” *Meccanica,* vol. 49, pp. 759-764, 2014.

[24] T. L. Anderson, Fracture Mechanics: Fundamentals and Applications, Boca Raton, Florida: CRC Press, 1995.

[25] D. E. Martin and G. M. Sinclair, “Crack propation under repeated loading,” *Proceedings of the Third U.S. National Congress of Applied Mechanics,* pp. 595-604, June 1958.

[26] P. Paris, M. Gomez and W. Anderson, “A rational analytic theory of fatigue,” *The Trend in Engineering,* vol. 13, p. 9–14, 1961.

[27] P. Paris and F. Erdogan, “A Critical Analysis of Crack Propagation Laws,” *ASME Journal of Basic Engineering,* vol. 85, no. 4, pp. 528-533, 1963.

[28] A. Hartman and J. Schijve, “The effects of environment and load frequency on the crack propagation law for macro fatigue crack growth in aluminium alloys,” *Engineering Fracture Mechanics,* vol. 1, pp. 615-631, 1970.

[29] T. C. Lindley, I. G. Palmer and C. E. Richards, “Acoustic Emission Monitoring Of Fatigue Crack Growth,” *Materials Science and Engineering,* vol. 32, pp. 1-15, 1978.

[30] W. Elber, “Fatigue Crack Closure Under Cyclic Tension,” *Engineering Fracture Mechanics,* vol. 2, pp. 37-45, 1970.

[31] W. Elber, “The Significance of Fatigue Crack Closure,” Damage Tolerance of Aircraft Structures, ASTM STP-486, pp. 230–242, 1971.

[32] R. M. Kemp, “Fatigue Crack Closure – A Review,” Technical Report 90046, Royal Aerospace Establishment, Farnborough, Hampshire, 1990.

[33] M. J. Adams, “Fatigue Crack Closure at Positive Stresses,” *Engineering Fracture Mechanics,* vol. 4, no. 3, pp. 543-554, 1972.

[34] R. Roberts and R. A. Schmidt, “Observations of Crack closure,” *International Journal of Fracture Mechanics,* vol. 8, no. 4, pp. 469-471, 1972.

[35] ASTM, “Standard Test Method for Measurement of fatigue crack growth rates, ASTM E647-13a,” 2014.

[36] J. C. Newman Jr. and Y. Yamada,, “Compression Precracking Methods to Generate Near - Threshold Fatigue-Crack-Growth-Rate Data,” *International Journal of Fatigue,* vol. 32, pp. 879-885, 2010.

[37] S. Suresh and R. O. Ritchie, “Propagation of Short Fatigue Cracks,” *International Metals Reviews,* vol. 29, no. 6, pp. 445-475, 1984.

[38] M. Lo, “Interaction of Fatigue Crack Growth and Intergranular Corrosion in Maritime Aircraft,” PhD Thesis, Monash University, Clayton, 2016.

[39] L. Molent, S. A. Barter and R. J. Wanhill, “The Lead Crack Fatigue Lifing Framework,” DSTO-RR-0353, DSTO, 2010.

[40] J. Schijve, “Fatigue life until small cracks in aircraft structures: Durability and damage tolerance,” in *NASA International Symposium on Advanced Structural Integrity Methods for Airframe Durability and Damage Tolerane, Part 2; pp 665-681*, 1994.

[41] D. A. Lados, D. Apeliana, P. Paris and J. K. Donald, “Closure Mechanisms in Al–Si–Mg Cast Alloys and Long-Crack to Small-Crack Corrections,” *International Journal of Fatigue,* vol. 27, pp. 1463-1472, 2005.

[42] S. Pearson, “Initiation of Fatigue Cracks in Commercial Aluminum Alloys and the Subsequent Propagation of Very Short Cracks,” *Engineering Fracture Mechanics,* vol. 7, pp. 235-247, 1975.

[43] J. Schijve, “Differences between the growth of small and large fatigue cracks. The relation to threshold K-values,” Report LR-327, Delft University of Technology, 1987.

[44] K. T. Rao, W. Yu and R. O. Ritchie, “On The Behavior Of Small Fatigue Cracks In Commercial Aluminum-Lithium Alloys,” *Engineering Fracture Mechanics,* vol. 31, no. 4, pp. 623-635, 1988.

[45] X. R. Wu, J. C. Newman, W. Zhao, M. H. Sawin, C. F. Ding and E. P. Phillips, “Small Crack Growth and Fatigue Life Predictions for High-Strength Aluminum Alloys: Part (I)—Experimental and Fracture Mechanics Analysis,” *Fatigue and Fracture of Engineering Materials and Structures,* vol. 21, pp. 1289-1306, 1998.

[46] J. C. Newman, W. R. Wu, M. H. Swain, W. Zhao, E. P. Phillips and C. F. Ding, “Small-Crack Growth and Fatigue Life Predictions for High-Strength Aluminium Alloys. Part II: Crack Closure and Fatigue Analyses.,” *Fatigue and Fracture of Engineering Materials and Structures,* vol. 23, pp. 59-72, 2000.

[47] R. Jones, L. Molent and S. Pitt, “Crack growth from physically small flaws,” *International Journal of Fatigue,* vol. 29, pp. 1658-1667, 2007.

[48] A. El Malki Alaoui, D. Thevenet and A. Zeghloul, “Short surface fatigue cracks,” *growth under constant and variable amplitude loading,* vol. 76, p. Engineering Fracture Mechanics, 2009.

[49] Y. Jones, S. Barter and F. Chen, “Experimental Studies into Short Crack Growth,” *Engineering Failure Analysis,* vol. 18, no. 7, pp. 1711-1722, 2011.

[50] R. Jones and D. Tamboli, “Implications of the Lead Crack Philosophy and the Role of Short Cracks In Combat Aircraft,” *Engineering Failure Analysis,* vol. 29, pp. 149-166, 2013.

[51] R. G. Forman, V. E. Kearney, and R. M. Engle, “Numerical Analysis of Crack Propagation in Cyclic-Loaded Structures,” *Journal of Basic Engineering,* vol. 89, no. 3, pp. 459-463, 1967.

[52] R. G. Forman and S. R. Mettu, “Behavior of surface and corner cracks subjected to tensile and bending loads in Ti–6Al–4V alloy,” Johnson Space Center, Houston, Texas, 1990.

[53] J. C. Newman Jr., “A Crack Opening Stress Equation for Fatigue Crack Growth,” *International Journal of Fracture,* vol. 24, pp. 131-135, 1984.

[54] R. Jones, L. Molent and K. Walker, “Fatigue crack growth in a diverse range of materials,” *International Journal of Fatigue,* vol. 40, pp. 43-50, 2012.

[55] R. Jone, “Fatigue crack growth and damage tolerance,” *atigue and Fracture of Engineering Materials and Structures,* vol. 37, no. 5, pp. 463-483, 2014.

[56] F. R. Shanley, “A theory of fatigue based on unbonding during reversed slip, AD422822,” 1953.

[57] N. E. Frost, and D. S. Dugdale, “The Propagation of Fatigue Cracks in Sheet Specimens,” *Journal of Mechanics and Physics of Solids,* vol. 6, pp. 92-110, 1958.

[58] R. A. Pell, L. Molent and A. J. Green, “The fractographical comparison of F/A-18 aluminium alloy 7050-T7451 bulkhead representative coupons tested under two fatigue load spectra at several stress levels,” DSTO-TR-1547, 2004.

[59] P. White, L. Molent and S. Barter, “Interpreting fatigue test results using a probabilistic fracture approach,” *International Journal of Fatigue,* vol. 27, no. 7, pp. 752-767, 2005.

[60] W. Zhuang, S. Barter, M. McDonald and L. Molent, “Fatigue crack growth life assessment of the F/A-18 aft fuselage frames (Y645 and Y657),” DSTO-TR-1826, 2006.

[61] W. Zhuang and L. Molent, “Block-by-block approaches for spectrum fatigue crack growth prediction,” *Engineering Fracture Mechanics,* vol. 75, no. 17, pp. 4933-4947, 2008.

[62] M. McDonald,, “Guide on the Effective Block Approach for the Fatigue Life Assessment of Metallic Structures,” DSTO-TR-2850, 2013.

[63] L. Molent and R. Jones, “A stress versus crack growth rate investigation (aka stress – cubed rule),” *International Journal of Fatigue,* vol. 87, pp. 435-443, 2016.

[64] J. Huynh, L. Molent and S. Barter, “Experimentally derived crack growth models for different stress concentration factors,” *International Journal of Fatigue,* vol. 30, pp. 1766-1786, 2008.

[65] S. Barter, “Fatigue Cracking in Aluminium Alloy 7050-T7451 – Quantitative Fractographic Methods and Life Prediction,” PhD Thesis, Monash University, Clayton, Victoria, 2007.

[66] S. Barter, “The quantification of fatigue crack initiators in aluminium alloy 7050-T7451 using quantitative fractography,” *International Journal of Structural Integrity,* vol. 2, no. 3, pp. 243-263, 2011.

[67] M. Burchill,, S. Barter and M. Jone, “The Effect of Crack Growth Retardation when Comparing Constant Amplitude to Variable Amplitude Loading in an Aluminium Alloy,” *Advanced Materials Research,* Vols. 891-892, pp. 948-954, 2014.

[68] S. S. Wang, J. F. Mandell and F. J. McGarry, “Analysis of crack tip stress-field in DCB adhesive fracture specimens,” *International Journal of Fracture,* vol. 14, no. 1, pp. 39-58, 1978.

[69] G. C. Sih, P. C. Paris and G. R. Irwin, “On cracks in rectilinearly anisotropic bodies,” *International Journal of Fracture Mechanics,* vol. 1, pp. 189-203, 1965.

[70] R. Jones, S. Pitt, A. J. Bunner and D. Hui, “Application of the Harman-Schijve equation to represent Mode I and Mode II fatigue delamination growth in composites,” *Composite Structures,* vol. 94, pp. 1343-1351, 2012.

[71] T. R. Brussat, S. T. Chiu and S. Mostovoy, “Fracture mechanics for structural adhesive bonds – final report,” AFML-TR-77-163, US Air Force Materials Laboratory, 1977.

[72] T. R. Brussat and S. T. Chiu, “Fatigue crack growth of bondline cracks in structural bonded joints,” *Journal of Engineering Materials and Technology,* vol. 100, pp. 39-45, 1978.

[73] S. Mall and W. S. Johnson, “Characterization of Mode I and Mixed-Mode Failure of Adhesive Bonds Between Composite Adherends,” NASA-TM-86355, Langley Research Center, Hampton, Virginia, 1985.

[74] S. Mall, G. Ramamurthy and M. A. Rezaizdeh, “Stress ratio effect on cyclic debonding in adhesively bonded joints,” *Composite Structures,* vol. 8, pp. 31-45, 1987.

[75] C.-G. Gustafson and M. Hojo, “Delamination fatigue crack growth in unidirectional graphite/epoxy laminates,” *Journal of Reinforced Plastics and Composites,* vol. 6, pp. 36-52, 1987.

[76] M. L. Benzeggagh and M. Kenane, “Measurement of Mixed-Mode Delamination Fracture Toughness of Unidirectional Glass/Epoxy Composites with Mixed-Mode Bending Apparatus,” *Composites Science and Technology,* vol. 56, pp. 439-449, 1996.

[77] M. Kenane and M. L. Benzeggagh, “Mixed-Mode Delamination Fracture Toughness of Unidirectional Glass/Epoxy Composites Under Fatigue Loading,” *Composites Science and Technology,,* vol. 57, pp. 597-605, 1997.

[78] P. T. Cheuk, L. Tong, C. H. Wang, A. A. Baker and P. Chalkley, “Fatigue crack growth in adhesively bonded composite-metal double-lap joints,” *Composite Structures,* vol. 57, pp. 109-115, 2002.

[79] M. Quaresimin and M. Ricotta, “Stress intensity factors and strain energy release rates in single lap bonded joints in composite materials,” *Composites Science and Technology,* vol. 66, no. 5, pp. 647-656, 2006.

[80] M. Quaresimin and M. Ricotta, “Life prediction of bonded joints in composite materials,” *International Journal of Fatigue,* vol. 28, no. 10, pp. 1166-1176, 2006.

[81] C. Rans, R. Alderliesten and R. Benedictus, “Misinterpreting the results: How similitude can improve our understanding,” *Composites Science and Technology,* vol. 71, pp. 230-238, 2011.

[82] M. J. Donough, A. J. Gunnion, A. C. Orifici and C. H. Wang, “Scaling parameter for fatigue delamination growth in composites under varying load ratios,” *Composites Science and Technology,* vol. 120, pp. 39-48, 2015.

[83] M. Hojo, K. Tanaka, C. G. Gustafson and R. Hayashi, “Effect of stress ratio on near-threshold propagation of delamiantion fatigue cracks in unidirectional CFRP,” *Composites Science and Technology,* vol. 29, pp. 273-292, 1987.

[84] C. T. Lin and P. W. Kao, “Fatigue Delamination Growth in Carbon Fibre-Reinforced Aluminium Laminates,” *Composites Part A,* vol. 27, pp. 9-15, 1996.

[85] M. Hojo, T. Ando, M. Tanaka, T. Adachi, S. Ochiai and Y. Endo, “Mode I and II interlaminar fracture toughness and fatigue delamination of CF/epoxy laminates with self-same epoxy interleaf,” *International Journal of Fatigue,* vol. 28, pp. 1154-1165, 2006.

[86] R. Jones, A. J. Kinloch, J. G. Michopoulos, A. J. Brunner and N. Phan, “Delamination growth in polymer-matrix fibre composites and the use of fracture mechanics data for material characterisation and life prediction,” *Composite Structures,* vol. 180, pp. 316-333, 2017.

[87] I. Simon, L. Banks-sills and V. Fourman, “Mode I delamination propagation and R-ratio effects in woven composite DCB specimens for a multi-directional layup,” *International Journal of Fatigue,* vol. 96, pp. 237-251, 2017.

[88] R. Jones, A. J. Kinloch, J. G. Michopoulos, A. J. Brunner and N. Phan, “Delamination growth in polymer-matrix fibre composites and the use of fracture mechanics data for material characterisation and life prediction,” *Composite Structures,* vol. 180, pp. 316-333, 2017.

[89] A. J. Brunner, N. Murphy and G. Pinter, “Development of a standardized procedure for the characterization of interlaminar delamination propagation in advanced composites under fatigue mode I loading conditions,” *Engineering Fracture Mechanics,* vol. 76, pp. 2678-2689, 2009.

[90] R. H. Martin and G. B. Murri, “Characterization of Mode I and Mode II delamination growth and thresholds in AS4/PEEK composites,” ASTM International, est Conshohocken, PA, 1990.

[91] G. Matsubara, H. Ono and K. Tanaka, “Mode II fatigue crack growth from delamination in unidirectional tape and satin-woven favric laminates of high strength GFRP,” *International Journal of Fatigue,* vol. 28, pp. 1177-1186, 2006.

[92] L. Yao, Y. Sun, L. Guo, M. Zhao, L. Jia, R. C. Alderliesten and R. Benedictus, “A modified Paris relation for fatigue delamination with fibre bridging in composite laminates,” *Composite Structures,* vol. 176, pp. 556-564, 2017.

[93] D. Roach and K. Rackow, “Development and Validation of Bonded Composite Doubler Repairs for Commercial Aircraft,” Sandia National Laboratories, U.S. Department of Energy, Oak Ridge, TN 37831, 2007.

[94] R. Jones, W. K. Chiu and J. Paul, “Designing for damage tolerant bonded joints,” *Composite Structures,* vol. 25, pp. 20-207, 1993.

[95] L. J. Hart-Smith, “Adhesive-bonded double-lap joints, NASA,” 1973.

[96] W. K. Chiu, D. Rees, P. Chalkley and R. Jones, “Designing for Damage Tolerant Repairs,” ARL Aircraft Structures Report 450, 1992.

[97] D. L. Potter, “Primary adhesively bonded structure technology (PABST): Design handbook for adhesive bonding,” USAF Technical Report, AFFDL-TR-79-3119, Long Beach, CA 90846, 1979.

[98] J. A. Pascoe, R. C. Alderliesten and R. Benedictus, “On the relationship between disbond growth and the release of strain energy,” *Engineering Fracture Mechanics,* vol. 133, pp. 1-13, 2015.

[99] P. C. Miedlar, A. P. Berens, A. Gunderson and J. P. Gallagher, “Analysis and Support Initiative for Structural Technology,” AFRL-VA-WP-TR-2003-3002, Ohio, USA, 2003.

[100] J. A. Pascoe, R. C. Alderliesten and R. Benedictus, “Methods for the prediction of fatigue delamination growth in composites and adhesive bonds – a critical review,” *Engineering Fracture Mechanics,* Vols. 112-113, pp. 72-96, 2013.

[101] S. Azari, G. Jhin, M. Papini and J. K. Spelt, “Fatigue threshold and crack growth rate of adhesively bonded joints as a function of load/displacement ratio,” *Composites Part A,* vol. 57, pp. 59-66, 2014.

[102] E. Ripling, S. Mostovoy and R. Patrick, “Application of fracture mechanics to adhesive joints,” ASTM International, West Conshohocken, PA, 1964.

[103] J. K. Jethwa and A. J. Kinloch, “The fatigue and durability behaviour of automotive adhesives. Part 1: fracture mechanics test,” *Journal of Adhesion,* vol. 61, pp. 71-95, 1996.

[104] A. J. Curley, H. Hadavinia, A. J. Kinloch and A. C. Taylor, “Predicting the service-life of adhesively-bonded joints,” *International Journal of Fracture,* vol. 103, pp. 41-69, 2000.

[105] R. Khan, R. Alderliesten, S. Badshah and R. Benedictus, “Effect of stress ratio or mean stress on fatigue delamination growth in composites: Critical review,” *Composite Structures,* vol. 124, pp. 214-227, 2015.

[106] R. Jones, A. J. Kinloch and W. Hu, “Cyclic-fatigue crack growth in composite and adhesively-bonded structures: The FAA slow crack growth approach to certification and the problem of similitude,” *International Journal of Fatigue,* vol. 88, pp. 10-18, 2016.

[107] S. Azari, M. Papini, J. A. Schroeder and J. K. Spelt, “The effect of mode ratio and bond interface on the fatigue behavior of a highly-toughened epoxy,” *Engineering Fracture Mechanics,* vol. 77, pp. 395-414, 2010.

[108] S. Azari, M. Papini, J. A. Schroeder and J. K. Spelt, “Fatigue threshold behavio rof adhesive joints,” *International Journal of Adhesion and Adhesives,* vol. 30, pp. 145-159, 2010.

[109] A. Pirondi and G. Nicoletto, “Fatigue crack growth in bonded DCB specimens,” *Engineering Fracture Mechanics,* vol. 71, pp. 859-871, 2004.

[110] J. Rouchon and M. J. Bos, "Fatigue and Damage Tolerance Evaluation of Structures: The Composite Materials Response," NLR-TP-2009-221, National Aerospace Laboratory NLR, 2009.

[111] A. J. Kinloch, M. S. G. Little and J. F. Watts, "The role of the interphase in the environmental failure of adhesive joints," *Acta Materialia,* vol. 48, pp. 4543-4553, 2000.

[112] A. J. Russell, "A Damage Tolerance Assessment of Bonded Repairs to CF-18 Composite Components. Part I: Adhesive Properties," DREP-TM-88-25, Department of National Defence, Canada, 1988.

[113] L. Molent, S. A. Barter and R. Wanhill, "The Lead Crack Fatigue Lifing Framework," *International Journal of Fatigue,* vol. 33, pp. 323-331, 2011.

[114] R. J. H. Wanhill, "Characteristic Stress Intensity Factor Correlations of Fatigue Crack Growth in High Strength Alloys: Reviews and Completion of NLR Investigations 1985–1990," NLR-TP-2009-256, National Aerospace Laboratory NLR, 2009.

[115] L. Molent, "A review of equivalent pre-crack sizes in aluminium alloy 7050-T7451," *Fatigue & Fracture of Engineering Materials & Structures,* vol. 37, pp. 1055-1074, 2014.

[116] L. Yao , R. C. Alderliesten, and R. Benedictus, "The effect of fibre bridging on the Paris relation for mode I fatigue delamination growth in composites," *Composite Structures,* vol. 140, pp. 125-135, 2016.

[117] L. Yao , R. Alderliesten, M. Zhao and R. Benedictus, "Bridging effect on mode I fatigue delamination behavior in composite laminates," *Composites: Part A,* vol. 63, pp. 103-109, 2014.

[118] J. A. Pascoe, C. D. Rans, R. C. Alderliesten and R. Benedictus, “Fatigue disbonding of bonded repairs – an application of the strain energy approach,” in *International Committee on Aeronautical Fatigue*, Jerusalem, Israel, 2013.

[119] A. A. Baker and R. Jones, Bonded Repair of Aircraft Structure, The Hague: Martinus Nijhoff Publishers, 1988.

[120] A. J. Kinloch, Adhesion and adhesives: science and technology, New York: Springer Science, 1987.

[121] R. O. Ritchie, “Mechanisms of fatigue-crack propagation in ductile and brittle solids,” *International Journal of Fracture,* vol. 100, pp. 55-83, 1999.

[122] A. A. Baker, “Structural health monitoring of a bonded composite patch repair on a fatigue-cracked F-111C Wing,” DSTO-RR-0335, DSTO, 2008.

[123] C. Kourloufas and J. Wittkopp, “F/A-18A/B Inner Wing Step Lap Joint Defect Management,” in *Continuing Airworthiness Conference,* Melbourne, 2016.

[124] P. T. Cheuk, L. Tong, N. Rider A and J. Wang, “Analysis of energy release rate for fatigue cracked metal-to-metal double-lap shear joints,” *International Journal of Adhesion and Adhesives,* vol. 25, pp. 181-191, 2005.

[125] D. A. Virkler, B. M. Hillberry and P. K. Goel, “The Statistical Nature of Fatigue Crack Propagation,” *Journal of Engineering Materials and Technology,* vol. 101, pp. 148-153, 1979.

[126] L. Molent and R. Jones, “The influence of cyclic stress intensity threshold on fatigue life scatter,” *International Journal of Fatigue,* vol. 82, pp. 748-756, 2016.

[127] T. A. Hafiz, M. M. Abdel-Wahab, A. D. Crocombe and P. A. Smith, “Mixed-mode fatigue crack growth in FM 73 bonded joints,” *International Journal of Adhesion & Adhesive,* vol. 40, pp. 188-196, 2013.

[128] W. S. Johnson and L. M. Butkus, “Considering environmental conditions in the design of bonded structures: a fracture mechanics approach,” *Fatigue and Fracture of Engineering Materials and Structures,* vol. 21, pp. 465-478, 1998.

[129] J. Ayling, A. Bowler, G. Brick and M. Ignjatovic, “Practical application of structural repair fatigue life determination on the AP-3C Orion platform,” *Advanced Materials Research,* Vols. 891-892, pp. 1065-1070, 2014.

[130] A. P. Berens, P. W. Hovey and D. A. Skinn, “Risk analysis for aging aircraft fleets - Volume 1: Analysis, WL-TR-91-3066,” Air Force Systems Command, Wright-Patterson Air Force Base, 1991.

[131] A. A. Baker, “A summary of work on applications of advanced fibre composites at the Aeronautical Research Laboratories, Australia,” *Composites,* vol. 9, pp. 11-16, 1978.

[132] R. Jones and R. J. Callinan, “Finite element analysis of patched cracks,” *Journal of Structural Mechanics,* vol. 7, pp. 107-130, 1979.

[133] R. Jones and R. J. Callinan, “Thermal considerations in the patching of metal sheets with composite overlays,” *Journal of Structural Mechanics,* vol. 8, pp. 143-149, 1980.

[134] R. Jones and R. J. Callinan, “Structural Design of BFRP Patches for Mirage Wing Repair, AR-002-214,” 1980.

[135] R. Jones, R. J. Callinan and K. C. Aggarwal, “Stress Analysis Of Adhesively Bonded Repairs To Fibre Composite Structures, AR-002-275,” 1981.

[136] A. A. Baker, “Repair of cracked or defective metallic aircraft components with advanced fibre composites–an overview of Australian work.,” *Composite Structures,* vol. 2, pp. 153-181, 1984.

[137] A. A. Baker, R. J. Callinan, M. J. Daivs, R. Jones and J. F. Williams, “Application of BFRP patching to Mirage III aircraft,” *Theoretical and Applied Fracture Mechanics,* vol. 2, no. 1, pp. 1-16, 1984.

[138] A. A. Baker, “Fatigue Crack Propagation Studies on Aluminium Panels Patched with Boron/Epoxy Composites,” in *nternational Conference on Aircraft Damage Assessment and Repair*, Melbourne, 1991.

[139] A. A. Baker, “Repair Efficiency In Fatigue-Cracked Aluminium Components Reinforced With Boron/Epoxy Patches,” *Fatigue & Fracture of Engineering Materials & Structures,* vol. 16, pp. 753-765, 1993.

[140] A. A. Baker, “Bonded composite repair of fatigue-cracked primary aircraft structure,” *Composite Structures,* vol. 47, p. 431–443, 1999.

[141] A. A. Baker, L. R. Rose and R. Jones, Advances in the Bonded Composite Repair of Metallic Aircraft Structure, Elsevier Science, 2003.

[142] A. B. Harman and K. F. Walker, “Review of improved methods for analysing load attraction and thermal effects in bonded composite repair design,” DSTO-TR-1546, DSTO, 2003.

[143] Cytec Engineered Materials, “FM 300-2 Film Adhesive, Technical Data Sheet,” 2011.

[144] N. M. Chowdbury, W. K. Chio, J. Wang and P. Chang, “Static and Fatigue Testing Thin Riveted, Bonded and Hybrid Carbon Fiber Double Lap Joints Used In Aircraft Structures,” *Composite Structures,* vol. 121, pp. 315-323, 2015.

[145] N. M. Chowdhury, J. Wang, W. K. Chiu and P. Chang, “Experimental and finite element studies of thin bonded and hybrid carbon fibre double lap joints used in aircraft structures,” *Composite Part B,* vol. 100, pp. 233-242, 2016.

[146] N. M. Chowdhury, W. K. Chiu, J. Wang and P. Chang, “Experimental and finite element studies of bolted, bonded and hybrid step lap joints of thick carbon fibre/epoxy panels used in aircraft,” *Composite Part B,* vol. 100, pp. 68-77, 2016.

[147] E. A. Starke Jr and J. R. Staley, “Application of modern aluminium alloys to aircraft,” *Progress in Aerospace Sciences,* vol. 32, pp. 131-172, 1996.

[148] A. P. Mouritz, Introduction to aerospace materials, Cambridge: Woodhead Publishing Limited, 2012.

[149] C. Meccanica, “Aluminum 7050-T7451 (7050-T73651),,” [Online]. Available: http://www.crpmeccanica.com/PDF/aluminium-7050-t7451-7050-t73651.pdf..

[150] R. Jones, M. Krishnapillai, K. Cairns and N. Matthews, “Application of infrared thermography to study crack growth and fatigue life extension procedures,” *Fatigue and Fracture of Engineering Materials and Structures,* vol. 33, no. 12, pp. 871-884, 2010.

[151] S. Stelzer, A. J. Brunner, A. Arguelles, N. Murpy, G. M. Cano and G. Pinter, “Mode I delamination fatigue crack growth in unidirectional fibre reinforced composites: Results from ESIS TC4 round robins,” *Engineering Fracture Mechanics,* vol. 116, pp. 92-107, 2014.

[152] R. Jones, L. Molent and S. Barter, “Calculating crack growth from small discontinuities in 7050-T7451 under combat aircraft spectra,” *International Journal of Fatigue,* vol. 55, pp. 178-182, 2013.

[153] J. N. Reddy and A. K. Pandey, "First-ply failure analysis of composite laminates," *Computers & Structures,* vol. 25, pp. 371-393, 1987.

[154] T. Y. Kam, Y. W. Liu and E. T. Lee, "First-ply failure strength of laminated composite pressure vessels," *Composite Structures,* vol. 38, pp. 65-70, 1997.

[155] B. G. Prusty, S. K. Satsangi and C. Ray, "First Ply Failure Analysis of Laminated Panels under Transverse Loading," *Journal of Reinforced Plastics and Composites,* vol. 20, pp. 671-684, 2001.

[156] R. Jones, M. Heller, D. Lombardo, S. Dunn, J. Paul and D. Saunders, "Thermoelastic Assessment of Damage Growth in Composites," *Composite Structures,* vol. 12, pp. 291-314, 1989.

[157] Y. R. Choi and N. Rajic, "In-situ Thermoelastic Stress Analysis for Airframe Full Scale Fatigue Testing: An Overview of Lessons Learnt," in *Australian International Aerospace Congress*, Melbourne, 2017.

[158] K. Ali, R. K. Singh, X. L. Zhao, R. Jones and A. J. McMillan, "Composite repairs to bridge steels demystified," *Composite Structures,* 2016.

[159] J. Park and W. Garcia, "Impacts on crack growth analysis of Ti-6Al-4V small crack," in *Aircraft Structural Integrity Program*, San Antonio, Texas, USA, 2015.

[160] J. F. Williams, R. Jones and N. Goldsmith, "An introduction to fracture mechanics theory and case studies," *Transactions of Mechanical Engineering,* vol. 14, no. 4, pp. 185-223, 1989.

[161] R. Jones, D. Peng, S. Pitt and C. Wallbrink, "Weight functions, CTOD, and related solutions for cracks at notches," *Engineering Failure Analysis,* vol. 11, pp. 79-114, 2004.

[162] R. Jones, “scientific evaluation of the approximate 2D theories for composite repairs to cracked metallic components,” *Composite Structures*, vol. 87, pp. 151-160, 2009.

[163] T. Brussat, “When "What we always do" won't solve the problem,” in *The Aircraft Structural Integrit Program Conference*, Bonita Springs, Florida, USA, 2013.